Airway Epithelium Organotypic Culture Models as a Platform for Adverse Outcome Pathway Assessment of Engineered Nanomaterials

Tyler Nicholas

A dissertation
submitted in partial fulfillment of the
requirements for the degree of

Doctor of Philosophy

University of Washington
2019

Reading Committee:
Elaine M. Faustman, Co-Chair
Terrance J. Kavanagh, Co-Chair
William A. Altemeier

Program Authorized to Offer Degree:
Public Health—Environmental and Occupational Health Sciences

University of Washington

Abstract

Airway Epithelium Organotypic Culture Models as a Platform for Adverse Outcome Pathway Assessment of Engineered Nanomaterials

Tyler Nicholas

Co-Chairs of the Supervisory Committee:
Professor Elaine M. Faustman
Professor Terrance J. Kavanagh
Department of Environmental and Occupational Health Sciences

Silver nanoparticles (AgNP) are one of the 84,000 chemicals regulated by the U.S. Environmental Protection Agency's (US EPA) Toxic Substances Control Act (TSCA) that have yet to be tested for potential respiratory toxicity. AgNP are used in multiple applications but primarily in the manufacturing of many antimicrobial products and are thus exposures in occupational settings that are of concern to public health.

Interactions between host genetic and acquired factors, or gene × environment interactions (G×E), may play a defining role in identifying sensitive populations to AgNP exposures in occupational settings. Host genetic factors, such as sex, genotype, or polymorphism, contribute to variation in certain genes that may increase an individual's sensitivity to occupational exposures. Host acquired factors, such as pre-existing chronic respiratory diseases, including asthma, acute bronchitis, and chronic obstructive

pulmonary disease (COPD), collectively affect 16% of the total United States population; these contribute to impairing host defense mechanisms, such as barrier function and immune regulation, mucocilliary clearance and permeability, as well as enzymatic and non-enzymatic oxidative stress regulation, and may also increase an individual's sensitivity to occupational exposures.

Few previous studies have characterized G×E effects on AgNP toxicity. Understanding G×E effects is important for identifying sensitive populations, whose underlying genetics or diseases could directly modify their response to AgNP exposures. Typically, these studies have used young, healthy animals or cell lines cultured toward a "Normal" phenotype and thus did not address the possibility of increased AgNP toxicity in asthmatics. In the present studies, we used organotypic cultures derived from murine tracheal epithelial cells (MTEC) as a high-content *in vitro* model of the conducting airway to characterize G×E effects, or in this case—the effects of genotype × phenotype interaction (G×P), in order to identify determinants of sensitivity and help define both regulatory and mechanistic bases for these effects on AgNP toxicity.

In our first study, we used organotypic cultures to characterize nominal and dosimetric dose-response relationships for AgNP-induced barrier dysfunction, glutathione (GSH) depletion, reactive oxygen species (ROS) production, lipid peroxidation, and cytotoxicity across genotypes, phenotypes, and exposures to understand G×P effects on AgNP toxicity. The "Type 2 (T2)-Skewed" phenotype was characterized as an *in vitro* model of chronic respiratory diseases and experienced an increased sensitivity to AgNP toxicity, suggesting that asthmatics could be a sensitive population to AgNP exposures in occupational settings.

In our second study, we used organotypic cultures to characterize global, differential, and targeted gene expression, canonical pathway enrichment, and upstream transcriptional regulation to understand G×P effects on transcriptional response to AgNP toxicity. We pursued a targeted analysis to characterize dose, genotype, and phenotype effects on expression patterns of genes involved in the secreted factors canonical pathway that were also associated with T1, pro-T2, T2, and T17 responses to AgNP toxicity. We observed

the “T2-Skewed” phenotype was marked by increased pro-inflammatory T17 responses to AgNP toxicity, which are significant predictors of neutrophilic/difficult-to-control asthma and suggests that asthmatics could be a sensitive population to AgNP exposures in occupational settings. In our third study, we utilized mechanistic information from *in vitro* and *in vivo* studies to highlight how key events (KE) can be modified by host genetic and host acquired factors at acute, subacute, and subchronic exposures, and identified two categories of knowledge gaps in order to more directly prioritize future research needs.

Taken together, our results highlight the importance of considering dosimetry as well as G×P effects when screening and prioritizing potential respiratory toxicants. This suggests the importance of considering other host factors, such as age, gender, and epigenetic effects when screening and prioritizing potential respiratory toxicants. This is challenging and important for engineered nanomaterials (ENM), since their mode of action (MoA) have been shown to differ considerably but are still used in hundreds of consumer products. Prior to anticipating potential adverse organism responses arising from ENM toxicity, ensuring safe development of the consumer products in which they are used will be the most critical and necessary step toward safeguarding public health.

Table of Contents

List of Figures

List of Tables

Acknowledgements

I am very grateful for the mentorship of Dr. William Altemeier, and for all of the time, energy, and financial support he provided for me over the last four years. Bill always took the time to review countless iterations of my fellowship applications, manuscripts, and presentations, and provided incredibly helpful feedback. Thanks to his patient guidance, I have become a better scientist and writer than I ever thought I could be. Bill's enthusiasm for science kept me motivated despite all of the failed experiments that came my way. Thank you for taking me on as your student and for giving me a chance to succeed.

I am also very grateful for the mentorship of Drs. Elaine Faustman and Terrance Kavanagh, and for all of the time, energy, and financial support they too have provided me over the last four years. Elaine and Terry always offered helping hands to pull me over the hurdles I had trouble clearing—and there were quite a few of them. They were a dynamic duo who always supported my interests, recognized the importance of having a life outside the lab, and also showed me incredible kindness and generosity over the years. Your genuine belief in my abilities will always mean the world to me.

I would also like to thank my other supervisory committee members, Drs. Michael Rosenfeld and Lara Gamble. Mike, thank you for supporting me as a pre-doctoral trainee in the Environmental Pathology/Toxicology Training Program. The EP/T Training Program was instrumental in fostering my development as an interdisciplinary thinker, and allowed me to incorporate different aspects of pathology, toxicology, and genomics into my research. Lara, thank you for saving the day and becoming my GSR just days before my general exam. I have greatly benefited from your expertise, thoughtful feedback, and willingness to share core resources at the Molecular Analysis Facility.

To the scientists in the Center for Lung Biology: thank you for taking me in as one of your own and for always being there to help me out in the lab. I would especially like to thank Nori Haick, who taught me everything I know about cell culture—without her patient guidance, these studies would not have been possible. Working in the CLB was an asset to my scientific training which instilled in me a genuine appreciation for being able to

answer research questions from an integrative clinical medicine and public health perspective.

To the faculty, staff, and students in the Department of Environmental and Occupational Health Sciences: thank you for giving me the opportunity to learn from you, and for shaping my experience in graduate school in many lasting and meaningful ways. Special shout out to Team Tox for being the best cohort anyone could have asked for.

To Hobbes: thank you for being my favorite co-author, for always “wow-ing” me with your feedback, and for walking on my keyboard while I was working—I know you were just trying to remind me to take a break. You brighten my day and make my house a home.

Dedication

For my sister: the one person on this earth who totally gets me, you are my best friend in this life, and words fail to describe how much I love you.

For my mom and Ken: you always told me to reach for the stars, loved me unconditionally, and gave me everything—thank you for being my rock.

For Lyddie, Maddie, and Emily: your boundless wisdom, strength, and curiosity are true sources of inspiration—thank you for being my sisters and for making us a modern family.

For Karen, Ian, and Sophia: you are three of my best friends and biggest supporters—thank you for always being there for me, I consider you a part of my family.

For Katie, Ellie, Sarah, and Bryce: you inspired me to run marathons, climb mountains, and never stop exploring—thank you for always packing me a beer on our adventures.

For Ben: you inspired me to become a scientist and embody what it means to be a best friend, thank you for that—and for giving me a sunny place to visit.

Chapter 1. Outline of Research Aims and Implications for Risk Assessment

Silver nanoparticles (AgNP) are one of the 84,000 chemicals regulated by the U.S. Environmental Protection Agency's (US EPA) Toxic Substances Control Act that have yet to be tested for potential respiratory toxicity. AgNP are used in multiple applications but primarily in the manufacturing of many antimicrobial products and are thus exposures in occupational settings that are of concern to public health. In recent years, we have seen a paradigm shift toward the use of *in vitro* models that reduce, replace, and refine the use of animals in toxicity testing (the three R's) from both the standpoint of economic imperative and animal welfare.[1,2] Despite these economic advantages over *in vivo* studies, *in vitro* studies are currently limited by: 1) the use of immortalized or transformed cell lines that may not recapitulate primary cell phenotypes, 2) the use of cells from a single genetic background or phenotype, which may not capture the impact of underlying genetics or diseases on toxicant response, and 3) the limited efforts to relate *in vitro* exposures to occupational exposures in order to provide a mechanistic basis for sensitivity to occupational exposures and inform regulatory policy aimed at protecting all populations, including individuals with pre-existing chronic respiratory diseases.[3,4] Therefore, it is crucial we continue to develop more robust *in vitro* models suitable for high-throughput screening in order to support global gene and protein expression analyses and the development of predictive, mechanistic-based biomarkers.[5-10]

Organotypic cultures attempt to recapitulate *in vivo* physiology by using multiple cell populations, addition of extracellular matrix, and/or microfluidic systems; therefore, they are well-suited to improve the predictive power of high-throughput screening programs, such as ToxCast, which serve to identify and prioritize chemicals of regulatory interest. In the present study, we used organotypic cultures derived from murine tracheal epithelial cells (MTEC) as a high-content *in vitro* model of the conducting airway. These organotypic cultures contain the cell populations in the proximal region of the conducting airway, including basal, ciliated, club, and mucin cells, and will be used to produce more biologically relevant results in the context of high-throughput screening for potential

respiratory toxicants. Using organotypic cultures as a tool for medium to high-throughput screening will allow us to capture determinants of sensitivity in order to screen and prioritize potential respiratory toxicants while providing relevant data on risk assessment for occupational exposures.

Interactions between host genetic and acquired factors, or gene × environment interactions (G×E), may play a defining role in identifying sensitive populations to AgNP exposures in occupational settings.[11-14] Host genetic factors, such as sex, genotype, or polymorphism, contribute to variation in certain genes that may increase an individual's sensitivity to occupational exposures. Host acquired factors, such as pre-existing chronic respiratory diseases, including asthma, acute bronchitis, and chronic obstructive pulmonary disease (COPD), collectively affect 16% of the total United States population; these contribute to impairing host defense mechanisms, such as barrier function and immune regulation,[15] mucocilliary clearance and permeability,[16-22] as well as enzymatic and non-enzymatic oxidative stress regulation,[23,24] and may also increase an individual's sensitivity to occupational exposures.[25-27]

Few studies have characterized G×E effects on AgNP toxicity.[28,29] Understanding G×E effects is important for identifying sensitive populations, whose underlying genetics or diseases could directly modify their response to AgNP exposures. Typically, these studies have used young, healthy animals or cell lines cultured toward a "Normal" phenotype and thus did not address the possibility of increased AgNP toxicity in asthmatics. In the present studies, we will use this high-content *in vitro* model of the conducting airway to characterize G×E effects, or in this case—the effects of genotype × phenotype interaction (G×P), in order to identify determinants of sensitivity and help define both regulatory and mechanistic bases for these effects on AgNP toxicity.

These studies will also allow us to support several important ongoing initiatives, including: 1) the development of methods to reduce animal usage and support ongoing three R's initiatives which advocate for sustainable research priorities, 2) the development of methods for nanotoxicity testing to capture determinants of sensitivity, and 3) the generation of new information to make better informed, and more timely decisions about

high-throughput screening.

The Effects of Gene × Environment Interactions on Silver Nanoparticle Toxicity in the Respiratory System

- **Research need:** There is presently a need to understand the effects of interactions between host genetic and acquired factors, or G×E, on AgNP toxicity in the respiratory system to assist in defining exposure limits to protect all populations in occupational settings.

- **Research aim:** Review host genetic and acquired factors identified across *in vitro* and *in vivo* studies and prioritize those necessary for defining exposure limits to protect all populations in occupational settings.

The Effects of Genotype × Phenotype Interactions on Silver Nanoparticle Toxicity in Organotypic Cultures of Murine Tracheal Epithelial Cells

- **Research need:** There is presently a need for *in vitro* models to provide a regulatory basis for sensitivity to occupational exposures.

- **Research aim:** Use organotypic cultures to characterize nominal and dosimetric dose-response relationships across genotypes, phenotypes, and exposures to understand G×P effects on AgNP toxicity.

- **Research hypothesis:** Genotype and phenotype (physiological environment) will define G×E, or genotype × phenotype interaction (G×P), effects on AgNP toxicity.

The Effects of Genotype × Phenotype Interactions on Transcriptional Response to Silver Nanoparticle Toxicity in Organotypic Cultures of Murine Tracheal Epithelial Cells

- **Research need:** There is presently a need for *in vitro* models to provide a mechanistic basis for sensitivity to occupational exposures.

- **Research aim:** Use organotypic cultures to characterize global and differential gene expression, canonical pathway enrichment, and upstream transcriptional

regulators to understand G×P effects on transcriptional response to AgNP toxicity.

- **Research hypothesis:** Genotype and phenotype will define G×P effects on transcriptional response to AgNP toxicity.

The Effects of Gene × Environment Interactions on Silver Nanoparticle Toxicity in The Respiratory System: Toward an Adverse Outcome Pathway

- **Research need:** There is presently a need to support regulatory decision-making for engineered nanomaterials (ENM) through highlighting knowledge gaps where they exist in order to more directly prioritize future research needs.

- **Research aim:** Use the Adverse Outcome Pathway (AOP) framework to organize and integrate data from *in vitro* and *in vivo* models to evaluate G×E effects on AgNP toxicity in the respiratory system.

- **Research hypothesis:** Molecular initiating events (MIE) and key events (KE) for AgNP toxicity can be modified by different host genetic and host acquired factors at acute, subacute, and subchronic exposures.

Chapter 2. The Effects of Gene × Environment Interactions on Silver Nanoparticle Toxicity in the Respiratory System

This chapter was submitted for publication in Chemical Research in Toxicology. The authors of the manuscript are:

Tyler P. Nicholas[1,2], Terrance J. Kavanagh[1,2], Elaine M. Faustman[1], and William A. Altemeier[2]

[1]Department of Environmental and Occupational Health Sciences, University of Washington, Seattle, Washington
[2]Department of Medicine—Division of Pulmonary, Critical Care, and Sleep Medicine, University of Washington, Seattle, Washington

Corresponding Author:
William A. Altemeier
UW Medicine Research / South Lake Union
850 Republican Street, S324
Box 358052
Seattle, Washington 98109
Phone: (206) 616-6140
Fax: (206) 221-0739
Email: billa@uw.edu

List of Abbreviations

Ag: silver mass
Ag^+: silver ions
AgNP: silver nanoparticles
$AgNP_{110CIT}$: 110 nm, citrate-coated silver nanoparticles
$AgNP_{110PVP}$: 110 nm, polyvinylpyrrolidone-coated silver nanoparticles
$AgNP_{20CIT}$: 20 nm, citrate-coated silver nanoparticles
$AgNP_{20PVP}$: 20 nm, polyvinylpyrrolidone-coated silver nanoparticles
AHR: airway hyperresponsiveness
Ano6: anoctamin 6
ApoE: Apolipoprotein E
BALF: bronchoalveolar lavage fluid
BAX: Bcl-2-associated X protein
BCL2: B-cell lymphoma 2 protein
BMD: benchmark dose
CAT: catalase
Cd: cadmium mass
CF-HBE: cystic fibrosis human bronchial epithelial cells
COPD: chronic obstructive pulmonary disease
ENaC: amiloride-sensitive epithelial Na^+ channel
ENM: engineered nanomaterials
G×E: gene × environment interactions
Gclm: glutamate-cysteine ligase modifier subunit
GPX: glutathione peroxidase
GSH: glutathione
HEC: human equivalent concentration
HIF1A: hypoxia-inducible factor 1 alpha
HMOX1: heme oxygenase 1
hnRNPA2B1: heterogeneous nuclear ribonucleoproteins A2/B1
IG ACC: Ig alpha chain C region
IG HCV 441: Ig heavy chain V region 441
IG HCV MOPC 47A: Ig heavy chain V region MOPC 47 A
IgE: immunoglobulin E
KEAP1: kelch ECH associating protein 1
LC3: microtubule-associated protein 1 light chain 3 alpha
LDH: lactate dehydrogenase
LDLR: low-density lipoprotein receptors
LTE_4: leukotriene E4
MAPK: mitogen-activated protein kinase
Marco: macrophage receptor with collagenous structure
MLKL: mixed lineage kinase domain like pseudokinase
MMD: mitochondrial membrane depolarization
MMP: mitochondrial membrane potential
MoA: mode of action
MOE: margin of exposure

MUC5AC: mucin 5AC
MYL6: myosin light polypeptide 6
N-HBE: normal human bronchial epithelial cells
Nedd4l: E3 ubiquitin-protein ligase NEDD4-like
NF-κB: nuclear factor kappa-light-chain-enhancer of activated B cells
NK: Natural Killer cells
NLRP3: NLR Family Pyrin Domain Containing 3
NRF2: nuclear factor erythroid 2-related factor 2
OEL: occupational exposure limit
OVA: ovalbumin
p53: tumor protein p53
PEL: permissible exposure limit
PI3K: phosphatidylinositide 3-kinase
PRDX: peroxiredoxin
Ptger4: prostaglandin E receptor 4
REL: recommended exposure limit
RIPK1/3: Receptor-interacting serine/threonine-protein kinase 1/3
RNA-seq: RNA sequencing
Rnf220: E3 ubiquitin-protein ligase RNF220
ROS: reactive oxygen species
SOD: superoxide dismutase
T1/T2/T17: type 1/type 2/type 17
TRX: thioredoxin
TRXR: thioredoxin reductase
Txnip: thioredoxin interacting protein
VCP: valosin-containing protein
VEGF: vascular endothelial growth factor
WNT: wingless/integrated
WT: wildtype

Chapter 2. The Effects of Gene × Environment Interactions on Silver Nanoparticle Toxicity in the Respiratory System

2.1 ABSTRACT

Silver nanoparticles (AgNP) are used in multiple applications but primarily in the manufacturing of many antimicrobial products. AgNP toxicity in the respiratory system is well characterized, but few *in vitro* or *in vivo* studies have evaluated the effects of interactions between host genetic and acquired factors, or gene × environment interactions (G×E), on AgNP toxicity in the respiratory system. The primary goal of this article is to review host genetic and acquired factors identified across *in vitro* and *in vivo* studies and prioritize those necessary for defining exposure limits to protect all populations in occupational settings. The impact of these exposures, and the work being done to address the current limited protections are also discussed. Future research on G×E effects on AgNP toxicity is warranted and will assist in defining exposure limits to protect all populations in occupational settings.

2.2 INTRODUCTION

Nanotechnology is the use of matter with at least one dimension sized 1 to 100 nanometers. These nanoscale dimensions give rise to engineered nanomaterials (ENM) with unique physicochemical properties compared to their counterparts on a macroscale. Silver nanoparticles (AgNP) are ENM whose antimicrobial, conductive, plasmonic, and photovoltaic properties are of great interest to the nanotechnology industry.[30-32] AgNP are used as antimicrobial agents in air filters, humidifiers, and purifiers as well as antimicrobial sprays.[32] AgNP are also used as conductive agents in plastics, composites, and adhesives to enhance their electrical conductivity; AgNP-enabled inks, pastes, and epoxies also have broad utilization in the electronics industry due to their excellent conductivity.[33,34] AgNP are also used as plasmonic agents in biomedical labels, sensors, and detectors as well as photovoltaic agents in solar panels; AgNP also support surface plasmons, which absorb and scatter specific wavelengths of light, and allow them to function as efficient optical antennas.[35]

In 2016, an estimated 32,000 tons of AgNP were produced worldwide for use in these applications; China being the largest consumer, followed by Japan, and the United States.[36] In the United States, AgNP have been used in 685 antimicrobial products, accounting for over one-third of those cataloged in the inventory of the Project on Emerging Nanotechnologies managed by the Woodrow Wilson International Center for Scholars.[37] Aerosols are produced during product manufacturing and thus pose a high risk for AgNP exposures in occupational settings. Exposure assessment studies in occupational settings observed AgNP exposures occur during gas- and liquid-phase synthesis.[32,38-42] There is currently a paucity of data that links these occupational exposures to adverse health responses; therefore, the use of AgNP in product manufacturing has continued to increase at a rate that presently exceeds the scientific community's capacity to evaluate AgNP toxicity, and thus inform exposure limits that enforce protections for all populations.[43]

A new draft recommended exposure limit (REL) for AgNP exposures has only recently been established for occupational settings, partially due to the complexity of evaluating the physicochemical properties attributed to their nanoscale dimensions.[44,45] AgNP release silver ions (Ag^+) upon dissolution, which have antimicrobial properties and play a defining role in AgNP toxicity.[46] AgNP are manufactured at different sizes, including 20 nm and 110 nm, and coated with different compounds, including citrate and polyvinylpyrrolidone, (20 and 110 nm, citrate-coated AgNP, or $AgNP_{20CIT}$ and $AgNP_{110CIT}$ respectively; 20 and 110 nm, PVP-coated AgNP, or $AgNP_{20PVP,}$ and $AgNP_{110PVP}$ respectively) to optimize their attributes for use in multiple applications.[47] By controlling size and coating, their dissolution profiles—and thus antimicrobial properties—can be tailored for specific applications. The effects of their physicochemical properties as well as interactions between host genetic and acquired factors, or gene × environment interactions (G×E), may also play a defining role in identifying sensitive populations to AgNP exposures in occupational settings.[11-14] Host genetic factors, such as sex, genotype, or polymorphism, contribute to variation in certain genes that may increase an individual's sensitivity to occupational exposures. Host acquired factors, such as pre-existing chronic respiratory diseases, including asthma, acute bronchitis, and chronic obstructive pulmonary disease (COPD), collectively affect 16% of the total United States

population; these contribute to impairing host defense mechanisms, such as barrier function and immune regulation,[15] mucocilliary clearance and permeability,[16-22] as well as enzymatic and non-enzymatic oxidative stress regulation,[23,24] and may also increase an individual's sensitivity to occupational exposures.[25-27] The effects of physicochemical properties on AgNP toxicity has been reviewed extensively, and this article will focus on reviewing current evidence supporting G×E effects on AgNP toxicity, which reflects a knowledge gap in the literature.

In vitro studies observed AgNP-induced oxidative stress, altered cell physiology, cytotoxicity, inflammation, mitochondrial dysfunction, and cell death in airway epithelial cells (bronchial and alveolar epithelial cells), specialized innate immune cells (e.g., neutrophils, eosinophils, mast cells, basophils, dendritic cells, alveolar macrophages, and Natural Killer [NK] cells), and specialized adaptive immune cells (e.g., B/T cells) **(Table 1)**. *In vivo* studies observed AgNP-induced altered organ physiology (marked by increased lung dysfunction, microbiome dysbiosis, and type 2 [T2] lung inflammation) in the lungs **(Table 2).** However, many of these *in vitro* and *in vivo* studies have not accounted for G×E effects on AgNP toxicity. One strategy for identifying these effects is to study host genetic and acquired factors that alter putative pathways shown to be relevant in AgNP toxicity using *in vitro* or *in vivo* models, which may help to better reflect adverse cellular and organ responses in sensitive populations.

These adverse cellular and organ responses compromise the airway epithelium's role in host defense as a physical barrier and an immune regulator through secreting cytokines, chemokines, growth factors, antimicrobial peptides, and recruiting leukocytes to sites of inflammation. Its role as an immune regulator is referred to as the epithelial-immune interface, where airway epithelial cells regulate innate and adaptive immunity by secreting upstream epithelial-derived cytokines, including IL-25, IL-33, TSLP, and CC-family chemokines to initiate and exacerbate T2 lung inflammation.[15] It is important to understand the mechanistic role of host genetic and acquired factors in modulating AgNP-induced T2 lung inflammation, which may exacerbate these pro-inflammatory effects to further increase an individual's sensitivity to occupational exposures.

Exposure limits should protect all populations, and especially sensitive populations, whose underlying genetics or diseases could directly modify their response to AgNP exposures. For example, individuals with pre-existing chronic respiratory diseases may be more sensitive to AgNP-induced T2 lung inflammation, which in turn, may further exacerbate their disease.[48] AgNP toxicity within the respiratory system is well characterized, but no study has evaluated G×E effects on AgNP toxicity. The primary goal of this article is to review host genetic and acquired factors identified across *in vitro* and *in vivo* studies and prioritize those necessary for defining exposure limits to protect all populations in occupational settings. Future research on G×E effects on AgNP toxicity is warranted and will assist in defining exposure limits to protect all populations in occupational settings

2.3 HOST GENETIC FACTORS

Here, we review the effects of host genetic factors on adverse cellular and organ responses identified in studies using *in vitro* and *in vivo* models of the respiratory system. Typically, these *in vitro* and *in vivo* studies have used different mice genotypes to model the broader effects of genetic background, or different polymorphic mice to model the specific effects of polymorphisms. Many *in vitro* studies have not accounted for the effects of host genetic factors on AgNP toxicity. Typically, these *in vitro* studies have used immortalized or transformed cell lines that may neither recapitulate primary cell phenotypes, nor capture the *in vitro* impact of underlying genetics on toxicant response. However, some *in vitro* studies have evaluated individual effects of host genetic factors, such as genotype or polymorphism, but have not accounted for the effects of interactions between host genetic factors on AgNP toxicity. For example: the use of a single mouse sex from multiple genotypes has ignored the potential interaction of sex with genotype effects on AgNP toxicity, and therefore does not fully capture the *in vitro* effects of underlying genetics on toxicant response. Similarly, some *in vivo* studies have evaluated individual effects of more host genetic factors, such as sex, genotype, and polymorphism, but have also not accounted for the effects of interactions between host genetic factors on AgNP toxicity. For example: the use of both rat sexes from a single genotype ignores the potential interaction of genotype with sex effects on AgNP toxicity. Therefore, these

in vivo studies also do not fully capture the *in vivo* effects of underlying genetics on toxicant response. The goal of this section is to review the effects of host genetic factors and prioritize those necessary for defining exposure limits to protect all populations in occupational settings.

In vitro models

One *in vitro* study has evaluated genotype effects on AgNP toxicity in specialized innate immune cells. Johnson et al. treated mast cells derived from 23 genotypes of male mice (20 nm, CIT-coated AgNP [primary particle size]; 0, 25, or 50 μg AgNP /mL medium; evaluated 1 h after treatment) and observed genotype effects on AgNP-induced altered cell physiology (marked by increased degranulation) compared to genetically-matched vehicle controls, with LP/J and C57BL/6J mice being the most differentially sensitive genotypes (C57BL/6J mice being the most sensitive). The authors used RNA sequencing (RNA-seq) on mast cells isolated from these differentially sensitive genotypes and observed that prostaglandin E receptor 4 (*Ptger4*) and thioredoxin interacting protein (*Txnip*) may function as candidate polymorphisms for AgNP-induced mast cell degranulation. *Ptger4* is a signal transduction gene involved in the mitogen-activated protein kinase (MAPK) signaling pathway, and *Txnip* is a stress response gene involved in kinase inhibitor activity and ubiquitin protein ligase activity.[49] One limitation of this *in vitro* study was its exclusive use of male mice, which precluded the authors from addressing sex effects on AgNP-induced mast cell degranulation. However, their study highlights the importance of using multiple mice genotypes to identify candidate polymorphisms for AgNP-induced mast cell degranulation. Their relevance as therapeutic targets should be evaluated in future studies that account for the effects of interactions between host genetic factors, such as sex and *Ptger4*/*Txnip* deficiency, on AgNP toxicity.

One *in vitro* study has evaluated polymorphism effects on AgNP toxicity in airway epithelial cells. Cystic fibrosis (CF) is a chronic lung disease caused by mutations in both copies of the gene encoding for the cystic fibrosis transmembrane conductance regulator (CFTR) protein. Jeannet et al. treated normal (N-HBE) and cystic fibrosis (CF-HBE) human bronchial epithelial cells (10-100 nm, uncoated AgNP [primary particle size]; 4×10^{7}-10^{9} ng AgNP/cm^2; evaluated 12 and 24 h after treatment) and observed CFTR

effects on AgNP-induced cytotoxicity (marked by increased LDH secretion), inflammation (marked by increased type 1/type 2 [T1/T2] cytokine secretion) and mitochondrial dysfunction (marked by caspase-3 activation) compared to N-HBE cells. The authors' characterization of CF-HBE cells showed higher levels of caspase-3 activation and T1/T2 cytokine secretion, indicating that the CFTR polymorphism was responsible for baseline differences in its resulting phenotype when compared to N-HBE cells, and that these differences were exacerbated by AgNP toxicity.[50] One limitation of this *in vitro* study was its limited dissociation of the CFTR polymorphism from its resulting phenotype, so therefore it was difficult to conclude as to whether AgNP toxicity was attributed either directly to the CFTR polymorphism, or indirectly to its resulting phenotype. However, one strength of this *in vitro* study was its use of primary cells, which allowed the authors to show how this polymorphism and its resulting phenotype captured the *in vitro* effects of underlying genetics and diseases on toxicant response. This *in vitro* study supports epidemiology studies suggesting that individuals with pre-existing chronic respiratory diseases may be more sensitive to particulate matter-induced toxicity and highlights the importance of evaluating polymorphism and phenotype effects on AgNP toxicity in future studies that account for interactions between these host genetic and acquired factors.

Similarly, one *in vitro* study has evaluated polymorphism effects on AgNP toxicity in specialized innate immune cells. Hamilton et al. treated alveolar macrophages isolated from wildtype (WT) and macrophage receptor with collagenous structure (*Marco*)-knockout, male C57BL/6J mice (20 and 110 nm, CIT- and PVP-coated AgNP [primary particle size]; 0, 6.25, 12.5, 25, or 50 μg AgNP /mL medium; evaluated 24 h after treatment) and observed *Marco* effects on AgNP-induced NLR family pyrin domain containing 3 (NLRP3) apoptosis (marked by increased IL-1β secretion) and cytotoxicity (marked by increased lactate dehydrogenase [LDH] secretion). The authors observed that $AgNP_{20CIT}$ induced NLRP3 apoptosis and cytotoxicity in alveolar macrophages isolated from WT mice, which was attributed to an interaction of host genetic factors (e.g., increased *MARCO*-mediated uptake of WT mice) and physicochemical properties (e.g., decreased coating stability), which facilitated their dissolution within acidic phagolysosomes.[51] One limitation of this *in vitro* study was its exclusive use of male mice, which precluded the authors from addressing sex effects on AgNP-induced NLRP3

apoptosis and cytotoxicity. Additionally, their comparison of primary cells to innate immune cell lines, (which have shown cell effects on AgNP-induced modes of programmed cell death) may not be physiologically relevant. However, this *in vitro* study highlights the importance of using polymorphic mice to identify *Marco's* relevance as a therapeutic target. This should be evaluated in future studies that account for the effects of interactions between host genetic factors, such as sex and *Marco* deficiency, on AgNP toxicity.

Innate immune cell lines have shown cell effects on AgNP-induced modes of programmed cell death, including: NLRP3 apoptosis; receptor-interacting serine/threonine-protein kinase 1/3 (RIPK1/3)/mixed lineage kinase domain like pseudokinase (MLKL) necroptosis; and pyroptosis. These mechanisms are also relevant to AgNP-induced modes of programmed cell death in airway epithelial cells, as *in vitro* studies observed particulate matter-, multi-wall carbon nanotube-, and zinc oxide nanoparticle-induced NLRP3 apoptosis (marked by caspase-4, NLRP3, and NF-κB activation, and subsequent inflammasome cytokine IL-1β secretion) in HBE and A549 cells.[52-55] Zielinska et al. observed AgNP-induced RIPK1/RIPK3/MLKL necroptosis (marked by caspase-3 activation and subsequent Bcl-2-associated X protein [BAX], B-cell lymphoma 2 protein [BCL2], tumor protein p53 [p53], RIPK1, RIPK3, MLKL, and the microtubule-associated protein 1 light chain 3 alpha [LC3] signaling pathway) in normal (hTERT-HPNE) and transformed (PANC-1) human pancreatic cells.[56] Simard et al. observed AgNP-induced pyroptosis (marked by caspase-1 and NLRP3 activation, NF-κB inhibition, as well as IL-1β secretion) in THP-1 cells.[57] The authors suggested that activation of caspase-4 is required for priming of the NLRP3 inflammasome, whose absence served to increase caspase-1 activation and decrease IL-1β secretion as well as pyroptosome positive THP-1 cells. Priming the NLRP3 inflammasome depends upon NF-κB activation, and since caspase-4-deficient THP-1 cells have lower baseline NF-κB activation, this suggests that differences in baseline NF-κB activation may also direct AgNP-induced activation of different caspases and lead to different modes of programmed cell death in addition to oxidative stress and mitochondrial dysfunction. These *in vitro* studies suggest that AgNP-induced caspase-1 and -4 activation is required for priming the NLRP3 inflammasome during apoptosis and pyroptosis; and that AgNP-induced caspase-3 activation mediates

inflammasome-independent RIPK1/RIPK3/MLKL necroptosis. While other *in vitro* studies observed AgNP-induced cytotoxicity (marked by increased LDH secretion) in BEAS-2B and A549 cells,[34,50,58-70] none have evaluated AgNP-induced NLRP3 apoptosis, RIPK1/RIPK3/MLKL necroptosis, or pyroptosis in airway epithelial cells. This should be evaluated in future studies that account for the effects of interactions between host genetic factors, such as cell population and baseline NF-κB activation, on AgNP toxicity.

In vivo models

Several *in vivo* studies have evaluated sex effects on AgNP toxicity in the lungs. One *in vivo* study observed that acute exposures do not produce AgNP-induced lung dysfunction. Sung et al. treated male and female Sprague-Dawley rats (18-20 nm, uncoated AgNP [primary particle size]; 75-750 mg/m^3; treated 4 h; evaluated 1, 3, 7, and 14 d after treatment) and did not find sex effects on AgNP-induced lung dysfunction (marked by decreased minute and tidal volume) compared to filtered air controls.[71] Interestingly, other *in vivo* studies observed that subchronic exposures do produce AgNP-induced T2 lung inflammation and lung dysfunction, which persist after a recovery period. In a follow up study, Sung et al. treated male and female Sprague-Dawley rats (18-20 nm, uncoated AgNP [primary particle size]; 50-515 mg/m^3; treated 6 h/d, 5 d/w, over 12 w; evaluated immediately after treatment) and observed sex effects on AgNP-induced T2 lung inflammation (marked by increased pro-inflammatory cell infiltrate, alveolar inflammation, and changes in histopathology) and lung dysfunction (marked by decreased minute and tidal volume) and in males after treatment with the high dose compared to filtered air controls, and suggested a NOAEL of 100 mg/m^3.[72,73] In a second follow-up study, Sung et al. treated male and female Sprague-Dawley rats (14-15 nm, uncoated AgNP [primary particle size]; 50-380 mg/m^3; treated for 6 h/d, 5 d/w, over 12 w; evaluated 0, 4, and 12 w after treatment) and observed sex effects on AgNP-induced T2 lung inflammation (marked by increased pro-inflammatory cell infiltrate, alveolar inflammation, perivascular inflammation, and changes in histopathology) and lung dysfunction (marked by decreased minute and tidal volume) and in males after treatment with the high dose compared to filtered air controls, at 0 and 12 w after the recovery period.[74] One possible explanation for these exposure effects on AgNP toxicity was the use of a single rat genotype across these *in vivo* studies, which may be resistant to AgNP

toxicity at acute exposures and sensitive at subchronic exposures. This precluded the authors from addressing genotype effects on AgNP-induced T2 lung inflammation and lung dysfunction, which should be evaluated in future studies that account for the effects of interactions between host genetic factors, such as sex and genotype, on AgNP toxicity.

Several *in vivo* studies have evaluated genotype effects on AgNP toxicity in the lungs. Scoville et al. treated 25 genotypes of male mice (20 nm, CIT-coated AgNP [primary particle size]; 0.25 mg/kg$_{BW}$; evaluated 24 h after treatment) and observed genotype effects on AgNP-induced T2 lung inflammation (marked by increased pro-inflammatory cell infiltrate) compared to genetically-matched vehicle controls, with BALB/cJ and SWR/J mice being the most differentially sensitive genotypes. In a separate study of genotype effects on quantum dot (QD) toxicity in the lungs, the authors quantified dosimetric doses of cadmium (Cd) mass in the lungs of these differentially sensitive genotypes and detected higher burdens in A/J mice compared to C57BL/6J mice. This suggested that airway physiology (marked by alveolar size and airway branching) may be a contributing factor in genotype effects on QD toxicity—which may be broadly applicable to other types of ENM, such as AgNP.[75-77] In the previous study, the authors used RNA-seq on lungs isolated from these differentially sensitive genotypes and observed that E3 ubiquitin-protein ligase NEDD4-like (*Nedd4l*), anoctamin 6 (*Ano6*), and E3 ubiquitin-protein ligase RNF220 (*Rnf220*) may function as candidate polymorphisms for AgNP-induced T2 lung inflammation. *Nedd4l* is a E3 ubiquitin ligase gene involved in ubiquitin protein ligase activity; AgNP-induced *Nedd4l* downregulation may increase amiloride-sensitive epithelial Na^+ channel (ENaC) activity and T2 lung inflammation. *Ano6* is small-conductance calcium-activated non-selective cation channel gene involved in calcium-dependent exposure of phosphatidylserine on the cell surface; AgNP-induced *Ano6* downregulation may impair ion transport, increase airway surface fluid volume and viscosity, as well as apoptosis, phagocytosis, and T2 lung inflammation and/or mast cell degranulation via the phosphatidylserine signaling pathway. *Rnf220* is another E3 ubiquitin ligase gene involved in ubiquitin protein ligase activity; AgNP-induced *Rnf220* downregulation may inhibit β-catenin stabilization and activate the wingless/integrated (WNT) signaling pathway to exacerbate T2 lung inflammation.[78] One limitation of this *in vivo* study was its exclusive use of male mice, which precluded the authors from

addressing sex effects on AgNP-induced T2 lung inflammation. However, this *in vivo* study highlights the importance of using multiple mice genotypes to identify candidate polymorphisms for AgNP-induced T2 lung inflammation. Their relevance as therapeutic targets should be evaluated in future studies that account for the effects of interactions between host genetic factors, such as sex and *Nedd4l/Ano6/Rnf220* deficiency, on AgNP toxicity.

Seiffert et al. treated male Brown-Norway and Sprague-Dawley rats (20 and 110 nm, CIT- and PVP-coated AgNP [primary particle size]; 0.10 mg/kg_{BW}; evaluated 1, 7, and 21 d after treatment) and observed size, coating, and genotype effects on AgNP-induced T2 lung inflammation (marked by increased T1/T2 cytokine secretion, pro-inflammatory cell infiltrate, immunoglobulin E [IgE], airway hyperresponsiveness [AHR], and changes in histopathology) compared to genetically-matched vehicle controls, with Brown-Norway rats being the more sensitive genotype.[79] In a separate study of genotype effects on AgNP toxicity in the lungs, the authors treated male Brown-Norway and Sprague-Dawley rats (13-16 nm, uncoated AgNP [primary particle size]; 600–800 μg/mm^3; evaluated 1 and 7 d after treatment) and observed genotype effects on AgNP-induced T2/T17 lung inflammation (marked by increased T2/T17 cytokine secretion, pro-inflammatory cell infiltrate, and changes in histopathology) and lung dysfunction (marked by decreased airway resistance and tissue elastance) compared to genetically-matched vehicle controls, with Brown-Norway rats being the more sensitive genotype. The authors also quantified dosimetric doses of silver (Ag) mass in the lungs of these differentially sensitive genotypes and detected higher burdens in Brown-Norway rats compared to Sprague-Dawley rats,[80] suggesting that airway physiology (marked by alveolar size and airway branching) may be a contributing factor in genotype effects on AgNP toxicity. One limitation of this *in vivo* study was its exclusive use of male rats, which precluded the authors from addressing sex effects on AgNP-induced T2/T17 lung inflammation and lung dysfunction. This precluded the authors from addressing sex effects on AgNP-induced T2/T17 lung inflammation and lung dysfunction, which should be evaluated in future studies that account for the effects of interactions between host genetic factors, such as sex and genotype, on AgNP toxicity.

Few *in vivo* studies have evaluated polymorphism effects on ENM toxicity in the lungs. McConnachie et al. treated WT, glutamate-cysteine ligase modifier subunit (*Gclm*)-knockdown, and *Gclm*-knockout male C57BL/6J mice (12-13 nm, TOPO-PMAT-coated, CdSe/ZnS core QD [primary particle size]; 1.53 μL/g_{BW}; evaluated 0.5, 1, 3, 8 or 24 h after treatment) and observed *Glcm* effects on QD-induced T2 lung inflammation (marked by increased pro-inflammatory cell infiltrate) compared to genetically-matched vehicle controls, with WT and *Gclm*-knockout mice being the most differentially sensitive genotypes (WT mice being the most sensitive). *Gclm*-knockout mice were hypothesized to the most sensitive genotype, and the authors suggested these findings may be attributed to their increased compensatory activation of alternative antioxidant and anti-inflammatory putative pathways, such as the nuclear factor erythroid 2-related factor 2/Kelch ECH associating protein 1 (NRF2/KEAP1) signaling pathway, and concluded that differences in GSH regulation may serve to exacerbate QD-induced T2 lung inflammation.[81] One limitation of this *in vivo* study was its exclusive use of male mice, which precluded the authors from addressing sex effects on QD-induced T2 lung inflammation. However, this *in vivo* study highlights the importance of using polymorphic mice to identify *Gclm's* relevance as a therapeutic target, which may be broadly applicable to other ENM, such as AgNP. Its relevance as a therapeutic target should be evaluated in future studies that account for the effects of interactions between host genetic factors, such as sex and *Gclm* deficiency, on AgNP toxicity.

2.4 HOST ACQUIRED FACTORS

Here, we review the effects of host acquired factors on adverse organ responses identified in studies using *in vivo* models of the respiratory system. No *in vitro* study has accounted for the effects of host acquired factors on AgNP toxicity in airway epithelial cells, which reflects a knowledge gap in the literature. However, some *in vivo* studies have accounted for the effects of host acquired factors on AgNP toxicity in the lungs. Typically, these *in vivo* studies have focused on a single mouse sex and genotype, and thus have not accounted for the effects of interactions between host genetic and acquired factors. For example, the use of a single mouse sex and genotype has ignored the potential interactions between sex and genotype with antigen effects on AgNP toxicity in the lungs.

Therefore, these *in vivo* studies also do not fully capture the *in vivo* effects of underlying genetics or diseases which may directly modify their response to AgNP exposures. The goal of this section is to review the effects of host acquired factors and prioritize those necessary for defining exposure limits to protect all populations in occupational settings.

In vivo models

Several *in vivo* studies have evaluated antigen effects on AgNP toxicity in the lungs. Typically, these *in vivo* studies have used ovalbumin (OVA)-sensitized female BALB/cJ mice, which develop increased AHR and T2 lung inflammation than male mice or other mice genotypes. These *in vivo* studies treated OVA-sensitized, female BALB/cJ or C57BL6/J mice with AgNP of various sizes and coatings **(Table 2)** and observed exacerbation of the allergic airway phenotype through increased AgNP-induced mucus production (marked by activation of the phosphatidylinositide 3-kinase [PI3K]/hypoxia-inducible factor 1 alpha [HIF1A]/vascular endothelial growth factor [VEGF] signaling pathway, and inhibition of the mucin 5AC [MUC5AC] signaling pathway), oxidative stress (marked by increased ROS production, NF-κB activation, leukotriene E4 [LTE_4] and 8-hydroxy-2'-deoxyguanosine [8-OHdG] production), and T2 lung inflammation (marked by increased T1/T2 cytokine secretion, pro-inflammatory cell infiltrate, IgE, and AHR) in allergic mice compared to healthy mice and filtered air controls.[82-85] In a unique study of antigen effects on AgNP toxicity in the lungs, Alessandrini et al. treated OVA-sensitized, female BALB/cJ mice (50, 200 nm; CIT and PVP coated AgNP [primary particle size]; 1-50 µg/mouse; evaluated 1 and 5 d after treatment) and observed antigen effects on AgNP-induced lung microbiome dysbiosis (marked by increased relative abundance of *Actinobacteria, Bacteroidetes, Firmicutes,* and *Proteobacteria)* and T2 lung inflammation (marked by increased T1/T2 cytokine secretion and changes in histopathology) in allergic mice compared to healthy mice and vehicle controls.[86] This suggests that a novel mechanism of lung microbiome dysbiosis may contribute toward AgNP-induced exacerbation of the allergic airway phenotype.

These *in vivo* studies suggest that an individual's chronic respiratory disease is a relevant host acquired factor in determining their response to occupational exposures. While AgNP-induced exacerbation of the allergic airway phenotype may occur indirectly through

a novel mechanism of lung microbiome dysbiosis, the immunological basis for these effects is not well understood. Su et al. treated OVA-sensitized, female BALB/cJ mice (33 nm, uncoated AgNP [primary particle size]; 3.3 mg/m^3; treated for 6 h/d, over 7 d; evaluated 5 d after treatment) and observed antigen effects on AgNP-induced T2 lung inflammation (marked by increased pro-inflammatory cell infiltrate) in allergic mice compared to healthy mice and filtered air controls. Additionally, the adjuvant effects of AgNP were exacerbated in allergic mice, marked by OVA-specific IgE. The authors also used mass spectrometry on bronchoalveolar lavage fluid (BALF) from these allergic and healthy mice to evaluate differences in their protein profiles and observed 79 and 106 commonly expressed proteins in allergic and healthy mice after AgNP treatment, respectively, which was suggestive of AgNP-induced perturbations in cellular, immune, and metabolic function. Specifically, these perturbations were associated with activation of: blood coagulation, the integrin signaling pathway, the ubiquitin proteasome signaling pathway, the cytokine/chemokine signaling pathway, the dopamine receptor signaling pathway, the Fas signaling pathway, T cell activation, tricarboxylic acid cycle activation, plasminogen activating cascade, and Rho GTPase cytoskeletal regulation.[83]

One limitation of these *in vivo* studies was their exclusive use of female BALB/cJ mice (except for one study [Park et al.], which used female C57BL6/J mice), as their use of a single mouse sex and genotype has ignored the potential interactions between sex and genotype with antigen effects on AgNP toxicity in the lungs. Chuang et al. compared their findings to those of Park et al. and attributed them, in part, to genotype effects on OVA-sensitization, or alternatively, to differences in study design with respect to particle, dose, or exposure. Though not OVA-sensitized, Scoville et al. observed BALB/cJ and C57BL/6J mice to be differentially sensitive genotypes to AgNP-induced T2 lung inflammation (marked by increased pro-inflammatory cell infiltrate, and specifically neutrophil influx; roughly 60% for BALB/cJ mice and 20% for C57BL/6J mice).[82] Together, this highlights the importance of evaluating sex, genotype, and antigen effects on AgNP toxicity in future studies that account for interactions between these host genetic and acquired factors.

2.5 HOST GENETIC AND ACQUIRED TARGETS

While multiple putative pathways are known to be implicated in AgNP toxicity, oxidative stress is perhaps the most critical putative pathway, and can be mediated by host genetic and acquired factors within sensitive populations. This putative pathway is activated upon the production of reactive oxygen species (ROS), depletion of antioxidant defense systems, and attenuation of mitochondrial membrane potential (MMP). ROS production both depletes antioxidant defense systems (e.g., heme oxygenase 1 [HMOX1],[87] catalase [CAT],[58] peroxiredoxin [PRDX],[88] glutathione peroxidase [GPX],[89] thioredoxin [TRX], thioredoxin reductase [TRXR],[90,91] and superoxide dismutase [SOD][58]) and attenuates MMP to induce cytotoxicity through either apoptosis, autophagy, or a combination thereof.[66,92-94] *In vitro* studies observed AgNP-induced ROS production was associated with mitochondrial-mediated cell death putative pathways through the formation of mitochondrial permeability transition pores,[94,95] known as mitochondrial membrane depolarization (MMD).[93,96] Therefore, attenuation of MMP, and putative pathways with crosstalk between the mitochondria and other cellular components, supports MMD-induced apoptosis as the mode of action (MoA) for AgNP toxicity.[94,97,98]

Host genetic targets

One way to potentially identify sensitive individuals with polymorphisms is to evaluate genes that are in putative pathways of AgNP toxicity and then determine which of those genes have known functional polymorphisms in human populations. *Ptger4, Txnip, Ano6, Nedd4l,* and *Rnf220* were candidate polymorphisms identified across *in vitro* and *in vivo* studies of genotype effects on AgNP toxicity, and *Marco* and *Gclm* were candidate polymorphisms evaluated across *in vitro* and *in vivo* studies of polymorphism effects on AgNP toxicity **(Table 3).** These genes have known functional polymorphisms in human populations and are involved in putative pathways of AgNP toxicity, such as oxidative stress. *Ptger4* is a signal transduction gene involved in the MAPK signaling pathway; this putative pathway can be activated by oxidative stress, and can lead to sustained activation of uncontrolled downstream processes, such as cytotoxicity.[99] *Txnip* is a stress response gene involved in kinase inhibitor activity; it is a potent TRX inhibitor whose sustained activation can lead to increased depletion of antioxidant defense systems in

the presence of oxidative stress.[100] *Ano6* is small-conductance calcium-activated non-selective cation channel gene involved in the phosphatidylserine signaling pathway; this putative pathway can be activated by oxidative stress, and can lead to sustained activation of controlled downstream processes, such as apoptosis.[101] *Nedd4l* is a E3 ubiquitin ligase gene involved in the ubiquitin proteasome signaling pathway and the TGF-β signaling pathway. By targeting activated Smad2/3, *Nedd4l* has been shown to be a negative regulator of the TGF-β signaling pathway, whose sustained activation can lead to increased depletion of antioxidant defense systems in the presence of oxidative stress.[102] *Rnf220* is another E3 ubiquitin ligase gene involved in the ubiquitin proteasome signaling pathway. By complexing with USP7, *Rnf220* has been shown to be a positive regulator of the WNT signaling pathway,[103] whose sustained deactivation can lead to increased T2 lung inflammation in the presence of oxidative stress.[104] *Marco* is a cell surface receptor gene involved in the binding and uptake of ligands by scavenger receptors; a polymorphism resulting in its deficiency in both sensitive and non-sensitive populations may provide a protective effect against mitochondrial dysfunction in the presence of oxidative stress.[51] *Gclm* is a regulatory enzyme-encoding gene involved in the first rate limiting enzyme of GSH synthesis; a polymorphism resulting in its deficiency in sensitive populations may lead to increased depletion of this antioxidant and impaired defense against oxidative stress.[81] Ultimately, these candidate polymorphisms may modulate AgNP toxicity by exacerbating its pro-inflammatory effects to further increase an individual's sensitivity to occupational exposures. Their respective mechanistic roles should be evaluated in future studies that account for interactions that include these host genetic targets.

Host acquired targets

One way to potentially evaluate sensitivity in individuals with pre-existing chronic respiratory diseases is to evaluate gene products whose expression is altered by these diseases and then determine which of those gene products are in putative pathways of AgNP toxicity. Apolipoprotein E (ApoE), heterogeneous nuclear ribonucleoproteins A2/B1 (hnRNPA2B1), Ig alpha chain C region (IG ACC), Ig heavy chain V region MOPC 47 A (IG HCV MOPC 47A), Ig heavy chain V region 441 (IG HCV 441), myosin light polypeptide 6 (MYL6), and valosin-containing protein (VCP) were amongst the most significant

candidate gene products identified in an *in vivo* study of antigen effects on AgNP toxicity **(Table 3).** These gene products were commonly expressed in allergic and healthy mice after AgNP treatment and are involved in putative pathways of AgNP toxicity, including oxidative stress and allergic inflammation. ApoE is an apolipoprotein with immunomodulatory and anti-inflammatory properties involved in the low-density lipoprotein receptor (LDLR) pathway.[105] By binding to LDLR, ApoE has been shown to be a negative regulator of AHR and goblet cell metaplasia in asthma; activators of the ApoE–LDLR pathway, such as ApoE mimetic peptides, might be developed into a therapeutic for asthmatics.[106] hnRNPA2B1 is a heterogeneous nuclear ribonucleoprotein associated with pre-mRNA processing, and was identified as a glucocorticoid receptor binding site and potential therapeutic target amongst a subset of genes associated with atopic status in asthmatics.[107] IG ACC, IG HCV MOPC 47A, and IG HCV 441 are immunoglobulin proteins used for antigen defense and are involved in innate immune response putative pathways; they were identified as potential therapeutic targets amongst a subset of genes associated with asthma induction via the IL-13 and TGF-β signaling pathways.[108] MYL6 is a myosin light polypeptide associated with airway smooth muscle contraction; it has been shown to be a positive regulator of AHR, as its overexpression leads to an increased velocity of shortening (and thus AHR) in asthmatics.[109] VCP is a transitional endoplasmic reticulum ATPase associated with facilitating degradation of polypeptides mediated by the proteasome; it is involved in response to cellular stress and innate immune response putative pathways. It has been associated with NLRP3 apoptosis and inflammation, with a recent *in vitro* study showing that both the NLRP3 inflammasome and local IL-1β$^{(+)}$F4/80$^{(+)}$Ly6C$^{(+)}$ inflammatory macrophages contribute to VCP-associated diseases;[110] inhibitors of the NLRP3/RXR axis, such as MCC950, might be also developed into a therapeutic for asthmatics.[111] Ultimately, these candidate gene products may exacerbate AgNP toxicity by modulating normal innate and adaptive immune responses to further increase an individual's sensitivity to occupational exposures. Their respective mechanistic roles should be evaluated in future studies that account for interactions that include these host acquired targets.

2.6 DISCUSSION

As illustrated in the *in vitro* and *in vivo* studies reviewed above, host genetic and acquired factors may play a role in defining sensitive populations to AgNP exposures in occupational settings. These G×E effects on AgNP toxicity are of relevance of public health as they may be broadly applicable to other types of ENM, which are used in manufacturing of many consumer products. Our review focused on host acquired factors, such as asthma, but other pre-existing chronic respiratory diseases, such as acute bronchitis or COPD, may also confer increased sensitivity to occupational exposures.[25-27] When defining exposure limits, it is important to determine whether sex effects on AgNP toxicity are present given the effects of sexual dimorphism on adverse health responses to oxidative stress and allergic inflammation. An additional consideration is whether there are known polymorphisms identified in the putative pathways by which different occupational exposures cause adverse health responses. It is also important to evaluate whether individuals with pre-existing chronic respiratory diseases, such as asthma, may be more sensitive to occupational exposures. Future studies should evaluate interactions between host genetic or acquired factors in order to identify genes or gene products that may contribute to risk for AgNP toxicity.

An individual's sex is a relevant host genetic factor in determining their response to a variety of infections, sterile injuries, or occupational exposures. One approach to determining risk for any given exposure is to use male and female mice to identify candidate sensitivity genes associated with increased risk to the target exposure. Sexual dimorphism is observed in the prevalence, progression, and severity of cardiovascular, autoimmune, and chronic respiratory diseases. Sexual dimorphism in the endocrine and immune systems likely contributes to these differences; recent studies suggest this may also extend to genetic background, which effects baseline phenotypes of reproductive, physiological, and disease states. It is likely that differential regulation of sex steroid-responsive genes across males and females plays a mechanistic role in sexual dimorphism.[112] Therefore, when defining exposure limits, it is important to evaluate whether an individual's sex confers increased sensitivity to occupational exposures.

An individual's genetic background is another relevant host genetic factor in determining their response to occupational exposures. Another approach to determining risk for any given exposure is to use mouse genetic resources such as the Collaborative Cross or Diversity Outbred mice to identify quantitative trait loci and candidate sensitivity genes associated with increased risk to the target exposure. However, this requires substantial investment in time and resources to identify and confirm specific candidate sensitivity genes. An alternative approach is to use existing information on putative pathways involved in exposure toxicity, e.g., oxidative stress for AgNP toxicity, and then determine what common functional polymorphisms have been identified for genes within this putative pathway. This can then serve as a basis for targeted analyses of specific genetic risks associated with exposure toxicity. While there are likely many potential sensitivity genes for a target exposure, each gene will usually exert a small effect rather than a few individual genes exerting a large effect when contributing to exposure toxicity. Due to the intersection of putative pathways associated with AgNP toxicity and asthma, there is a strong potential for variation in these genes (amongst many others) to increase an individual's sensitivity to occupational exposures.

An individual's chronic respiratory disease is a relevant host acquired factor in determining their response to occupational exposures. Our review focused on asthma, which is a complex airway disease whose prevalence, progression, and severity are can be affected by host genetic and acquired factors as well as occupational exposures.[28] Exposure assessment studies on AgNP exposures in occupational settings are in their infancy, and given the potential for effects of G×E on AgNP toxicity, there is an urgent need to develop better methods for exposure assessment as well as biomarker development. If we cannot relate the genetic effects of AgNP exposures to specific quantities in occupational settings, our ability to define a mechanistic basis for G×E effects on AgNP toxicity will continue to be limited. Therefore, the progress in the fields of toxicology, genetics, and genomics calls for a greater investment in the development of improved methods for exposure assessment.

When defining exposure limits, it is important to use models of pre-existing chronic respiratory diseases which may directly modify their response to AgNP exposures. For

example, *in vivo* models suggest that asthma may increase risk of AgNP toxicity. Therefore, using *in vitro* or *in vivo* models of asthma may identify a more appropriate exposure limit. Epidemiology studies would also be useful to confirm that these pre-clinical findings are relevant in human populations. The impacts of AgNP exposures on public health have the potential to be significant, as they can occur during the lifecycle of the products in which they are utilized, either directly through raw materials extraction, synthesis, product manufacturing, product use, or indirectly through release into the environment, or disposal at the end of product life.[113-118] Weldon et al. observed multiple routes of AgNP exposures in their review of exposure assessment studies in occupational settings, and identified the most critical route of exposure as cleaning the systems in which the particles are synthesized.[38-40] While identifying these routes of exposure is an important first step, follow-up for adverse health responses is both critical and necessary to inform whether AgNP exposures produce biologically significant effects. Future exposure assessment studies on AgNP exposures in occupational settings should conduct follow-up and include workers with polymorphisms and/or pre-existing chronic respiratory diseases to understand G×E effects on AgNP toxicity in human populations.

It is very likely that many of the *in vitro* and *in vivo* studies reviewed above utilized extreme doses rather than realistic tissue burdens which may have implications for the interpretation of their findings when predicting response to AgNP exposures. The use of dosimetry methods to derive physiologically-relevant, dosimetric dose response relationships as well as additional exposure assessment studies in occupational settings would be important for reconciling the findings of some *in vitro* and *in vivo* studies. Weldon et al. used a benchmark dose (BMD) approach to derive a health-based occupational exposure limit (OEL) of 0.19 μg AgNP/m^3 using dosimetric human equivalent concentrations (HEC) based upon the faction of deposited Ag mass in different target organs; the authors identified the liver, followed by the lungs, as the most sensitive targets for adverse organ responses.[119] The dosimetric BMD for T2 lung inflammation was recognized as a tissue burden between 1 and 20 μg AgNP/mg tissue. This approach allowed for a comparison of physiologically-relevant, dosimetric dose response relationships in order to anchor these within a mechanistic framework and inform regulatory policy aimed at protecting all populations. Similar approaches should be

implemented in future *in vitro* studies, as there is presently a need for *in vitro* models to provide relevant data on risk assessment for occupational exposures.

While NIOSH has established REL for total Ag, including dusts, fumes, and soluble compounds for occupational settings, a draft REL for AgNP exposures has only recently been established for occupational settings. In August 2018, NIOSH revised its draft Current Intelligence Bulletin on the Health Effects of Occupational Exposure to Silver Nanomaterials, which contains an updated review of scientific literature on AgNP exposures in occupational settings and proposes a new draft REL that would apply to processes involved in product manufacturing. NIOSH now recommends that AgNP exposures in occupational settings not exceed 0.9 μg AgNP/m^3 measured as an airborne respirable 8-hour time-weighted average concentration. NIOSH continues to recommend its existing REL for Ag mass of 10.0 μg Ag/m^3 as an 8-hour time-weighted average concentration of dusts, fumes, and soluble compounds, which is the same as the OSHA permissible exposure limit (PEL) for Ag. Further, NIOSH continues to recommend the use of exposure assessments, engineering controls, safe working practices, as well as worker training and education, and surveillance programs to prevent adverse health responses from AgNP exposures in occupational settings.

NIOSH has proposed the following priority areas for research to address knowledge gaps on these adverse health responses from AgNP exposures in occupational settings: 1) assure that the hazards of exposure are consistent with current scientific knowledge; 2) assure that the proposed sampling and analytical methods are adequate to measure exposure; 3) assure that the recommended strategies (e.g., engineering controls, personal protective equipment, and/or work practices) are reasonable to control exposure; 4) assure that the accuracy of the relationship between exposure and toxicity are consistent with current scientific knowledge; 5) assure that the risk assessment and dosimetry methods are consistent with current scientific practice; 6) assure that the evidence of adverse health responses is consistent with current scientific knowledge; 7) assure that the new draft REL for AgNP exposures is well-supported by current scientific knowledge; 8) assure that the knowledge gaps and future research needs are completely and clearly described.[120] To address some of these knowledge gaps and future research

needs, we recommend that future studies focus on G×E effects on AgNP toxicity. Further, we recommend that regulatory agencies consider G×E effects on AgNP toxicity when finalizing the REL for AgNP exposures, as the studies reviewed above illustrate that underlying genetics or diseases may directly modify response to AgNP exposures.

AUTHOR CONTRIBUTIONS

The manuscript was written through contributions of all authors. All authors have given approval to the final version of the manuscript.

FUNDING SOURCES

This work was supported by the US EPA under Grant R835738 (E.M.F., T.J.K., W.A.A); NIH under Grants P30 ES007033 (T.J.K.) and T32 ES007032-38 (T.P.N.); the Washington State Department of Labor and Industries under the Medical Aid/Accident Fund; (T.P.N.) and the University of Washington under the GO-MAP Dissertation Fellowship (T.P.N.).

NOTES

The authors declare no competing financial interest.

2.7 DATA

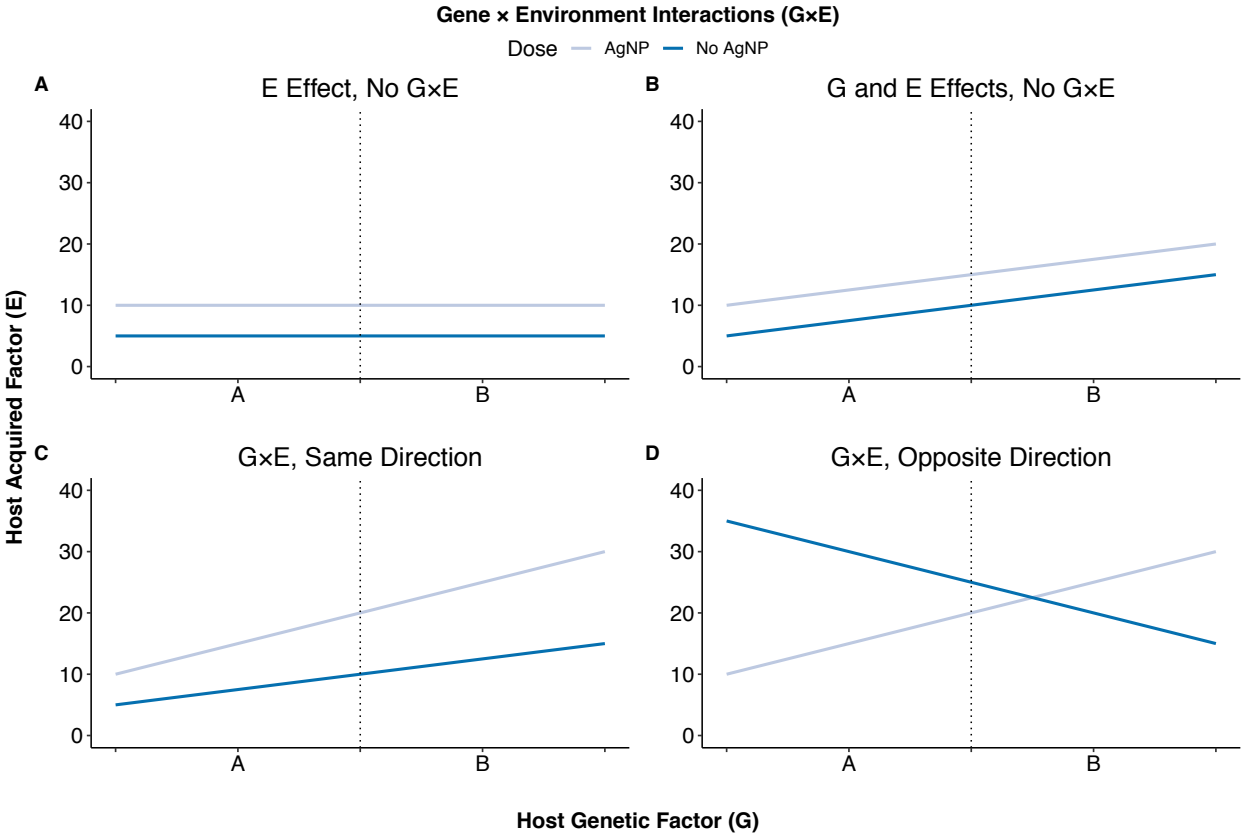

Figure 2.1 G×E effects on AgNP toxicity. Representative G×E effects on AgNP toxicity under four different model scenarios: **(A)** individual effect of host acquired factor, no G×E; **(B)** individual effects of host genetic and acquired factors, no G×E; **(C)** interaction of host genetic and acquired factors in the same direction, G×E; **(D)** interaction of host genetic and acquired factors in the opposite direction, G×E.

		Size (nm)	Coating	Dose	Exposure	Cell Line/Species/Genotype	Adverse Cellular Response	Significance (*P*)	Reference
Airway Epithelial Cells	Bronchial Epithelial Cells	50-250	Uncoated	0.1-10 μg/mL	24 h	BEAS-2B/Human	Cytotoxicity DNA damage ROS production	*** *** **	58
		250-385	Uncoated	0.1-10 μg/mL	4, 24 h	BEAS-2B/Human	Cytotoxicity DNA damage	NS NS	59
		10-100	PVP	2-180 μg/mL	4-48 h	BEAS-2B/Human	Chromosomal aberration Cytokinesis inhibition Cytotoxicity DNA damage Micronuclei induction	NS NS *** *** NS	34
		10-75	CIT, PVP	5-100 μg/mL	4, 24 h	BEAS-2B/Human	Cytotoxicity DNA damage Mitochondrial activity ROS production	*** ** *** NS	60
		100-500	Uncoated	0.1-10 μg/mL	4, 24 h	BEAS-2B/Human	Cytotoxicity	NS	61
		10-100	Uncoated	4×10^{7}-10^{9} ng/cm^2	12, 24 h	N-HBE/Human CF-HBE/Human	Apoptosis Cytotoxicity T1 cytokine secretion	*** ** ***	50
		50-300	Uncoated	1.8-7.4 μg/mL	24 h	BEAS-2B/Human	Apoptosis DNA damage ROS production Scavenger enzyme activity	* * * *	121
		7-10	CIT	0.1-0.7 ug/cm^2	4, 24 h	BEAS-2B/Human	Cytotoxicity ROS production	*** **	62
		20	CIT, PVP	0.1-50 μg/mL	24 h	BEAS-2B/Human	Antioxidant enzyme activity GSH depletion Mitochondrial activity	* * *	87
		20-200	Uncoated	0.13-1.33 μg/mL	16 w	BEAS-2B/Human	Apoptosis Cytotoxicity	** **	63
	Alveolar Epithelial Cells	40	Uncoated	3-6 μg/mL	22-66 h	R3-1/Rat	ROS production	*	122
		80	PVP	0.5-20 μg/mL	24 h	A549/Human	Apoptosis Cytotoxicity DNA adducts Mitochondrial activity ROS production	* * * * *	64
		20, 200	PVP	10-100 μg/mL	2-72 h	A549/Human	Cytotoxicity	*	69
		<100	PVP	25-200 μg/mL	24-72 h	A549/Human	Apoptosis Cytotoxicity Mitochondrial activity Mitochondrial membrane potential ROS production S phase cell cycle arrest Sub-G1 phase cell cycle arrest	* * * * * * *	65
		250-385	Uncoated	0.1-10 μg/mL	4, 24 h	A549/Human	Cytotoxicity DNA damage	NS NS	59
		20	CIT	30, 270 ng/cm^2	4, 24 h	A549/Human	Cytotoxicity Inflammation Oxidative stress T1 cytokine secretion	NS NS NS NS	67
		70	PVP	0.03-3 ug/cm^2	4, 24 h	A549/Human	Cytotoxicity T1 cytokine secretion	NS NS	68
		10-40	Uncoated	3.0625-50 μg/mL	24 h	A549/Human	Cytotoxicity DNA damage	** *	66

						Mitochondrial activity ROS production	*** ***	
		7-10	CIT	0.1-0.7 ug/cm^2	4, 24 h	A549/Human	Cytotoxicity ROS production	NS NS	62
		20, 200	PVP	10-100 µg/mL	2-72 h	A549/Human	Inflammation NF-κB activation Oxidative stress T1 cytokine secretion	*** * * *	123
Innate Immune Cells	Mast Cells	20, 110	CIT, PVP	6.25-50 µg/mL	1 h	Primary/Mouse/C57BL/6J	Cell degranulation Osteopontin production	* *	124
		20	CIT	25 µg/mL	1 h	Primary/Mouse/C57BL/6J	Ca^{2+} influx Cell degranulation Mitochondrial activity	* * *	125
		20	CIT	25 µg/mL	1 h	Primary/Mouse/129X1/SvJ Primary/Mouse/BALB/cByJ Primary/Mouse/BALB/cJ Primary/Mouse/BXD100/RwwJ Primary/Mouse/BXD50/RwwJ Primary/Mouse/BXD61/RwwJ Primary/Mouse/BXD73/RwwJ Primary/Mouse/BXD90/RwwJ Primary/Mouse/C3H/HeJ Primary/Mouse/C57BL/6J Primary/Mouse/CAST/EiJ Primary/Mouse/CBA/J Primary/Mouse/DBA/2J Primary/Mouse/FVB/NJ Primary/Mouse/I/LnJ Primary/Mouse/LP/J Primary/Mouse/NOD/ShiLtJ Primary/Mouse/NZW/LacJ Primary/Mouse/PL/J Primary/Mouse/PWD/PhJ Primary/Mouse/RIIIS/J Primary/Mouse/SJL/J Primary/Mouse/SWR/J	Candidate genes Cell degranulation	*** *	49
	Basophils	15	Uncoated	50 µg/mL	5-20 m	RBL-2H3/Rat	Ca^{2+} influx Cell degranulation Cell size	* ** *	126
		20	CIT	25 µg/mL	1 h	RBL-2H3/Rat	Ca^{2+} depletion Cell degranulation Mitochondrial activity	* * *	125
	Eosinophils	1-2.5	Uncoated	1-30 ppm	72 h	Primary/Human	Cell influx T1 cytokine secretion T2 cytokine secretion	* * *	127
		20, 70	CIT	100 µg/mL	6-24 h	AML14.3D10/Human	Apoptosis T1 cytokine secretion T2 cytokine secretion	* * *	128
	Neutrophils	20	CIT	10, 100 µg/mL	24 h	Primary/Human	Apoptosis Cell size Cytotoxicity *De novo* protein synthesis	* * * *	129
		20	CIT	10, 100 µg/mL	24 h	Primary/Human	Apoptosis Cell degranulation Cytotoxicity NLRP3 inflammasome activation	*** *** *** ***	130

						ROS production	NS	
	Dendritic Cells	40-300	Uncoated	10 µg/mL	24 h	Primary/Mouse/C57BL/6J, Primary/Mouse/OTII.2	Cell proliferation T1 cytokine secretion T2 cytokine secretion	*** ** ***	131
		2 nm	PVP	0.125-3 µg/mL	12-48 h	DC2.4/Mouse	Apoptosis Cytotoxicity Mitochondrial activity ROS production	*** *** ** ***	132
	Alveolar Macrophages	15-55	Uncoated	10-75 µg/mL	24 h	Primary/Rat	GSH depletion Mitochondrial activity ROS production T1 cytokine secretion	* * ** *	133
		20, 110	CIT, PVP	6.25-50 µg/mL	24 h	Primary/C57BL/6J/Mouse Primary/*Marco*/Mouse	Cytotoxicity Mitochondrial Activity NLRP3 Inflammasome Activation	*** *** ***	51
	NK Cells	1-2.5	Uncoated	1-30 ppm	72 h	Primary/Human	Cell proliferation T1 cytokine secretion T2 cytokine secretion	* * *	127
		20	CIT	1-10 µg/mL	12 h	Primary/Human	Killing potential Mitochondrial activity Surface receptor activation	* * NS	134
Adaptive Immune Cells	B Cells	3-8	Uncoated	5-80 µg/mL	2, 24 h	Primary/Human	Cell proliferation Chromosomal aberration Cytokinesis inhibition DNA damage Lipid peroxidation Micronuclei induction	* * * * * *	135
		80	CIT, PVP	12.5-50 µg/mL	72 h	Primary/Human	Cell proliferation Mitochondrial activity	* *	136
	T Cells	50-90	PVP	5-30 µg/mL	24 h	Primary/Human	Apoptosis Cell proliferation ROS production Surface receptor activation T1 cytokine secretion	NS NS * NS *	137
		80	CIT, PVP	12.5-50 µg/mL	72 h	Primary/Human	Cell proliferation Mitochondrial activity	* *	136

Table 2.1. Adverse cellular responses. Coating: CIT (citrate); PVP (polyvinylpyrrolidone). Exposure: m (minutes); h (hours); w (weeks). Significance: NS (P>0.05); * (P<0.05); ** (P<0.01); *** (P<0.001) for the highest dose only, as reported in the respective paper.

	Size (nm)	Coating	Dose	Exposure	Genotype/Sex	Adverse Organ Response	Significance (P)	Reference

Mouse	Genotype	20	CIT	0.25 mg/kg	Period: 0 h Assessment: 1 d	129S1/SvImJ/Male A/J/Male AKR/J/Male BALB/cJ/Male BTBRT^{+} tf/J/Male C3H/HeJ/Male C57BL/10J/Male C57BL/6J/Male C57L/J/Male CBA/J/Male DBA/2J/Male FVB/NJ/Male MRL/MpJ/Male NOD/ShiLtJ/Male NZB/BINJ/Male NZO/HlLtJ/Male NZW/LacJ/Male PL/J/Male PWD/PhJ/Male PWK/PhJ/Male SJL/J/Male SM/J/Male SWR/J/Male TALLYHO/JngJ/Male WSB/EiJ/Male	Candidate genes Cell count: BALF	* *	78
	Antigen	50, 200	CIT, PVP	1-50 µg/mL	Period: 0 h Assessment: 1, 5 d	BALB/cJ/Female	Cell count: BALF Histopathology Microbiome dysbiosis T2 cytokine secretion	** * * *	86
		6	Uncoated	20 ppm	Period: 1 h/d, 5 d Assessment: 2 d	BALB/cJ/Female	Airway resistance Cell count: BALF Histopathology T2 cytokine secretion VEGF signaling	* * * * *	84
		33	Uncoated	3.3 mg/m^3	Period: 6 h/d, 7 d Assessment: 7 d	BALB/cJ/Female	Ag quantification Airway resistance Allergic reaction Cell count: blood Histopathology Inflammation Oxidative stress T2 cytokine secretion	NS ** * ** NS ** * *	82
		33	Uncoated	3.3 mg/m^3	Period: 6 h/d, 7 d Assessment: 5 d	BALB/cJ/Female	OVA-specific IgE secretion Blood coagulation Chemokine signaling Cytokine signaling Dopamine receptor signaling Fas signaling Integrin signaling Plasminogen activating cascade Rho GTPas cytoskeletal regulation T cell activation Tricarboxylic acid cycle activation Ubiquitin proteasome signaling	* * * * * * * * * * * *	83
		5, 20	Uncoated	20 ppm	Period: 1 h/d, 5 d Assessment: 2 d	C57BL/6J/Female	Airway resistance Biochemistry: blood Cell count blood	* NS NS	85

Rat						Cell count: BALF Histopathology NF-κB activation T2 cytokine secretion	NS * * *	
	Genotype/Sex	15	Uncoated	133 μg/m^3	Period: 6 h Assessment: 0 h, 1, 4, 7 d	Fischer 344/Female	Ag quantification	NS, *	138
		15, 410	PVP	179, 167 μg/m^3	Period: 6 h/d, 4 d Assessment: 1, 7 d	Fischer 344/Male	Ag quantification Cell count: BALF Cell count: blood Cytotoxicity GSH depletion Histopathology T1 cytokine secretion	* * NS * * NS *	139
		18	Uncoated	0.5-61 μg/m^3	Period: 6 h/d, 5 d/w, 4 w Assessment: 0 h	Sprague-Dawley/Male, Female	Ag quantification Biochemistry: blood Cell count: blood Histopathology	** * * NS	140
		18	Uncoated	49-515 μg/m^3	Period: 6 h/d, 5 d/w, 13 w Assessment: 0 h	Sprague-Dawley/Male, Female	Biochemistry: blood Cell count: BALF Histopathology Lung function: minute volume Lung function: peak inspiration Lung function: tidal volume	** ** * ** ** **	72
		18	Uncoated	49-515 μg/m^3	Period: 6 h/d, 5 d/w, 13 w Assessment: 0 h	Sprague-Dawley/Male, Female	Ag quantification Biochemistry: blood Cell count: blood Histopathology	*** NS * **	73
		18-20	Uncoated	76-750 μg/m^3	Period: 4 h Assessment: 2 w	Sprague-Dawley/Male, Female	Lung Function: minute volume Lung Function: tidal volume	NS NS	71
		14-15	Uncoated	49-381 μg/m^3	Period: 6 h/d, 5 d/w, 12 w Assessment: 4, 12 w	Sprague-Dawley/Male, Female	Ag quantification Histopathology Lung function: minute volume Lung function: peak inspiration Lung function: tidal volume	** * ** ** **	74
		20, 110	CIT, PVP	0.10 mg/kg$_{BW}$	Period: 0 h Assessment: 1, 7, 21 d	Brown-Norway/Male Sprague-Dawley/Male	Cell count: BALF Histopathology IgE secretion Lung function: airway resistance Lung function: airway responsiveness Lung function: dynamic compliance T2 cytokine secretion	*** *** ** *** *** *** **	79
		13-16	Uncoated	600-800 μg/mm^3	Period: 3 h/d, 4 d Assessment: 1	Brown-Norway/Male Sprague-Dawley/Male	Ag quantification Cell count: BALF Histopathology Lung function: airway resistance Lung function: tissue elastance T2 cytokine secretion T17 cytokine secretion	*** *** *** * ** *** **	80

Table 2.2. Adverse organ responses. Coating: CIT (citrate); PVP (polyvinylpyrrolidone). Exposure: m (minutes); h (hours); w (weeks); # (exposure prior to ovalbumin challenge and sensitization). Significance: NS (P>0.05); * (P<0.05); ** (P<0.01); *** (P<0.001) for the highest dose only, as reported in the respective paper.

		Target	Target ID	Study	Host Genetic Factor	Host Acquired Factor	Putative Pathway	Reference
Host Genetic Targets	Genotype/Polymorphism	*Ano6*	MGI:2145890	*In Vivo*	Genotype	-	Immune system Innate immune system Ion channel transport Neutrophil degranulation Stimuli-sensing channels Transport of small molecules	78
		Gclm	MGI:104995	*In Vivo*	Polymorphism	-	Biological oxidations Glutathione conjugation Glutathione synthesis and recycling Metabolism Phase II - conjugation of compounds	81
		Marco	MGI:1309998	*In Vitro*	Polymorphism	-	Binding and uptake of ligands by scavenger receptors Scavenging by class A receptors Vesicle-mediated transport	51
		Nedd4l	MGI:1933754	*In Vivo*	Genotype	-	Adaptive immune system Antigen processing: ubiquitination & proteasome degradation Class I MHC mediated antigen processing & presentation Downregulation of SMAD2/3:SMAD4 transcriptional activity Gene expression (transcription) Generic transcription pathway Immune system Ion channel transport RNA Polymerase II transcription Signal transduction Signaling by TGF-beta family members Signaling by TGF-beta receptor complex Stimuli-sensing channels Transcriptional activity of SMAD2/SMAD3:SMAD4 heterotrimer Transport of small molecules	78
		Ptger4	MGI:104311	*In Vitro*	Genotype	-	Class A/1 (Rhodopsin-like receptors) Eicosanoid ligand-binding receptors G alpha (s) signaling events GPCR downstream signaling GPCR ligand binding Prostanoid ligand receptors Signal transduction Signaling by GPCR	49
		Rnf220	MGI:1913993	*In Vivo*	Genotype	-	Adaptive immune system Antigen processing: ubiquitination & proteasome degradation Class I MHC mediated antigen processing & presentation Immune system	78
		Txnip	MGI:1889549	*In Vitro*	Genotype	-	-	49

Host Acquired Targets	Antigen	*ANXA2*	P07356	*In Vivo*	-	Antigen	Dissolution of fibrin clot Hemostasis Immune system Innate immune system Neutrophil degranulation	83
		APOE	P08226	*In Vivo*	-	Antigen	Binding and uptake of ligands by scavenger receptors Chylomicron assembly Chylomicron clearance Chylomicron remodeling G alpha (i) signaling events GPCR downstream signaling HDL remodeling Metabolism Metabolism of fat-soluble vitamins Metabolism of proteins Metabolism of vitamins and cofactors Plasma lipoprotein assembly, remodeling, and clearance Post-translational protein modification Post-translational protein phosphorylation Regulation of IGF transport Regulation of IGFBP uptake Retinoid metabolism and transport Scavenging by class A receptors Signal transduction Signaling by GPCR Transport of small molecules Vesicle-mediated transport Visual phototransduction	83
		CFTR	P26361	*In Vitro*	Polymorphism	Phenotype	ABC-family proteins mediated transport Cargo recognition for clathrin-mediated endocytosis Clathrin-mediated endocytosis Deubiquitination Membrane trafficking Metabolism of proteins Post-translational protein modification Transport of small molecules Ub-specific processing proteases Vesicle-mediated transport	50
		HIF1A	Q61221	*In Vivo*	-	Antigen	Cellular responses to hypoxia Cellular responses to external stimuli Cellular responses to stress Deubiquitination Metabolism of proteins Neddylation Oxygen-dependent asparagine hydroxylation of HIF1A Oxygen-dependent proline hydroxylation of HIF1A Post-translational protein modification PTK6 promotes HIF1A stabilization Regulation of gene expression by HIF Regulation of HIF by oxygen Signal transduction Signaling by non-receptor tyrosine kinases Signaling by PTK6 Ub-specific processing proteases	84
		HIST1H2AF	Q8CGP5	*In Vivo*	-	Antigen	Chromatin organization	83
		HIST1H4A	P62806	*In Vivo*	-	Antigen	Nucleosome assembly	83

HNRNPA2B1	O88569	*In Vivo*	-	Antigen	Metabolism of RNA mRNA splicing mRNA splicing - major pathway Processing of capped intron-containing Pre-mRNA	83
HSPA4	Q61316	*In Vivo*	-	Antigen	Cellular responses to external stimuli Cellular responses to heat stress Cellular responses to stress Regulation of HSF1-mediated heat shock response	83
GLOD4	Q9CPV4	*In Vivo*	-	Antigen	-	83
IG ACC	P01878	*In Vivo*	-	Antigen	Binding and uptake of ligands by scavenger receptors Cell surface interactions at the vascular wall Hemostasis Scavenging of heme from plasma Vesicle-mediated transport	83
IG HCV MOPC 47A	P01786	*In Vivo*	-	Antigen	Adaptive immune response B cell activation B cell receptor signaling Defense response to bacterium Humoral immune response Immune effector process Innate immune response Membrane invagination Phagocytosis Positive regulation of lymphocyte activation Protein metabolic process Vesicle budding from membrane	83
IG HCV 441	P01806	*In Vivo*	-	Antigen	Adaptive immune response B cell activation B cell receptor signaling Defense response to bacterium Humoral immune response Immune effector process Innate immune response Membrane invagination Phagocytosis Positive regulation of lymphocyte activation Protein metabolic process Vesicle budding from membrane	83
IG LCC	P01843	*In Vivo*	-	Antigen	Response to stimulus	83
ITIH2	Q61703	*In Vivo*	-	Antigen	-	83
MYL6	Q60605	*In Vivo*	-	Antigen	Muscle contraction RHO GTPase effectors RHO GTPases activate PAKs Signal transduction Signaling by Rho GTPases Smooth muscle contraction	83
MYL9	Q9CQ19	*In Vivo*	-	Antigen	Developmental process Muscle contraction	83

PI3K	Q9JHG7	*In Vivo*	-	Antigen	G beta:gamma signaling through PI3Kgamma G-protein beta:gamma signaling GPCR downstream signaling GPVI-mediated activation cascade Hemostasis Metabolism Metabolism of lipids Phospholipid metabolism PI Metabolism Platelet activation, signaling and aggregation Signal Transduction Signaling by GPCR Synthesis of PIPs at the plasma membrane	84
PSMA1	Q9R1P4	*In Vivo*	-	Antigen	Proteasome-mediated Ub-dependent protein catabolic process Protein ubiquitination	83
SOD3	O09164	*In Vivo*	-	Antigen	Cellular responses to oxidative stress Cellular responses to oxygen-containing compound Reactive oxygen species metabolic process Response to inorganic substance Response to reactive oxygen species Response to toxic substance	83
VCP	Q01853	*In Vivo*	-	Antigen	ABC-family proteins mediated transport Asparagine N-linked glycosylation Cellular responses to external stimuli Cellular responses to heat stress Cellular responses to stress Deubiquitination DNA damage bypass DNA repair Hedgehog ligand biogenesis HSF1 activation Immune system Innate immune system Metabolism of proteins N-glycan trimming in the ER and calnexin/calreticulin cycle Neutrophil degranulation Ovarian tumor domain proteases Post-translational protein modification Protein methylation Signal transduction Signaling by hedgehog Translesion synthesis by POLH Translesion synthesis by Y family DNA polymerases Transport of small molecules	83

VEGF	Q00731	*In Vivo*	-	Antigen	Axon guidance Developmental biology EGF ligand-receptor interactions EPH-Ephrin signaling EPHB-mediated forward signaling Hemostasis Platelet activation, signaling, and aggregation Platelet degranulation Response to elevated platelet cytosolic Ca2+ Signal transduction Signaling by receptor tyrosine kinases Signaling by VEGF VEGF binds to VEGFR leading to receptor dimerization VEGFA-VEGFR2 Pathway VEGFR2 mediated cell proliferation	84
VIM	P20152	*In Vivo*	-	Antigen	-	83

Table 2.3. Host genetic and acquired targets. Host Genetic Targets: *Ano6* (anoctamin 6); *Gclm* (glutamate-cysteine ligase modifier subunit); *Marco* (macrophage receptor with collagenous structure); *Nedd4l* (E3 ubiquitin-protein ligase NEDD4-like); *Ptger4* (prostaglandin E receptor 4); *Rnf220* (E3 ubiquitin-protein ligase RNF220); *Txnip* (thioredoxin interacting protein). Host Acquired Targets: ANXA2 (Annexin A2); APOE (Apolipoprotein E); CFTR (Cystic fibrosis transmembrane conductance regulator); HIF1A (Hypoxia-inducible factor 1-alpha); HIST1H2AF (Histone H2A type 1-F); HIST1H4A (Histone H4); HNRNPA2B1 (Heterogeneous nuclear ribonucleoproteins A2/B1); HSPA4 (Heat shock 70 kDa protein 4); GLOD4 (Glyoxalase domain-containing protein 4); IG ACC (Ig alpha chain C region); IG HCV MOPC 47A (Ig heavy chain V region MOPC 47 A); IG HCV 441 (Ig heavy chain V region 441); IG LCC (Ig lambda-1 chain C region); ITIH2 (Inter-alpha-trypsin inhibitor heavy chain H2); MYL6 (Myosin light polypeptide 6); MYL9 (Myosin regulatory light polypeptide 9); PI3K (Phosphoinositide 3-kinase); PSMA1 (Proteasome subunit alpha type-1); SOD3 (Extracellular superoxide dismutase [Cu-Zn]); VCP (Valosin-containing protein); VEGF (Vascular endothelial growth factor); VIM (Vimentin).

Chapter 3. The Effects of Genotype × Phenotype Interactions on Silver Nanoparticle Toxicity in Organotypic Cultures of Murine Tracheal Epithelial Cells

This chapter was submitted for publication in Nanotoxicology. The authors of the manuscript are:

Tyler P. Nicholas[1,2], Anoria K. Haick[2], Tomomi W. Workman[1], William C. Griffith[1], James D. Nolin[2], Terrance J. Kavanagh[1,2], Elaine M. Faustman[1], and William A. Altemeier[2]

[1]Department of Environmental and Occupational Health Sciences, University of Washington, Seattle, Washington
[2]Department of Medicine—Division of Pulmonary, Critical Care, and Sleep Medicine, University of Washington, Seattle, Washington

Corresponding Author:
William A. Altemeier
UW Medicine Research / South Lake Union
850 Republican Street, S324
Box 358052
Seattle, Washington 98109
Phone: (206) 616-6140
Fax: (206) 221-0739
Email: billa@uw.edu

List of Abbreviations

5×4 h: subacute exposure of 4 hours, every other day, over 5 days
Ag: silver mass
Ag^+: silver ions
AgNP: silver nanoparticles
AJ or B6:Normal: A/J or C57BL6/J, “Normal” phenotype
AJ or B6:T2-Skewed: A/J or C57BL6/J, “T2-Skewed” phenotype
ALI: air-liquid interface
Au: gold mass
BMD: benchmark dose
BMDL: benchmark dose lower 95% confidence limit
Cd: cadmium mass
Clca1: calcium-activated chloride channel 1
COPD: chronic obstructive pulmonary disease
DCF: 2,7-dichlorofluorescein
DIV: day *in vitro*
DMEM: Dulbecco’s Modified Eagle Media
ENaC: amiloride-sensitive epithelial Na^+ channel
ENM: engineered nanomaterials
G×E: gene × environment interactions
G×P: genotype × phenotype interactions
GSH: glutathione
HEC: human equivalent concentration
ICPMS: inductively coupled plasma mass spectrometry
IHC: immunohistochemistry
ILC2: type 2 innate lymphoid cells
LDH: lactate dehydrogenase
MDA: malondialdehyde
MoA: mode of action
MTEC: murine tracheal epithelial cells
Muc5ac: mucin 5AC
NACIVT: Nano Aerosol Chamber for *in vitro* Toxicity studies
NDA: 2,3-naphthalenedicarboxaldehyde
Nedd4l: E3 ubiquitin-protein ligase NEDD4-like
NRC: National Research Council
OEL: occupational exposure limit
OR: odds ratio
PBPK: physiologically-based pharmacokinetic/toxicokinetic
QD: quantum dots
qRT-PCR: quantitative reverse transcription polymerase chain reaction
ROS: reactive oxygen species
T1/T2: type 1/type 2
TEER: transepithelial electrical resistance
TSCA: Toxic Substances Control Act
US EPA: U.S. Environmental Protection Agency

Chapter 3. The Effects of Genotype × Phenotype Interactions on Silver Nanoparticle Toxicity in Organotypic Cultures of Murine Tracheal Epithelial Cells

3.1 ABSTRACT

Silver nanoparticles (AgNP) are used in multiple applications but primarily in the manufacturing of many antimicrobial products. Previous studies have identified AgNP toxicity in airway epithelial cells, but no *in vitro* studies to date have used organotypic cultures as a high-content *in vitro* model of the conducting airway to characterize the effects of interactions between host genetic and acquired factors, or gene × phenotype interactions (G×P), on AgNP toxicity. In the present study, we derived organotypic cultures from primary murine tracheal epithelial cells (MTEC) to characterize nominal and dosimetric dose-response relationships for AgNP-induced barrier dysfunction, glutathione (GSH) depletion, reactive oxygen species (ROS) production, lipid peroxidation, and cytotoxicity across two genotypes (A/J and C57BL/6J mice), two phenotypes ("Normal" and "Type 2 [T2]-Skewed"), and two AgNP exposures (an acute 24 h exposure and a subacute exposure of 4 hours, every other day, over 5 days [5×4 h]). We characterized the "T2-Skewed" phenotype as an *in vitro* model of chronic respiratory diseases, which was marked by increased sensitivity to AgNP-induced barrier dysfunction, GSH depletion, ROS production, lipid peroxidation, and cytotoxicity, suggesting that asthmatics could be a sensitive population to AgNP exposures in occupational settings. This also suggests that exposure limits, which should be based upon the most sensitive population, should be derived using *in vitro* and *in vivo* models of chronic respiratory diseases. This study highlights the importance of considering dosimetry as well as G×P effects when screening and prioritizing potential respiratory toxicants. Such *in vitro* studies can be used to inform regulatory policy aimed at protecting all populations.

3.2 INTRODUCTION

There is presently a need for *in vitro* models to provide relevant data on risk assessment for occupational exposures. In recent years, there has been a gradual paradigm shift toward the use of *in vitro* models that reduce, replace, and refine the use of animals in

toxicity testing (the three R's) from both the standpoint of economic imperative and animal welfare.[1,2] Despite these economic advantages over *in vivo* models, *in vitro* models are currently limited by: 1) the use of immortalized or transformed cell lines that may not recapitulate primary cell phenotypes, 2) the use of cells from a single genetic background or phenotype, which may not capture the impact of underlying genetics or diseases on toxicant response, and 3) the limited efforts to relate *in vitro* exposures to occupational exposures in order to provide a regulatory basis for sensitivity to occupational exposures and inform regulatory policy aimed at protecting all populations.[3,4]

Chronic respiratory diseases, including asthma, acute bronchitis, and chronic obstructive pulmonary disease (COPD), collectively affect 16% of the United States population; these diseases impair host defense mechanisms, such as barrier function and immune regulation,[15] mucocilliary clearance and permeability,[16-22] as well as enzymatic and non-enzymatic regulation of oxidative stress,[23,24] and may increase an individual's sensitivity to occupational exposures.[25-27] Chronic respiratory diseases place a major burden on individuals, their workplaces, and the healthcare system, and yet less than 1% of the chemicals regulated by the U.S. Environmental Protection Agency's (US EPA) Toxic Substances Control Act (TSCA) have been tested for respiratory toxicity.[3,141] Together, the above limitations highlight a need to develop *in vitro* models suitable for high-throughput screening that also capture determinants of sensitivity in order to screen and prioritize potential respiratory toxicants while providing relevant data on risk assessment for occupational exposures.[142,143]

Silver nanoparticles (AgNP) have been tested for respiratory toxicity in previous studies, as they are used in the manufacturing of many antimicrobial consumer products, including air filters, humidifiers, and purifiers as well as antimicrobial sprays.[31,32,37] Previous *in vitro* studies observed the mode of action (MoA) for their antimicrobial properties (e.g., release of bioactive silver ions [Ag^+] upon dissolution[11-13]) is also a defining factor of AgNP toxicity in mammalian cells.[144] One MoA in airway epithelial cells is Ag^+-mediated reactive oxygen species (ROS) production, which leads to adverse cellular responses including oxidative stress, mitochondrial dysfunction, inflammation, and cytotoxicity.[50,58-63,87,121,145] Asthmatics are possibly a sensitive population to AgNP exposures in occupational

settings, as these adverse cellular responses may further modulate innate and adaptive immune responses at the epithelial-immune interface to exacerbate this chronic airway disease.[48]

Few previous studies have characterized the effects of interactions between host genetic and acquired factors, or gene × environment interactions (G×E),[28,29] on AgNP toxicity. Understanding G×E effects is important for identifying sensitive populations, whose underlying genetics or diseases could directly modify their response to AgNP exposures. Typically, these studies have used young, healthy animals or cell lines cultured toward a "Normal" phenotype and thus did not address the possibility of increased AgNP toxicity in asthmatics. The present study was designed to test the hypothesis that genotype and phenotype (physiological environment) will define G×E, or genotype × phenotype interaction (G×P), effects on AgNP toxicity.

We derived organotypic cultures from primary murine tracheal epithelial cells (MTEC) of differentially sensitive genotypes (A/J and C57BL/6J mice) to airway hyperresponsiveness,[146-148] antigen sensitization,[149] T2 lung inflammation,[150] and engineered nanomaterial (ENM) toxicity[77,78] to model the effects of host genetic factors on AgNP toxicity. We differentiated organotypic cultures toward either "Normal" or "Type 2 [T2]-Skewed" phenotypes to model the effects of host acquired factors on AgNP toxicity. To acquire the "Normal" phenotype, we used a defined differentiation media to achieve differentiation toward the cell populations in the proximal region of the conducting airway, including basal, ciliated, club, and mucin cells.[151] To acquire the "T2-Skewed" phenotype, we used a defined differentiation media supplemented with IL-13 to skew differentiation toward an *in vitro* model of chronic respiratory diseases, characterized by barrier dysfunction,[152] mucus production,[153] allergic responses,[153] and T2 responses.[154-156]

Using this high-content *in vitro* model of the conducting airway, we characterized nominal and dosimetric dose-response relationships for AgNP-induced barrier dysfunction, GSH depletion, ROS production, lipid peroxidation, and cytotoxicity across genotypes, phenotypes, and exposures to understand G×P effects on AgNP toxicity. To our knowledge, this is the first study to use organotypic cultures as a high-content *in vitro*

model of the conducting airway to characterize G×P effects on AgNP toxicity. By pairing organotypic cultures with dosimetry, we can define the basis for physiologically-relevant dose-response relationships by accounting for association and dissolution, and by using a benchmark dose (BMD) approach, we can identify the most sensitive adverse cellular responses to help define a regulatory basis for G×P effects on AgNP toxicity.

3.3 METHODS

Cell culture

All animal studies were approved by the Institutional Animal Care and Use Committee at the University of Washington. We harvested tracheas from A/J and C57BL/6J mice (The Jackson Laboratory, Bar Harbor, ME, USA), and isolated MTEC using enzymatic digestion, as previously described.[151,157,158] We suspended MTEC in a defined proliferation media [Dulbecco's Modified Eagle Media (DMEM) with 10 μg/mL insulin, 5 μg/mL apo-transferrin, 0.1 μg/mL cholera toxin, 25 ng/mL epidermal growth factor, 30 μg/mL bovine pituitary extract, and 50 nM retinoic acid (Sigma-Aldrich, St. Louis, MO, USA)] to culture at a density of 1.5×10^4 cells/well in collagen-coated 24-Transwell plates (Corning, Corning, NY, USA). We allowed organotypic cultures to proliferate with media in both apical and basal compartments starting on day *in vitro* (DIV) 0. We changed the defined proliferation media every other day until DIV 7-9, when transepithelial electrical resistance (TEER) exceeded 1000 $\Omega\times cm^2$, which marked the end of proliferation.

For the "Normal" phenotype, we allowed organotypic cultures to differentiate at an air-liquid interface (ALI) in a defined differentiation media [DMEM with 2% v/v NuSerum (BD BioSciences, San Jose, CA, USA), and 50 nM retinoic acid (Sigma-Aldrich, St. Louis, MO, USA)] in the basal compartment starting on DIV 7. We changed the defined differentiation media every other day until DIV 28, which marked the end of differentiation.

For the "T2-Skewed" phenotype, we allowed organotypic cultures to differentiate at an ALI in a defined differentiation media supplemented with IL-13 [DMEM with 2% v/v NuSerum (BD BioSciences, San Jose, CA, USA), 50 nM retinoic acid (Sigma-Aldrich, St. Louis, MO, USA)], and 25 ng/mL IL-13 (PeproTech, Rocky Hill, NJ, USA)]. We identified

this concentration of IL-13 in a preliminary study and supplemented it to the defined proliferation media starting on DIV 5, and then to the defined differentiation media from DIV 7-28, which we changed every other day until DIV 28.

Immunohistochemistry

We used immunohistochemistry (IHC) to characterize organotypic morphology in unexposed organotypic cultures on DIV 28. We washed organotypic cultures three times with 1× PBS (each wash for 10 min), fixed in 4% PFA (for 24 h at 4°C), embedded in paraffin, sectioned, and then stained with hematoxylin and eosin using an Autostainer XL (Leica Biosystems, Buffalo Grove, IL, USA). We acquired images at 40× on an Eclipse *90i* light microscope and processed using associated digital microscopy software (Nikon Instruments, Melville, NY, USA).

Quantitative reverse transcription-polymerase chain reaction

We used quantitative reverse transcription polymerase chain reaction (qRT-PCR) to quantify gene expression for markers of barrier function, cell populations, allergic responses (airway remodeling and hyperresponsiveness), as well as type 1 (T1), T2, and pro-T2 cytokines in unexposed organotypic cultures on DIV 28. We isolated total RNA from organotypic cultures using a RNEasy Micro Kit (Qiagen, Hilden, Germany), and synthesized cDNA using a RevertAid RT Reverse Transcription Kit (ThermoFisher Scientific, Waltham, MA, USA). We performed qRT-PCR using 20 ng cDNA per reaction with commercially available primer probe sets **(Table 1)**, and master mix (Integrated DNA Technologies, Coralville, IA, USA) on a 7900HT Fast Real-Time PCR System (Applied BioSystems, Foster City, CA, USA). We normalized data to a baseline condition of the *Ct* values for each gene averaged across AJ:Normal, B6:Normal, AJ:T2-Skewed, and B6:T2-Skewed and then to the average *Ct* values of housekeeping genes *Hprt1*, *Pol2ra*, and *Tbp* using the $2^{-\Delta\Delta Ct}$ method, as previously described.[78]

AgNP exposure

We exposed organotypic cultures in the apical compartment on DIV 28 to either 2 mM sodium citrate (vehicle control; 0 µg AgNP/mL media), or to silver nanoparticles (AgNP;

20 nm, gold-core, citrate-coated, at 1 mg/mL in 2 mM sodium citrate; nanoComposix, San Diego, CA, USA) for an acute exposure of 24 hours, or a subacute exposure of 4 hours, every other day, over 5 days (5×4 h) at nominal doses of 12.5, 25, or 50 µg AgNP/mL media, as freshly prepared in suspensions of defined differentiation media.

Inductively coupled plasma-mass spectrometry

We used inductively coupled plasma mass spectrometry (ICP-MS) to quantify dosimetric doses of silver (Ag), gold (Au), and the ratio of silver to gold (Ag:Au) mass associated on organotypic cultures. We washed organotypic cultures three times, each wash for 10 m, with 1× PBS to remove unassociated AgNP. We lysed organotypic cultures with CelLytic M Cell Lysis Reagent (Sigma-Aldrich, St. Louis, MO, USA) for 10 m at 4°C and pelleted the lysates at 50,000×g for 1 h at 4°C using an Optima MAX-XP ultracentrifuge (Beckman Coulter, Brea, CA, USA). We re-suspended cell fractions in 500 µL water and stored the samples at 4°C until analysis, as previously described.[159] We used a Bradford assay (Bio-Rad Laboratories, Hercules, CA, USA) to measure protein content, as previously described.[160] We normalized data by dividing the Ag, Au, and Ag:Au mass in each cell fraction by the protein content. The Ag:Au mass is an indirect measurement of the colocation of Ag and Au mass, and a high Ag:Au mass therefore suggests that the two metals have not separated through dissolution.

Transepithelial electrical resistance assay

We used a EVOM2 Epithelial Volt/Ohm Meter (World Precision Instruments, Sarasota, FL, USA) to quantify TEER as a measure of barrier function in exposed organotypic cultures, as previously described.[161] We normalized data by subtracting the average background resistance (in 1× PBS) and multiplying by the area of the semi-permeable transwell membrane (0.33 cm^2).

2,3-Naphthalenedicarboxaldehyde assay

We used a 2,3-naphthalenedicarboxaldehyde (NDA) assay to quantify NDA fluorescence at 472/528 nm as a measure of GSH depletion/oxidative stress in exposed organotypic cultures, as previously described.[162] We normalized data by subtracting the average

background absorbance of defined differentiation media, multiplying by a sample dilution factor (1/100) for fitting to a standard curve of known GSH concentrations in media, and dividing by the protein content.

2,7-Dichlorofluorescein assay

We used a 2,7-dichlorofluorescein (DCF) assay (Abcam, Cambridge, MA, USA) to quantify DCF fluorescence at 485/535 nm as a measure of ROS production/oxidative stress in exposed organotypic cultures, as previously described.[163] We normalized data by subtracting the average background absorbance of defined differentiation media and dividing by the DCF fluorescence of vehicle controls.

Malondialdehyde assay

We used a malondialdehyde (MDA) assay (Abcam, Cambridge, MA, USA) to quantify MDA fluorescence at 523/553 nm as a measure of lipid peroxidation/oxidative stress in exposed organotypic cultures, as previously described.[164] We normalized data by subtracting the average background absorbance in media, multiplying by a correction factor (4) for using 200 µL of the 800 µL reaction mix, multiplying by a dilution factor (1/100) for fitting to a standard curve of known MDA concentrations in media, and dividing by the protein content.

Lactate dehydrogenase assay

We used a lactate dehydrogenase (LDH) assay (Promega, Madison, WI, USA) to quantify LDH absorbance in cell culture supernatant at 490 nm as a measure of cytotoxicity in exposed organotypic cultures, as previously described.[165] We normalized data by subtracting the average background absorbance in media and dividing by the LDH absorbance of positive controls.

3.4 STATISTICS

We used linear mixed effects models to test the fixed effects of genotype, phenotype, and exposure using R statistical software.[166] We adjusted each model for random effects to account for variability across and within biological and technical replicates. We used

ANOVA to test the significance of each fixed effect as well as interactions between these fixed effects using the nominal dose of AgNP mass as a categorical variable. We tested the significance of interactions between these fixed effects to characterize G×P effects on AgNP toxicity. For all analyses, we considered an effect with a *P*-value less than 0.05 ($P<0.05$) statistically significant and adjusted all effects for multiple comparisons when comparing each nominal dose of AgNP mass to vehicle controls. We used a BMD approach to characterize G×P effects on the sensitivity of adverse cellular responses by accounting for differences in the effective dose ranges to induce AgNP toxicity measured by the nominal and dosimetric BMD and their lower 95% confidence limits (BMDL) across genotypes, phenotypes, and exposures using the dosimetric dose of Ag mass as a continuous variable **(Equation 1).**

3.5 RESULTS

The "T2-Skewed" phenotype is an in vitro model of chronic respiratory diseases

We compared genotype and phenotype effects for organotypic morphology and gene expression to achieve baseline characterization of organotypic cultures. We did not observe genotype effects on organotypic morphology; however, we observed phenotype effects on organotypic morphology **(Figure 1).** We observed organotypic morphology of the "T2-Skewed" phenotype recapitulated clinical features of airway remodeling, marked by a shift toward a pseudostratified columnar epithelium with an abundance of epithelial glycoproteins. We observed an increase in epithelial thickness due to cell proliferation (marked by blue-stained nuclei), shifted the simple cuboidal epithelium under the "Normal" phenotype to the pseudostratified columnar epithelium under the "T2-Skewed" phenotype. An increase in the density of ciliated cells is a distinguishing feature of pseudostratified columnar epithelium, which we also observed on the apical surface under the "T2-Skewed" phenotype. An increase in epithelial glycoproteins, including mucus and chitin (marked by unstained or light pink-stained inclusion bodies), is a distinguishing feature of T2 airway inflammation, which we also observed under the "T2-Skewed" phenotype.

We did not observe genotype effects on gene expression ($P>0.05$); however, we

observed phenotype effects on gene expression (*P*<0.001) **(Figure 2).** We observed gene expression under the "T2-Skewed" phenotype recapitulated clinical features of chronic respiratory diseases, including barrier dysfunction,[22] mucus production,[19] allergic responses,[20] and T2 responses.[154,167] We observed barrier dysfunction under the "T2-Skewed" phenotype by downregulation of *Tuba1a*, *Tubb4a*, *Tjp1*, *Jup*, and *Gja1,* which are markers for α-tubulin, β-tubulin, tight, adherens, and gap junctions, respectively. We observed genotype effects on gene expression for *Tubb4a*, *Jup*, and *Gja1* under the "Normal" phenotype (*P*<0.001 - *P*<0.05). We observed mucus production under the "T2-Skewed" phenotype by upregulation of *Muc5ac,* a marker for mucin cells; however, we did not observe mucin cell metaplasia under the "T2-Skewed" phenotype due to no evidence of reciprocal regulation with *Foxj1,* a marker for ciliated cells. We observed genotype effects on gene expression for *Scgb1a1* and *Muc5ac* under the "T2-Skewed" phenotype (*P*<0.001 - *P*<0.01). We observed allergic responses associated with airway remodeling and hyperresponsiveness under the "T2-Skewed" phenotype by upregulation of *Pcna*, *Ym1/2,* and *Pla2g10*, which are markers for cellular proliferation, agglutination, and eicosanoid production, respectively. We observed genotype effects on gene expression for *Pcna* and *Pla2g10* under the "T2-Skewed" phenotype (*P*<0.001). We observed reciprocal regulation of T1/T2 responses under the "T2-Skewed" phenotype by downregulation of T1 cytokines *Il2*, *Infg*, and *Tnfb* and upregulation of upstream pro-T2 cytokines *Il25*, *Il33*, and *Tslp* as well as downstream T2 cytokines *Il4*, *Il5*, *Il6*, *Il9*, *Il10*, and *Il13*. We observed genotype effects on gene expression for *Il2* and *Infg* under the "Normal" phenotype (*P*<0.001) as well as *Tnfb*, *Il33*, *Il6*, *and Il10* under the "T2-Skewed" phenotype (*P*<0.001 - *P*<0.01).

Exposure and phenotype effects on the linear relationship between the nominal dose of AgNP mass and the dosimetric dose of Ag, Au, and Ag:Au mass

We compared genotype, phenotype, and exposure effects for linear relationships between the nominal dose of AgNP mass and the dosimetric dose of Ag, Au, and Ag:Au mass. We observed positive linear relationships between the nominal dose of AgNP mass and the dosimetric dose of Ag mass **(Figure 3A-B; Supplementary Data)** and Au mass **(Figure 3C-D; Supplementary Data)** for AJ:Normal, B6:Normal, AJ:T2-Skewed, and

B6:T2-Skewed at the acute 24 h exposure and the subacute 5×4 h exposure. We did not observe genotype or phenotype effects on the dosimetric dose of Ag and Au mass (P>0.05); however, we observed exposure effects on the dosimetric dose of Ag and Au mass, with the highest dosimetric dose of Ag and Au mass detected at the acute 24 h exposure (P<0.001). Additionally, we observed G×P effects on the dosimetric dose of Ag and Au mass at the acute 24 h exposure and the subacute 5×4 h exposure (P<0.001). We did not observe a linear relationship between the nominal dose of AgNP mass and the dosimetric dose of Ag:Au mass **(Figure 3E-F; Supplementary Data)** for AJ:Normal, B6:Normal, AJ:T2-Skewed, and B6:T2-Skewed at the acute 24 h exposure and the subacute 5×4 h exposure. We did not observe genotype or exposure effects on the dosimetric dose of Ag:Au mass (P>0.05); however, we observed phenotype effects on the dosimetric dose of Ag:Au mass, with the lowest dosimetric dose of Ag:Au mass detected in the "T2-Skewed" phenotype (P<0.05). Additionally, we observed G×P effects on the dosimetric dose of Ag:Au mass at the acute 24 h exposure (P<0.05) and the subacute 5×4 h exposure (P<0.001).

Genotype and phenotype effects on AgNP-induced barrier dysfunction

We compared genotype, phenotype, and exposure effects for nominal and dosimetric dose-response relationships for TEER as a measure of barrier function. We observed negative dose-response relationships for AgNP-induced barrier dysfunction for AJ:T2-Skewed at the acute 24 h exposure and the subacute 5×4 h exposure (P<0.001) **(Figure 4; Supplementary Data).** We observed genotype and phenotype effects on AgNP-induced barrier dysfunction (P<0.001), with increased sensitivity to barrier dysfunction detected in AJ:T2-Skewed. We did not observe exposure effects on AgNP-induced barrier dysfunction (P>0.05); however, we observed G×P effects on AgNP-induced barrier dysfunction at the acute 24 h exposure and the subacute 5×4 h exposure (P<0.001).

Genotype and phenotype effects on AgNP-induced GSH depletion

We compared genotype, phenotype, and exposure effects for nominal and dosimetric dose-response relationships for NDA fluorescence as a measure of GSH content. We observed negative dose-response relationships for AgNP-induced GSH depletion for

AJ:Normal, B6:Normal, AJ:T2-Skewed, and B6:T2-Skewed at the acute 24 h exposure and the subacute 5×4 h exposure (P<0.001 - P<0.05) **(Figure 5; Supplementary Data).** We observed genotype and phenotype effects on AgNP-induced GSH depletion (P<0.001), with increased sensitivity to GSH depletion detected in AJ:T2-Skewed. We did not observe exposure effects on AgNP-induced GSH depletion (P>0.05); however, we observed G×P effects on AgNP-induced GSH depletion at the acute 24 h exposure and the subacute 5×4 h exposure (P<0.001).

Genotype, phenotype, and exposure effects on AgNP-induced ROS production

We compared genotype, phenotype, and exposure effects for nominal and dosimetric dose-response relationships for DCF fluorescence as a measure of ROS production. We observed positive dose-response relationships for AgNP-induced ROS production for AJ:Normal, B6:Normal, AJ:T2-Skewed, and B6:T2-Skewed at the acute 24 h exposure and the subacute 5×4 h exposure (P<0.001) **(Figure 6; Supplementary Data).** We observed genotype, phenotype, and exposure effects on AgNP-induced ROS production (P<0.001), with increased sensitivity to ROS production detected in AJ:T2-Skewed at the acute 24 h exposure. Additionally, we observed G×P effects on AgNP-induced ROS production at the acute 24 h exposure and the subacute 5×4 h exposure (P<0.001).

Genotype, phenotype, and exposure effects on AgNP-induced lipid peroxidation

We compared genotype, phenotype, and exposure effects for nominal and dosimetric dose-response relationships for MDA fluorescence as a measure of lipid peroxidation. We observed positive dose-response relationships for AgNP-induced lipid peroxidation for AJ:Normal, B6:Normal, AJ:T2-Skewed, and B6:T2-Skewed at the acute 24 h exposure and the subacute 5×4 h exposure (P<0.001) **(Figure 7; Supplementary Data).** We observed genotype, phenotype, and exposure effects on AgNP-induced lipid peroxidation (P<0.001), with increased sensitivity to lipid peroxidation detected in AJ:T2-Skewed at the acute 24 h exposure. Additionally, we observed G×P effects on AgNP-induced lipid peroxidation at the acute 24 h exposure and the subacute 5×4 h exposure (P<0.001).

Genotype and phenotype effects on AgNP-induced cytotoxicity

We compared genotype, phenotype, and exposure effects for nominal and dosimetric dose-response relationships for LDH absorbance as a measure of cytotoxicity. We observed positive dose-response relationships for AgNP-induced cytotoxicity for AJ:Normal, B6:Normal, AJ:T2-Skewed, and B6:T2-Skewed at the acute 24 h exposure and the subacute 5×4 h exposure (P<0.001) **(Figure 8; Supplementary Data).** We observed genotype and phenotype effects on AgNP-induced cytotoxicity (P<0.001), with increased sensitivity to cytotoxicity detected in AJ:T2-Skewed. We did not observe exposure effects on AgNP-induced cytotoxicity (P>0.05); however, we observed G×P effects on AgNP-induced cytotoxicity at the acute 24 h exposure and the subacute 5×4 h exposure (P<0.001).

Genotype, phenotype, and exposure effects on sensitivity to AgNP-induced adverse cellular responses

We compared genotype, phenotype, and exposure effects for nominal and dosimetric BMD (BMDL) as a measure of sensitivity to adverse cellular responses by accounting for differences in the effective dose ranges to induce AgNP toxicity. We observed similar patterns of nominal and dosimetric BMD (BMDL) across genotypes, phenotypes, and exposures for each adverse cellular response **(Figure 9; Supplementary Data).** The most sensitive adverse cellular response across nominal and dosimetric dose-response relationships was marked by the lowest effective dose to induce AgNP toxicity, which was ROS production at the acute 24 h exposure and the subacute 5×4 h exposure.

3.6 DISCUSSION

This is the first study to use organotypic cultures as a high-content *in vitro* model of the conducting airway to characterize G×P effects on AgNP toxicity. We characterized nominal and dosimetric dose-response relationships for AgNP-induced barrier dysfunction, GSH depletion, ROS production, lipid peroxidation, and cytotoxicity across genotypes, phenotypes, and exposures to understand G×P effects on AgNP toxicity. Across each of the nominal and dosimetric dose-response relationships, we observed increased sensitivity to AgNP toxicity under AJ:T2-Skewed at the acute 24 h exposure. We observed higher dosimetric doses of Ag and Au mass under the “T2-Skewed”

phenotype at the acute 24 h exposure and lower dosimetric doses of Ag:Au mass under the “T2-Skewed” phenotype at the subacute 5×4 h exposure, suggesting that phenotype and exposure effects on association and dissolution are greatest for the “T2-Skewed” phenotype at acute and subacute exposures, respectively. The dosimetric dose of Ag:Au mass is an indirect measurement of the colocation of Ag and Au mass, and a low Ag:Au mass suggests that the two metals have separated through dissolution, potentially leading to increased AgNP bioavailability and bioactivity. We used a BMD approach to characterize G×P effects on the sensitivity of adverse cellular responses by accounting for differences in the effective dose ranges to induce AgNP toxicity across genotypes, phenotypes, and exposures, and identified ROS production as the most sensitive adverse cellular response at the acute 24 h exposure and the subacute 5×4 h exposure.

These data suggest that phenotype and exposure effects on AgNP particokinetics are greatest for the “T2-Skewed” phenotype at the acute 24 h exposure, rather than the subacute 5×4 h exposure. For the subacute 5×4 h exposure, when the delivered dose was separated across days, the peak exposures per day seemed to drive the overall exposure. The subacute 5×4 h exposure was chosen to model a work-week exposure scenario, as previous studies have suggested a potential high-risk for AgNP exposures in occupational settings.[32,38-41] Together, this highlights the importance of using multiple genotypes, phenotypes, and exposures when screening and prioritizing other potential respiratory toxicants in order to produce more biologically robust predictions of adverse organism responses resulting from occupational exposures.[119]

We used dosimetric dose-response relationships to account for genotype, phenotype, and exposure effects on AgNP particokinetics and/or airway physiology of organotypic cultures. However, when we used these data to derive dosimetric BMD (BMDL), the sensitivity of the “T2-Skewed” phenotype decreased for the acute 24 h exposure but increased (alongside the “Normal” phenotype) for the subacute 5×4 h exposure. This suggests the importance of considering exposure effects on AgNP toxicity. While electron microscopy may better inform whether these genotype, phenotype, and exposure effects on association and dissolution lead to differences in uptake of whole particles, the approach used in the present study allowed for the detection of AgNP toxicity that can be

translated to physiologically-relevant units measurable in occupational settings.

While we addressed some of these differences in AgNP particokinetics and/or airway physiology using dosimetric dose-response relationships, the *in vitro* to *in vivo* extrapolation (IVIVE) from organotypic cultures to the lungs may still exhibit significant variability. This was highlighted by Bachler et al., who developed a physiologically-based pharmacokinetic/toxicokinetic (PBPK) model for AgNP toxicity in various organ systems. For the lungs, the authors calibrated their human respiratory tract model to estimate the deposition fraction of inhaled particles from 1 to 1000 nm among the extrathoracic, endothoracic, bronchial, bronchiolar, and alveolar-interstitial compartments, and accounted for mucociliary clearance as well as time-dependent uptake of particles to the systemic blood circulation.[168] While deposition and dissolution can occur throughout the conducting and respiratory airways, deposition in the conducting airway of healthy individuals will be reduced by mucociliary clearance, with a fraction of deposited Ag mass undergoing dissolution upon inhalation. However, this host defense mechanism may be impaired in individuals with pre-existing chronic respiratory diseases, and raises the potential for increased deposition, dissolution, and thus AgNP toxicity. This could be evaluated in future studies using healthy and allergic mice that also incorporate IVIVE or PBPK models to derive human equivalent concentrations (HEC). Weldon et al. used HEC based upon the dosimetric dose of Ag mass associated in the lungs, which showed the highest retention time and burden compared to other organs as reported in the *in vivo* study by Sung et al., to derive a health-based occupational exposure limit (OEL) of 0.19 μg AgNP/m^3.[119] Together, this highlights the importance of considering PBPK parameters within sensitive populations when deriving dose-response relationships, HEC, and OEL which can be used to contribute relevant data and efficient characterization toward risk assessment for occupational exposures.

Our observations were supported by previous *in vitro* and *in vivo* studies on the effects of host genetic and acquired factors on ENM toxicity. With regard to host genetic factors, Weldon et al. exposed organotypic cultures derived from primary murine embryonic midbrain cells, and observed size, coating, genotype, and developmental stage effects on AgNP-induced cytotoxicity, with A/J and C57BL/6J mice being differentially sensitive

genotypes.[165] Scoville et al. exposed eight genotypes of male mice and observed genotype effects on quantum dot (QD)-induced T2 lung inflammation, with A/J and C57BL/6J mice being the most differentially sensitive genotypes. The authors quantified dosimetric doses of cadmium (Cd) mass in the lungs of these differentially sensitive genotypes and detected higher burdens in A/J mice compared to C57BL/6J mice, suggesting that airway physiology (marked by alveolar size and airway branching) may be a contributing factor in genotype effects on QD toxicity—which may be broadly applicable to other types of ENM, such as AgNP.[75-77] With regard to host acquired factors, Chuang et al. treated OVA-sensitized, female BALB/cJ mice by inhalation and observed antigen effects on AgNP-induced oxidative stress in allergic mice compared to healthy mice and fresh air controls, with allergic and healthy mice being differentially sensitive to AgNP toxicity.[82] In a similar study, Alessandrini et al. exposed OVA-sensitized, female BALB/cJ mice by tracheal instillation and observed size, coating, dose, and antigen effects on AgNP-induced T2 lung inflammation in allergic mice compared to healthy mice and vehicle controls, with allergic and healthy mice also being differentially sensitive to AgNP toxicity.[86] Interestingly, the authors observed AgNP-induced T2 lung inflammation in a biphasic manner, with $AgNP_{CIT200}$ and $AgNP_{PVP200}$ attenuating T2 lung inflammation, and $AgNP_{CIT50}$ and $AgNP_{PVP50}$ exacerbating T2 lung inflammation. In the present study; we observed genotype effects to be more understated than phenotype effects on baseline characterization of organotypic cultures. However, we observed G×P effects on AgNP toxicity and therefore suggest these were primarily driven by phenotype rather than genotype effects on AgNP toxicity.

The “T2-Skewed” phenotype’s sensitivity to AgNP toxicity may be attributed to increased association and dissolution, which can be mediated by particle interactions with chloride ions (Cl^-) within secreted mucus. Yasuo et al. observed IL-13 induced upregulation of *Muc5ac* and calcium-activated chloride channel 1 (*Clca1*) when skewing differentiation of airway epithelial cells.[169] Therefore, under the “T2-Skewed” phenotype, IL-13 may induce upregulation of *Clca1* in addition to *Muc5ac*, potentially leading to increased AgNP bioavailability and bioactivity. The “T2-Skewed” phenotype’s sensitivity to AgNP toxicity may also be attributed to impaired ion transport, which can be mediated by amiloride-sensitive epithelial Na^+ channel (ENaC) activity. Kimura et al. observed E3 ubiquitin-

protein ligase NEDD4-like (*Nedd4l*) regulates ENaC activity in the lungs, and under normal conditions, it inhibits ENaC activity to prevent T2 airway inflammation.[170] Campbell et al. observed a positive association between a 6 kbp deletion in an intron of *Nedd4l* and the odds of asthma (Odds Ratio [OR] = 3.13; $P<0.05$);[171] and as a critical mediator of asthma, IL-13 may induce downregulation of *Nedd4l* to promote ENaC activity and T2 airway inflammation.

The "T2-Skewed" phenotype's sensitivity to AgNP toxicity may also be attributed to GSH depletion, which can be mediated by T2 responses and/or NF-κB activation. Nam et al. observed IL-13 induced NADPH oxidase activity and iNOS to promote ROS/RNS production and GSH depletion in hippocampal neurons.[172] Although no studies have confirmed this mechanism of IL-13-induced GSH depletion in airway epithelial cells, GSH depletion has been shown to promote T2 responses during chronic respiratory diseases. Kato et al. observed endocrine disrupting chemicals induced both GSH depletion and reciprocal regulation of IL-10/IL-12 production in airway epithelial cells.[173] Reductive redox status, marked by high levels of GSH content, has been shown to promote IL-12 production via MAPK signaling in monocytes,[174] whereas oxidative redox status, marked by low levels of GSH content, has been shown to promote IL-10 production via NF-κB activation in monocytes, B cells, T cells, and NK cells.[175,176] The "T2-Skewed" phenotype was marked by oxidative redox status, and thus AgNP-induced pro-inflammatory cytokine production likely contributed toward higher levels of ROS production, and potentially toward inhibition of GSH synthesis enzymes. GSH has regulatory mechanisms in apoptosis, vascularisation, mitochondrial integrity, and the immune system. GSH is not only inhibitory for the pro-inflammatory response to respiratory toxicants, it is critical for mounting innate and adaptive immune responses, including: T-lymphocyte proliferation,[177] polymorphonuclear leukocyte phagocytosis, and dendritic cell functions such as antigen presentation, degradation, and processing which depend upon the GSH-mediated reduction of disulfide bonds.[178,179] Although GSH inhibits the production of most pro-inflammatory cytokines, it is required to maintain sufficient IFN-γ production by dendritic cells.[180] Therefore, the regulatory mechanisms of GSH in the immune system might explain why in chronic respiratory diseases, including asthma, acute bronchitis, and COPD, GSH depletion is associated with T1/T2 imbalance and an increased sensitivity

to occupational exposures.[181] No studies have confirmed these mechanisms of GSH depletion-induced T2 responses in organotypic cultures. These hypotheses should be tested in future studies to better understand G×P effects on association, dissolution, impaired ion transport, and GSH depletion in relation to AgNP toxicity.

This is the first study to use organotypic cultures as a high-content *in vitro* model of the conducting airway to characterize G×P effects on AgNP toxicity, and therefore, refining this *in vitro* model in future studies is warranted. One limitation of this study was our use of only one sex and two genotypes; the use of both sexes and additional genotypes (e.g., BALB/cJ and SWR/J mice) or knockouts (e.g., *Nedd4l*$^{-/-}$ or *Nfkb1*$^{-/-}$ *mice*) would increase genetic diversity and assist in defining a mechanistic basis for G×P effects on AgNP toxicity in future studies. A second limitation of this study was our use of IL-13 to skew differentiation toward an *in vitro* model of chronic respiratory diseases; the use of co-cultures with relevant cell populations, including mast cells or type 2 innate lymphoid cells (ILC2), would increase cellular diversity and improve the physiological relevance of this *in vitro* model in future studies. A third limitation of this study was our administration of the nominal dose of AgNP using suspensions in defined differentiation media. This approach may have contributed to their dissolution; the use of a Nano Aerosol Chamber for *in vitro* Toxicity studies (NACIVT) would allow for direct deposition of ENM onto the apical surface of organotypic cultures;[50,61,182] or alternatively, the use of microfluidic systems would improve our understanding of the kinetics and dynamics of the conducing airway in future studies.[183] Both approaches would allow this *in vitro* model to better recapitulate the physiological conditions of AgNP exposures in occupational settings.

Despite these limitations, this study establishes organotypic cultures derived from MTEC as a medium-throughput, high-content *in vitro* model for the conducing airway to characterize chemical perturbation as a means to screen and prioritize potential respiratory toxicants. Our results highlight the importance of considering dosimetry as well as G×P effects when screening and prioritizing potential respiratory toxicants. This is challenging and important for ENM, since their MoA have been shown to differ considerably but are still used in hundreds of consumer products. Prior to anticipating potential adverse organism responses arising from ENM toxicity, ensuring safe

development of the consumer products in which they are used will be the most critical and necessary step toward safeguarding public health.

AUTHOR CONTRIBUTIONS

The manuscript was written through contributions of all authors. All authors have given approval to the final version of the manuscript.

FUNDING SOURCES

This work was supported by the US EPA under Grant R835738 (E.M.F., T.J.K., W.A.A); NIH under Grants P30 ES007033 (T.J.K.) and T32 ES007032-38 (T.P.N.); the Washington State Department of Labor and Industries under the Medical Aid/Accident Fund; (T.P.N.) and the University of Washington under the GO-MAP Dissertation Fellowship (T.P.N.).

NOTES

The authors declare no competing financial interest.

ACKNOWLEDGEMENTS

The authors gratefully acknowledge Dowon An for her technical support with animals, and Brian Johnson for his technical support with immunohistochemistry. Part of this work was conducted at the Environmental Health Laboratory, a National Nanotechnology Coordinated Infrastructure site at the University of Washington which is supported in part by the Washington State Department of Labor and Industries. Part of this work was conducted at the Molecular Analysis Facility, a National Nanotechnology Coordinated Infrastructure site at the University of Washington which is supported in part by the National Science Foundation under Grant NNCI-1542101, the University of Washington, the Molecular Engineering & Sciences Institute, and the Clean Energy Institute.

3.7 DATA

$$Y_i = A + BX_i + R_i + E_i$$
$$R_i \sim N(0, r) \; and \; E \sim (0, s) for \; i = 1 \ldots sample$$

$$\text{BMD} = \frac{\sigma}{\text{B}}$$

$$\text{BMDL} = \left(\frac{\sigma}{\text{Upper Limit}_{95\% \text{ CI}}}, \frac{\sigma}{\text{Lower Limit}_{95\% \text{ CI}}} \right)$$

Equation 3.1. Nominal and dosimetric BMD (BMDL). Y_i = adverse cellular response, A = intercept, B = slope, X_i = dose, R_i = random effect of preparation date for i^{th} sample, r = variance for random effects, s = residual variance for fixed effects, σ = population variability.

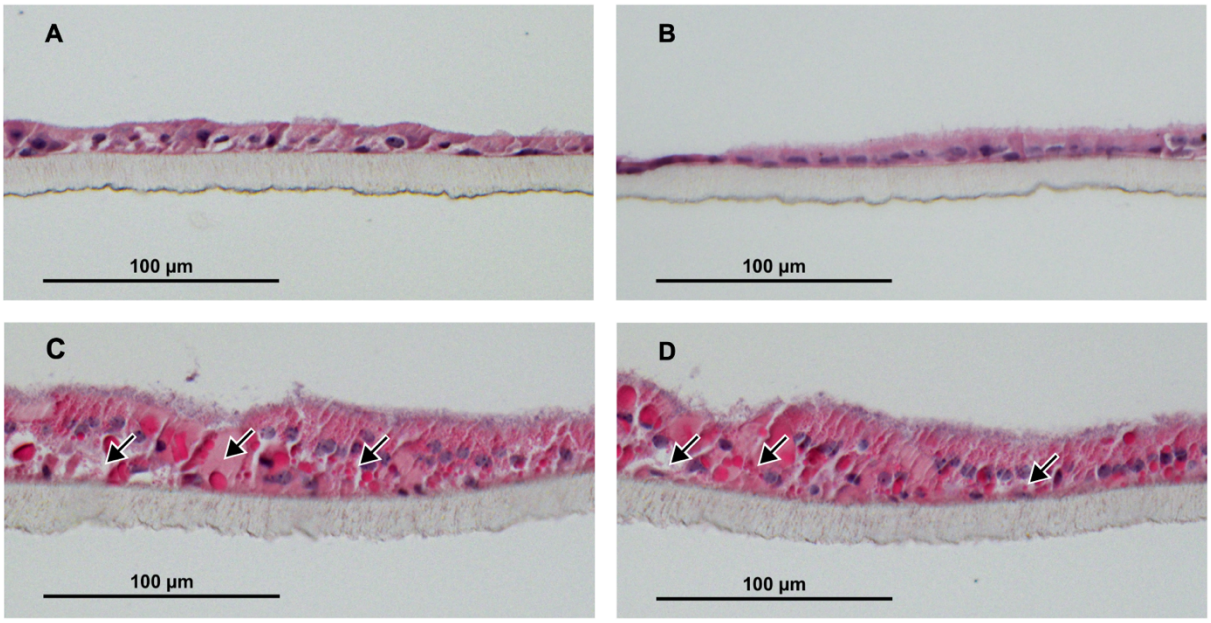

Figure 3.1. The "T2-Skewed" phenotype is characterized by baseline organotypic morphology associated with clinical features of chronic respiratory diseases, or a pseudostratified columnar epithelium with an abundance of epithelial glycoproteins. Representative H&E staining of untreated organotypic cultures **(A)** AJ:Normal, **(B)** B6:Normal, **(C)** AJ:T2-Skewed, and **(D)** B6:T2-Skewed on DIV 28. Scale bar: 100 µm. Arrows: epithelial glycoproteins.

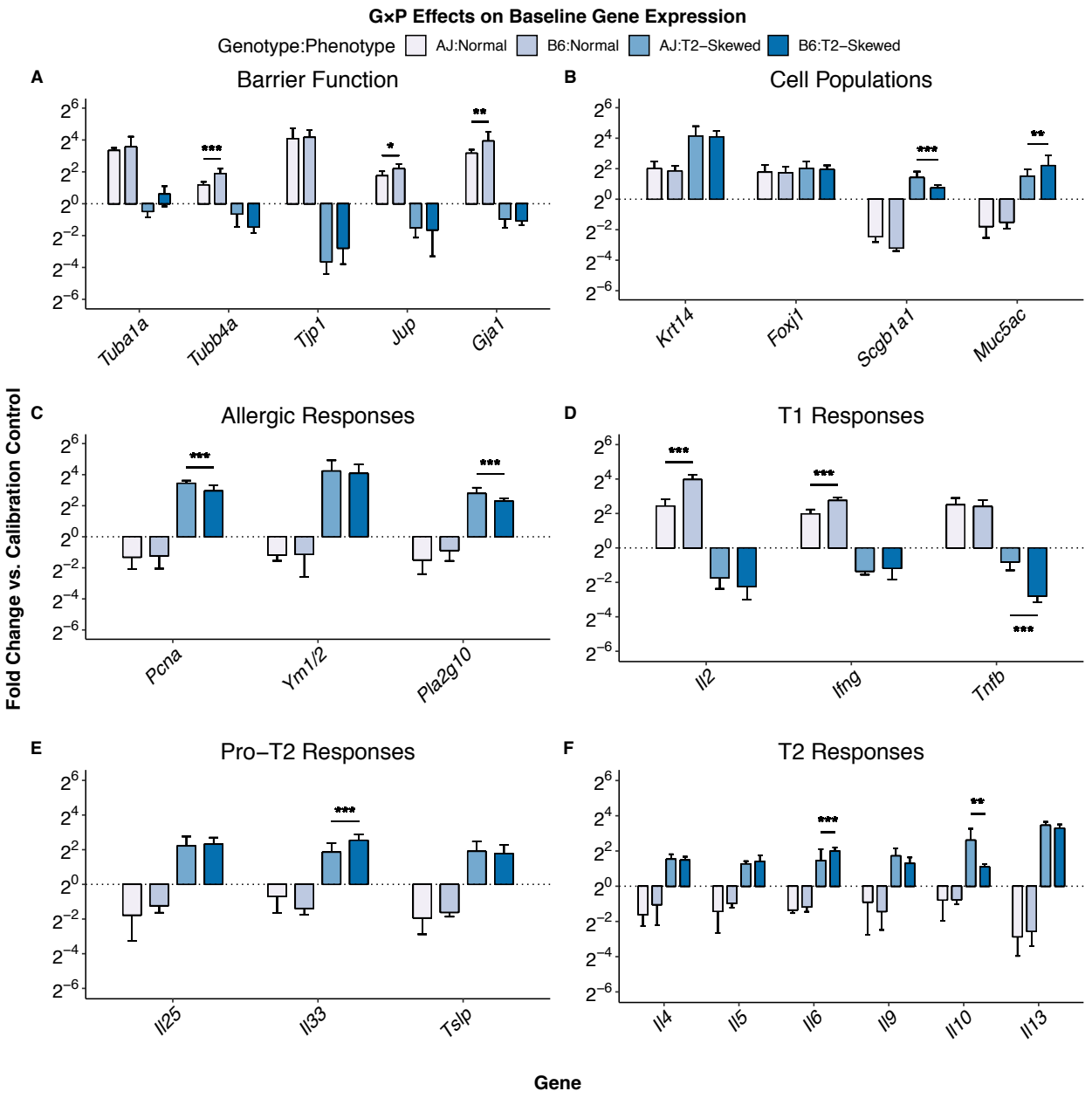

Figure 3.2. The "T2-Skewed" phenotype is characterized by baseline gene expression associated with clinical features of chronic respiratory diseases, including barrier dysfunction, mucus production, allergic responses, and T2 responses. Total RNA was isolated from untreated organotypic cultures on DIV 28, and cDNA was subjected to qRT-PCR analysis for gene expression of markers associated with **(A)** barrier function, **(B)** cell populations, **(C)** allergic responses, **(D)** T1 responses, **(E)** pro-T2 responses, and **(F)** T2 responses. The fold change in gene expression was compared between genotypes (asterisks) for each phenotype. *n* = 3 biological replicates with technical replicates. Data represent mixed effects estimate ± 95% CI; NS (P>0.05); * (P<0.05); *** (P<0.001).

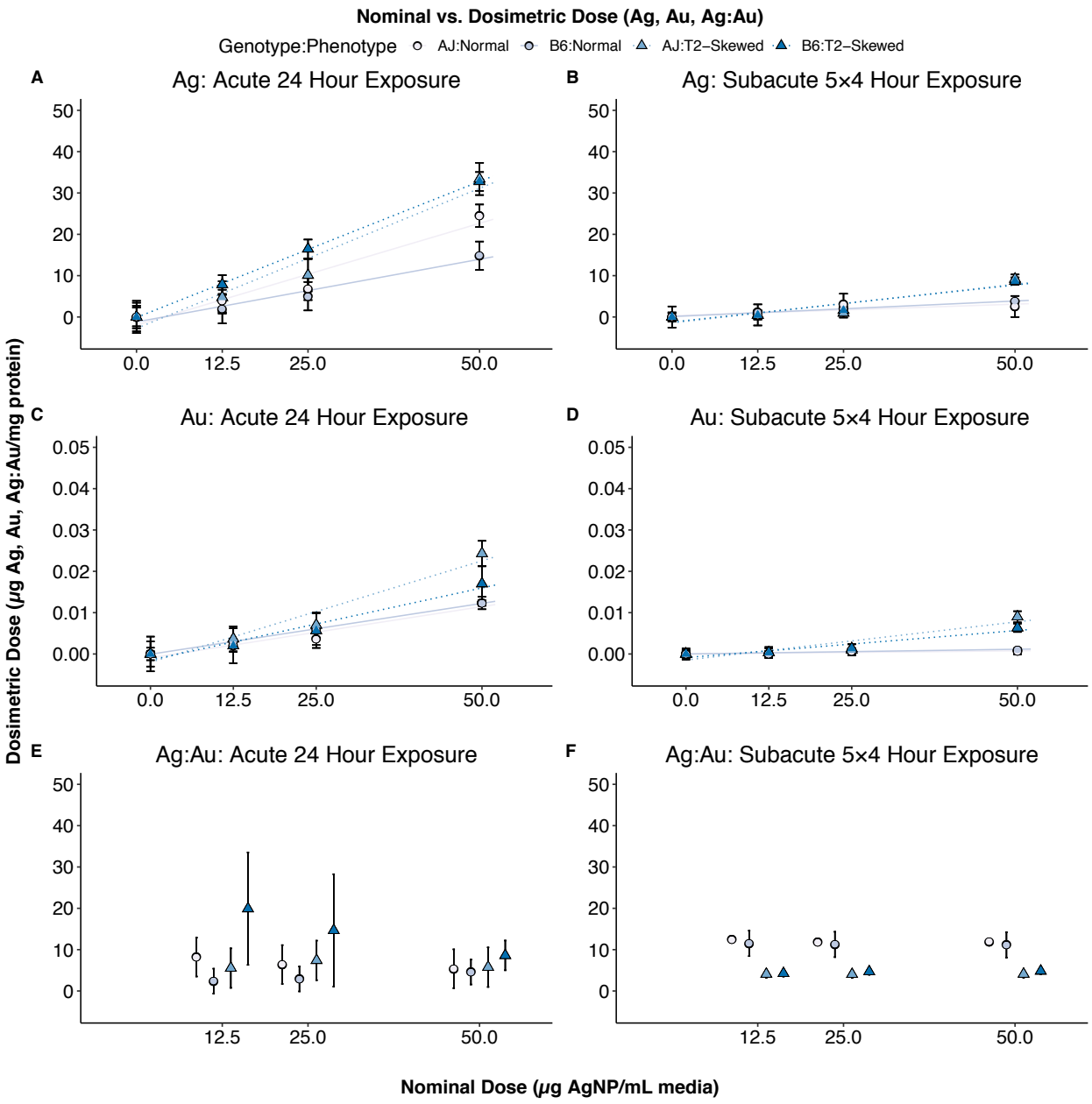

Figure 3.3. Phenotype and exposure effects on the linear relationship between the nominal dose of AgNP mass and the dosimetric doses of Ag, Au, and Ag:Au mass. Organotypic cultures were exposed to nominal doses of 0, 12.5, 25, or 50 μg AgNP/mL media for an acute 24 h exposure and a subacute 5×4 h exposure, and cell lysates were subjected to ICP-MS analysis for dosimetric doses of Ag **(A, B)**, Au **(C, D)**, and Ag:Au **(E, F)** mass. Dosimetric doses of Ag and Au mass were normalized to the protein content and were then divided to derive dosimetric doses of Ag:Au mass. *n* = 3 biological replicates. Data represent mixed effects estimate ± 95% CI.

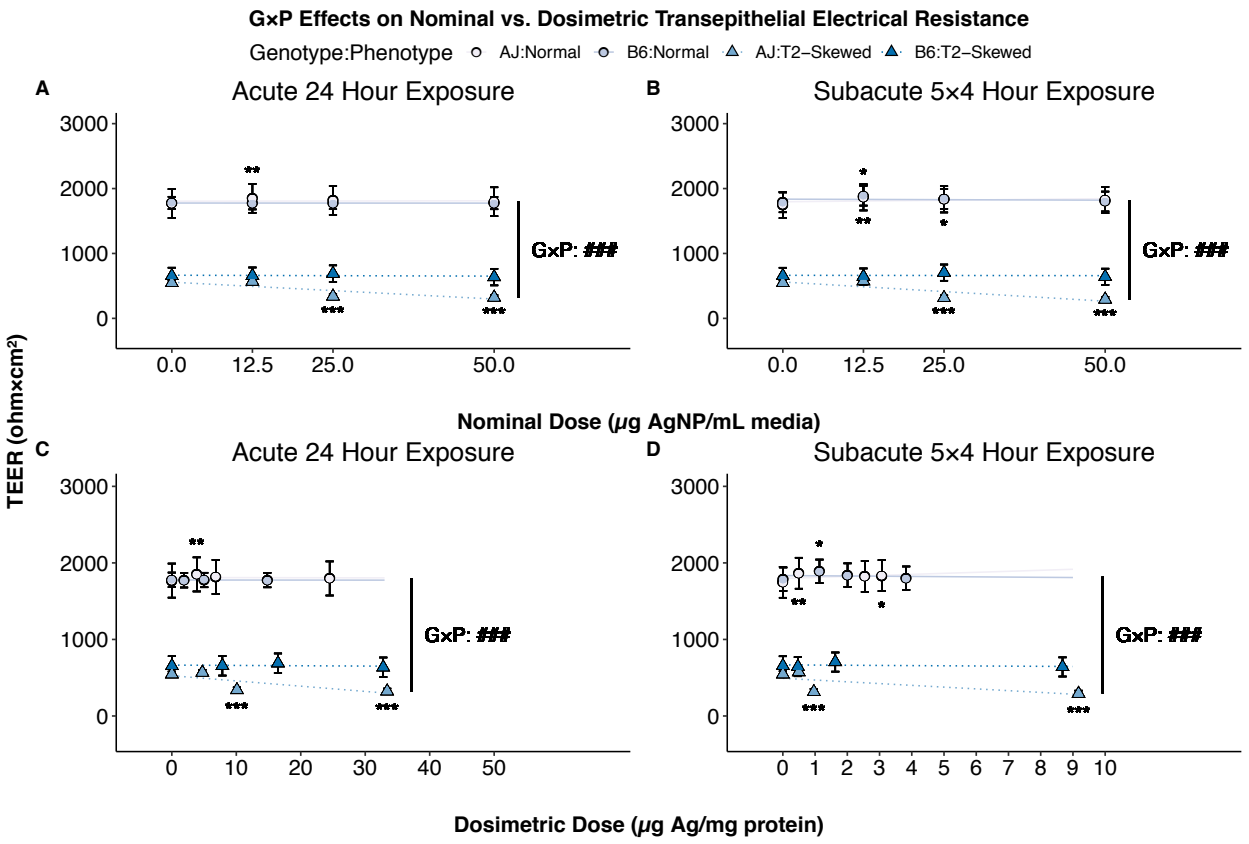

Figure 3.4. Genotype and phenotype effects on AgNP-induced barrier dysfunction. TEER, a non-specific method to assay barrier function in epithelial monolayers, was assayed in organotypic cultures exposed to nominal doses of 0, 12.5, 25, or 50 µg AgNP/mL media for an acute 24 h exposure and a subacute 5×4 h exposure. TEER was normalized to the background resistance and area of the semi-permeable transwell membrane, then compared to vehicle controls (asterisks) across genotypes and phenotypes; G×P effects were compared across genotypes and phenotypes (pounds) for each exposure across nominal **(A, B)** and dosimetric **(C, D)** dose-response relationships. *n* = 3 biological replicates with technical replicates. Data represent mixed effects estimate ± 95% CI; NS (*P*>0.05); * (*P*<0.05); ** (*P*<0.01); *** (*P*<0.001); ### (*P*<0.001).

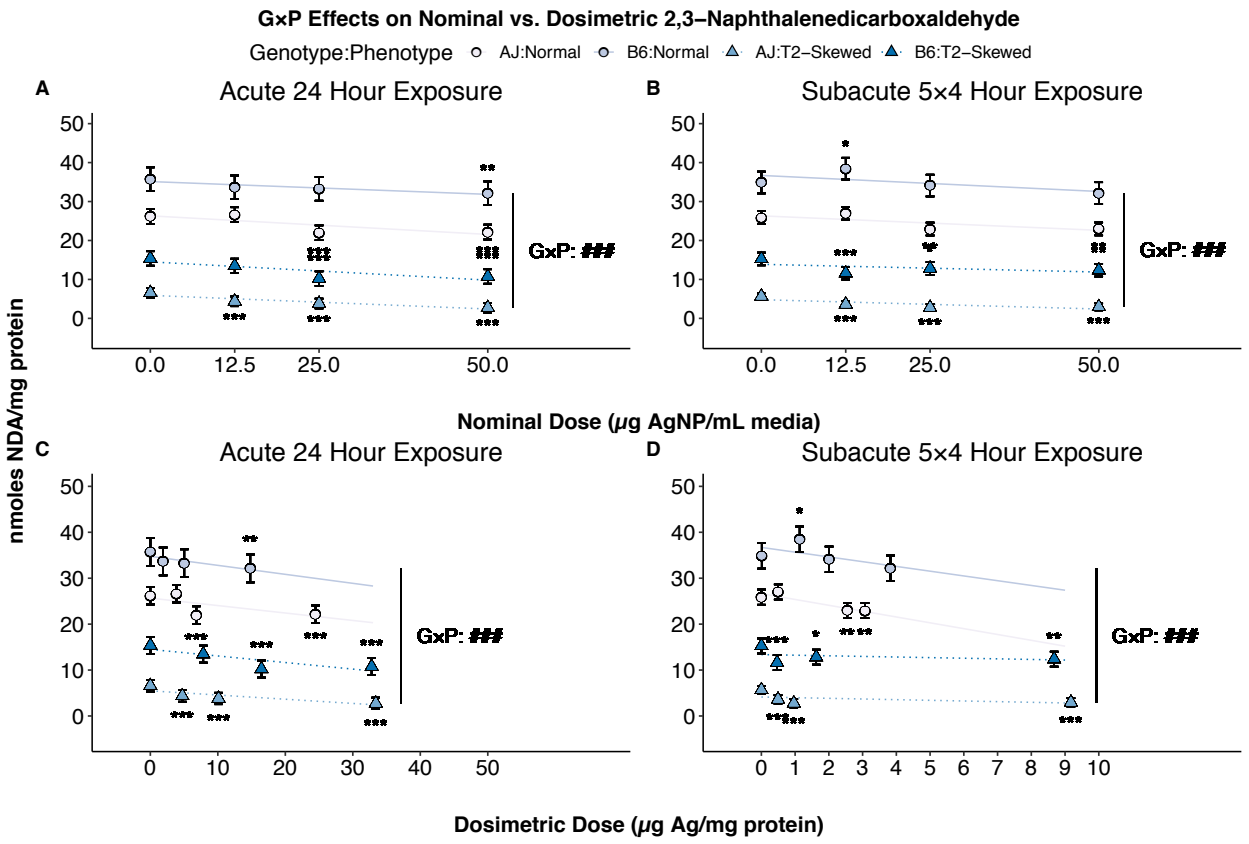

Figure 3.5. Genotype and phenotype effects on AgNP-induced GSH depletion. NDA fluorescence, a specific method to assay dissolved GSH concentrations in media, was assayed in organotypic cultures exposed to nominal doses of 0, 12.5, 25, or 50 μg AgNP/mL media for an acute 24 h exposure and a subacute 5×4 h exposure. NDA fluorescence was normalized to the protein content, then compared to vehicle controls (asterisks) across genotypes and phenotypes; G×P effects were compared across genotypes and phenotypes (pounds) for each exposure across nominal **(A, B)** and dosimetric **(C, D)** dose-response relationships. *n* = 3 biological replicates with technical replicates. Data represent mixed effects estimate ± 95% CI; NS (*P*>0.05); * (*P*<0.05); ** (*P*<0.01); *** (*P*<0.001); ### (*P*<0.001).

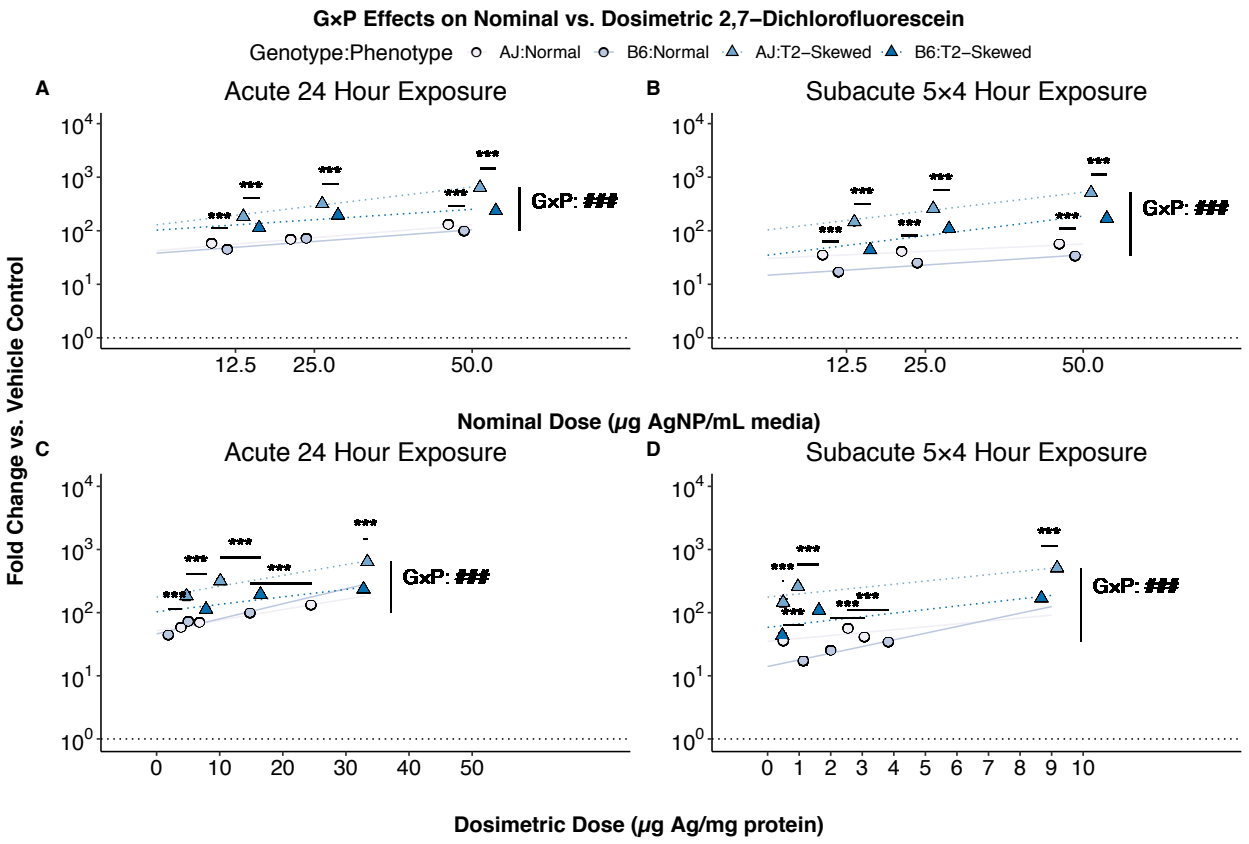

Figure 3.6. Genotype, phenotype, and exposure effects on AgNP-induced ROS production. DCF fluorescence, a non-specific method to assay ROS production in media, was assayed in organotypic cultures exposed to nominal doses of 0, 12.5, 25, or 50 µg AgNP/mL media for an acute 24 h exposure and a subacute 5×4 h exposure. The fold change in DCF fluorescence was normalized to the vehicle controls, then compared between genotypes (asterisks) for each phenotype; G×P effects were compared across genotypes and phenotypes (pounds) for each exposure across nominal **(A, B)** and dosimetric **(C, D)** dose-response relationships. *n* = 3 biological replicates with technical replicates. Data represent mixed effects estimate ± 95% CI; NS (*P*>0.05); *** (*P*<0.001); ### (*P*<0.001).

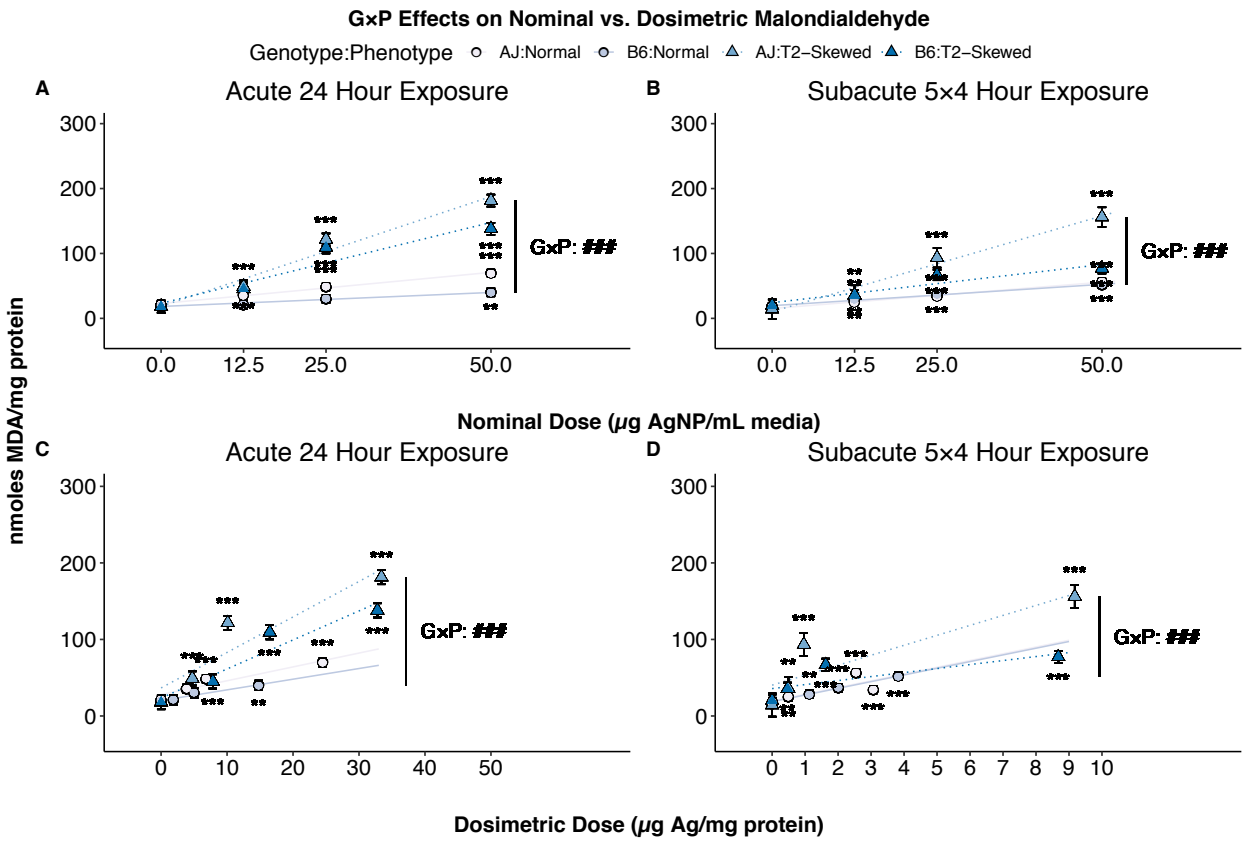

Figure 3.7. Genotype, phenotype, and exposure effects on AgNP-induced lipid peroxidation. MDA fluorescence, a specific method to assay dissolved MDA concentrations in media, was assayed in organotypic cultures exposed to nominal doses of 0, 12.5, 25, or 50 µg AgNP/mL media for an acute 24 h exposure and a subacute 5×4 h exposure. MDA fluorescence was normalized to the protein content, then compared to vehicle controls (asterisks) across genotypes and phenotypes; G×P effects were compared across genotypes and phenotypes (pounds) for each exposure across nominal **(A, B)** and dosimetric **(C, D)** dose-response relationships. *n* = 3 biological replicates with technical replicates. Data represent mixed effects estimate ± 95% CI; NS (*P*>0.05); ** (*P*<0.01); *** (*P*<0.001); ### (*P*<0.001).

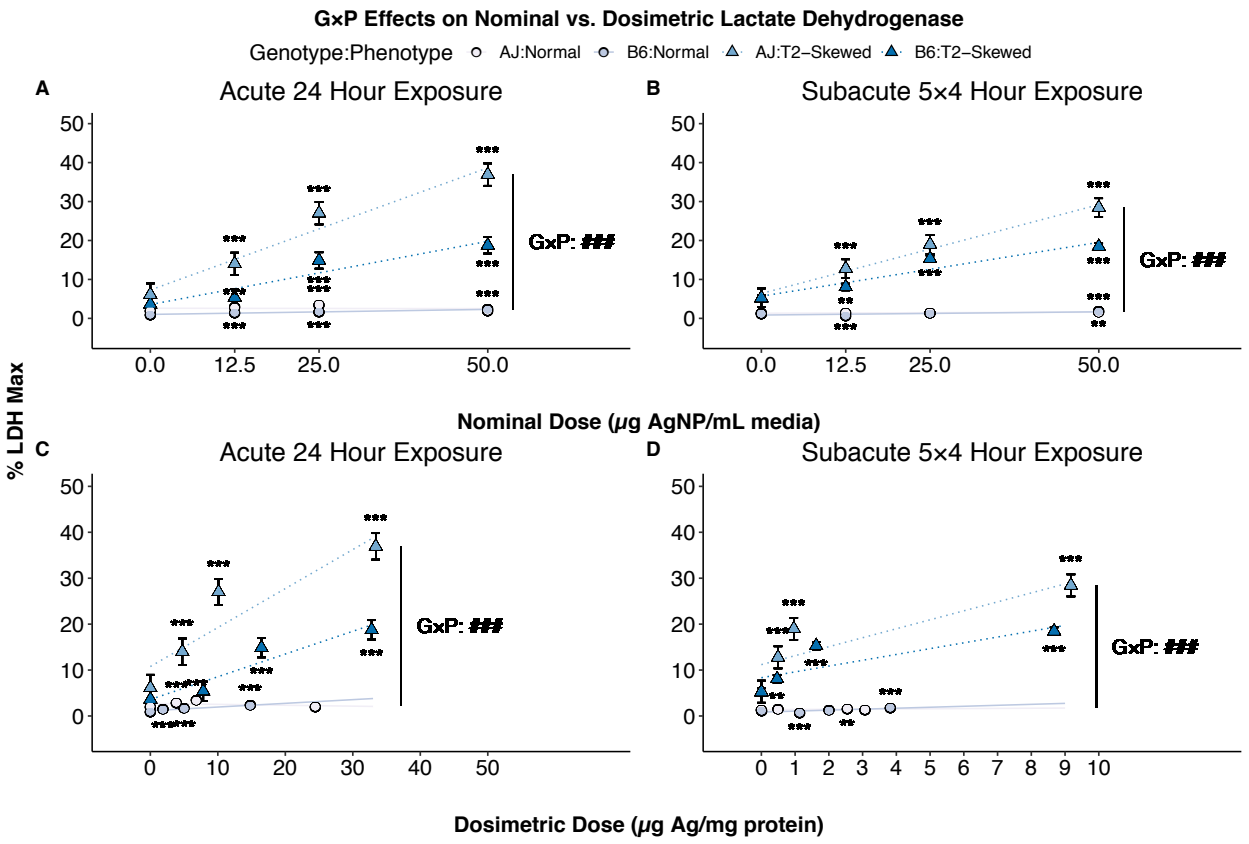

Figure 3.8. Genotype and phenotype effects on AgNP-induced cytotoxicity. LDH absorbance, a specific method to assay dissolved LDH concentrations in media, was assayed in organotypic cultures exposed to nominal doses of 0, 12.5, 25, or 50 µg AgNP/mL media for an acute 24 h exposure and a subacute 5×4 h exposure. LDH absorbance was normalized to positive controls, then compared to vehicle controls (asterisks) across genotypes and phenotypes; G×P effects were compared across genotypes and phenotypes (pounds) for each exposure across nominal **(A, B)** and dosimetric **(C, D)** dose-response relationships. *n* = 3 biological replicates with technical replicates. Data represent mixed effects estimate ± 95% CI; NS (*P*>0.05); * (*P*<0.05); ** (*P*<0.01); *** (*P*<0.001); ### (*P*<0.001).

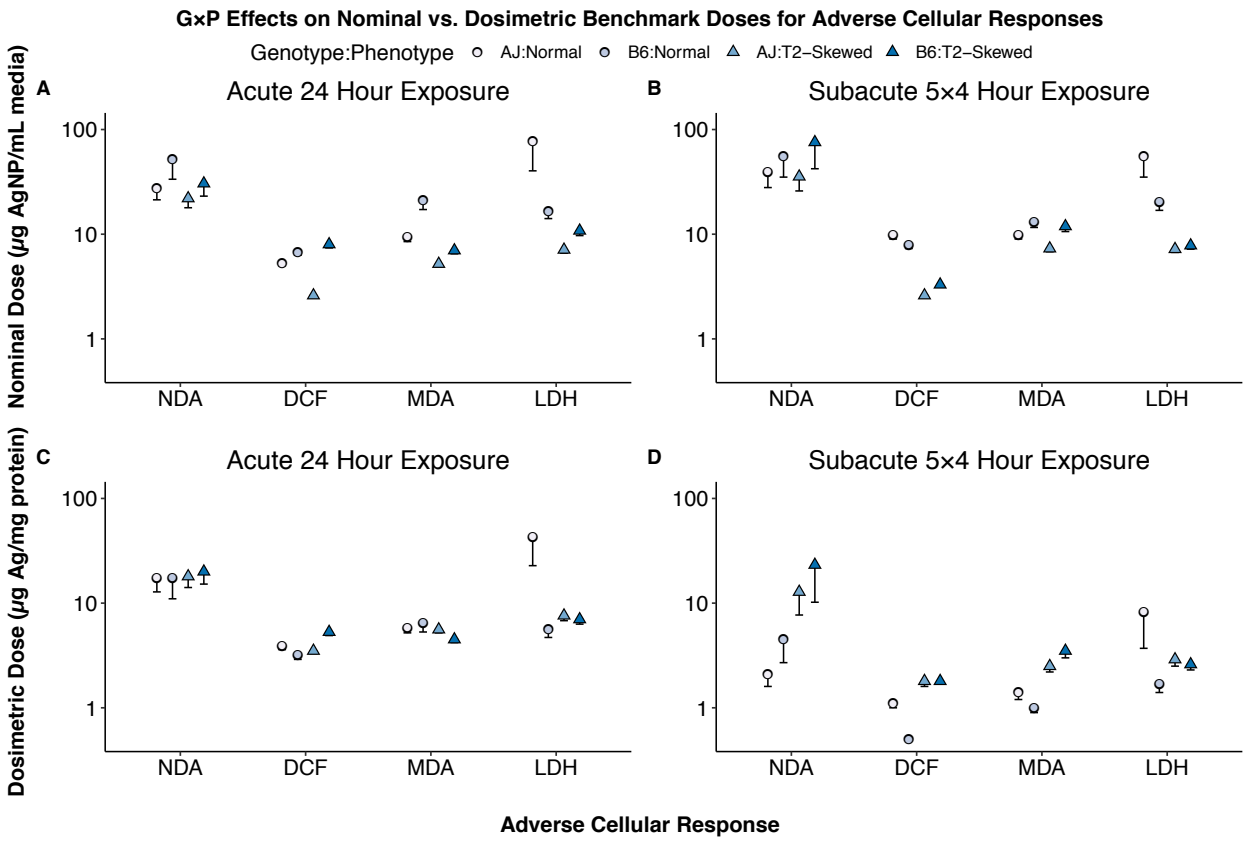

Figure 3.9. Genotype, phenotype, and exposure effects on sensitivity to AgNP-induced adverse cellular responses. BMD (BMDL) were used to compare sensitivity to adverse cellular responses. BMD (BMDL) were derived from significant nominal **(A, B)** and dosimetric **(C, D)** dose-response relationships for each genotype, phenotype, and exposure using the dosimetric dose of Ag mass as a continuous variable. *n* = 3 biological replicates with technical replicates. Data represent BMD - BMDL.

3.8 SUPPLEMENTARY DATA

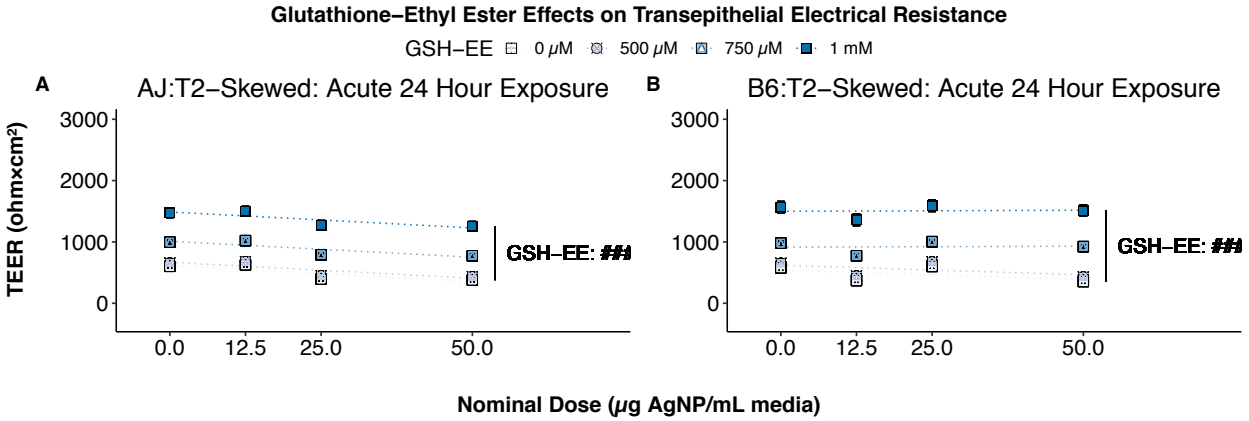

GSH-EE supplementation attenuates AgNP-induced barrier dysfunction. TEER, a non-specific method to assay barrier function in epithelial monolayers, was assayed under the "T2-Skewed" phenotype pre-exposed with concentrations of 0, 500, 750, or 1000 µM GSH-EE for 1 h, and then exposed to nominal doses of 0, 12.5, 25, or 50 µg AgNP/mL media for an acute 24 h exposure. TEER was normalized to the background resistance and area of the semi-permeable transwell membrane, then compared to non-supplemented controls (pounds) for AJ:T2-Skewed **(A)** and B6:T2-Skewed **(B)**. *n* = 3 biological replicates with technical replicates. Data represent mixed effects estimate ± 95% CI; ### (*P*<0.001).

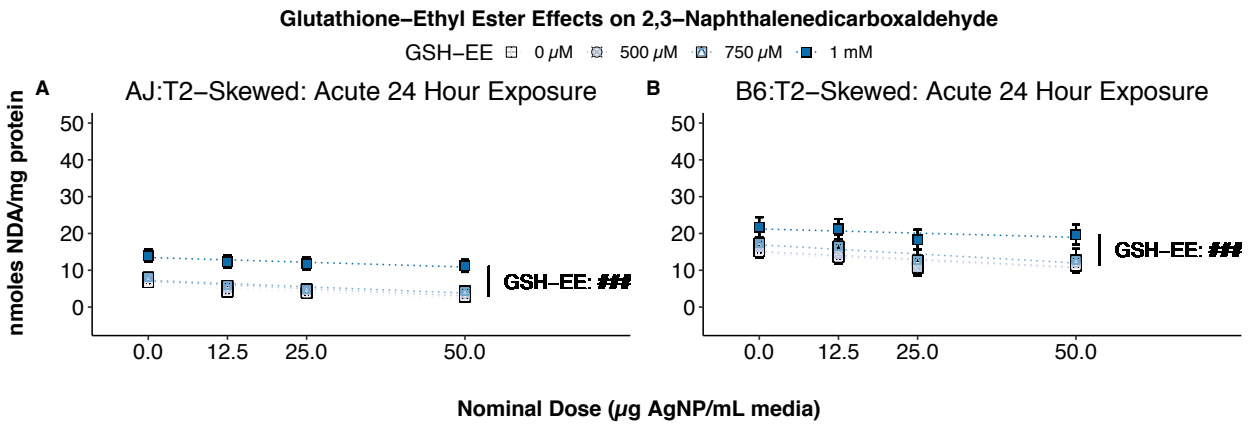

GSH-EE supplementation attenuates AgNP-induced GSH depletion. NDA fluorescence, a specific method to assay dissolved GSH concentrations in media, was assayed under the "T2-Skewed" phenotype pre-exposed with concentrations of 0, 500, 750, or 1000 μM GSH-EE for 1 h, and then exposed to nominal doses of 0, 12.5, 25, or 50 μg AgNP/mL media for an acute 24 h exposure. NDA fluorescence was normalized to the protein content, then compared to non-supplemented controls (pounds) for AJ:T2-Skewed **(A)** and B6:T2-Skewed **(B)**. *n* = 3 biological replicates with technical replicates. Data represent mixed effects estimate ± 95% CI; ### (P<0.001).

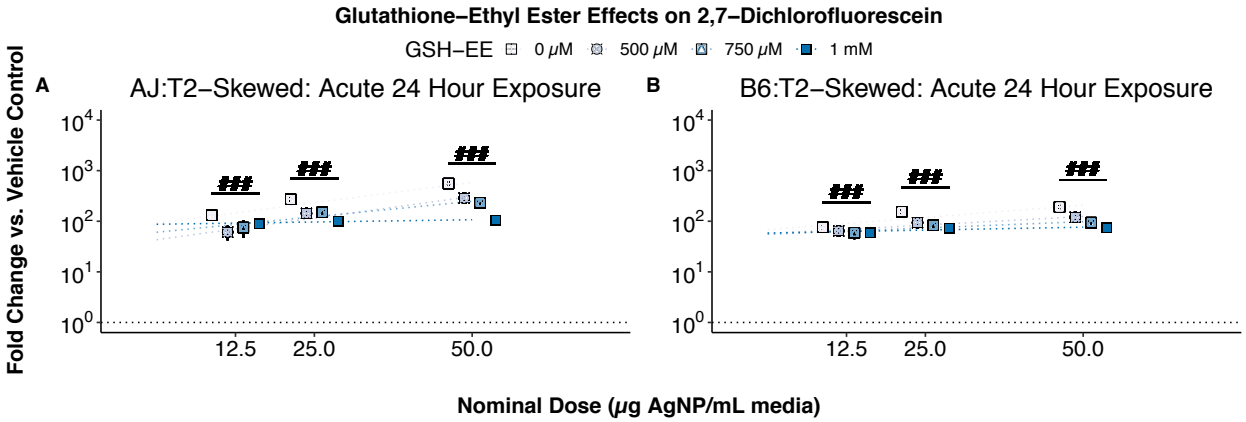

GSH-EE supplementation attenuates AgNP-induced ROS production. DCF fluorescence, a non-specific method to assay ROS production in media, was assayed under the "T2-Skewed" phenotype pre-exposed with concentrations of 0, 500, 750, or 1000 μM GSH-EE for 1 h, and then exposed to nominal doses of 0, 12.5, 25, or 50 μg AgNP/mL media for an acute 24 h exposure. The fold change in DCF fluorescence was normalized to the vehicle controls, then compared to non-supplemented controls (pounds) for AJ:T2-Skewed **(A)** and B6:T2-Skewed **(B)**. *n* = 3 biological replicates with technical replicates. Data represent mixed effects estimate ± 95% CI; ### (*P*<0.001).

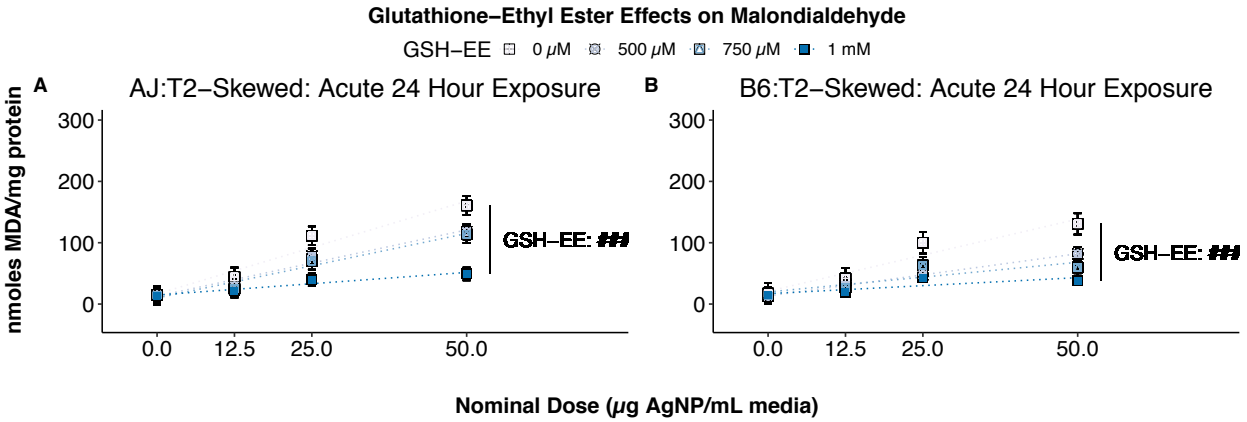

GSH-EE supplementation attenuates AgNP-induced lipid peroxidation. MDA fluorescence, a specific method to assay dissolved MDA concentrations in media, was assayed under the "T2-Skewed" phenotype pre-exposed with concentrations of 0, 500, 750, or 1000 µM GSH-EE for 1 h, and then exposed to nominal doses of 0, 12.5, 25, or 50 µg AgNP/mL media for an acute 24 h exposure. MDA fluorescence was normalized to the protein content, then compared to non-supplemented controls (pounds) for AJ:T2-Skewed **(A)** and B6:T2-Skewed **(B)**. *n* = 3 biological replicates with technical replicates. Data represent mixed effects estimate ± 95% CI; ### (*P*<0.001).

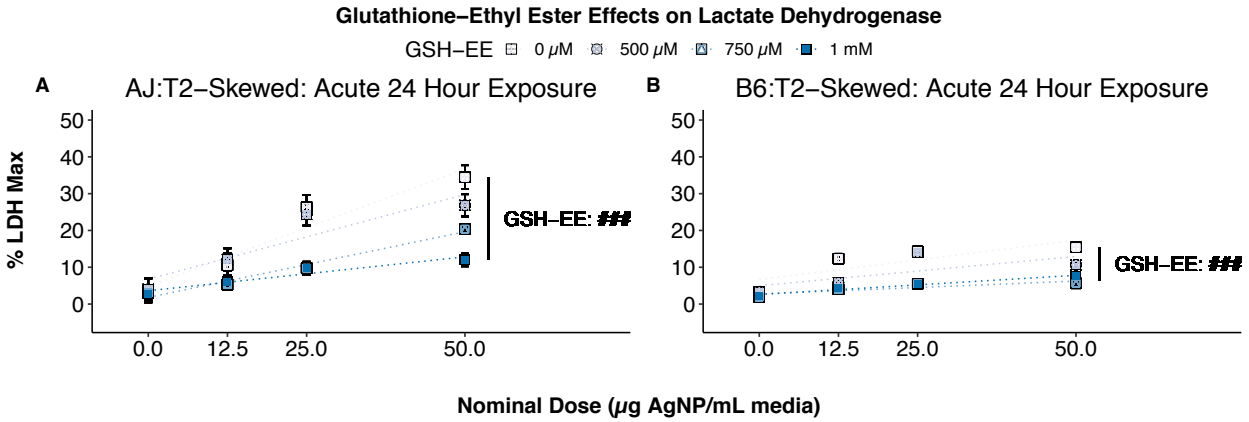

GSH-EE supplementation attenuates AgNP-induced cytotoxicity. LDH absorbance, a specific method to assay dissolved LDH concentrations in media, was assayed under the "T2-Skewed" phenotype pre-exposed with concentrations of 0, 500, 750, or 1000 μM GSH-EE for 1 h, and then exposed to nominal doses of 0, 12.5, 25, or 50 μg AgNP/mL media for an acute 24 h exposure. LDH absorbance was normalized to positive controls, then compared to non-supplemented controls (pounds) for AJ:T2-Skewed **(A)** and B6:T2-Skewed **(B)**. *n* = 3 biological replicates with technical replicates. Data represent mixed effects estimate ± 95% CI; NS (p>0.05); ### (*P*<0.001).

Gene Cluster	Gene	Biological Function	Reference
Barrier Function	*Tuba1a*	Forms and organizes microtubules	184
	Tubb4a	Forms and organizes microtubules	151,184
	Tjp1	Forms tight junctions	151
	Jup	Forms adherens junctions	185
	Gja1	Forms gap junctions	186
Cell Distribution	*Krt14*	Controls production of intermediate filaments	187
	Foxj1	Controls production of motile cilia	188
	Scgb1a1	Controls production and secretion of uteroglobin	189
	Muc5ac	Controls production and secretion of mucus	151,190
Allergic Responses	*Pcna*	Correlated with epithelial thickness	191
	Ym1/2	Inhibits 12(S)-HETE production via 12/15-LOX	192-194
	Pla2g10	Promotes eicosanoid formation and arachidonic release	195,196
T1 Responses	*Il2*	Promotes effector memory, and regulatory T cell differentiation	197
	Infg	Inhibits T2 cell differentiation	198,199
	Tnfb	Activates NF-κB signaling	200
Pro-T2 Responses	*Il25*	Promotes IL-4, IL-5, and IL-13 production to increase eosinophils	201
	Il33	Promotes IL-9 production to induce airway remodeling and hyperresponsiveness	202
	Tslp	Promotes dendritic cell activation to increase regulatory T cells	203
T2 Responses	*Il4*	Promotes B cell activation to increase IgE and T2 cells	198,199
	Il5	Promotes B cell activation to increase IgE and eosinophils	204
	Il6	Promotes B cell activation to increase IgE and neutrophils	205
	Il9	Promotes B cell activation to increase IgE and mast cells	161
	Il10	Inhibits NF-κB signaling	206
	Il13	Promotes B cell activation to increase IgE and mucin cells	156,161,198,207-209

Genes used for baseline characterization of organotypic cultures. Gene: *Tuba1a* (tubulin alpha 1a); *Tubb4a* (tubulin beta 4A class IVa); *Tjp1* (tight junction protein 1); *Jup* (junction plakoglobin); *Gja1* (gap junction protein alpha 1); *Krt14* (keratin 14); *Foxj1* (forkhead box J1); *Scgb1a1* (secretoglobin family 1A member 1) ; *Muc5ac* (mucin 5AC); *Pcna* (proliferating cell nuclear antigen); *Ym1/2* (chitinase-3-like protein 1); *Pla2g10* (group 10 secretory phospholipase A2); *Il2* (interleukin 2); *Ifng* (interferon gamma); *Tnfb* (tumor necrosis factor beta); *Il25* (interleukin 25); *Il33* (interleukin 33); *Tslp* (thymic stromal lymphopoietin); *Il4* (interleukin 4); *Il5* (interleukin 5); *Il6* (interleukin 6); *Il9* (interleukin 9); *Il10* (interleukin 10); *Il13* (interleukin 13).

Exposure	Genotype:Phenotype	Nominal Dose (AgNP)	Dosimetric Dose (Ag)	Dosimetric Dose Au)	Dosimetric Dose (Ag:Au)
24 h	AJ:Normal	0	0.00	0.00	-
		12.5	4.03	0.75	5.41
		25	9.43	1.06	8.90
		50	21.07	4.00	5.27
	B6:Normal	0	0.00	0.00	-
		12.5	1.18	0.78	1.51
		25	2.63	1.67	1.57
		50	20.40	2.98	6.85
	AJ:T2-Skewed	0	0.00	0.00	-
		12.5	5.39	0.94	5.72
		25	8.18	2.37	3.45
		50	29.12	5.04	5.78
	B6:T2-Skewed	0	0.04	0.00	-
		12.5	7.34	0.31	23.76
		25	15.94	0.70	22.81
		50	29.25	5.91	4.95
5×4 h	AJ:Normal	0	0.00	0.00	-
		12.5	0.69	0.06	12.46
		25	7.89	0.70	11.23
		50	3.94	0.33	12.10
	B6:Normal	0	0.01	0.00	22.80
		12.5	1.20	0.10	11.74
		25	1.93	0.17	11.46
		50	3.79	0.33	11.36
	AJ:T2-Skewed	0	0.00	0.00	-
		12.5	0.37	0.09	4.08
		25	0.26	0.06	4.12
		50	7.86	1.87	4.21
	B6:T2-Skewed	0	0.00	0.00	-
		12.5	0.28	0.06	4.58
		25	2.05	0.43	4.73
		50	7.84	1.57	5.01

Nominal dose of AgNP mass vs. dosimetric dose of Ag, Au, and Ag:Au mass. Exposure: h (hours). Genotype:Phenotype: AJ:Normal (A/J, “Normal” phenotype); B6:Normal (C57BL6/J, “Normal” phenotype); AJ:T2-Skewed (A/J, “T2-Skewed” phenotype); B6:T2-Skewed (C57BL6/J, “T2-Skewed” phenotype). Nominal Dose: AgNP (µg AgNP/mL media). Dosimetric Dose: Ag mass (µg Ag/mg protein); Au mass (µg Au/mg protein); Ag:Au mass (µg Ag:Au/mg protein). *n* = 3 biological replicates.

Dosimetric Dose	Exposure	Genotype:Phenotype	Slope (β)	Intercept (B)	Correlation (r^2)	Significance (*P*)
Ag	24 h	AJ:Normal	0.49	-1.98	0.91	***
		B6:Normal	0.30	-1.20	0.83	***
		AJ:T2-Skewed	0.68	-2.76	0.92	***
		B6:T2-Skewed	0.66	-0.12	0.98	***
	5×4 h	AJ:Normal	0.06	0.31	0.24	NS
		B6:Normal	0.08	0.10	0.99	*
		AJ:T2-Skewed	0.19	-1.44	0.82	***
		B6:T2-Skewed	0.18	-1.22	0.87	***
Au	24 h	AJ:Normal	2.48E-04	-9.33E-04	0.91	***
		B6:Normal	2.47E-04	-6.67EE-05	0.99	***
		AJ:T2-Skewed	4.91E-04	-2.00E-03	0.91	***
		B6:T2-Skewed	3.49E-04	-1.47E-03	0.81	***
	5×4 h	AJ:Normal	1.52E-05	0.00E+00	0.29	NS
		B6:Normal	2.29E-05	-1.88E-19	0.73	***
		AJ:T2-Skewed	1.85E-04	-1.47E-03	0.81	***
		B6:T2-Skewed	1.31E-04	-8.67E-04	0.85	***
Ag:Au	24 h	AJ:Normal	-0.01	6.40	0.00	NS
		B6:Normal	0.02	3.23	0.02	NS
		AJ:T2-Skewed	0.01	5.98	0.00	NS
		B6:T2-Skewed	-0.56	33.13	0.22	NS
	5×4 h	AJ:Normal	0.07	8.96	0.40	*
		B6:Normal	-0.19	18.46	0.44	*
		AJ:T2-Skewed	-0.03	5.14	0.30	*
		B6:T2-Skewed	0.03	3.47	0.49	**

Linear mixed effects model parameters of nominal dose of AgNP mass vs. dosimetric dose of Ag, Au, and Ag:Au mass. Dosimetric Dose: Ag mass (µg Ag/mg protein); Au mass (µg Au/mg protein); Ag:Au mass (µg Ag:Au/mg protein). Exposure: h (hours). Genotype:Phenotype: AJ:Normal (A/J, "Normal" phenotype); B6:Normal (C57BL6/J, "Normal" phenotype); AJ:T2-Skewed (A/J, "T2-Skewed" phenotype); B6:T2-Skewed (C57BL6/J, "T2-Skewed" phenotype). *n* = 3 biological replicates. Data represent mixed effects estimate of the linear slope parameters for each model; NS (*P*>0.05); * (*P*<0.05); ** (*P*<0.01); *** (*P*<0.001).

Adverse Cellular Response	Exposure	Genotype:Phenotype	Slope (β)	Intercept (B)	Correlation (r^2)	Significance (*P*)
Barrier dysfunction	24 h	AJ:Normal	0.13	1805.10	0.91	NS
		B6:Normal	-0.03	1776.83	0.86	NS
		AJ:T2-Skewed	-5.20	557.70	0.67	***
		B6:T2-Skewed	-0.28	664.73	0.42	NS
	5×4 h	AJ:Normal	0.96	1796.30	0.81	NS
		B6:Normal	-0.32	1836.78	0.62	NS
		AJ:T2-Skewed	-5.92	560.78	0.68	***
		B6:T2-Skewed	-0.11	663.41	0.43	NS
GSH depletion	24 h	AJ:Normal	-0.09	26.33	0.34	***
		B6:Normal	-0.07	35.13	0.26	**
		AJ:T2-Skewed	-0.07	5.91	0.46	***
		B6:T2-Skewed	-0.09	14.51	0.27	***
	5×4 h	AJ:Normal	-0.07	26.32	0.18	***
		B6:Normal	-0.08	36.70	0.12	**
		AJ:T2-Skewed	-0.05	4.80	0.22	***
		B6:T2-Skewed	-0.04	13.88	0.06	*
ROS production	24 h	AJ:Normal	2.46	11.55	0.92	***
		B6:Normal	1.89	13.09	0.88	***
		AJ:T2-Skewed	12.56	9.76	0.98	***
		B6:T2-Skewed	4.50	37.59	0.84	***
	5×4 h	AJ:Normal	0.99	11.76	0.78	***
		B6:Normal	0.63	5.68	0.85	***
		AJ:T2-Skewed	10.02	8.73	0.98	***
		B6:T2-Skewed	3.43	5.85	0.97	***
Lipid peroxidation	24 h	AJ:Normal	0.96	22.83	0.80	***
		B6:Normal	0.43	18.34	0.41	***
		AJ:T2-Skewed	3.38	18.61	0.93	***
		B6:T2-Skewed	2.49	23.17	0.87	***
	5×4 h	AJ:Normal	0.81	15.23	0.78	***
		B6:Normal	0.66	19.53	0.66	***
		AJ:T2-Skewed	2.95	10.36	0.87	***
		B6:T2-Skewed	1.17	24.18	0.70	***
Cytotoxicity	24 h	AJ:Normal	0.00	2.60	0.00	NS
		B6:Normal	0.03	1.06	0.32	***
		AJ:T2-Skewed	0.63	7.28	0.83	***
		B6:T2-Skewed	0.32	3.55	0.72	***
	5×4 h	AJ:Normal	0.01	1.32	0.10	NS
		B6:Normal	0.02	0.85	0.45	***
		AJ:T2-Skewed	0.46	6.39	0.82	***
		B6:T2-Skewed	0.28	5.70	0.85	***

Linear mixed effects model parameters of nominal dose-response relationships. Exposure: h (hours). Genotype:Phenotype: AJ:Normal (A/J, "Normal" phenotype); B6:Normal (C57BL6/J, "Normal" phenotype); AJ:T2-Skewed (A/J, "T2-Skewed" phenotype); B6:T2-Skewed (C57BL6/J, "T2-Skewed" phenotype). *n* = 3 biological replicates with technical replicates. Data represent mixed effects estimate of the linear slope parameters for each model; NS (*P*>0.05); * (*P*<0.05); ** (*P*<0.01); *** (*P*<0.001).

Adverse Cellular Response	Exposure	Genotype:Phenotype	Slope (β)	Intercept (B)	Correlation (r^2)	Significance (*P*)
Barrier dysfunction	24 h	AJ:Normal	-0.15	1809.30	0.90	NS
		B6:Normal	-0.06	1776.53	0.86	NS
		AJ:T2-Skewed	-6.85	526.51	0.56	***
		B6:T2-Skewed	-0.42	664.59	0.42	NS
	5×4 h	AJ:Normal	13.31	1796.98	0.81	NS
		B6:Normal	-2.87	1834.73	0.62	NS
		AJ:T2-Skewed	-23.10	492.59	0.43	***
		B6:T2-Skewed	-2.32	667.34	0.43	NS
GSH depletion	24 h	AJ:Normal	-0.16	25.66	0.27	***
		B6:Normal	-0.20	34.76	0.25	**
		AJ:T2-Skewed	-0.09	5.49	0.40	***
		B6:T2-Skewed	-0.14	14.50	0.27	***
	5×4 h	AJ:Normal	-1.27	26.64	0.26	***
		B6:Normal	-1.04	36.71	0.11	*
		AJ:T2-Skewed	-0.14	4.13	0.08	*
		B6:T2-Skewed	-0.13	13.37	0.02	NS
ROS production	24 h	AJ:Normal	4.65	24.38	0.85	***
		B6:Normal	5.68	23.53	0.76	***
		AJ:T2-Skewed	17.66	71.50	0.93	***
		B6:T2-Skewed	6.83	38.53	0.84	***
	5×4 h	AJ:Normal	12.21	14.95	0.58	***
		B6:Normal	8.47	4.69	0.87	***
		AJ:T2-Skewed	44.76	108.97	108.97	***
		B6:T2-Skewed	16.30	36.98	0.79	***
Lipid peroxidation	24 h	AJ:Normal	1.81	27.93	0.73	***
		B6:Normal	1.39	20.20	0.41	***
		AJ:T2-Skewed	4.64	36.63	0.84	***
		B6:T2-Skewed	3.79	23.51	0.88	***
	5×4 h	AJ:Normal	8.83	19.44	0.46	***
		B6:Normal	8.73	18.69	0.67	***
		AJ:T2-Skewed	13.02	40.28	0.70	***
		B6:T2-Skewed	5.23	35.78	0.50	***
Cytotoxicity	24 h	AJ:Normal	-0.02	2.73	0.03	NS
		B6:Normal	0.08	1.14	0.30	***
		AJ:T2-Skewed	0.85	10.77	0.73	***
		B6:T2-Skewed	0.50	3.60	0.73	***
	5×4 h	AJ:Normal	0.04	1.38	0.07	NS
		B6:Normal	0.21	0.85	0.41	***
		AJ:T2-Skewed	1.95	11.18	0.63	***
		B6:T2-Skewed	1.27	8.33	0.64	***

Linear mixed effects model parameters of dosimetric dose-response relationships. Exposure: h (hours). Genotype:Phenotype: AJ:Normal (A/J, "Normal" phenotype); B6:Normal (C57BL6/J, "Normal" phenotype); AJ:T2-Skewed (A/J, "T2-Skewed" phenotype); B6:T2-Skewed (C57BL6/J, "T2-Skewed" phenotype). *n* = 3 biological replicates with technical replicates. Data represent mixed effects estimate of the linear slope parameters for each model; NS ($P>0.05$); * ($P<0.05$); ** ($P<0.01$); *** ($P<0.001$).

Adverse Cellular Response	Exposure	Genotype:Phenotype	Nominal BMD (BMDL)	Significance (*P*)	Dosimetric BMD (BMDL)	Significance (*P*)
GSH depletion	24 h	AJ:Normal	27.40 (21.30)	***	17.40 (12.80)	***
		B6:Normal	51.70 (33.50)	***	17.50 (11.00)	***
		AJ:T2-Skewed	22.00 (17.90)	***	18.00 (14.10)	***
		B6:T2-Skewed	35.50 (25.90)	***	20.00 (15.20)	***
	5×4 h	AJ:Normal	39.40 (27.90)	***	2.10 (1.60)	***
		B6:Normal	55.60 (35.10)	***	4.50 (2.70)	***
		AJ:T2-Skewed	35.50 (25.90)	***	12.80 (7.70)	***
		B6:T2-Skewed	75.60 (42.20)	*	>8.70	NS
ROS production	24 h	AJ:Normal	5.30 (5.00)	***	3.90 (3.60)	***
		B6:Normal	6.70 (6.30)	***	3.20 (2.90)	***
		AJ:T2-Skewed	2.60 (2.50)	***	3.50 (3.30)	***
		B6:T2-Skewed	8.00 (7.40)	***	5.30 (4.90)	***
	5×4 h	AJ:Normal	9.90 (9.00)	***	1.10 (1.00)	***
		B6:Normal	7.90 (7.30)	***	0.60 (0.50)	***
		AJ:T2-Skewed	2.60 (2.50)	***	1.80 (1.60)	***
		B6:T2-Skewed	3.30 (3.20)	***	1.80 (1.70)	***
Lipid peroxidation	24 h	AJ:Normal	9.40 (8.50)	***	5.80 (5.20)	***
		B6:Normal	21.00 (17.20)	***	6.50 (5.30)	***
		AJ:T2-Skewed	5.20 (4.90)	***	5.60 (5.20)	***
		B6:T2-Skewed	7.00 (6.50)	***	4.50 (4.20)	***
	5×4 h	AJ:Normal	9.90 (9.00)	***	1.40 (1.20)	***
		B6:Normal	13.20 (11.60)	***	1.00 (0.90)	***
		AJ:T2-Skewed	7.30 (6.80)	***	3.50 (3.00)	***
		B6:T2-Skewed	11.90 (10.60)	***	8.30 (3.70)	***
Cytotoxicity	24 h	AJ:Normal	>50.00	NS	>24.50	NS
		B6:Normal	16.50 (14.10)	***	5.60 (4.70)	***
		AJ:T2-Skewed	7.10 (6.60)	***	>33.50	NS
		B6:T2-Skewed	10.80 (9.70)	***	7.00 (6.30)	***
	5×4 h	AJ:Normal	55.40 (35.10)	***	8.30 (3.70)	***
		B6:Normal	20.50 (16.90)	***	1.70 (1.40)	***
		AJ:T2-Skewed	7.20 (6.70)	***	2.90 (2.50)	***
		B6:T2-Skewed	7.80 (7.20)	***	2.60 (2.30)	***

Nominal BMD (BMDL) vs. dosimetric BMD (BMDL) for adverse cellular responses. Exposure: h (hours). Genotype:Phenotype: AJ:Normal (A/J, "Normal" phenotype); B6:Normal (C57BL6/J, "Normal" phenotype); AJ:T2-Skewed (A/J, "T2-Skewed" phenotype); B6:T2-Skewed (C57BL6/J, "T2-Skewed" phenotype). Nominal BMD (BMDL): µg AgNP/mL media; Dosimetric BMD (BMDL): µg Ag/mg protein. $n = 3$ biological replicates with technical replicates. Data represent BMD (BMDL); NS ($P>0.05$); * ($P<0.05$); ** ($P<0.01$); *** ($P<0.001$).

Chapter 4. The Effects of Genotype × Phenotype Interactions on Transcriptional Response to Silver Nanoparticle Toxicity in Organotypic Cultures of Murine Tracheal Epithelial Cells

This chapter will be submitted for publication in Toxicological Sciences. The authors of the manuscript are:

Tyler P. Nicholas[1,2], Anoria K. Haick[2], Theo K. Bammler[1], Tomomi W. Workman[1], Terrance J. Kavanagh[1,2], Elaine M. Faustman[1], Sina A. Gharib[2,*], William A. Altemeier[2,*]

[1]Department of Environmental and Occupational Health Sciences, University of Washington, Seattle, Washington
[2]Department of Medicine—Division of Pulmonary, Critical Care, and Sleep Medicine, University of Washington, Seattle, Washington
*Co-senior authors

Corresponding Author:
William A. Altemeier
UW Medicine Research / South Lake Union
850 Republican Street, S324
Box 358052
Seattle, Washington 98109
Phone: (206) 616-6140
Fax: (206) 221-0739
Email: billa@uw.edu

List of Abbreviations

5×4 h: repeated exposure of 4 hours, every other day, over 5 days
Ag: silver metals
Ag^{+}: silver ions
AgNP: silver nanoparticles
AJ or B6:Normal: A/J or C57BL6/J, “Normal” phenotype
AJ or B6:T2-Skewed: A/J or C57BL6/J, “T2-Skewed” phenotype
AOP: Adverse Outcome Pathways
COPD: chronic obstructive pulmonary disease
DEG: differentially expressed genes
DMEM: Dulbecco’s Modified Eagle Media
G×E: gene × environment interactions
G×P: genotype × phenotype interactions
GSEA: gene set enrichment analysis
GSH: glutathione
ILC2: type 2 innate lymphoid cells
IPA: Ingenuity Pathway Analysis
MIE: molecular initiating event
MoA: mode of action
MTEC: murine tracheal epithelial cells
NES: normalized enrichment score
NRC: National Research Council
PCA: Principal Components Analysis
RNA-seq: RNA sequencing
ROS: reactive oxygen species
STAR: Spliced Transcripts Alignment to a Reference
T1/T2/T17: type 1/type 2/type 17
TEER: transepithelial electrical resistance
TSCA: Toxic Substances Control Act
US EPA: U.S. Environmental Protection Agency

Chapter 4. The Effects of Genotype × Phenotype Interactions on Transcriptional Response to Silver Nanoparticle Toxicity in Organotypic Cultures of Murine Tracheal Epithelial Cells

4.1 ABSTRACT

The airway epithelium is critical for maintaining innate and adaptive immune responses, and occupational exposures that disrupt its immune homeostasis may initiate and amplify airway inflammation. In our previous study, we demonstrated that silver nanoparticles (AgNP), which are engineered nanomaterials used in multiple applications but primarily in the manufacturing of many antimicrobial products, induce toxicity in organotypic cultures derived from murine tracheal epithelial cells (MTEC), and those differentiated toward a “Type 2 [T2]-Skewed” phenotype experienced an increased sensitivity to AgNP toxicity, suggesting that asthmatics could be a sensitive population to AgNP exposures in occupational settings. However, the mechanistic basis for this genotype × phenotype interaction (G×P) has yet to be defined. In the present study, we conducted transcriptional profiling using RNA-sequencing (RNA-seq) to predict the enrichment of specific canonical pathways and upstream transcriptional regulators to assist in defining a mechanistic basis for G×P effects on AgNP toxicity. Organotypic cultures were derived from MTEC across two genetically inbred mouse strains (A/J and C57BL/6J mice), two phenotypes (“Normal” and “T2-Skewed”), and one AgNP exposure (an acute 24 h exposure) to characterize G×P effects on transcriptional response to AgNP toxicity. The “T2-Skewed” phenotype was marked by increased pro-inflammatory T17 responses to AgNP toxicity, which are significant predictors of neutrophilic/difficult-to-control asthma and suggests that asthmatics could be a sensitive population to AgNP exposures in occupational settings. This study highlights the importance of considering G×P effects when identifying these sensitive populations, whose underlying genetics or diseases could directly modify their response to AgNP exposures.

4.2 INTRODUCTION

Upstream perturbations of canonical inflammatory pathways within the respiratory system

can lead to adverse cellular responses, such as inflammation, which can profoundly impact the ability of exposed airways to maintain cellular function and overall health. These perturbations can be caused by many environmental toxicants, and in the airway epithelium, they can impair host defense mechanisms by altering its secretion of different cytokines, chemokines, growth factors, antimicrobial peptides, and recruited immune cells to sites of inflammation.[15] Immune dysregulation is a clinical feature of many chronic respiratory diseases, including asthma, acute bronchitis, and chronic obstructive pulmonary disease (COPD),[210] which collectively affect 16% of the United States population. Pre-existing chronic respiratory diseases impair other host defense mechanisms, including barrier function,[15] mucocilliary clearance and permeability,[16-22] as well as enzymatic and non-enzymatic regulation of oxidative stress,[23,24] and together with immune dysregulation, may increase an individual's sensitivity to occupational exposures.[25-27]

Chronic respiratory diseases place a major burden on individuals, their workplaces, and the healthcare system, and yet less than 1% of the chemicals regulated by the U.S. Environmental Protection Agency's (US EPA) Toxic Substances Control Act (TSCA) have been tested for potential respiratory toxicity.[3] In a pivotal report, the National Research Council (NRC) outlined a vision for toxicity testing that shifts the focus from downstream pathological changes in animals to upstream perturbations of toxicant response canonical pathways using lower, and more environmentally relevant doses.[4] This incited a paradigm shift in toxicity testing toward the use of *in vitro* models suitable for high-throughput screening in order to support global gene and protein expression analyses and the development of predictive, mechanistic-based biomarkers.[5-10] Validation of these *in vitro* models will enable screening and prioritization of potential respiratory toxicants in order to inform regulatory policy aimed at protecting all populations. However, the sensitivity and specificity of these *in vitro* models must be well characterized before they can be translated into regulatory frameworks.[143]

There is presently a need for the development of *in vitro* models to provide relevant data on risk assessment for occupational exposures. In recent years, there has been a gradual paradigm shift toward the use of *in vitro* models that reduce, replace, and refine the use

of animals in toxicity testing (the three R's) from both the standpoint of economic imperative and animal welfare.[1,2] Despite these economic advantages over *in vivo* models, *in vitro* models are currently limited by: 1) the use of immortalized or transformed cell lines that may not recapitulate primary cell phenotypes, 2) the use of cells from a single genetic background or phenotype, which may not capture the impact of underlying genetics or diseases on toxicant response, and 3) the limited efforts to relate *in vitro* exposures to occupational exposures in order to provide a mechanistic basis for sensitivity to occupational exposures and inform regulatory policy aimed at protecting all populations.[3,4] Together, the above limitations highlight a need to develop *in vitro* models suitable for high-throughput screening that also capture determinants of sensitivity in order to screen and prioritize potential respiratory toxicants while providing relevant data on risk assessment for occupational exposures.[142,143]

Silver nanoparticles (AgNP) have been tested for respiratory toxicity in previous studies, as they are used in the manufacturing of many antimicrobial consumer products, including air filters, humidifiers, and purifiers as well as antimicrobial sprays.[31,32,37] Previous *in vitro* studies observed the mode of action (MoA) for their antimicrobial properties (e.g., release of bioactive silver ions [Ag^+] upon dissolution[11-13]) is also a defining factor of AgNP toxicity in mammalian cells.[144] One MoA in airway epithelial cells is Ag^+-mediated reactive oxygen species (ROS) production, which leads to adverse cellular responses including oxidative stress, mitochondrial dysfunction, inflammation, and cytotoxicity.[50,58-63,87,121,145] Cytokines are critical mediators of asthma, and regulate this heterogeneous chronic airway disease through divergent mechanisms of type 2 (T2) and T17 inflammation to produce the distinct endotypes of increasing severity, T2/T17-low, T2-high, and T17-high.[211] The T2-high endotype is associated with eosinophilic/easy-to-control asthma,[212,213] whereas the T17-high endotype is associated with neutrophilic/difficult-to-control asthma, and is thus characterized by the secretion of potent neutrophil-attractant chemokines.[214,215] Asthmatics are possibly a sensitive population to AgNP exposures in occupational settings, as these adverse cellular responses may further modulate innate and adaptive immune responses at the epithelial-immune interface to exacerbate this chronic airway disease by shifting it toward a T17-high endotype.[48]

We previously characterized the effects of interactions between host genetic and acquired factors, or gene × environment interactions (G×E),[28,29] on AgNP toxicity. Understanding G×E effects is important for identifying sensitive populations, whose underlying genetics or diseases could directly modify their response to AgNP exposures. The present study was designed to test the hypothesis that genotype and phenotype (physiological environment) will define G×E, or genotype × phenotype interaction (G×P), effects on transcriptional response to AgNP toxicity. We derived organotypic cultures from primary murine tracheal epithelial cells (MTEC) of differentially sensitive genotypes (A/J and C57BL/6J mice) to airway hyperresponsiveness,[146-148] antigen sensitization,[149] T2 lung inflammation,[150] and engineered nanomaterial toxicity[77,78] to model the effects of host genetic factors on AgNP toxicity. We differentiated organotypic cultures toward either "Normal" or "T2-Skewed" phenotypes to model the effects of host acquired factors on AgNP toxicity. To acquire the "Normal" phenotype, we used a defined differentiation media to achieve differentiation toward the cell populations in the proximal region of the conducting airway, including basal, ciliated, club, and mucin cells.[151] To acquire the "T2-Skewed" phenotype, we used a defined differentiation media supplemented with IL-13 to skew differentiation toward an *in vitro* model of chronic respiratory diseases, characterized by barrier dysfunction,[152] mucus production,[153] allergic responses,[153] and T2 responses.[154-156]

Using this high-content *in vitro* model of the conducting airway, we characterized global, differential, and targeted gene expression, canonical pathway enrichment, and upstream transcriptional regulation to understand G×P effects on transcriptional response to AgNP toxicity. To our knowledge, this is the first study to use organotypic cultures as a high-content *in vitro* model of the conducting airway paired with RNA sequencing (RNA-seq) to characterize G×P effects on transcriptional response to AgNP toxicity. RNA-seq and other omics technologies can be used to extract information that has mechanistic and diagnostic value by associating changes in global and targeted gene, protein, or metabolite expression with a physiological endpoint of interest. By pairing organotypic cultures with RNA-seq, we can capture the enrichment of specific canonical pathways and identify their transcriptional regulators to assist in defining a mechanistic basis for G×P effects on AgNP toxicity.

4.3 METHODS

Cell culture

All animal studies were approved by the Institutional Animal Care and Use Committee at the University of Washington. We harvested tracheas from A/J and C57BL/6J mice (The Jackson Laboratory, Bar Harbor, ME, USA), and isolated MTEC using enzymatic digestion, as previously described.[151,157,158] We suspended MTEC in a defined proliferation media [Dulbecco's Modified Eagle Media (DMEM) with 10 μg/mL insulin, 5 μg/mL apo-transferrin, 0.1 μg/mL cholera toxin, 25 ng/mL epidermal growth factor, 30 μg/mL bovine pituitary extract, and 50 nM retinoic acid (Sigma-Aldrich, St. Louis, MO, USA)] to culture at a density of 1.5×10^4 cells/well in collagen-coated 24-Transwell plates (Corning, Corning, NY, USA). We allowed organotypic cultures to proliferate with media in both apical and basal compartments starting on day *in vitro* (DIV) 0. We changed the defined proliferation media every other day until DIV 7-9, when transepithelial electrical resistance (TEER) exceeded 1000 $\Omega\times cm^2$, which marked the end of proliferation.

For the "Normal" phenotype, we allowed organotypic cultures to differentiate at an air-liquid interface (ALI) in a defined differentiation media [DMEM with 2% v/v NuSerum (BD BioSciences, San Jose, CA, USA), and 50 nM retinoic acid (Sigma-Aldrich, St. Louis, MO, USA)] in the basal compartment starting on DIV 7. We changed the defined differentiation media every other day until DIV 28, which marked the end of differentiation.

For the "T2-Skewed" phenotype, we allowed organotypic cultures to differentiate at an ALI in a defined differentiation media supplemented with IL-13 [DMEM with 2% v/v NuSerum (BD BioSciences, San Jose, CA, USA), 50 nM retinoic acid (Sigma-Aldrich, St. Louis, MO, USA)], and 25 ng/mL IL-13 (PeproTech, Rocky Hill, NJ, USA)]. We identified this concentration of IL-13 in a preliminary study and supplemented it to the defined proliferation media starting on DIV 5, and then to the defined differentiation media from DIV 7-28, which we changed every other day until DIV 28.

AgNP exposure

We exposed organotypic cultures in the apical compartment on DIV 28 to either 2 mM

sodium citrate (vehicle control; 0 µg AgNP/mL media), or to silver nanoparticles (AgNP; 20 nm, gold-core, citrate-coated, at 1 mg/mL in 2 mM sodium citrate; nanoComposix, San Diego, CA, USA) for an acute exposure of 24 hours at nominal doses of 12.5 or 50 µg AgNP/mL media, as freshly prepared in suspensions of defined differentiation media.

RNA-sequencing

We used RNA-seq to quantify global, differential, and targeted gene expression in exposed organotypic cultures on DIV 28. We isolated total RNA from organotypic cultures using a RNEasy Micro Kit (Qiagen, Hilden, Germany), and estimated RNA quality and quantity using an Agilent 2100 Bioanalyzer (Agilent Technologies, Santa Clara, CA, USA) to visualize the 18S and 28S rRNA bands. We performed library preparation was using a combination of two protocols which allowed for smaller volumes while minimizing handling steps, first using a SMART-seq v4 Ultra Low Input RNA Kit (Clontech Laboratories, Mountain View, CA, USA) to convert the RNA to full length cDNA and to amplify it, and then using a Nextera XT Library Preparation Kit (Fluidigm, San Francisco, CA, USA) to fragment the cDNA and add Illumina adapters. We sequenced the library products using the Illumina HiSeq2500 platform (Illumina, San Diego, CA, USA), and aligned the trimmed sequencing reads to the Ensembl mouse transcriptome (version GRCm38.84) using Spliced Transcripts Alignment to a Reference (STAR) software.[216]

4.4 STATISTICS

We used average read counts (≥ 10; n = 9,642) to characterize dose, genotype, and phenotype effects on: 1) global gene expression, 2) differential gene expression, 3) canonical pathway enrichment, 4) targeted gene expression for the secreted factors canonical pathway, 5) ingenuity pathway analysis for the secreted factors canonical pathway, and 6) targeted gene expression for T1, pro-T2, T2, and T17 responses. We characterized hierarchical clustering of global gene expression using z-scores of $\log_2$(average read counts) on the pheatmap package for R statistical software.[166] We characterized principal components of global gene expression using $\log_2$(average read counts) on the DESeq2 package for R statistical software.[166] We characterized differential gene expression using $\log_2$(average read counts) with a false discovery rate (*FDR*<0.10)

to generate more robust networks and to adjust for multiple comparisons on the DESeq2 package for R statistical software.[166] We characterized canonical pathway enrichment using Gene Set Enrichment Analysis (GSEA; Broad Institute, Cambridge, MA, USA) with the Benjamini-Hochberg method (*FDR*<0.10) for rank-ordered z-scores of $\log_2$(average read counts) (*n* = 9,642) on the clusterProfiler package for R statistical software.[166] We repeated these analyses using more stringent cut-offs (*FDR*<0.01 and *FDR*<0.05) and observed similar numbers of differentially expressed genes (DEG) and patterns of canonical pathway enrichment. We characterized targeted gene expression for the secreted factors canonical pathway using z-scores of $\log_2$(average read counts) (*n* = 54) on the pheatmap package for R statistical software.[166] We characterised upstream transcriptional regulators and downstream functions and diseases associated with the secreted factors canonical pathway using Ingenuity Pathway Analysis (IPA; Ingenuity Systems, Redwood City, CA, USA).

4.5 RESULTS

Genotype, phenotype, and dose effects on global gene expression

We characterized dose, genotype, and phenotype effects on hierarchical clustering of global gene expression using Pearson correlation distance and average linkage distance on z-scores of $\log_2$(average read counts) (*n* = 9,642) for AJ:Normal **(Figure 1A)**, B6:Normal **(Figure 1B)**, AJ:T2-Skewed **(Figure 1C)**, and B6:T2-Skewed **(Figure 1D)** exposed to nominal doses of 0, 12.5, or 50 µg AgNP/mL media for an acute 24 h exposure. We observed dose, genotype and phenotype effects on hierarchical clustering of global gene expression, with the largest differences between the “Normal” and “T2-Skewed” phenotypes. We characterized dose, genotype, and phenotype effects on principal components of global gene expression using principal components analysis (PCA) on $\log_2$(average read counts) (*n* = 9,642) for AJ:Normal, B6:Normal, AJ:T2-Skewed, and B6:T2-Skewed exposed to nominal doses of 0 **(Figure 2A)**, 12.5 **(Figure 2B)**, or 50 **(Figure 2C)** µg AgNP/mL media for an acute 24 h exposure. We observed dose, genotype effects on principal components of global gene expression, which explained 3%, 4%, and 19% of the total variance at 0, 12.5, and 50 µg AgNP/mL media,

respectively. We observed phenotype effects on principal components of global gene expression, which explained 89%, 90%, and 77% of the total variance at 0, 12.5, and 50 μg AgNP/mL media, respectively. We observed the largest separation between AJ:T2-Skewed and B6:T2-Skewed at 50 μg AgNP/mL media.

Genotype, phenotype, and dose effects on differential gene expression

We characterized dose, genotype, and phenotype effects on differential gene expression using a *t*-test for significant differences in $\log_2$(average read counts) (n = 9,642) for AJ:Normal, B6:Normal, AJ:T2-Skewed, and B6:T2-Skewed exposed to nominal doses of 0, 12.5, or 50 μg AgNP/mL media for an acute 24 h exposure (*FDR*<0.10). We observed dose effects on upregulated DEG, with 49 and 38 genes uniquely expressed in AJ:Normal (12.5 and 50 μg AgNP/mL media vs. vehicle controls, respectively), 2 and 4 genes uniquely expressed in B6:Normal (12.5 and 50 μg AgNP/mL media vs. vehicle controls, respectively), 15 and 122 genes uniquely expressed in AJ:T2-Skewed (12.5 and 50 μg AgNP/mL media vs. vehicle controls, respectively), and 188 and 163 genes uniquely expressed in B6:T2-Skewed (12.5 and 50 μg AgNP/mL media vs. vehicle controls, respectively) **(Supplementary Data)**. We observed dose effects on downregulated DEG, with 43 and 262 genes uniquely expressed in AJ:Normal (12.5 and 50 μg AgNP/mL media vs. vehicle controls, respectively), 4 and 37 genes uniquely expressed in B6:Normal (12.5 and 50 μg AgNP/mL media vs. vehicle controls, respectively), 84 and 93 genes uniquely expressed in AJ:T2-Skewed (12.5 and 50 μg AgNP/mL media vs. vehicle controls, respectively), and 160 and 202 genes uniquely expressed in B6:T2-Skewed (12.5 and 50 μg AgNP/mL media vs. vehicle controls, respectively) **(Supplementary Data)**.

Genotype, phenotype, and dose effects on canonical pathway enrichment

We characterized dose, genotype, and phenotype effects on canonical pathway enrichment using GSEA with the Benjamini-Hochberg method (*FDR*<0.10) on rank-ordered z-scores of $\log_2$(average read counts) (n = 9,642) for AJ:Normal, B6:Normal, AJ:T2-Skewed, and B6:T2-Skewed exposed to nominal doses of 0 **(Figure 3A-3D)**, 12.5 **(Figure 3E-3H)**, or 50 **(Figure 3I-3J)** μg AgNP/mL media for an acute 24 h exposure. We defined directionality of enrichment using a normalized enrichment score > 0 to represent

activation, and a normalized enrichment score < 0 to represent inhibition.

Five of the top activated canonical pathways predicted for AJ:Normal at 0 µg AgNP/mL media were “N-Glycan Trimming” (*n* = 12 genes; -log[*P*-value] = 2.70), “GCR Signaling Pathway” (*n* = 13 genes; -log[*P*-value] = 2.69), “β-Catenin Signaling Pathway” (*n* = 13 genes; -log[*P*-value] = 2.69), “DNA Unwinding” (*n* = 11 genes; -log[*P*-value] = 2.69), and “Antigen Presentation Folding Assembly” (*n* = 15 genes; -log[*P*-value] = 2.69). Five of the top inhibited canonical pathways predicted for AJ:Normal at 0 µg AgNP/mL media were “Ribosome” (*n* = 50 genes; -log[*P*-value] = 2.74), “Influenza vRNA Transcription” (*n* = 64 genes; -log[*P*-value] = 2.74), “Peptide Chain Elongation” (*n* = 49 genes; -log[*P*-value] = 2.74), “Class 1A Rhodopsin Like Receptor Binding” (*n* = 43 genes; -log[*P*-value] = 2.74), and “Nonsense-Mediated Decay” (*n* = 70 genes; -log[*P*-value] = 2.73) **(Figure 3A)**.

Five of the top activated canonical pathways predicted for AJ:Normal at 12.5 µg AgNP/mL media were “L1 Recycling Pathway” (*n* = 20 genes; -log[*P*-value] = 2.68), “Lipid Digestion, Mobilization, and Transport” (*n* = 19 genes; -log[*P*-value] = 2.68), “Antigen Presentation Folding Assembly” (*n* = 15 genes; -log[*P*-value] = 2.68), “Adherens Junctions Interactions” (*n* = 15 genes; -log[*P*-value] = 2.68), and “TRiC/CCT-Mediated Protein Biosynthesis” (*n* = 24 genes; -log[*P*-value] = 2.68). Five of the top inhibited canonical pathways predicted for AJ:Normal at 12.5 µg AgNP/mL media were “Influenza vRNA Transcription” (*n* = 64 genes; -log[*P*-value] = 2.76), “Nonsense-Mediated Decay” (*n* = 70 genes; -log[*P*-value] = 2.76), “Peptide Chain Elongation” (*n* = 49 genes; -log[*P*-value] = 2.73), “Ribosome” (*n* = 50 genes; -log[*P*-value] = 2.72), and “N-Glycan Biosynthesis” (*n* = 25 genes; -log[*P*-value] = 2.11) **(Figure 3E)**.

Five of the top activated canonical pathways predicted for AJ:Normal at 50 µg AgNP/mL media were “TNF Signaling Pathway” (*n* = 27 genes; -log[*P*-value] = 2.71), “Ribonucleoprotein Transport” (*n* = 27 genes; -log[*P*-value] = 2.71), “Rho Signaling Pathway” (*n* = 27 genes; -log[*P*-value] = 2.71), “NS2-Mediated Cellular Export” (*n* = 27 genes; -log[*P*-value] = 2.71), and “Aurora Signaling Pathway” (*n* = 27 genes; -log[*P*-value] = 2.71). Five of the top inhibited canonical pathways predicted for AJ:Normal at 50 µg AgNP/mL media were “Peptide Chain Elongation” (*n* = 49 genes; -log[*P*-value] = 2.73),

“Ribosome” (*n* = 50 genes; -log[*P*-value] = 2.72), “Influenza vRNA Transcription” (*n* = 64 genes; -log[*P*-value] = 2.41), “Non-Homologous End-Joining” (*n* = 11 genes; -log[*P*-value] = 2.41), and “Glycosaminoglycan Biosynthesis” (*n* = 15 genes; -log[*P*-value] = 1.86) **(Figure 3I)**.

Five of the top activated canonical pathways predicted for B6:Normal at 0 µg AgNP/mL media were “Tight Junction Interactions” (*n* = 10 genes; -log[*P*-value] = 2.68), “RAF MAPK Cascade” (*n* = 10 genes; -log[*P*-value] = 2.68), “Lipoprotein Metabolism” (*n* = 10 genes; -log[*P*-value] = 2.68), “Calnexin Calreticulin Cycle” (*n* = 10 genes; -log[*P*-value] = 2.68), and “SDC2 Signaling Pathway” (*n* = 25 genes; -log[*P*-value] = 2.67). Five of the top inhibited canonical pathways predicted for B6:Normal at 0 µg AgNP/mL media were “Nonsense-Mediated Decay” (*n* = 70 genes; -log[*P*-value] = 2.73), “Cotranslational Protein Targeting” (*n* = 70 genes; -log[*P*-value] = 2.73), “Peptide Chain Elongation” (*n* = 49 genes; -log[*P*-value] = 2.73), “Influenza vRNA Transcription” (*n* = 64 genes; -log[*P*-value] = 2.73), and “Ribosome” (*n* = 20 genes; -log[*P*-value] = 2.72) **(Figure 3B)**.

Five of the top activated canonical pathways predicted for B6:Normal at 12.5 µg AgNP/mL media were “TCA Cycle” (*n* = 18 genes; -log[*P*-value] = 2.66), “Lipid Digestion, Mobilization, and Transport” (*n* = 19 genes; -log[*P*-value] = 2.66), “Proteasome Pathway” (*n* = 28 genes; -log[*P*-value] = 2.66), “Dilated Cardiomyopathy” (*n* = 33 genes; -log[*P*-value] = 2.66), and “CXCR3 Signaling Pathway” (*n* = 33 genes; -log[*P*-value] = 2.66). Five of the top inhibited canonical pathways predicted for B6:Normal at 12.5 µg AgNP/mL media were “Nonsense-Mediated Decay” (*n* = 70 genes; -log[*P*-value] = 2.75), “Influenza vRNA Transcription” (*n* = 64 genes; -log[*P*-value] = 2.74), “3’ UTR-Mediated Translation” (*n* = 67 genes; -log[*P*-value] = 2.74), “Peptide Chain Elongation” (*n* = 49 genes; -log[*P*-value] = 2.74), and “Ribosome” (*n* = 50 genes; -log[*P*-value] = 2.73) **(Figure 3F)**.

Five of the top activated canonical pathways predicted for B6:Normal at 50 µg AgNP/mL media were “N-Cadherin Signaling Pathway” (*n* = 26 genes; -log[*P*-value] = 2.70), “FMLP Signaling Pathway” (*n* = 26 genes; -log[*P*-value] = 2.70), “Antigen Processing and Presentation” (*n* = 26 genes; -log[*P*-value] = 2.70), “SDC2 Signaling Pathway” (*n* = 25 genes; -log[*P*-value] = 2.70), and “Citric Acid Cycle” (*n* = 25 genes; -log[*P*-value] = 2.70).

Five of the top inhibited canonical pathways predicted for B6:Normal at 50 µg AgNP/mL media were “Influenza vRNA Transcription” (*n* = 64 genes; -log[*P*-value] = 2.75), “3’ UTR-Mediated Translation” (*n* = 67 genes; -log[*P*-value] = 2.74), “Peptide Chain Elongation” (*n* = 49 genes; -log[*P*-value] = 2.74), “Nonsense-Mediated Decay” (*n* = 70 genes; -log[*P*-value] = 2.74), and “Ribosome” (*n* = 50 genes; -log[*P*-value] = 2.73) **(Figure 3J)**.

Five of the top activated canonical pathways predicted for AJ:T2-Skewed at 0 µg AgNP/mL media were “N-Glycan Trimming” (*n* = 12 genes; -log[*P*-value] = 2.70), “Innate Immune System” (*n* = 138 genes; -log[*P*-value] = 2.70), “Stress Response Pathway” (*n* = 22 genes; -log[*P*-value] = 2.70), “mTOR Signaling Pathway” (*n* = 22 genes; -log[*P*-value] = 2.70), and “WNT Signaling Pathway” (*n* = 95 genes; -log[*P*-value] = 2.69). Five of the top inhibited canonical pathways predicted for AJ:T2-Skewed at 0 µg AgNP/mL media were “Ribosome” (*n* = 50 genes; -log[*P*-value] = 2.73), “Peptide Chain Elongation” (*n* = 49 genes; -log[*P*-value] = 2.72), “Influenza vRNA Transcription” (*n* = 64 genes; -log[*P*-value] = 2.42), “Nuclear Factor Transcription Pathway” (*n* = 22 genes; -log[*P*-value] = 2.09), and “Nonsense-Mediated Decay” (*n* = 70 genes; -log[*P*-value] = 1.94) **(Figure 3C)**.

Five of the top activated canonical pathways predicted for AJ:T2-Skewed at 12.5 µg AgNP/mL media were “Carbohydrate Metabolism” (*n* = 141 genes; -log[*P*-value] = 2.72), “B Cell Receptor Signaling Pathway” (*n* = 43 genes; -log[*P*-value] = 2.72), “DNA Replication” (*n* = 176 genes; -log[*P*-value] = 2.71), “Secreted Factors” (*n* = 98 genes; -log[*P*-value] = 2.71), and “Interferon Signaling Pathway” (*n* = 98 genes; -log[*P*-value] = 2.71). Five of the top inhibited canonical pathways predicted for AJ:T2-Skewed at 12.5 µg AgNP/mL media were “Peptide Chain Elongation” (*n* = 49 genes; -log[*P*-value] = 2.71), “Ribosome” (*n* = 50 genes; -log[*P*-value] = 2.70), “Nonsense-Mediated Decay” (*n* = 70 genes; -log[*P*-value] = 2.70), “Influenza vRNA Transcription” (*n* = 64 genes; -log[*P*-value] = 2.70), and “Glutathione Metabolism” (*n* = 34 genes; -log[*P*-value] = 2.70) **(Figure 3G)**.

Five of the top activated canonical pathways predicted for AJ:T2-Skewed at 50 µg AgNP/mL media were “Secreted Factors” (*n* = 98 genes; -log[*P*-value] = 2.80), “Adaptive Immune System” (*n* = 349 genes; -log[*P*-value] = 2.79), “Lipoprotein Metabolism” (*n* = 305 genes; -log[*P*-value] = 2.78), “IL-23 Signaling Pathway” (*n* = 24 genes; -log[*P*-value] =

2.78), and “WNT Signaling Pathway” (*n* = 95 genes; -log[*P*-value] = 2.78). Five of the top inhibited canonical pathways predicted for AJ:T2-Skewed at 50 µg AgNP/mL media were “Glutathione Metabolism” (*n* = 34 genes; -log[*P*-value] = 2.67), “Peptide Chain Elongation” (*n* = 49 genes; -log[*P*-value] = 2.65), “Ribosome” (*n* = 50 genes; -log[*P*-value] = 2.65), “Influenza vRNA Transcription” (*n* = 64 genes; -log[*P*-value] = 2.62), and “Nonsense-Mediated Decay” (*n* = 70 genes; -log[*P*-value] = 2.61) **(Figure 3K)**.

Five of the top activated canonical pathways predicted for B6:T2-Skewed at 0 µg AgNP/mL media were “N-Cadherin Signaling Pathway” (*n* = 26 genes; -log[*P*-value] = 2.70), “L1 Signal Transduction” (*n* = 26 genes; -log[*P*-value] = 2.70), “FMLP Signaling Pathway” (*n* = 26 genes; -log[*P*-value] = 2.70), “Antigen Processing and Presentation” (*n* = 26 genes; -log[*P*-value] = 2.70), and “HIV-NEF Signaling Pathway” (*n* = 50 genes; -log[*P*-value] = 2.70). Five of the top inhibited canonical pathways predicted for B6:T2-Skewed at 0 µg AgNP/mL media were “3’ UTR-Mediated Translation” (*n* = 67 genes; -log[*P*-value] = 2.70), “Peptide Chain Elongation” (*n* = 49 genes; -log[*P*-value] = 2.70), “Nonsense-Mediated Decay” (*n* = 70 genes; -log[*P*-value] = 2.70), “Influenza vRNA Transcription” (*n* = 64 genes; -log[*P*-value] = 2.70), and “Cotranslational Protein Targeting” (*n* = 70 genes; -log[*P*-value] = 2.70) **(Figure 3D)**.

Five of the top activated canonical pathways predicted for B6:T2-Skewed at 12.5 µg AgNP/mL media were “Spliceosome” (*n* = 118 genes; -log[*P*-value] = 2.72), “Amino Acid Metabolism” (*n* = 118 genes; -log[*P*-value] = 2.72), “Adaptive Immune System” (*n* = 349 genes; -log[*P*-value] = 2.72), “Secreted Factors” (*n* = 98 genes; -log[*P*-value] = 2.71), and “Mitotic G1 G1/S Phases” (*n* = 125 genes; -log[*P*-value] = 2.71). Five of the top inhibited canonical pathways predicted for B6:T2-Skewed at 12.5 µg AgNP/mL media were “Influenza vRNA Transcription” (*n* = 64 genes; -log[*P*-value] = 2.70), “Nonsense-Mediated Decay” (*n* = 70 genes; -log[*P*-value] = 2.69), “Peptide Chain Elongation” (*n* = 49 genes; -log[*P*-value] = 2.69), “Ribosome” (*n* = 50 genes; -log[*P*-value] = 2.68), and “3’ UTR-Mediated Translation” (*n* = 67 genes; -log[*P*-value] = 2.39) **(Figure 3H)**.

Five of the top activated canonical pathways predicted for B6:T2-Skewed at 50 µg AgNP/mL media were “Adaptive Immune System” (*n* = 349 genes; -log[*P*-value] = 2.74),

"Secreted Factors" (*n* = 98 genes; -log[*P*-value] = 2.73), "Lipoprotein Metabolism" (*n* = 305 genes; -log[*P*-value] = 2.73), "IL-23 Signaling Pathway" (*n* = 24 genes; -log[*P*-value] = 2.74), and "Cytokine-Cytokine Receptor Interaction" (*n* = 113 genes; -log[*P*-value] = 2.73). Five of the top inhibited canonical pathways predicted for B6:T2-Skewed at 50 µg AgNP/mL media were "Nonsense-Mediated Decay" (*n* = 70 genes; -log[*P*-value] = 2.70), "Cotranslational Protein Targeting" (*n* = 70 genes; -log[*P*-value] = 2.70), "3' UTR-Mediated Translation" (*n* = 67 genes; -log[*P*-value] = 2.69), "Influenza vRNA Transcription" (*n* = 98 genes; -log[*P*-value] = 2.69), and "Influenza Life Cycle" (*n* = 64 genes; -log[*P*-value] = 2.69) **(Figure 3L)**.

Genotype, phenotype, and dose effects on targeted gene expression for the secreted factors canonical pathway

We identified "Secreted Factors" as an important enriched canonical pathway that may play a role in defining the mechanistic basis for G×P effects on AgNP toxicity. To better understand this mechanistic basis, we characterized dose, genotype, and phenotype effects on targeted gene expression for the secreted factors canonical pathway using z-scores of $\log_2$(average read counts) (*n* = 54) for AJ:Normal **(Figure 4A)**, B6:Normal **(Figure 4B)**, AJ:T2-Skewed **(Figure 4C)**, and B6:T2-Skewed **(Figure 4D)** exposed to nominal doses of 0, 12.5, or 50 µg AgNP/mL media for an acute 24 h exposure. We chose this subset of genes based on leading-edge analysis, which identifies the subsets of genes (referred to as the leading-edge subset) that contributed the most to the enrichment score of a given gene set's core enrichment. We observed dose, genotype and phenotype effects on targeted gene expression, specifically upregulated genes for chemokines responsible for attracting leukocyte populations including T lymphocytes (e.g., *Ccl20* and *Ccl22*), dendritic cells (e.g., *Ccl25*), eosinophils (e.g., *Ccl24* and *Ccl26*) and neutrophils (e.g., *Cxcl1*, *Cxcl2*, *Cxcl3*, and *Cxcl5*). We observed dose, phenotype effects on upregulated genes for cytokines associated with T2/T17 responses, specifically upregulated genes for T2 cytokines in the "Normal" phenotype (e.g., *Il4*, *Il5*, *Il6*, *Il9*, *Il10*, and *Il13*), and upregulated genes for T17 cytokines in the "T2-Skewed" phenotype (e.g., *Ccl20*, *Ccl25*, *Csf3*, *Cxcl1*, *Cxcl2*, *Cxcl3*, *Cxcl5, Il17c,* and *Il23a*).

Genotype, phenotype, and dose effects on upstream transcriptional regulation of the secreted factors canonical pathway

We identified "Secreted Factors" as an important enriched canonical pathway that may play a role in defining the mechanistic basis for G×P effects on AgNP toxicity. To better understand this mechanistic basis, we also characterized dose, genotype, and phenotype effects on upstream regulators, downstream functions and diseases of the secreted factors canonical pathway using IPA with the Fischer's Exact method (*FDR*<0.10) on fold changes of $\log_2$(average AgNP/vehicle control) (*n* = 54) for AJ:Normal **(Figure 5A, 6A)**, B6:Normal **(Figure 5B, 6A)**, AJ:T2-Skewed **(Figure 5C, 6C)**, and B6:T2-Skewed **(Figure 5D, 6D)** exposed to nominal doses of 0, 12.5, or 50 µg AgNP/mL media for an acute 24 h exposure. These predictions were based on the overlap *P*-value, which measures the significance of the overlap between affected genes and all of the genes within the secreted factors canonical pathway. We used the upstream analysis module of IPA to identify dose, genotype, and phenotype effects on upstream regulators of the secreted factors canonical pathway. Across doses, genotypes, and phenotypes, we identified *Stat3* as one of the most significant upstream activators of the secreted factors canonical pathway **(Figure 5)**, and *Bcl6* as one of the most significant upstream inhibitors of the secreted factors canonical pathway **(Figure 6)**. We used the pathway analysis module of IPA to identify dose, genotype, and phenotype effects on specific cytokines that may serve as upstream activators of the T17 canonical pathway. Across doses, genotypes, and phenotypes, we identified IL-23 as the most significant upstream activator of STAT3 within the T17 canonical pathway **(Supplementary Data)**. We used the downstream analysis module of IPA to identify dose, genotype, and phenotype effects on downstream functions and diseases of the secreted factors canonical pathway. Across doses, genotypes, and phenotypes, we identified neutrophil chemotaxis as one of the most significant downstream functions of the secreted factors canonical pathway **(Supplementary Data)**, and lung inflammation as one of the most significant downstream diseases of the secreted factors canonical pathway **(Supplementary Data)**.

Genotype, phenotype, and dose effects on targeted gene expression for T1, pro-T2, T2, and T17 responses

We identified dose, genotype and phenotype effects on IL-23-mediated STAT3 activation, which may define a potential mechanistic basis for G×P effects on AgNP toxicity. To better understand how this mechanism may differentially regulate AgNP-induced T1/pro-T2/T2/T17 responses, we characterized dose effects on targeted gene expression for T1, pro-T2, T2, and T17 cytokines. We observed discordant regulation across T1, pro-T2, T2, and T17 responses. We observed no consistent dose, genotype or phenotype effects on AgNP-induced T1 responses **(Figure 7A-B)**. However, we observed dose, phenotype effects on AgNP-induced pro-T2 **(Figure 7C-D)** and T2 responses **(Figure 7E-F)**, with downregulation of upstream pro-T2 cytokines *Il25*, *Il33*, and *Tslp* as well as downstream T2 cytokines *Il4*, *Il5*, *Il6*, *Il9*, *Il10*, and *Il13* under the "T2-Skewed" phenotype (P<0.05 - NS) compared to the "Normal" phenotype (P<0.001). We observed dose, phenotype effects on AgNP-induced regulation of T17 responses **(Figure 7G-H)**, with upregulation of T17 activator *Stat3* and downregulation of T17 inhibitor *Bcl6* under the "T2-Skewed" phenotype (P<0.001 - P>0.05) compared to the "Normal" phenotype (P<0.001 - P>0.05). We observed dose, phenotype effects on AgNP-induced T17 responses **(Figure 7G-H)**, with stronger, more persistent upregulation of T17 cytokines *Ccl20*, *Ccl25*, *Csf3*, *Cxcl1*, *Cxcl2*, *Cxcl3*, *Cxcl5*, *Il17c*, *Il23a*, and *Tgfb1* under the "T2-Skewed" phenotype (P<0.001) compared to the "Normal" phenotype (P<0.001 - P>0.05). The observed dose, phenotype effects on targeted gene expression suggest G×P effects on the "T2-Skewed" phenotype's shift toward a "T17-Like" phenotype, or an *in vitro* model of severe chronic respiratory diseases characteristic of neutrophilic/difficult-to-control asthma.

4.6 DISCUSSION

This is the first study to use organotypic cultures as a high-content *in vitro* model of the conducting airway to characterize G×P effects on transcriptional response to AgNP toxicity. We characterized global, differential, and targeted gene expression, canonical pathway enrichment, and upstream transcriptional regulation to understand G×P effects on transcriptional response to AgNP toxicity. We observed the "T2-Skewed" phenotype was marked by increased pro-inflammatory T17 responses to AgNP toxicity, which are significant predictors of neutrophilic/difficult-to-control asthma. This suggests that asthmatics could be a sensitive population to AgNP exposures in occupational settings,

as these adverse cellular responses may further modulate innate and adaptive immune responses at the epithelial-immune interface to exacerbate this chronic airway disease.[48] Understanding G×P effects is important for identifying these sensitive populations, whose underlying genetics or diseases could directly modify their response to AgNP exposures.

Asthma is a heterogeneous chronic airway disease regulated by divergent mechanisms of T2 and T17 inflammation. In a cross-sectional study by Brown et al., observed IL-4 and IL-13 were significant predictors of the T2-high endotype, or eosinophilic/easy-to-control asthma, whereas CXCL1, IL-5, IL-8, and IL-17A were significant predictors of the T17-high endotype, or neutrophilic/difficult-to-control asthma.[217] In another cross-sectional study by Choy et al., endobronchial tissue gene expression in asthmatics revealed three distinct endotypes of increasing severity: T2/17-low, T2-high, and T17-high.[211] To better understand this heterogeneity, the authors investigated how suppression of T2 cytokines may drive the potentiation of T17 responses in house dust mite (HDM)-sensitized, female BALB/cJ mice injected with anti-IL-4, anti-IL-13, and anti–IL-17 antibodies prior to sensitization. They observed that neutralization of IL-4 and/or IL-13 produced increased levels of T17 cells and exacerbated T17 lung inflammation, and that neutralization of both IL-13 and IL-17A was protective against mucus production, airway remodeling and hyperresponsiveness, as well as T2/T17 lung inflammation, suggesting that combination therapies targeting both mechanisms may maximize therapeutic efficacy in asthmatics comprising both T2-high and T17-high endotypes. These cytokines are differentially regulated across endotypes and have the potential to be shifted by AgNP toxicity. In the present study, we observed dose, phenotype effects on AgNP-induced T17 responses, with stronger, more persistent upregulation of T17 cytokines *Ccl20*, *Ccl25*, *Csf3*, *Cxcl1*, *Cxcl2*, *Cxcl3*, *Cxcl5*, *Il17c*, *Il23a*, and *Tgfb1* under the “T2-Skewed” phenotype compared to the “Normal” phenotype. The observed dose, phenotype effects on targeted gene expression suggest these cytokines are differentially regulated across phenotypes and were shifted by AgNP toxicity.

Our observations were supported by previous *in vivo* studies on the effects of host genetic factors on AgNP toxicity. Seiffert et al. exposed male Brown-Norway and Sprague-Dawley rats, and observed size, coating, and genotype effects on AgNP-induced T2/T17 lung

inflammation (marked by increased IL-6 and IL-17A secretion, pro-inflammatory cell infiltrate, and changes in histopathology) and lung dysfunction (marked by decreased airway resistance, tissue elastance), with Brown-Norway rats being the more sensitive genotype.[79,80] The authors also quantified dosimetric doses of silver (Ag) mass in the lungs of these differentially sensitive genotypes and detected higher burdens in Brown-Norway rats compared to Sprague-Dawley rats, suggesting that airway physiology (marked by alveolar size and airway branching) may be a contributing factor in genotype effects on AgNP toxicity, marked by AgNP-induced T2/T17 lung inflammation. Our observations were also supported by IPA in the present study, which identified *Stat3* as one of the most significantly activated upstream transcriptional regulators, and *Bcl6* as one of the most significantly inhibited upstream transcriptional regulators of the secreted factors canonical pathway. *Stat3* is recognized as the essential regulator of T17 cells, analogous to *Stat1* and *Stat4* in T1 cells, and *Stat6* in T2 cells. *Il6* and *Il23a* have been shown to synergistically regulate *Stat3*,[218] and while IL-23 is mostly produced by dendritic cells and macrophages, Lee et al. observed that this IL-17 inducible cytokine was produced in airway epithelial cells derived from antigen-sensitized female BALB/cJ mice.[219] IL-23 induces the differentiation of naive $CD4^+$ T cells into T17 cells; inhibiting IL-23 or its downstream factors, including IL-17, can attenuate the progression of inflammatory bowel diseases in animal models, which suggests the IL-23/IL-17 axis's relevance as a therapeutic target for chronic respiratory diseases.[220] *Stat3* has been shown to regulate *Bcl6*,[221] which is recognized as another essential regulator of T17 cells. Mondal et al. observed that *Bcl6* deficiency promoted T17 responses through suppression of T2 responses in *Bcl6*-knockout, C57BL/6J-129Sv mice.[222] In the present study, the shift toward a "T17-Like" phenotype may have also been orchestrated by reciprocal regulation of *Stat3* and *Bcl6* to suppress T2 cytokines *Il4*, *Il5*, *Il6*, *Il9*, *Il10*, and *Il13*. In addition to *Stat3* and *Bcl6*, T17 responses have also been shown to be tightly regulated by TGF-β and WNT signaling.[223,224] However, in the present study, we observed more limited dose, genotype, and phenotype effects on TGF-β and WNT signaling canonical pathway enrichment **(Supplementary Data)**, which suggests these canonical pathways may have played a more understated role when compared to the secreted factors canonical pathway with regard to driving the mechanistic basis for G×P effects on AgNP

toxicity. Overall, the observed dose, genotype and phenotype effects on IL-23-mediated *Stat3* activation are suggestive of G×P effects on upstream transcriptional regulation of the secreted factors canonical pathway, which produced a shift toward a “T17-Like” phenotype, or an *in vitro* model of severe chronic respiratory diseases characteristic of neutrophilic/difficult-to-control asthma.

This is first study to use organotypic cultures as a high-content *in vitro* model of the conducting airway paired with RNA-seq to characterize G×P effects on transcriptional response to AgNP toxicity, and therefore, refining this *in vitro* model in future studies is warranted. One limitation of this study was the use of only one sex and two genotypes; the use of both sexes and additional genotypes (e.g., BALB/cJ and SWR/J mice) or knockouts (e.g., *Il23*$^{-/-}$, *Stat3*$^{-/-}$, or *Bcl6*$^{-/-}$ mice) would increase genetic diversity and further assist in defining a mechanistic basis for G×P effects on AgNP toxicity in future studies. A second limitation of this study was the use of IL-13 to skew differentiation toward an *in vitro* model of chronic respiratory diseases; the use of additional cytokines, such as IL-17, to skew differentiation toward an *in vitro* model of severe chronic respiratory diseases would better reflect the diversity of T2-high and T17-high endotypes and improve the physiological relevance of this *in vitro* model in future studies. A third limitation of this study was the fact the we did not address whether these differences in gene expression translate into differences in protein expression for secreted factors in bronchoalveolar lavage fluid (BALF). Characterizing these differences in gene expression in humans depends upon invasive procedures and therefore precludes routine use, which emphasises the need to identify less invasive mechanistic-based biomarkers of AgNP toxicity still capable of producing biologically robust predictions of adverse organism responses resulting from these occupational exposures.

Despite these limitations, this study establishes organotypic cultures derived from MTEC as a medium-throughput, high-content *in vitro* model of the conducing airway to characterize chemical perturbation as a means to screen and prioritize potential respiratory toxicants. Our results highlight the importance of considering G×P effects on transcriptional regulation when screening and prioritizing potential respiratory toxicants. This is challenging and important for engineered nanomaterials, since their MoA have

been shown to differ considerably but are still used in hundreds of consumer products. Prior to anticipating potential adverse organism responses arising from engineered nanomaterial toxicity, ensuring safe development of the consumer products in which they are used will be the most critical and necessary step toward safeguarding public health.

AUTHOR CONTRIBUTIONS

The manuscript was written through contributions of all authors. All authors have given approval to the final version of the manuscript.

FUNDING SOURCES

This work was supported by the US EPA under Grant R835738 (E.M.F., T.J.K., W.A.A); NIH under Grants P30 ES007033 (T.J.K.), T32 ES007032-38 (T.P.N.), and NIH R01 AI137111 (S.A.G.); the Washington State Department of Labor and Industries under the Medical Aid/Accident Fund; (T.P.N.) and the University of Washington under the GO-MAP Dissertation Fellowship (T.P.N.).

NOTES

The authors declare no competing financial interest.

ACKNOWLEDGEMENTS

The authors gratefully acknowledge Dowon An for her technical support with animals, and Yu Hua Chow for her technical support with RNA isolation and purification. Part of this work was conducted at the Genomics Core Laboratory of the Benaroya Research Institute at Virginia Mason.

4.7 DATA

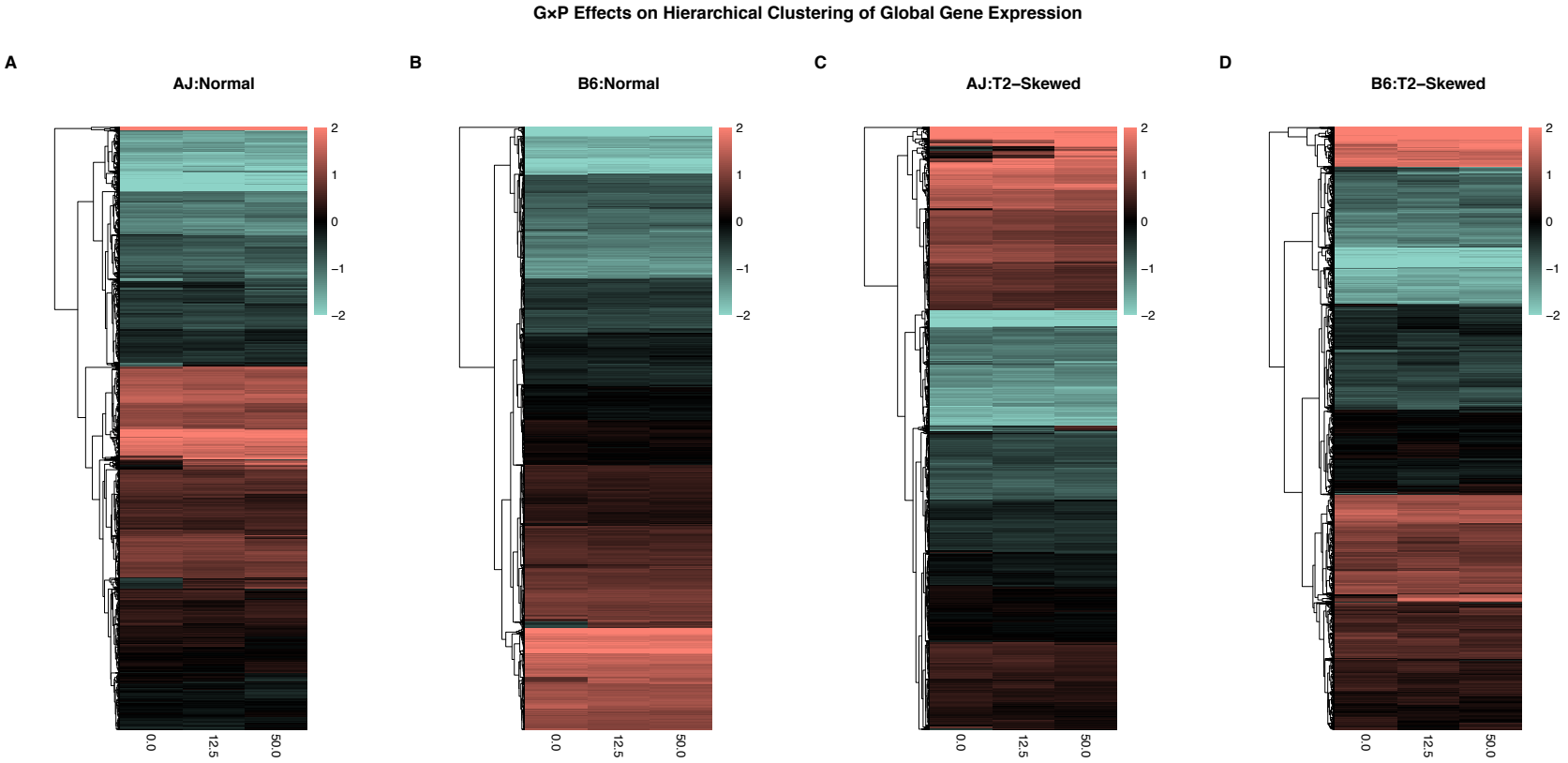

Figure 4.1. Genotype, phenotype, and dose effects on hierarchical clustering of global gene expression. Hierarchical clustering of global gene expression was characterized using Pearson correlation distance and average linkage distance of $\log_2$(average read counts) (n = 9,642) for AJ:Normal **(A)**, B6:Normal **(B)**, AJ:T2-Skewed **(C)**, and B6:T2-Skewed **(D)** exposed to nominal doses of 0, 12.5, or 50 µg AgNP/mL media for an acute 24 h exposure. Data represent average z-scores (red = positive; green = negative); rows represent genes, and columns represent genotypes and phenotypes. n = 3 biological replicates.

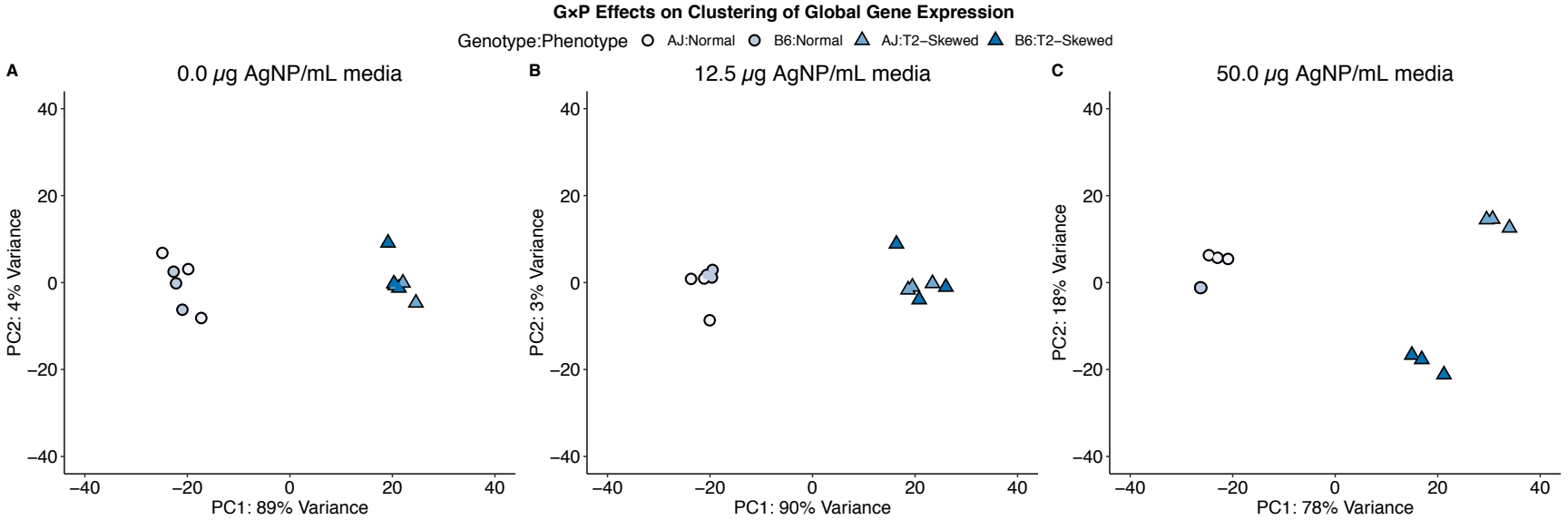

Figure 4.2. Genotype, phenotype, and dose effects on principal components of global gene expression. Principal components of global gene expression were characterized using PCA of $\log_2$(average read counts) (n = 9,642) for AJ:Normal, B6:Normal, AJ:T2-Skewed, and B6:T2-Skewed exposed to nominal doses of 0 **(A)**, 12.5 **(B)**, or 50 **(C)** µg AgNP/mL media for an acute 24 h exposure. n = 3 biological replicates.

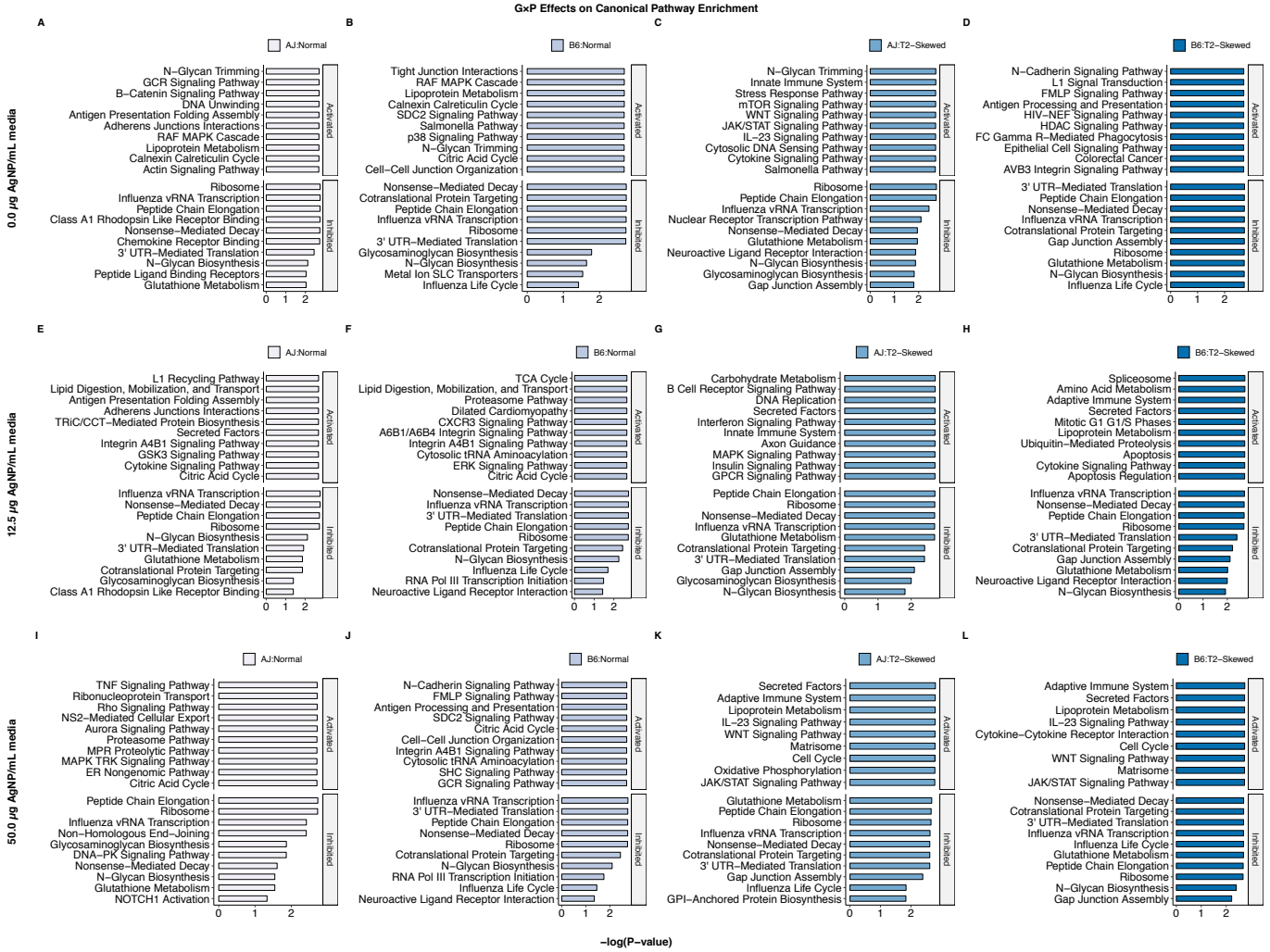

Figure 4.3. Genotype, phenotype, and dose effects on canonical pathway enrichment. Canonical pathway enrichment was characterized using GSEA with the Benjamini-Hochberg method (*FDR*<0.10) on rank-ordered z-scores of $\log_2$(average read counts) (*n* = 9,642) for AJ:Normal, B6:Normal, AJ:T2-Skewed, and B6:T2-Skewed exposed to nominal doses of 0 **(A-D)**, 12.5 **(E-H)**, or 50 **(I-J)** μg AgNP/mL media for an acute 24 h exposure. Data represent the top ten enriched canonical pathways with significant -log(*P*-values), where activated = normalized enrichment score > 0, inhibited = normalized enrichment score < 0. *n* = 3 biological replicates.

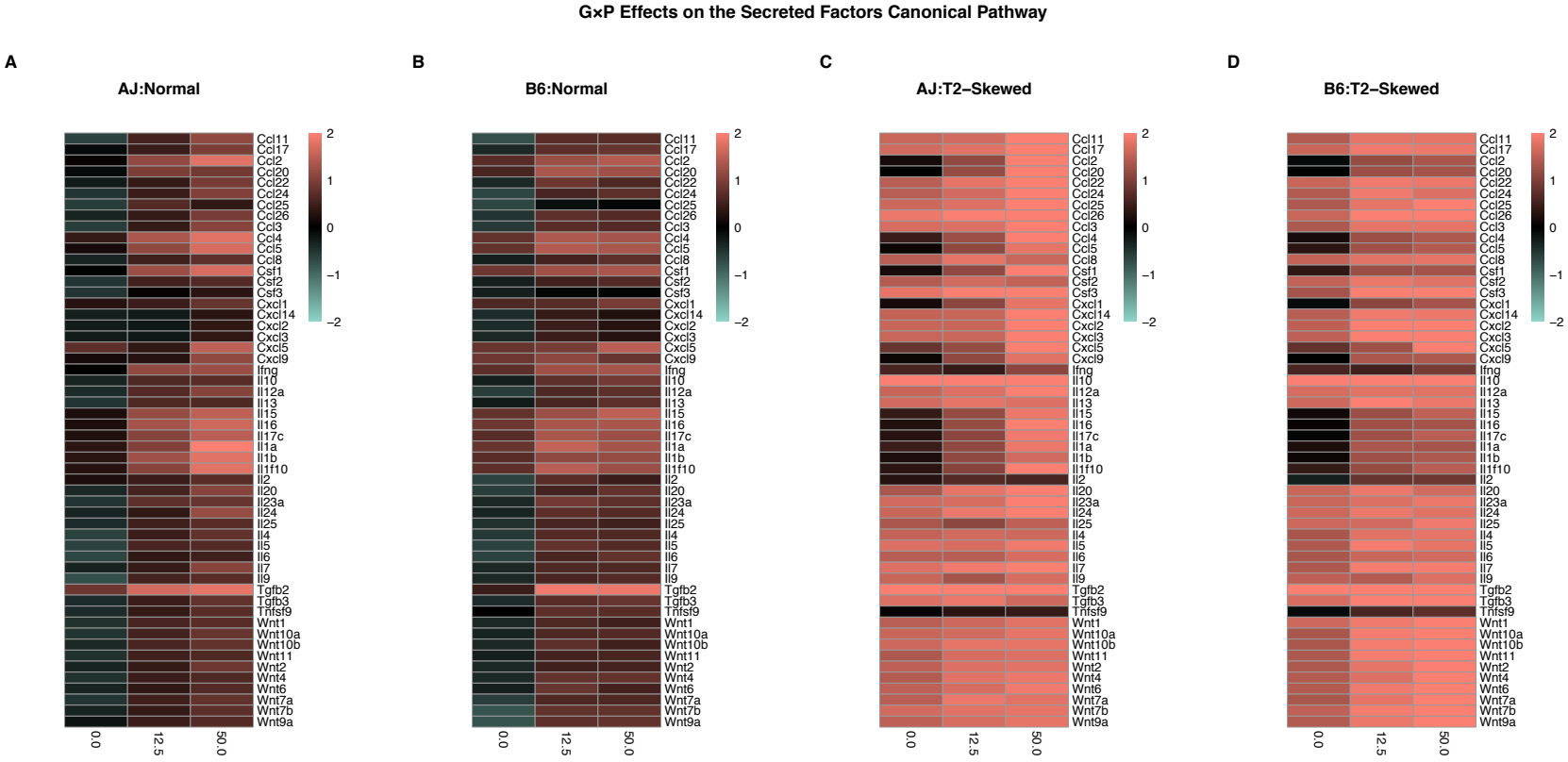

Figure 4.4. Genotype, phenotype, and dose effects on targeted gene expression for the secreted factors canonical pathway. Targeted gene expression for the secreted factors canonical pathway was characterized using z-scores of $\log_2$(average read counts) (*n* =54) for AJ:Normal **(A)**, B6:Normal **(B)**, AJ:T2-Skewed **(C)**, and B6:T2-Skewed **(D)** exposed to nominal doses of 0, 12.5, or 50 µg AgNP/mL media for an acute 24 h exposure. Data represent average z-scores (red = positive; green = negative); rows represent genes, and columns represent doses. *n* = 3 biological replicates.

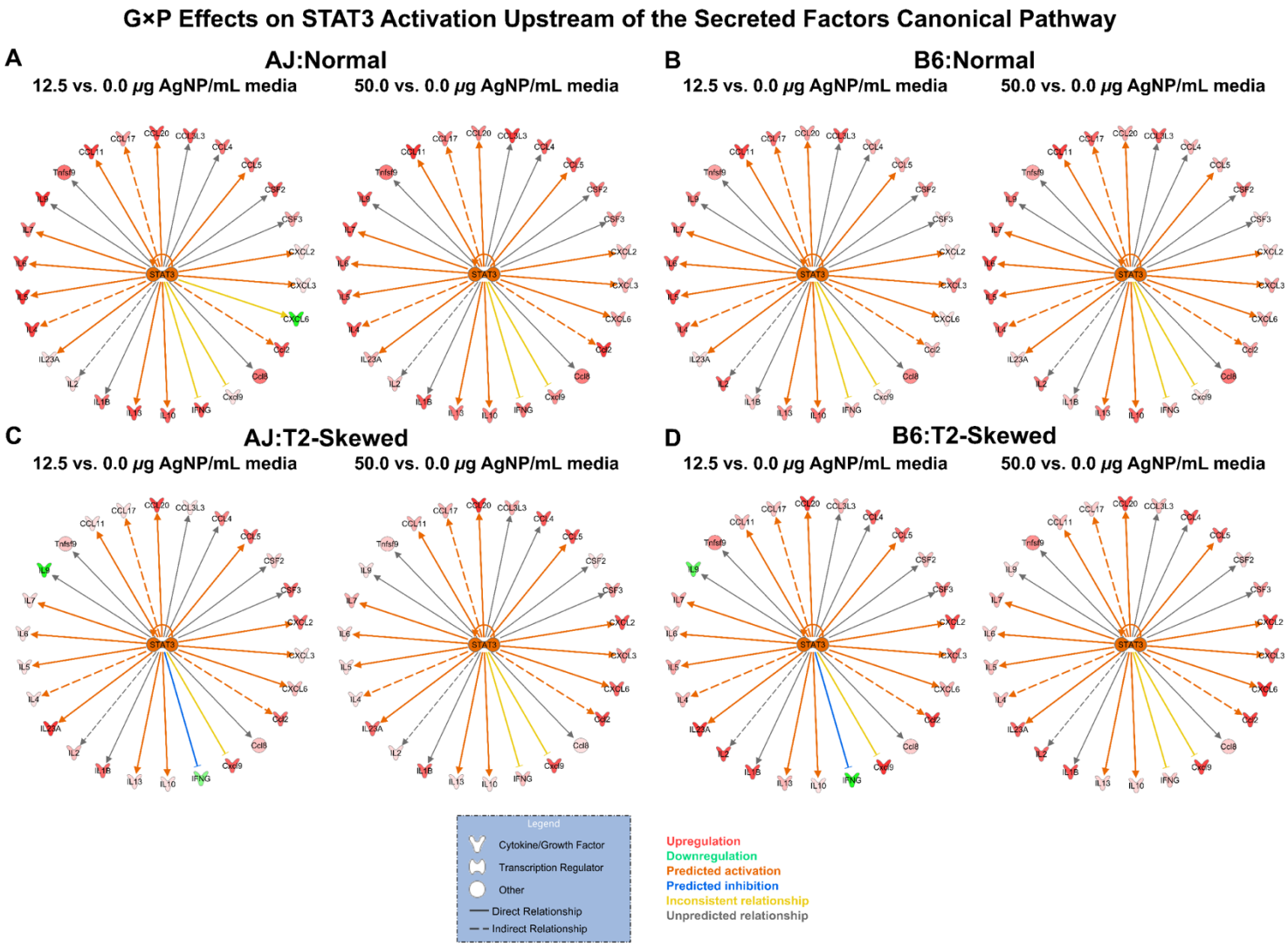

Figure 4.5. Genotype, phenotype, and dose effects on *Stat3* activation upstream of the secreted factors canonical pathway. Upstream activation of the secreted factors canonical pathway was characterized using IPA with the Fischer's Exact method (*FDR*<0.10) on fold changes of $\log_2$(average AgNP/vehicle control) (n = 54) for AJ:Normal **(A)**, B6:Normal **(B)**, AJ:T2-Skewed **(C)**, and B6:T2-Skewed **(D)** exposed to nominal doses of 0, 12.5, or 50 μg AgNP/mL media for an acute 24 h exposure. Central icons represent the upstream activator (*Stat3*), peripheral icons represent cytokine/growth factors, and arrows represent predicted relationships. n = 3 biological replicates.

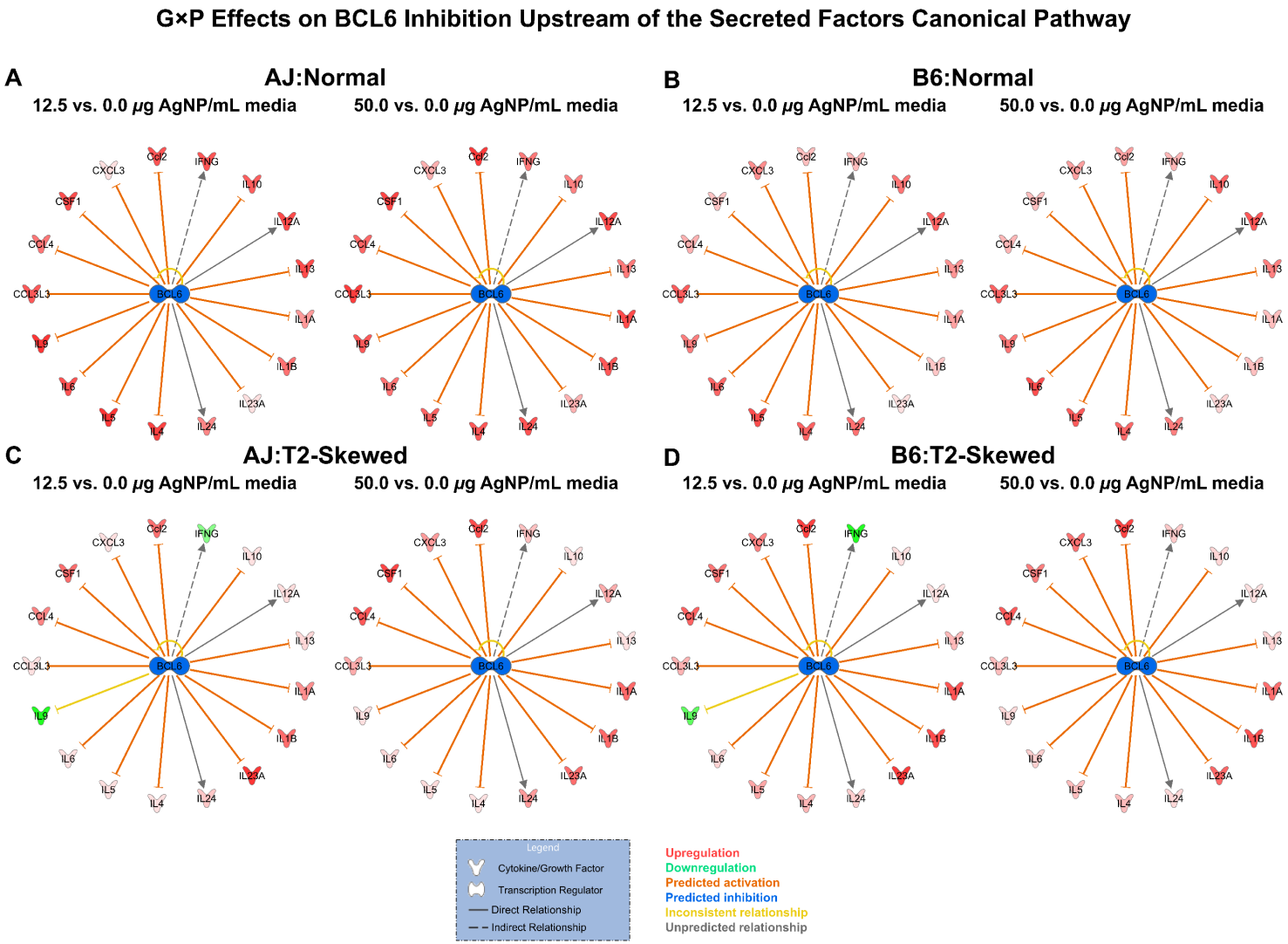

Figure 4.6. Genotype, phenotype, and dose effects on *Bcl6* inhibition upstream of the secreted factors canonical pathway. Upstream inhibition of the secreted factors canonical pathway was characterized using IPA with the Fischer's Exact method (*FDR*<0.10) on fold changes of $\log_2$(average AgNP/vehicle control) (n = 54) for AJ:Normal **(A)**, B6:Normal **(B)**, AJ:T2-Skewed **(C)**, and B6:T2-Skewed **(D)** exposed to nominal doses of 0, 12.5, or 50 μg AgNP/mL media for an acute 24 h exposure. Central icons represent the upstream inhibitor (*Bcl6*), peripheral icons represent cytokine/growth factors, and arrows represent predicted relationships. n = 3 biological replicates.

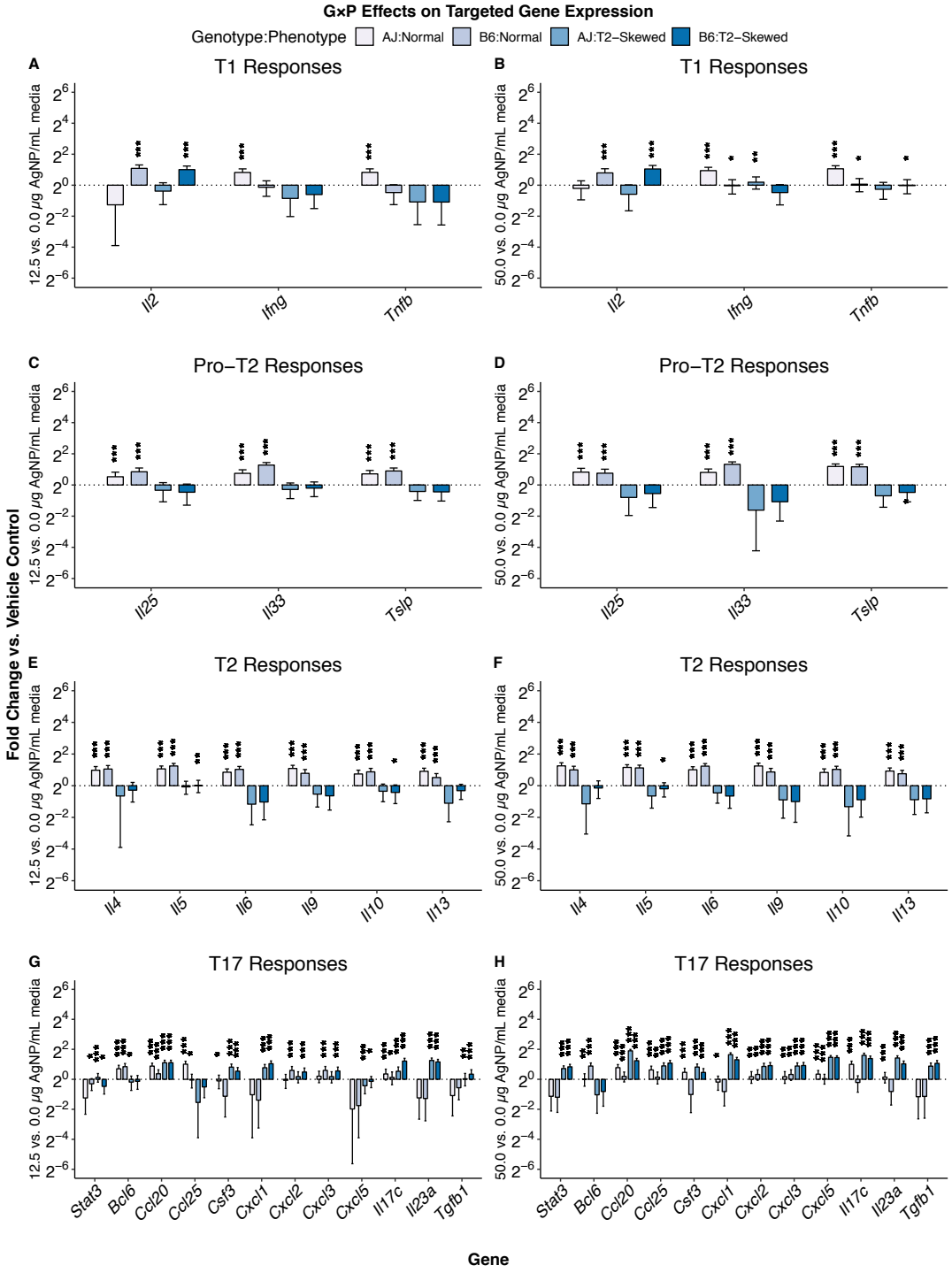

Figure 4.7. Genotype, phenotype, and dose effects on targeted gene expression associated with clinical features of severe chronic respiratory diseases.Differential gene expression for T1 responses **(A-B)**, pro-T2 responses **(C-D)**, T2 responses **(E-F)**, and T17 responses **(G-H)** was characterized using a *t*-test for significant differences in gene expression (*FDR*<0.10) on fold changes of $\log_2$(average AgNP/vehicle control) (n = 24) for AJ:Normal, B6:Normal, AJ:T2-Skewed, and B6:T2-Skewed exposed to nominal doses of 0, 12.5, or 50 µg AgNP/mL media for an acute 24 h exposure. Data represent average $\log_2$(AgNP/vehicle control) fold changes ± SE; NS (P>0.05); * (P<0.05); ** (P<0.01); *** (P<0.001). n = 3 biological replicates.

4.8 SUPPLEMENTARY DATA

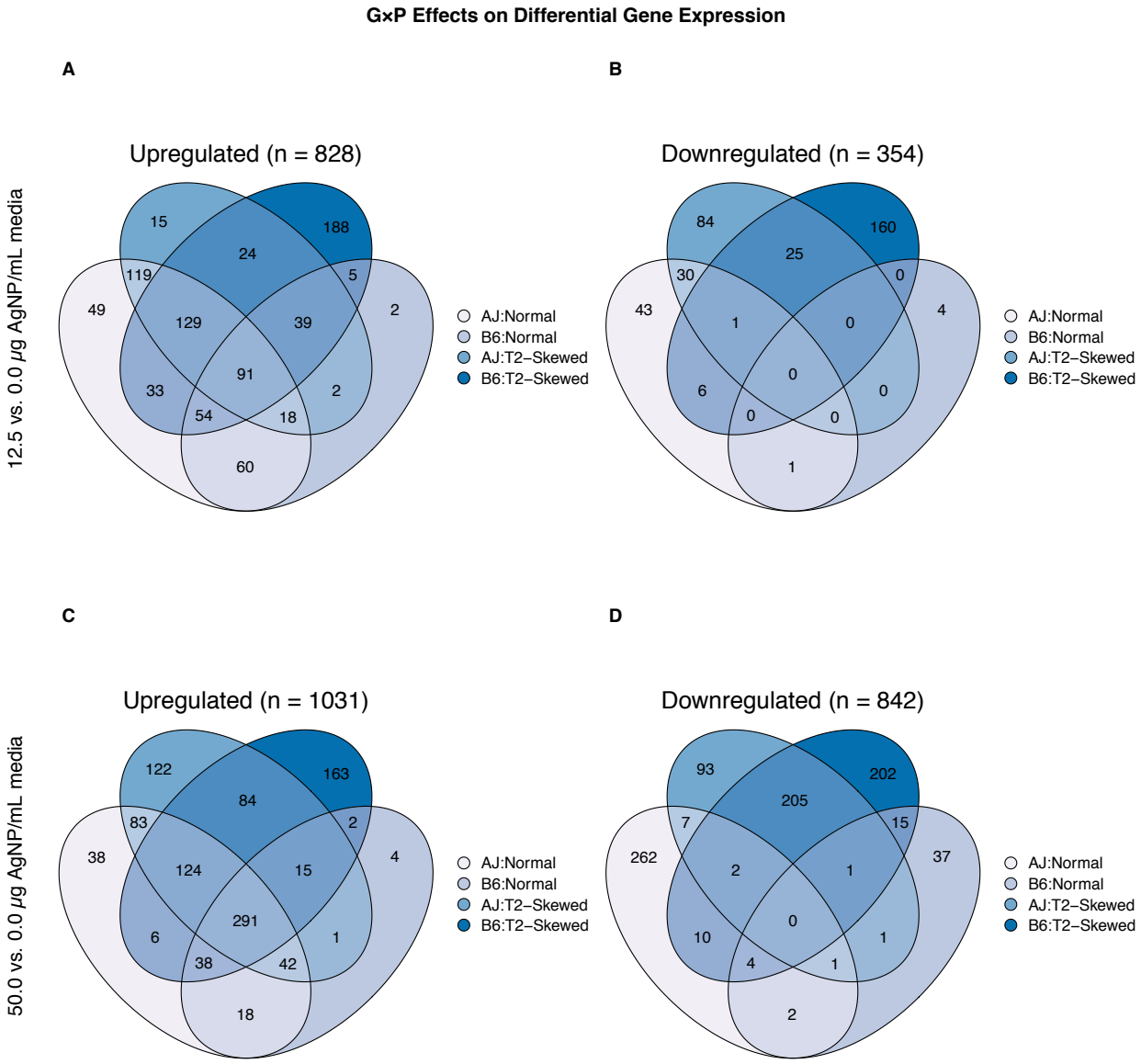

Genotype, phenotype, and dose effects on differential gene expression. Differential gene expression was characterized using a *t*-test for significant differences in gene expression (*FDR*<0.10). Dose effects = 12.5 **(A-B)** and 50 **(C-D)** μg AgNP/mL media vs. vehicle controls. Data represent the number of significant $\log_2$(AgNP/vehicle control) fold changes, where upregulated = $\log_2$(AgNP/vehicle control) fold change < 0, downregulated = $\log_2$(AgNP/vehicle control) fold change > 0. *n* = 3 biological replicates.

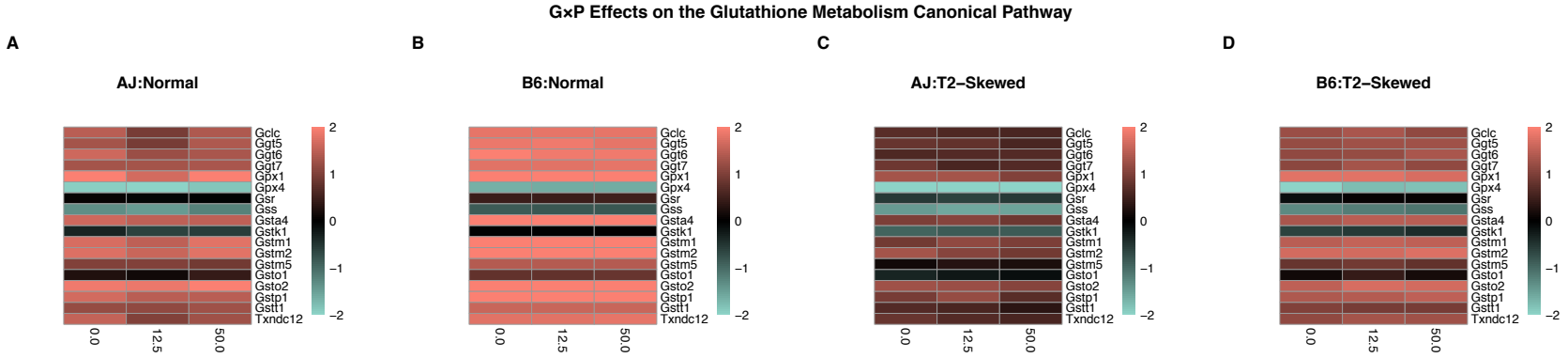

Genotype, phenotype, and dose effects on targeted gene expression for the glutathione metabolism canonical pathway. Targeted gene expression for the glutathione metabolism canonical pathway was characterized using z-scores of $\log_2$(average read counts) (*n* = 14) for AJ:Normal **(A)**, B6:Normal **(B)**, AJ:T2-Skewed **(C)**, and B6:T2-Skewed **(D)** exposed to nominal doses of 0, 12.5, or 50 µg AgNP/mL media for an acute 24 h exposure. Data represent average z-scores (red = positive; green = negative); rows represent genes, and columns represent doses. *n* = 3 biological replicates.

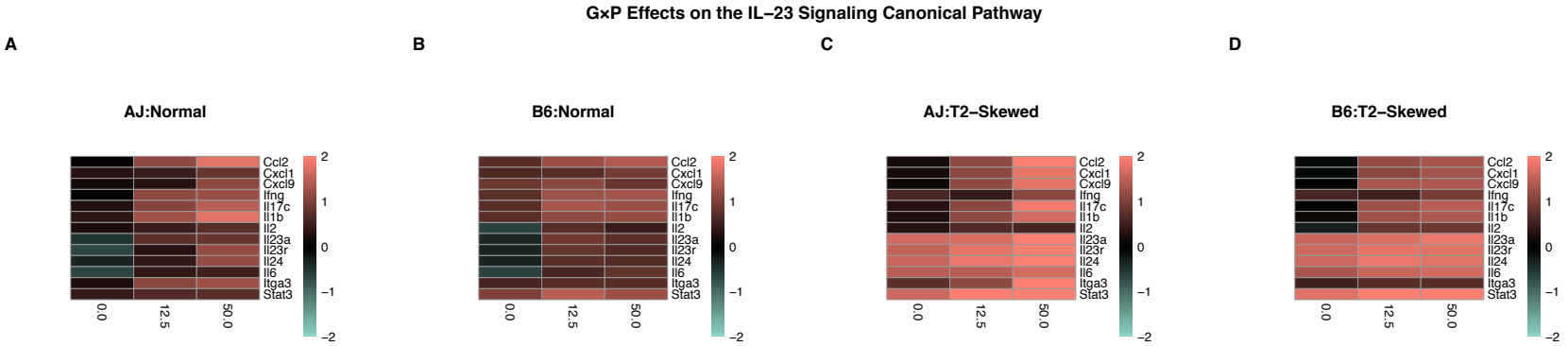

Genotype, phenotype, and dose effects on targeted gene expression for the IL-23 signaling canonical pathway. Targeted gene expression for the IL-23 signaling canonical pathway was characterized using z-scores of $\log_2$(average read counts) (*n* = 13) for AJ:Normal **(A)**, B6:Normal **(B)**, AJ:T2-Skewed **(C)**, and B6:T2-Skewed **(D)** exposed to nominal doses of 0, 12.5, or 50 µg AgNP/mL media for an acute 24 h exposure. Data represent average z-scores (red = positive; green = negative); rows represent genes, and columns represent doses. *n* = 3 biological replicates.

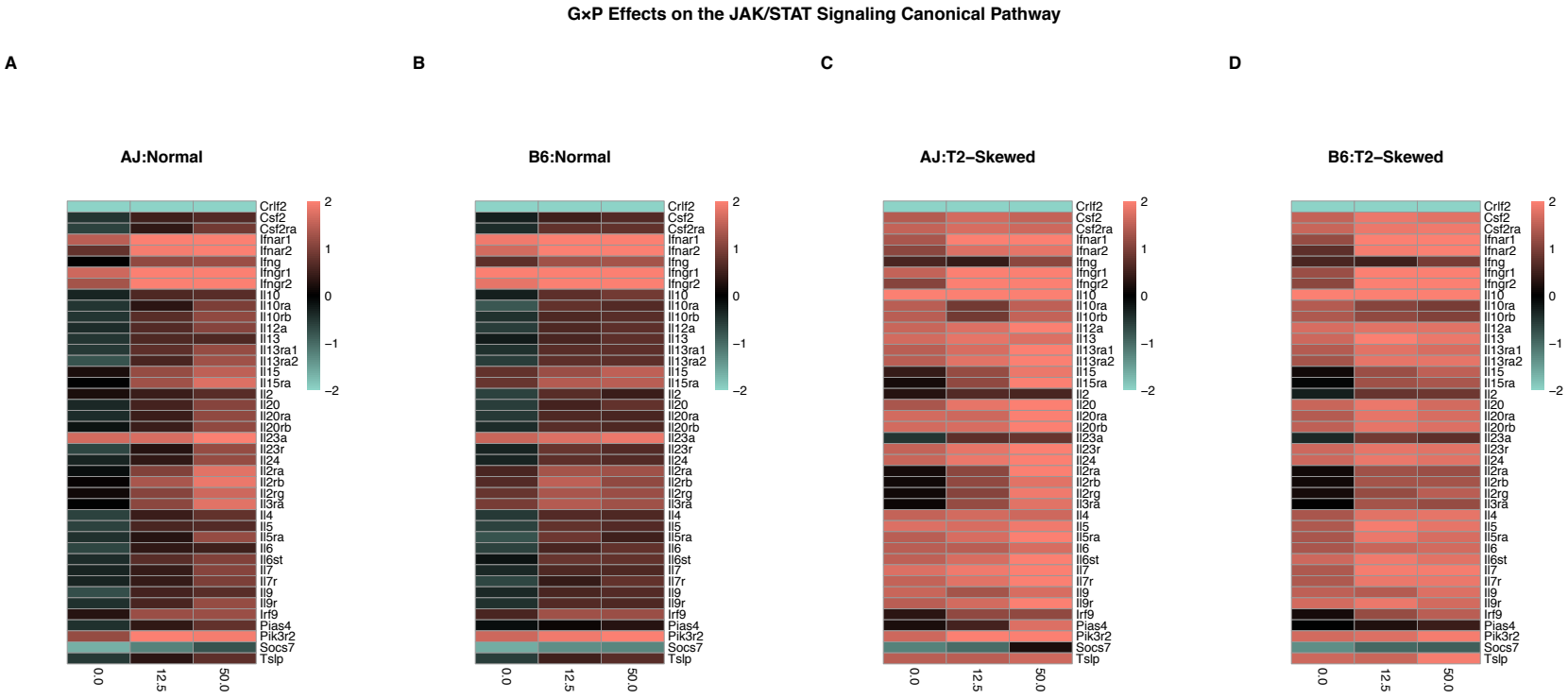

Genotype, phenotype, and dose effects on targeted gene expression for the JAK/STAT signaling canonical pathway. Targeted gene expression for the JAK/STAT signaling canonical pathway was characterized using z-scores of $\log_2$(average read counts) (n = 42) for AJ:Normal **(A)**, B6:Normal **(B)**, AJ:T2-Skewed **(C)**, and B6:T2-Skewed **(D)** exposed to nominal doses of 0, 12.5, or 50 µg AgNP/mL media for an acute 24 h exposure. Data represent average z-scores (red = positive; green = negative); rows represent genes, and columns represent doses. n = 3 biological replicates.

Cytokine Activation of the T17 Canonical Pathway

AJ:Normal

12.5 vs. 0.0 μg AgNP/mL media

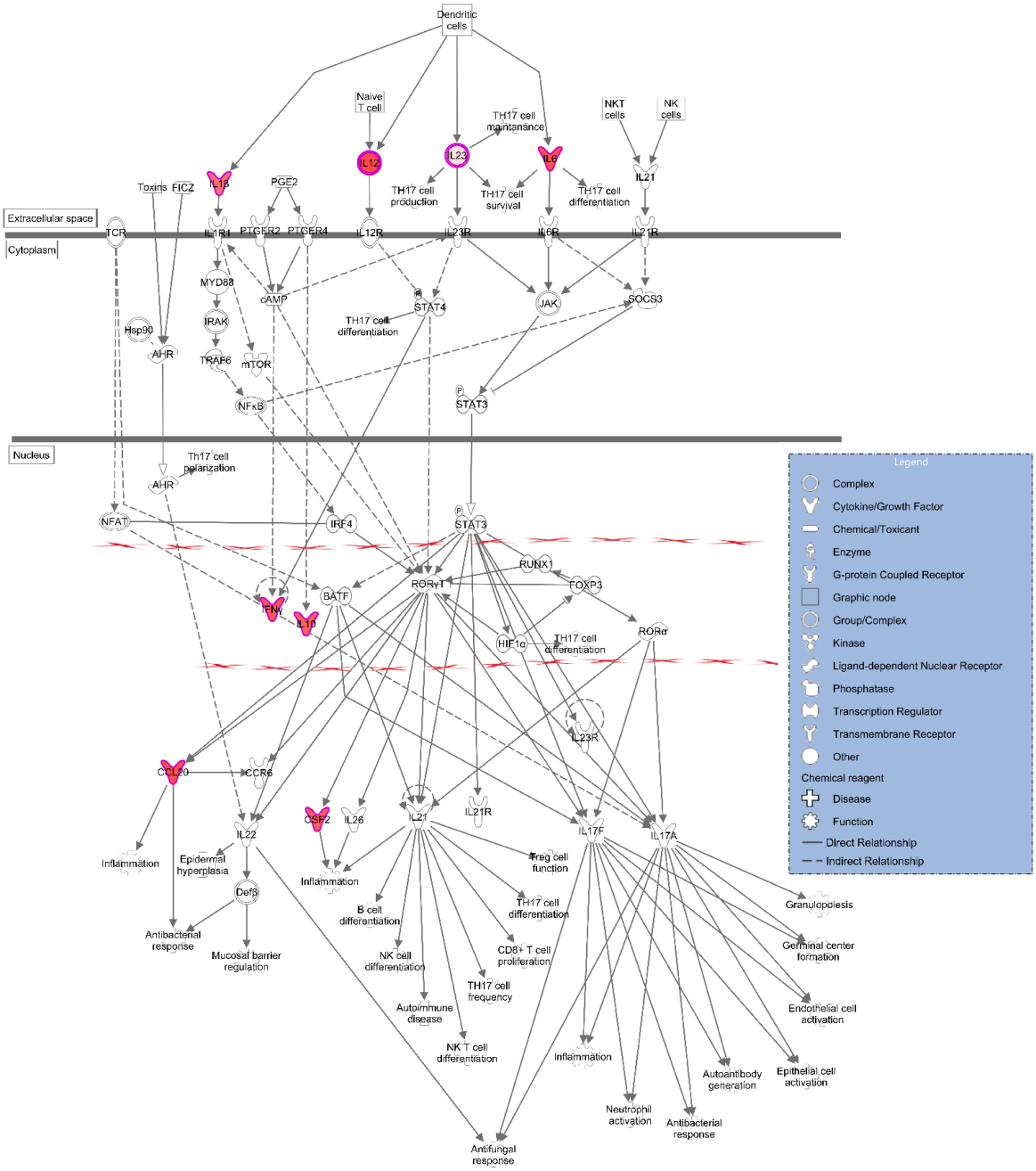

Cytokine activation of the T17 canonical pathway. Cytokine activation of the secreted factors canonical pathway was characterized using IPA with the Fischer's Exact method (*FDR*<0.10) on fold changes of $\log_2$(average AgNP/vehicle control) (n = 54) for AJ:Normal exposed to nominal doses of 0 or 12.5 μg AgNP/mL media for an acute 24 h exposure. Highlighted icons represent cytokine/growth factors, and arrows represent predicted relationships. n = 3 biological replicates.

Cytokine Activation of the T17 Canonical Pathway

AJ:Normal
50.0 vs. 0.0 μg AgNP/mL media

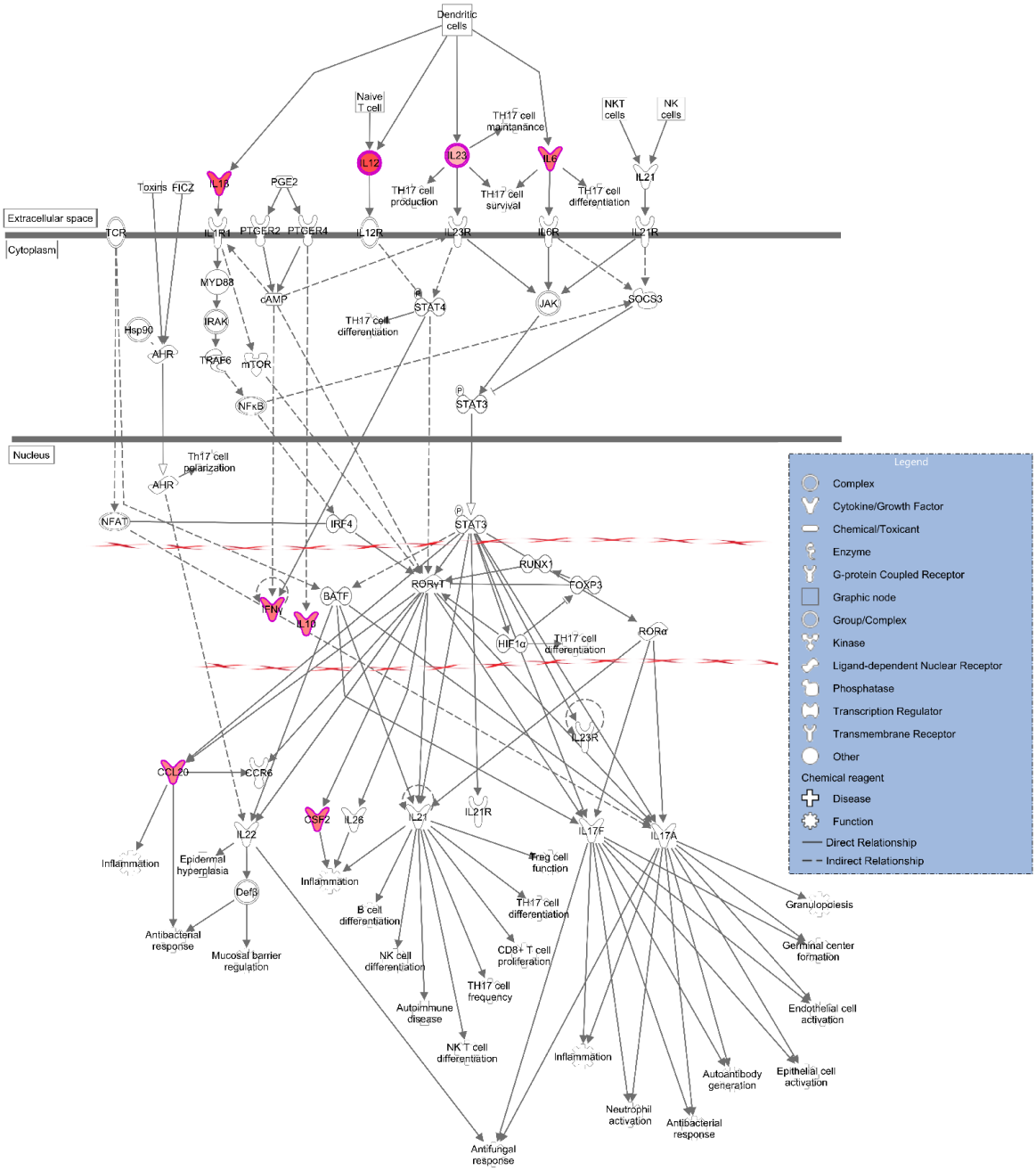

Cytokine activation of the T17 canonical pathway. Cytokine activation of the secreted factors canonical pathway was characterized using IPA with the Fischer's Exact method (*FDR*<0.10) on fold changes of $\log_2$(average AgNP/vehicle control) (n = 54) for AJ:Normal exposed to nominal doses of 0 or 50 μg AgNP/mL media for an acute 24 h exposure. Highlighted icons represent cytokine/growth factors, and arrows represent predicted relationships. n = 3 biological replicates.

Cytokine Activation of the T17 Canonical Pathway

B6:Normal
12.5 vs. 0.0 μg AgNP/mL media

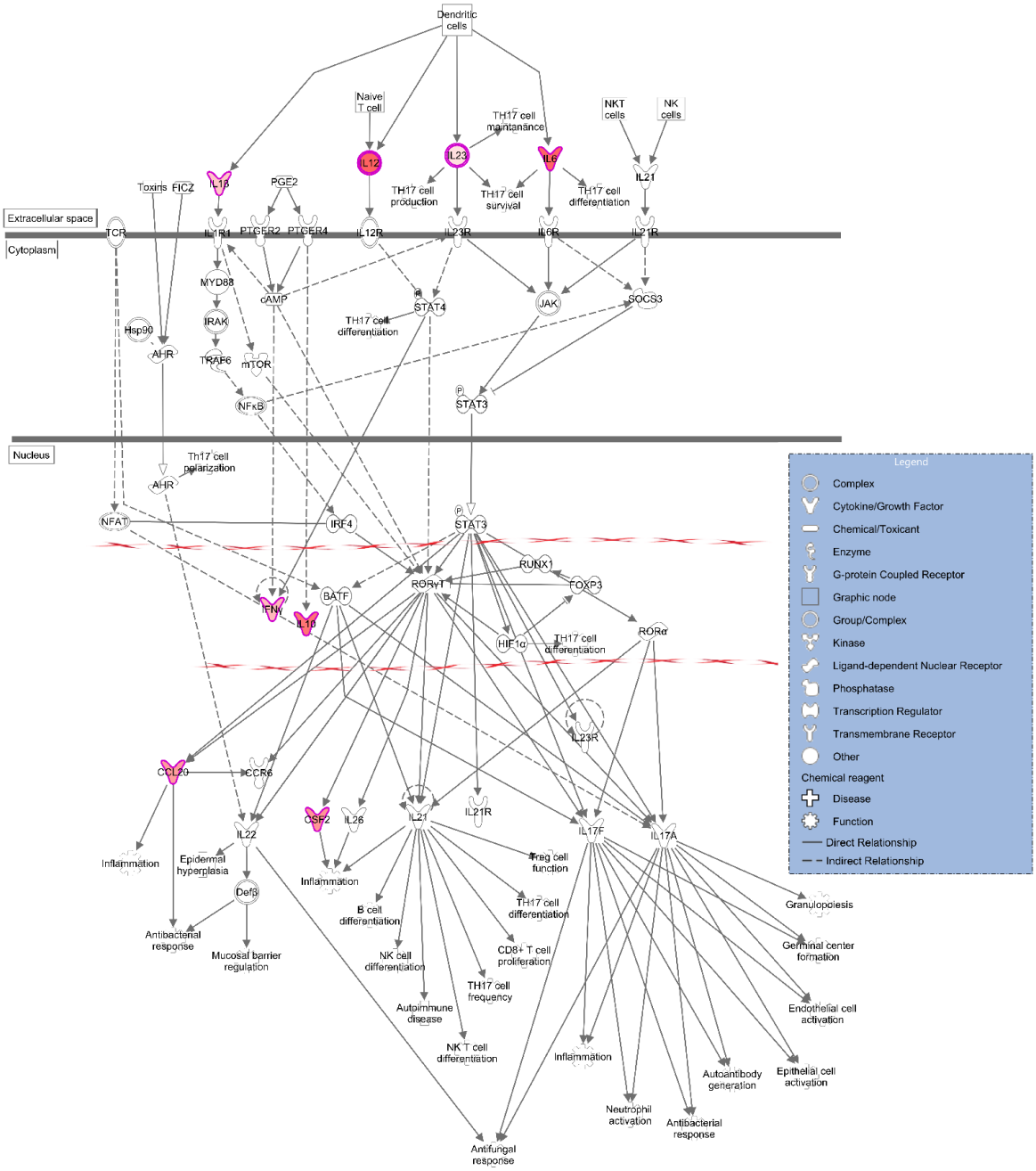

Cytokine activation of the T17 canonical pathway. Cytokine activation of the secreted factors canonical pathway was characterized using IPA with the Fischer's Exact method (*FDR*<0.10) on fold changes of $\log_2$(average AgNP/vehicle control) (n = 54) for B6:Normal exposed to nominal doses of 0 or 12.5 μg AgNP/mL media for an acute 24 h exposure. Highlighted icons represent cytokine/growth factors, and arrows represent predicted relationships. n = 3 biological replicates.

Cytokine Activation of the T17 Canonical Pathway

B6:Normal
50.0 vs. 0.0 μg AgNP/mL media

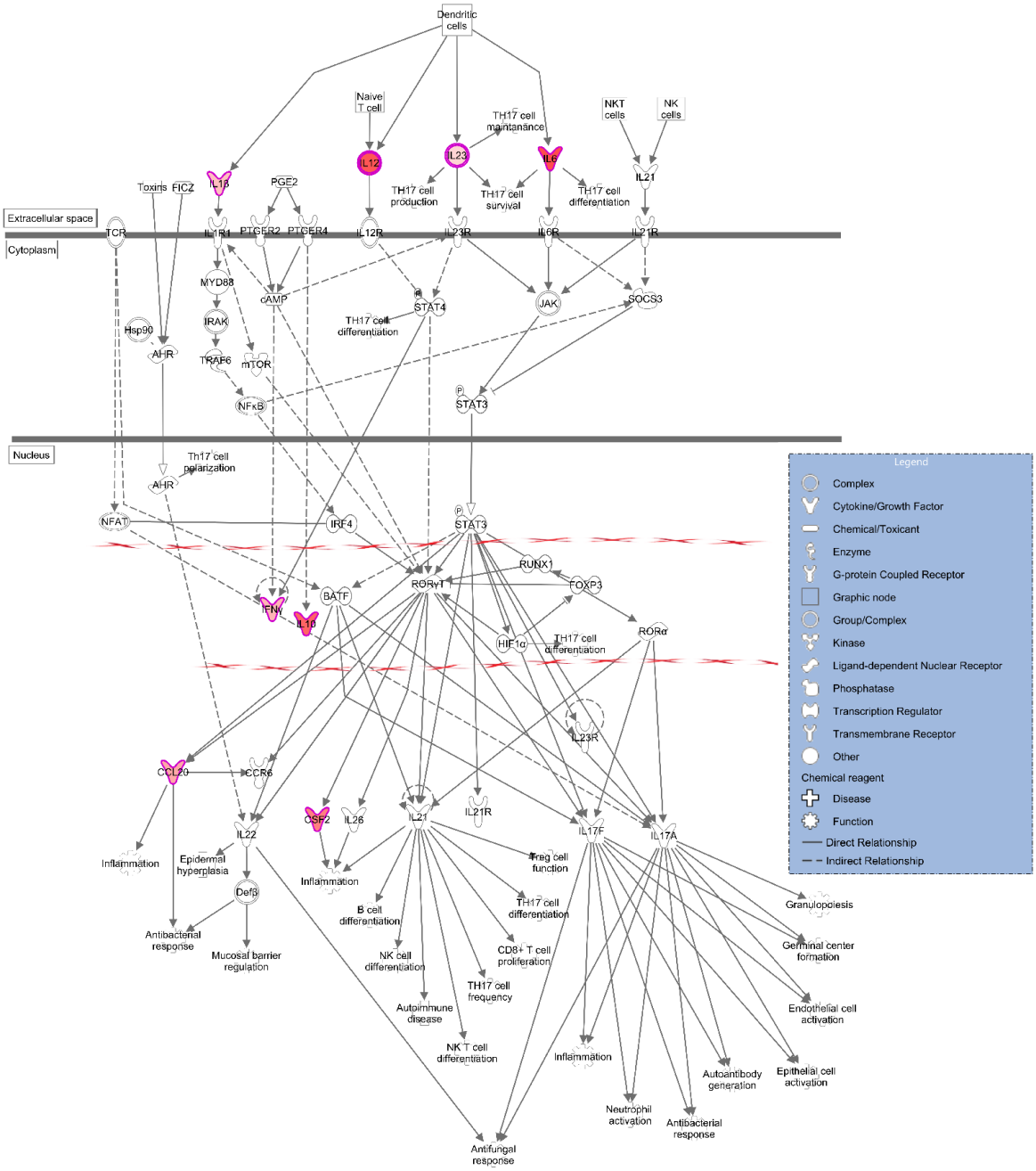

Cytokine activation of the T17 canonical pathway. Cytokine activation of the secreted factors canonical pathway was characterized using IPA with the Fischer's Exact method (*FDR*<0.10) on fold changes of $\log_2$(average AgNP/vehicle control) (n = 54) for B6:Normal exposed to nominal doses of 0 or 50 μg AgNP/mL media for an acute 24 h exposure. Highlighted icons represent cytokine/growth factors, and arrows represent predicted relationships. n = 3 biological replicates.

Cytokine Activation of the T17 Canonical Pathway

AJ:T2-Skewed
12.5 vs. 0.0 μg AgNP/mL media

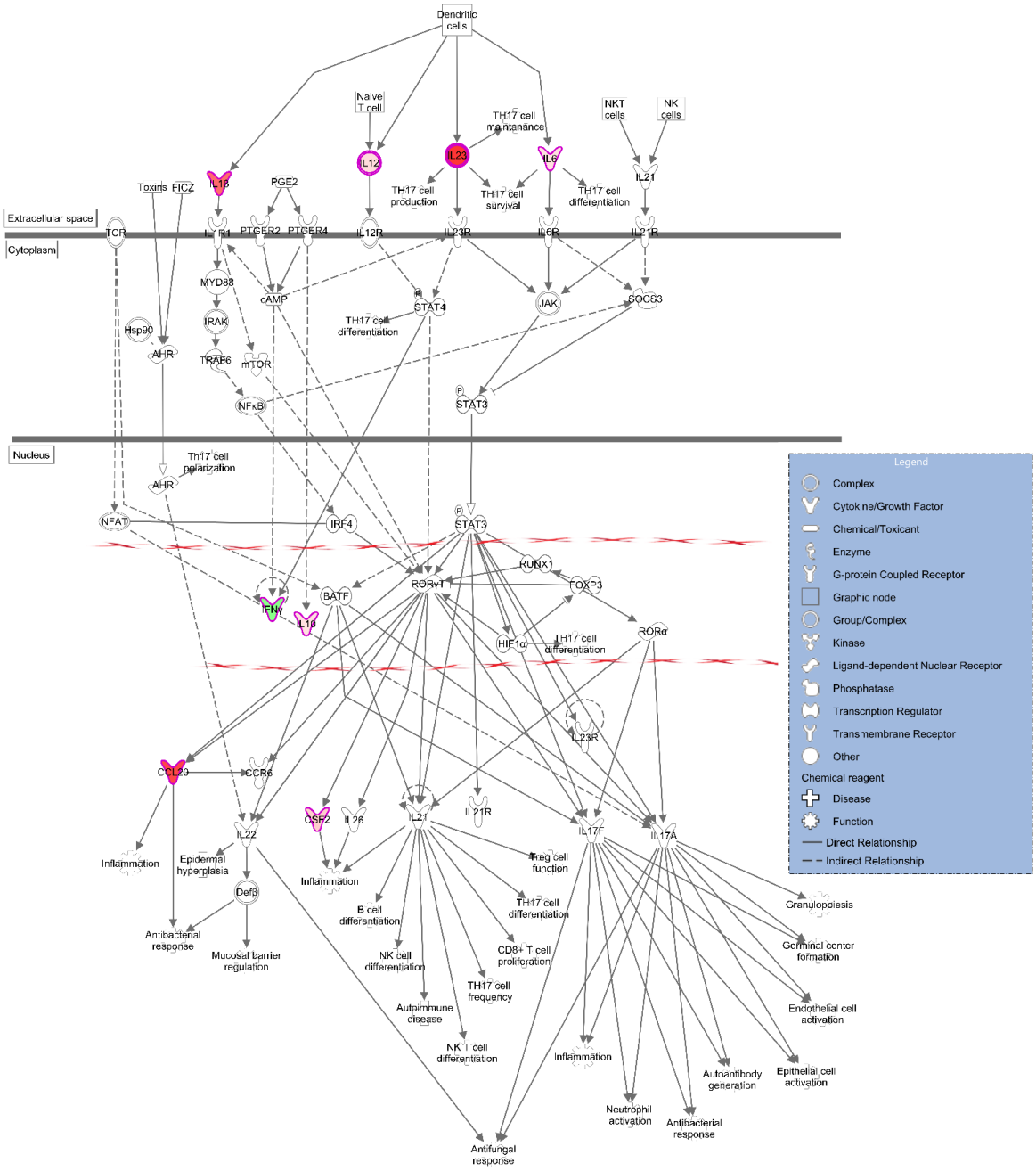

Cytokine activation of the T17 canonical pathway. Cytokine activation of the secreted factors canonical pathway was characterized using IPA with the Fischer's Exact method (*FDR*<0.10) on fold changes of $\log_2$(average AgNP/vehicle control) (n = 54) for AJ:T2-Skewed exposed to nominal doses of 0 or 12.5 μg AgNP/mL media for an acute 24 h exposure. Highlighted icons represent cytokine/growth factors, and arrows represent predicted relationships. n = 3 biological replicates.

Cytokine Activation of the T17 Canonical Pathway

AJ:T2-Skewed
50.0 vs. 0.0 μg AgNP/mL media

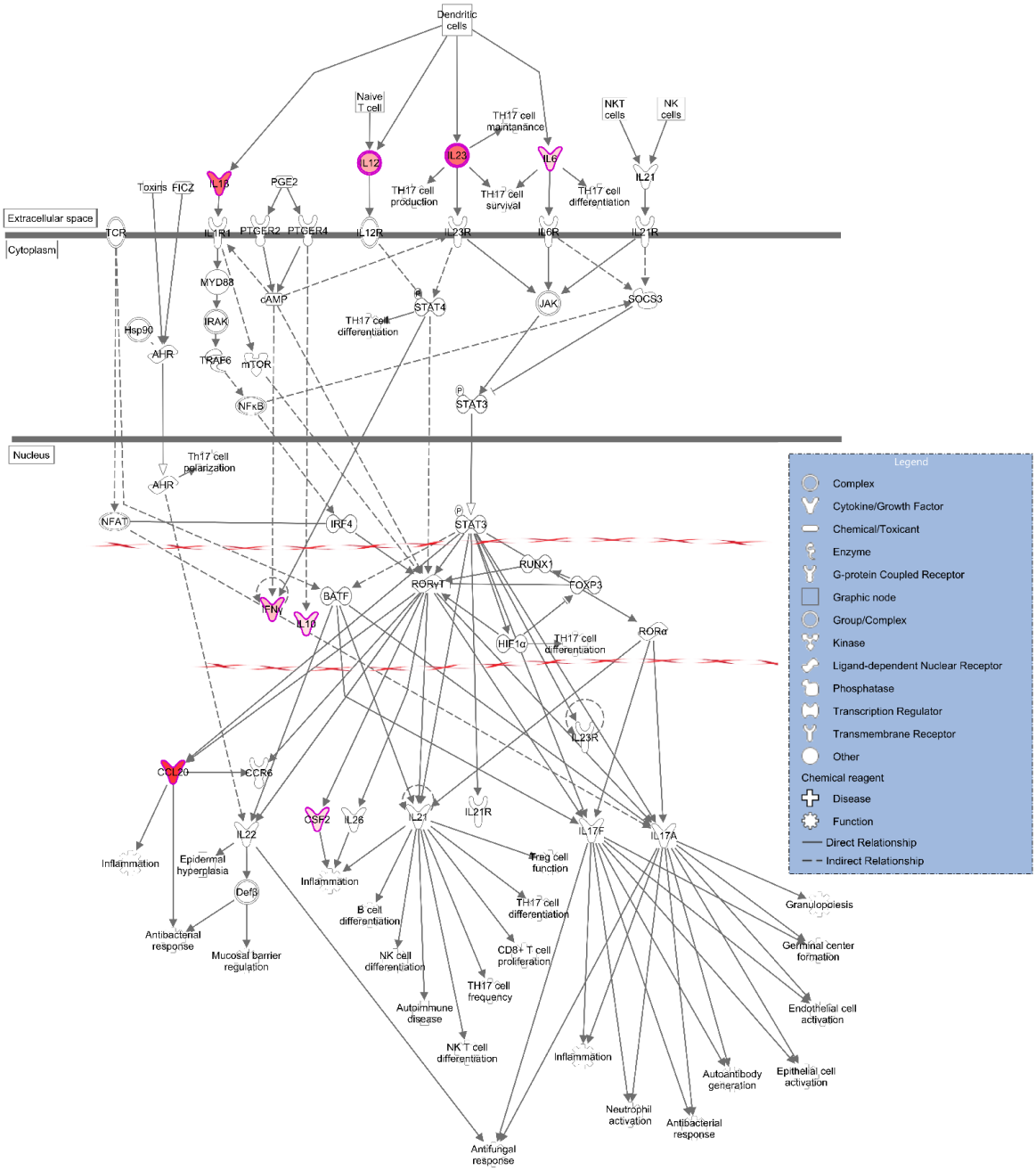

Cytokine activation of the T17 canonical pathway. Cytokine activation of the secreted factors canonical pathway was characterized using IPA with the Fischer's Exact method (*FDR*<0.10) on fold changes of $\log_2$(average AgNP/vehicle control) (n = 54) for AJ:T2-Skewed exposed to nominal doses of 0 or 50 μg AgNP/mL media for an acute 24 h exposure. Highlighted icons represent cytokine/growth factors, and arrows represent predicted relationships. n = 3 biological replicates.

Cytokine Activation of the T17 Canonical Pathway

B6:T2-Skewed
12.5 vs. 0.0 μg AgNP/mL media

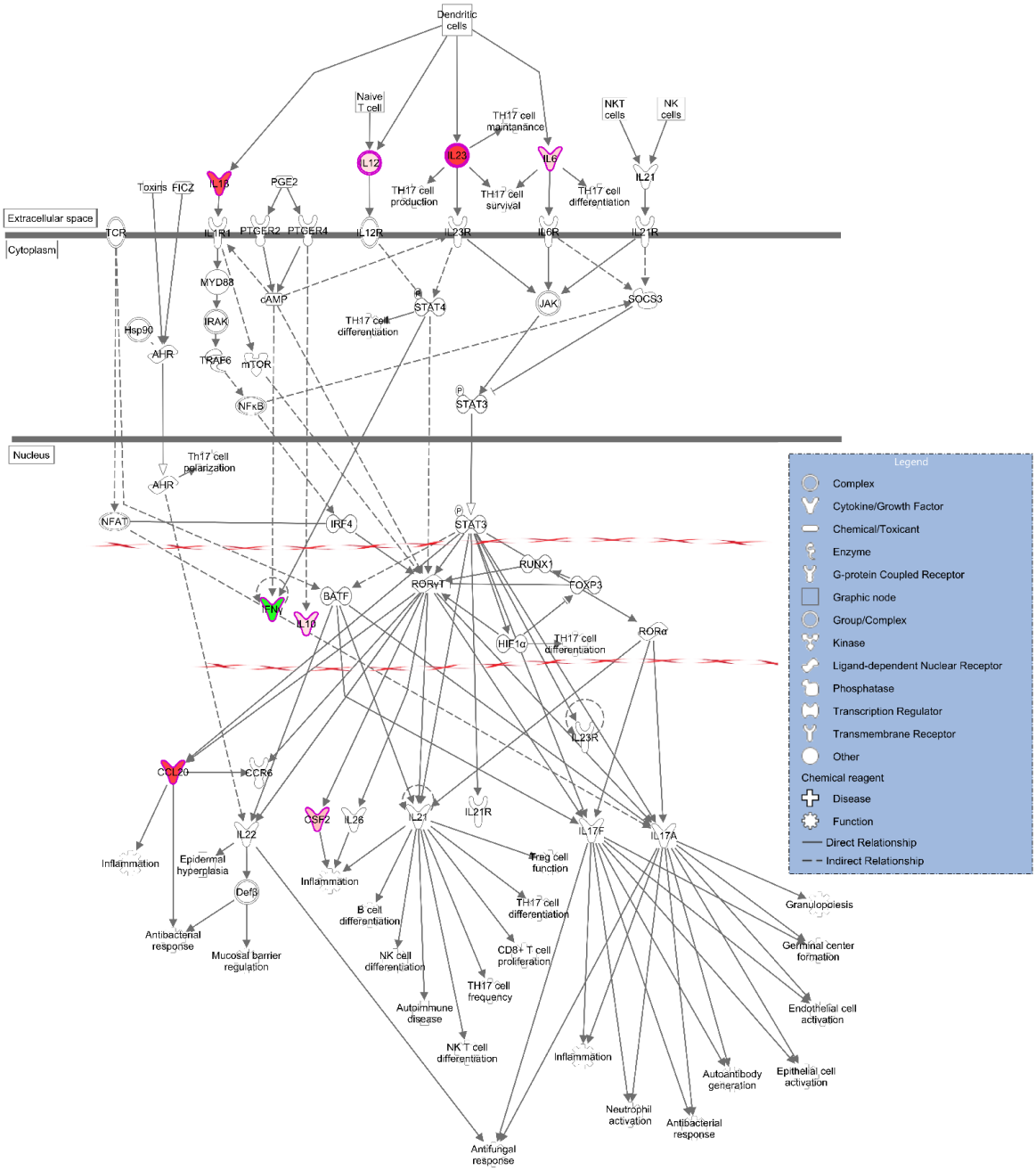

Cytokine activation of the T17 canonical pathway. Cytokine activation of the secreted factors canonical pathway was characterized using IPA with the Fischer's Exact method (*FDR*<0.10) on fold changes of $\log_2$(average AgNP/vehicle control) (n = 54) for B6:T2-Skewed exposed to nominal doses of 0 or 12.5 μg AgNP/mL media for an acute 24 h exposure. Highlighted icons represent cytokine/growth factors, and arrows represent predicted relationships. n = 3 biological replicates.

Cytokine Activation of the T17 Canonical Pathway

B6:T2-Skewed

50.0 vs. 0.0 μg AgNP/mL media

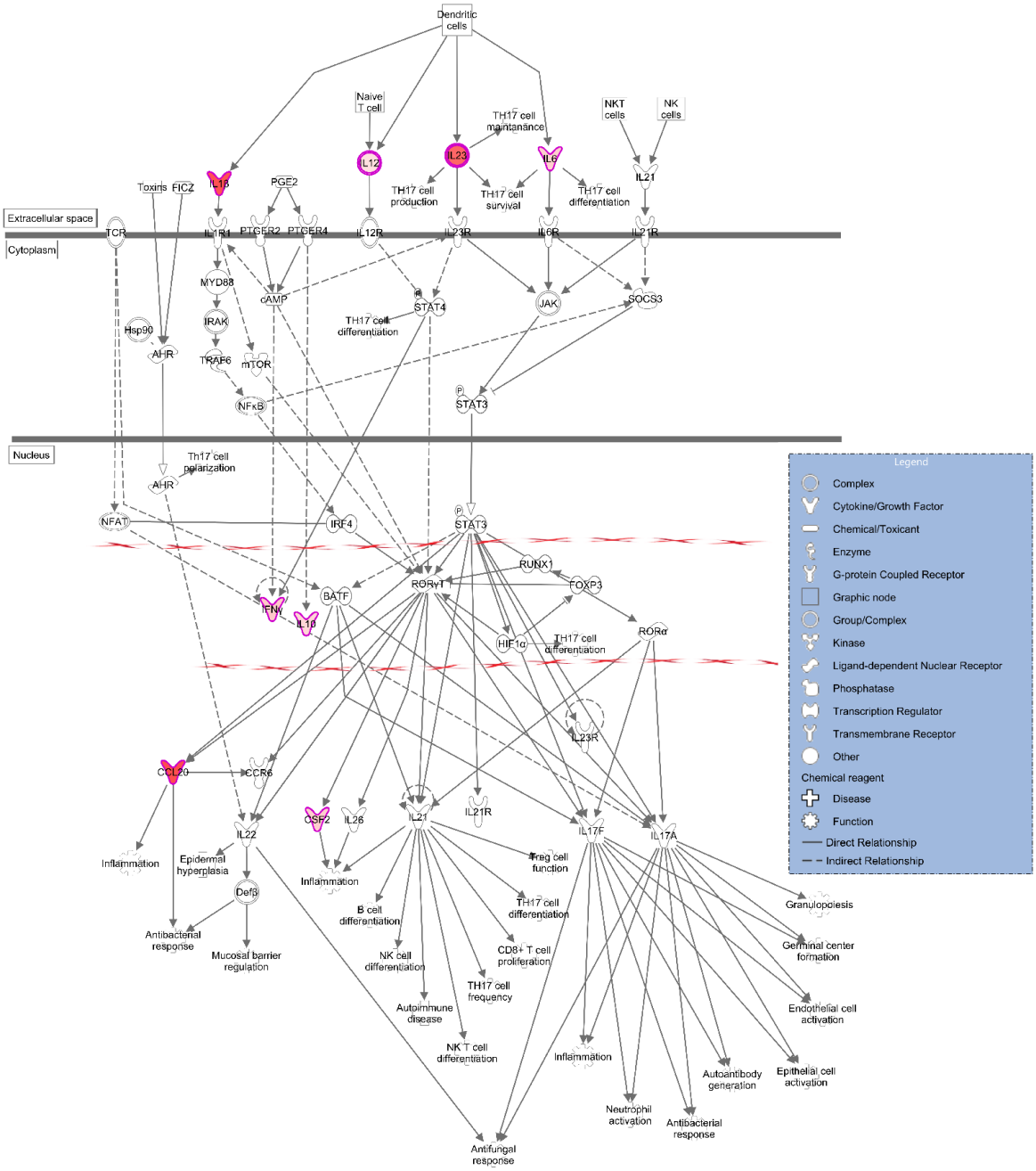

Cytokine activation of the T17 canonical pathway. Cytokine activation of the secreted factors canonical pathway was characterized using IPA with the Fischer's Exact method (*FDR*<0.10) on fold changes of $\log_2$(average AgNP/vehicle control) (n = 54) for B6:T2-Skewed exposed to nominal doses of 0 or 50 μg AgNP/mL media for an acute 24 h exposure. Highlighted icons represent cytokine/growth factors, and arrows represent predicted relationships. n = 3 biological replicates.

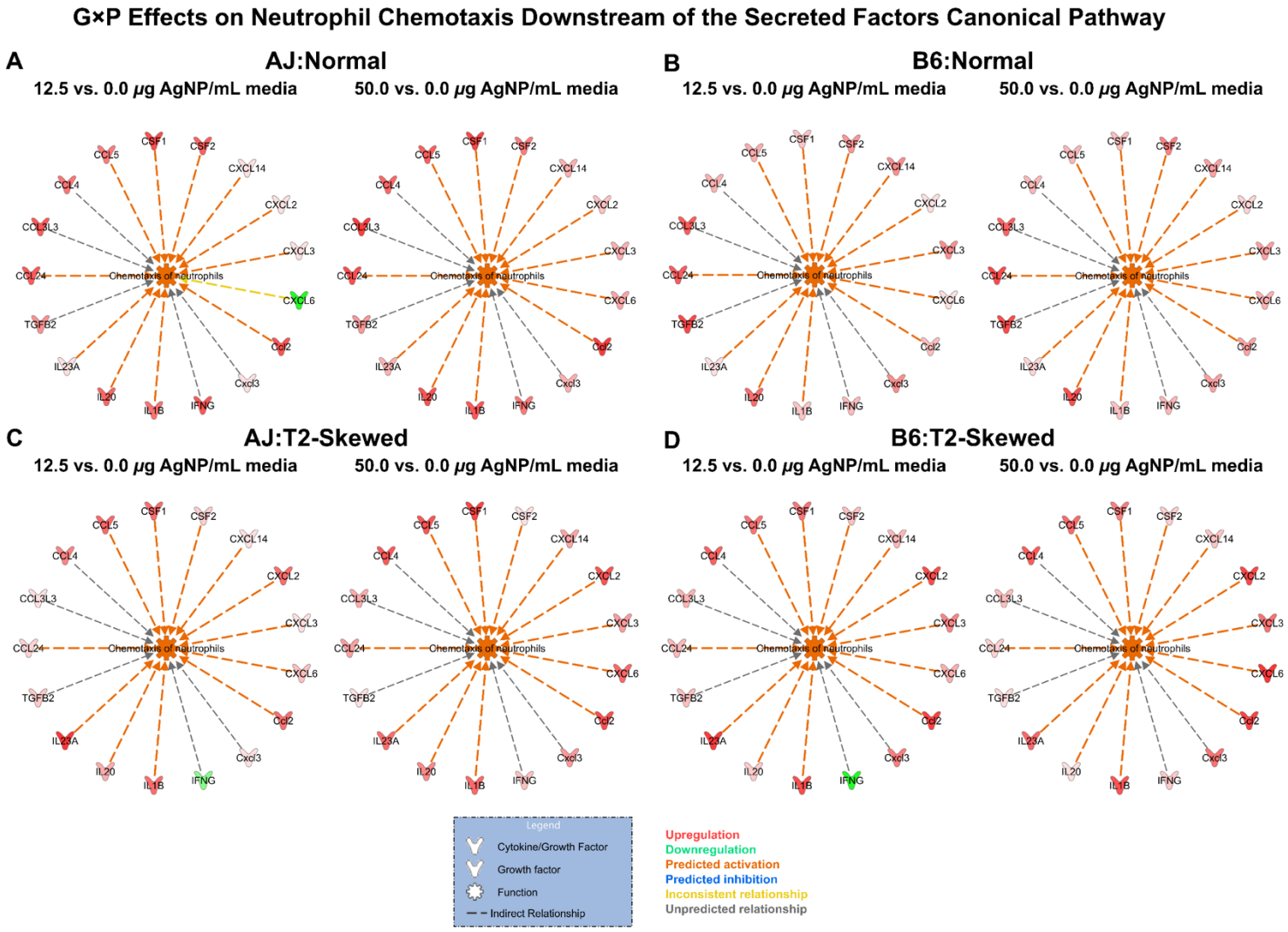

Genotype, phenotype, and dose effects on neutrophil chemotaxis downstream of the secreted factors canonical pathway. Downstream functions of the secreted factors canonical pathway were characterized using IPA with the Fischer's Exact method (*FDR*<0.10) on fold changes of $\log_2$(average AgNP/vehicle control) (n = 54) for AJ:Normal **(A)**, B6:Normal **(B)**, AJ:T2-Skewed **(C)**, and B6:T2-Skewed **(D)** exposed to nominal doses of 0, 12.5, or 50 μg AgNP/mL media for an acute 24 h exposure. Central icons represent the downstream function (neutrophil chemotaxis), peripheral icons represent cytokine/growth factors, and arrows represent predicted relationships. n = 3 biological replicates.

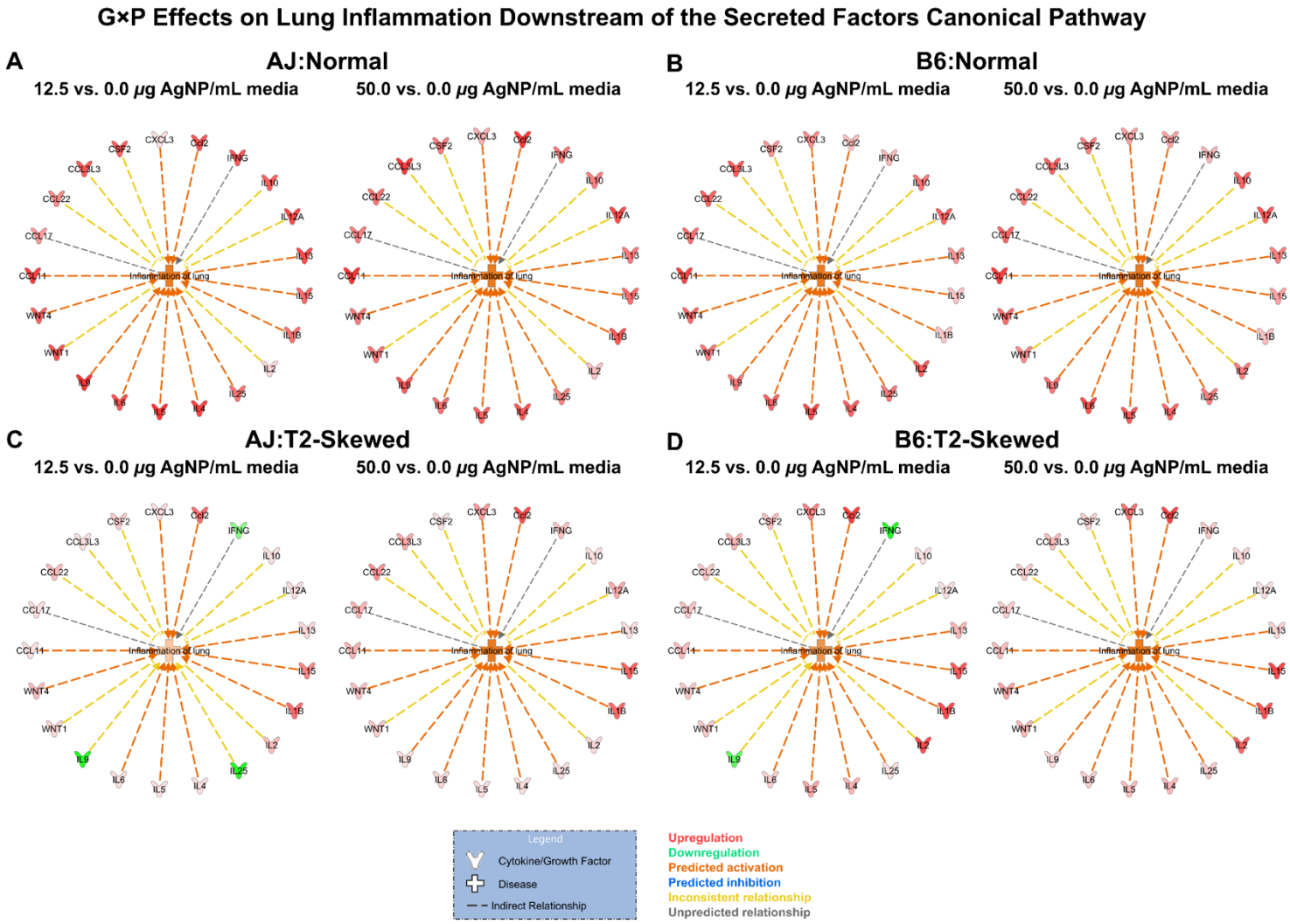

Genotype, phenotype, and dose effects on lung inflammation downstream of the secreted factors canonical pathway. Downstream diseases of the secreted factors canonical pathway were characterized using IPA with the Fischer's Exact method (*FDR*<0.10) on fold changes of $\log_2$(average AgNP/vehicle control) (n = 54) for AJ:Normal **(A)**, B6:Normal **(B)**, AJ:T2-Skewed **(C)**, and B6:T2-Skewed **(D)** exposed to nominal doses of 0, 12.5, or 50 μg AgNP/mL media for an acute 24 h exposure. Central icons represent the downstream disease (lung inflammation), peripheral icons represent cytokine/growth factors, and arrows represent predicted relationships. n = 3 biological replicates.

Chapter 5. The Effects of Gene × Environment Interactions on Silver Nanoparticle Toxicity in the Respiratory System: Toward an Adverse Outcome Pathway

This chapter will be submitted for publication in WIREs Nanomedicine & Nanobiotechnology. The authors of the manuscript are:

Tyler P. Nicholas[1,2], William K. Boyes[3], Terrance J. Kavanagh[1,2], William A. Altemeier[2], and Elaine M. Faustman[1]

[1]Department of Environmental and Occupational Health Sciences, University of Washington, Seattle, Washington
[2]Department of Medicine, Division of Pulmonary, Critical Care, and Sleep Medicine, University of Washington, Seattle, Washington
[3]National Health and Environmental Effects Research Laboratory, Office of Research and Development, U.S. Environmental Protection Agency, Research Triangle Park, North Carolina

Corresponding Author:
Elaine M. Faustman
UW Medicine / Roosevelt Clinic
4225 Roosevelt Way NE, STE100
Box 354695
Seattle, Washington 98105
Phone: (206) 685-2269
Fax: (206) 685-4696
Email: faustman@uw.edu

List of Abbreviations

5×4 h: subacute exposure of 4 hours, every other day, over 5 days
8-OHdG: 8-hydroxy-2'-deoxyguanosine
Ag: silver mass
Ag^+: silver ions
AgNP: silver nanoparticles
AHR: airway hyperresponsiveness
AJ or B6:Normal: A/J or C57BL6/J, "Normal" phenotype
AJ or B6:T2-Skewed: A/J or C57BL6/J, "T2-Skewed" phenotype
Ano6: anoctamin 6
AOP: adverse outcome pathway
Au: gold mass
BALF: bronchoalveolar lavage fluid
BMD: benchmark dose
BMDL: benchmark dose lower 95% confidence limit
Cd: cadmium mass
COPD: chronic obstructive pulmonary disease
ENM: engineered nanomaterials
ENaC: amiloride-sensitive epithelial Na^+ channel
G×E: gene × environment interactions
G×P: gene × phenotype interactions
GSH: glutathione
HEC: human equivalent concentration
IATA: Integrated Approaches to Testing and Assessment
IPCS: International Programme on Chemical Safety
ITS: Integrated Testing Strategies
IVIVE: *in vitro* to *in vivo* extrapolation
KE: key event
LDH: lactate dehydrogenase
LTE_4: leukotriene E4
MIE: molecular initiating event
MoA: mode of action
MTEC: murine tracheal epithelial cells
Nedd4l: E3 ubiquitin-protein ligase NEDD4-like
OECD: Organisation for Economic Co-operation and Development
OEL: occupational exposure limit
OVA: ovalbumin
PBPK: physiologically-based pharmacokinetic/toxicokinetic
QD: quantum dots
QSAR: quantitative structure–activity relationship
REACH: Registration, Evaluation, Authorisation and Restriction of Chemicals
RNA-seq: RNA sequencing
Rnf220: E3 ubiquitin-protein ligase RNF220

ROS: reactive oxygen species
T1/T2/T17: type 1/type 2/type 17
TEER: transepithelial electrical resistance
TSCA: Toxic Substances Control Act
US EPA: U.S. Environmental Protection Agency
WHO: World Health Organization

Chapter 5. The Effects of Gene × Environment Interactions on Silver Nanoparticle Toxicity in the Respiratory System: Toward an Adverse Outcome Pathway

5.1 ABSTRACT

The Adverse Outcome Pathway (AOP) framework has served as the foundation of predictive toxicology. It has been proposed as a systems-based approach for pathway analysis that collects, describes, and quantifies toxicity data across multiple levels of biological organization to identify causal relationships between interactions of stressors with their molecular targets and adverse organism responses of regulatory relevance. AOP development for engineered nanomaterials (ENM), including silver nanoparticles (AgNP), is currently lagging behind other chemicals of regulatory interest since 1) their modes of action (MoA) have been shown to differ considerably due to differences in their particokinetics, and 2) the *in vitro* and *in vivo* effects of how underlying genetics or diseases directly modify response to AgNP exposures are presently not well understood. For example, AgNP are used in multiple applications but primarily in the manufacturing of many antimicrobial products, and asthmatics may be a sensitive population to AgNP exposures in occupational settings. The primary goal of this study is to use the AOP framework to organize and integrate data from *in vitro* and *in vivo* models to evaluate the effects of interactions between host genetic and acquired factors, or gene × environment interactions (G×E), on AgNP toxicity in the respiratory system. Using this framework will help us to identify plausible linkages between MoA and adverse organism responses when key events (KE) are not measured using the same assay in order to derive future predictive models, guide research, and support development of tools for making risk-based, regulatory decisions on ENM.

5.2 INTRODUCTION

The respiratory system is critical for maintaining gas exchange and overall health. It can be damaged by many environmental toxicants and is a sensitive target organ for toxicity for numerous occupational exposures. Chronic respiratory diseases, including asthma, acute bronchitis, and chronic obstructive pulmonary disease (COPD), collectively affect

16% of the United States population; these diseases impair host defense mechanisms, such as barrier function and immune regulation,[15] mucocilliary clearance and permeability,[16-22] as well as enzymatic and non-enzymatic regulation of oxidative stress,[23,24] and may increase an individual's sensitivity to occupational exposures.[25-27] Chronic respiratory diseases place a major burden on individuals, their workplaces, and the healthcare system, and yet less than 1% of the chemicals regulated by the U.S. Environmental Protection Agency's (US EPA) Toxic Substances Control Act (TSCA) have been tested for respiratory toxicity.[3,141]

Silver nanoparticles (AgNP) are one of the 84,000 chemicals of regulatory interest to TSCA. They are used in the manufacturing of many antimicrobial consumer products, including air filters, humidifiers, and purifiers as well as antimicrobial sprays.[31,32,37] Previous *in vitro* studies observed the mode of action (MoA) for their antimicrobial properties (e.g., release of bioactive silver ions [Ag^+] upon dissolution[11-13]) is also a defining factor of AgNP toxicity in mammalian cells.[144] One MoA in airway epithelial cells is Ag^+-mediated reactive oxygen species (ROS) production, which leads to adverse cellular responses including oxidative stress, mitochondrial dysfunction, inflammation, and cytotoxicity.[50,58-63,87,121,145] Asthmatics are possibly a sensitive population to AgNP exposures in occupational settings, as these adverse cellular responses may further modulate innate and adaptive immune responses at the epithelial-immune interface to exacerbate this chronic airway disease.[48] Despite this, in the United States, AgNP have been used in nearly 700 consumer products, accounting for over one-third of those cataloged in the inventory of the Project on Emerging Nanotechnologies managed by the Woodrow Wilson International Center for Scholars.[37]

Few previous studies have assessed the effects of interactions between host genetic and acquired factors, or gene × environment interactions (G×E),[28,29] on AgNP toxicity. Understanding G×E effects is important for identifying sensitive populations, whose underlying genetics or diseases could directly modify their response to AgNP exposures. Typically, these studies have used young, healthy animals or cell lines cultured toward a "Normal" phenotype and thus did not address the possibility of increased AgNP toxicity in asthmatics. While these studies identified multiple determinants of AgNP toxicity and

have helped us to better understand adverse cellular and organ responses under physiological conditions, there is currently no MoA that adequately describes G×E effects on AgNP toxicity.

The sensitivity and specificity of *in vitro* and *in vivo* models must be well characterized before they can be translated into regulatory frameworks,[143,225] which are currently moving toward utilizing this MoA concept. This has been exemplified by the development of Integrated Testing Strategies (ITS) to support the implementation of legislation such as Registration, Evaluation, Authorisation and Restriction of Chemicals (REACH) in the European Union,[226,227] and by more recent efforts within the Organisation for Economic Co-operation and Development (OECD) to develop Integrated Approaches to Testing and Assessment (IATA) that utilize existing data from *in vitro* studies and prediction models to satisfy specific information requirements.[228]

The International Programme on Chemical Safety (IPCS) of the World Health Organization (WHO) initiated this MoA concept to better identify and prioritize chemicals of regulatory interest.[229] Utilizing aspects of the WHO/IPCS MoA concept, the OECD launched the Programme for the Development of Adverse Outcome Pathways (AOP).[230] The AOP framework has served as the foundation of predictive toxicology. It has been proposed as a systems-based approach for pathway analysis that collects, describes, and quantifies toxicity data across multiple levels of biological organization to identify causal relationships between interactions of stressors with their molecular targets and adverse organism responses of regulatory relevance.[231-235] The AOP framework identifies MoA by outlining a molecular initiating event (MIE) followed by key events (KE) along a biological pathway, ending with the adverse organism response **(Figure 1)**.[236] Following OECD guidance, the AOP framework aims to support regulatory decision-making by: 1) prioritizing MIE and KE for further study, 2) identifying knowledge gaps to propose new MoA, and 3) supporting the development of IATA, OECD test guidelines, and quantitative structure–activity relationship (QSAR) tools.[143,230]

While this program has been successful in proposing a large number of AOP for multiple chemicals of regulatory interest, it has been less successful for engineered nanomaterials

(ENM), since: 1) their MoA have been shown to differ considerably due to differences in their particokinetics, and 2) the *in vitro* and *in vivo* effects of how underlying genetics or diseases directly modify the risk of ENM toxicity are presently not well understood.[230,237-239] To our knowledge, Vietti et al. has published the only AOP to date that evaluates ENM toxicity in the respiratory system, and specifically for carbon nanotubes (CNT). The authors' AOP outlined adverse cellular responses in multiple cell types, including airway epithelial cells, fibroblasts, and macrophages, leading to adverse organ responses, including extracellular matrix accumulation and lung fibrotic reactions, and ultimately lung fibrosis as an adverse organism response. The primary goals of the authors' AOP was to highlight a need to develop functional *in vitro* assays suited for better *de novo* predictions of CNT toxicity, and to support risk-based, regulatory decisions aimed toward preventing CNT-induced lung fibrosis.[240]

Predicting the *in vitro* and *in vivo* activity of ENM toxicity is difficult due to the dynamic interactions between their particokinetics and similarly complex G×E effects within biological systems. Therefore, effective and complete characterization of ENM prior to and upon entry into different biological systems is important for establishing plausible linkages between their MoA and adverse organism responses. This very problem was previously highlighted by Boyes et al., who proposed a modified version of the AOP framework designed to serve as a basis for: 1) screening based on a minimal set of assay data and then prioritize for more in-depth testing and evaluation, 2) identifying KE that are critical drivers of bioactivity, and 3) identifying knowledge gaps to further develop and parametrize the structure of the AOP framework.[239] In the present study, we illustrate how this AOP framework can be used to describe G×E effects on AgNP toxicity by utilizing mechanistic information from *in vitro* and *in vivo* models to highlight how KE can be modified by different host genetic and host acquired factors at subacute, acute, and subchronic exposures. Using this AOP framework helped us to identify plausible linkages between MoA and adverse organism responses when endpoints are not measured using the same assay.[241] This AOP will help support regulatory decision-making for ENM by prioritizing MIE and KE for further study while identifying knowledge gaps to propose new MoA for AgNP toxicity. This is not intended to be fully comprehensive in any one area, but rather to highlight these most recent findings, while identifying knowledge gaps

regarding G×E effects on AgNP toxicity in the context of environmental health and safety issues to enable a value of information assessment that better prioritizes future research needs.

5.3 METHODS

AOP framework

In the present study, the modified version of AOP framework was used to organize data from *in vitro* and *in vivo* studies to evaluate G×P effects on AgNP toxicity **(Figure 1)**. We connected the KE for AgNP toxicity using color-coded linkages to highlight knowledge gaps where they exist, specifically: plausible linkages based on limited or no data, empirical linkages based on quantitative *in vitro* dose-response data, and empirical linkages based on quantitative *in vivo* exposure-response data. Plausible linkages based on limited or no data refer to relationships between two intervening adverse cellular or organ responses where one intervening response was not assayed or was predicted using RNA-sequencing (RNA-seq). Empirical linkages based on quantitative *in vitro* dose-response relationships refer to relationships between two intervening adverse cellular responses where both were measured using *in vitro* assays. Empirical linkages based on quantitative *in vivo* dose-response relationships refer to relationships between two intervening adverse organ responses where both were measured using *in vivo* assays.

Adverse cellular responses

We outlined the KE for adverse cellular responses at subacute and acute exposures by integrating data from our previous *in vitro* studies, where the genotype and phenotype (physiological environment) were hypothesized to define G×E, or genotype × phenotype interaction (G×P), effects on AgNP toxicity. All animal studies were approved by the Institutional Animal Care and Use Committee at the University of Washington. We harvested tracheas from A/J and C57BL/6J mice (The Jackson Laboratory, Bar Harbor, ME, USA), and isolated MTEC using enzymatic digestion, as previously described.[151,157,158] We suspended MTEC in a defined proliferation media [Dulbecco's Modified Eagle Media (DMEM) with 10 µg/mL insulin, 5 µg/mL apo-transferrin, 0.1 µg/mL

cholera toxin, 25 ng/mL epidermal growth factor, 30 µg/mL bovine pituitary extract, and 50 nM retinoic acid (Sigma-Aldrich, St. Louis, MO, USA)] to culture at a density of 1.5×10^4 cells/well in collagen-coated 24-Transwell plates (Corning, Corning, NY, USA). We allowed organotypic cultures to proliferate with media in both apical and basal compartments starting on day *in vitro* (DIV) 0. We changed the defined proliferation media every other day until DIV 7-9, when transepithelial electrical resistance (TEER) exceeded 1000 $\Omega\times cm^2$, which marked the end of proliferation.

For the "Normal" phenotype, we allowed organotypic cultures to differentiate at an air-liquid interface (ALI) in a defined differentiation media [DMEM with 2% v/v NuSerum (BD BioSciences, San Jose, CA, USA), and 50 nM retinoic acid (Sigma-Aldrich, St. Louis, MO, USA)] in the basal compartment starting on DIV 7. We changed the defined differentiation media every other day until DIV 28, which marked the end of differentiation.

For the "T2-Skewed" phenotype, we allowed organotypic cultures to differentiate at an ALI in a defined differentiation media supplemented with IL-13 [DMEM with 2% v/v NuSerum (BD BioSciences, San Jose, CA, USA), 50 nM retinoic acid (Sigma-Aldrich, St. Louis, MO, USA)], and 25 ng/mL IL-13 (PeproTech, Rocky Hill, NJ, USA)]. We identified this concentration of IL-13 in a preliminary study and supplemented it to the defined proliferation media starting on DIV 5, and then to the defined differentiation media from DIV 7-28, which we changed every other day until DIV 28.

We exposed organotypic cultures in the apical compartment on DIV 28 to either 2 mM sodium citrate (vehicle control; 0 µg AgNP/mL media), or to silver nanoparticles (AgNP; 20 nm, gold-core, citrate-coated, at 1 mg/mL in 2 mM sodium citrate; nanoComposix, San Diego, CA, USA) for an acute exposure of 24 hours, or a subacute exposure of 4 hours, every other day, over 5 days (5×4 h) at nominal doses of 12.5, 25, or 50 µg AgNP/mL media, as freshly prepared in suspensions of defined differentiation media.

We used inductively coupled plasma mass spectrometry (ICP-MS) to quantify dosimetric doses of silver (Ag), gold (Au), and the ratio of silver to gold (Ag:Au) mass associated on organotypic cultures. Data were normalized by dividing the Ag, Au, and Ag:Au mass in each cell fraction by the protein content, as previously described.[160] The Ag:Au mass is

an indirect measurement of the colocation of Ag and Au mass, and a high Ag:Au mass therefore suggests that the two metals have not separated through dissolution.

We assayed ROS production as an MIE for AgNP toxicity using a 2,7-dichlorofluorescein (DCF) assay (Abcam, Cambridge, MA, USA) to quantify DCF fluorescence as a measure of ROS production, as previously described.[163] We assayed barrier function, oxidative stress, mitochondrial function, inflammation, and cytotoxicity as adverse cellular responses for AgNP toxicity. We assayed organotypic physiology using an EVOM2 Epithelial Volt/Ohm Meter (World Precision Instruments, Sarasota, FL, USA) to quantify transepithelial electrical resistance (TEER) as a measure of barrier function, as previously described.[161] We assayed oxidative stress using a 2,3-naphthalenedicarboxaldehyde (NDA) assay to quantify NDA fluorescence as a measure of glutathione (GSH) depletion, as previously described,[162] and a malondialdehyde (MDA) assay (Abcam, Cambridge, MA, USA) to quantify MDA fluorescence as a measure of lipid peroxidation, as previously described.[164] We assayed mitochondrial function and inflammation using RNA-seq to generate molecular information to support evidence for the MIE by predicting canonical pathway enrichment associated with mitochondrial function and T2/T17 inflammation, as previously described by Nicholas et al. (summitted). We assayed cytotoxicity using a lactate dehydrogenase (LDH) assay (Promega, Madison, WI, USA) to quantify LDH absorbance as a measure of cytotoxicity, as previously described.[165]

Adverse organ responses

We outlined the KE for adverse organ responses at subacute and subchronic exposures by integrating data from previous *in vivo* studies. We implemented the following inclusion criteria for integrating these *in vivo* data into the AOP framework: 1) studied the effects of at least one host genetic or acquired factor on AgNP toxicity, 2) studied either subacute or subchronic effects on AgNP toxicity, where subacute effects refer to a subacute exposure (5-14 d) and subchronic effects refer to a subchronic exposure (21-90 d) using inhalation as the route of AgNP exposure, 3) assayed relevant adverse organ responses associated with oxidative stress, lung inflammation, and organ physiology, and 4) assayed dosimetric doses of Ag mass associated in the lungs using ICP-MS.

We integrated *in vivo* data on sex, genotype, and antigen effects on AgNP toxicity, where sex refers to the animal sex (mouse or rat), genotype refers to the genetically inbred animal strain (e.g., A/J and C57BL/6J mice, or Fischer 344 and Sprague-Dawley rats), and antigen refers to the *in vivo* airway phenotype produced by OVA sensitization prior to AgNP exposure. We integrated *in vivo* data on subacute and subchronic effects on AgNP toxicity, where subacute effects refer to a subacute exposure (5-14 d) and subchronic effects refer to a subchronic exposure (21-90 d) using inhalation as the route of AgNP exposure. We integrated *in vivo* data on adverse organ responses associated with oxidative stress, lung inflammation, as well as lung function and/or airway hyperresponsiveness (AHR) whose physiological relevance was improved by assayed dosimetric doses of Ag mass associated in the lungs using ICP-MS.

5.4 RESULTS

Key events for AgNP toxicity are impacted by genetics, diseases, and exposures

We stratified KE for AgNP toxicity identified in previous *in vitro* and *in vivo* studies by host genetic and acquired factors to highlight additional knowledge gaps related to the *in vitro* and *in vivo* effects of how underlying genetics or diseases directly modify their response to AgNP exposures. Specifically, we stratified sex, genotype, phenotype, and antigen effects on AgNP toxicity across *in vitro* and *in vivo* models, where sex refers to the animal sex (male or female), genotype refers to the genetically inbred animal strain (e.g., A/J and C57BL/6J mice, or Fischer 344 and Sprague-Dawley rats), phenotype refers to the *in vitro* airway phenotype produced by defined differentiation media (“Normal” and “T2-Skewed”) prior to AgNP exposure, and antigen refers to the *in vivo* airway phenotype produced by ovalbumin (OVA) sensitization prior to AgNP exposure. We also stratified the KE for AgNP toxicity by exposures to highlight additional knowledge gaps related to the acute to subchronic *in vitro* and *in vivo* impacts of AgNP toxicity. Specifically, we stratified acute, subacute, and subchronic effects on AgNP toxicity across *in vitro* and *in vivo* models, where acute effects refer to an acute exposure (24 h), subacute effects refer to a subacute exposure (5-14 d), and subchronic effects refer to a subchronic exposure (21-90 d).

Genotype and phenotype effects on key events for AgNP-induced adverse

cellular responses at acute exposures

Two *in vitro* studies evaluated G×E effects on AgNP toxicity in organotypic cultures at an acute 24 h exposure, and we integrated these *in vitro* data into the AOP framework **(Figure 2)**. Nicholas et al. (submitted) compared G×E effects on association and dissolution (marked by Ag, Au, and Ag:Au mass) **(Figure 2, Row 1)** across genotypes, phenotypes, and exposures, and observed the strongest G×E effects in the "T2-Skewed phenotype" at an acute 24 h exposure when normalized by ICP-MS for both AgNP association by Ag mass and by Ag^+ dissolution as estimated by Ag:Au mass. The authors also compared G×E effects on dosimetric dose-response relationships across genotypes, phenotypes, and exposures, and observed the strongest G×E effects in the "T2-Skewed" phenotype at an acute 24 h exposure for AgNP-induced MIE (marked by increased ROS production) **(Figure 2, Row 1)**, oxidative stress (marked by increased GSH depletion and lipid peroxidation) **(Figure 2, Column 2)**, mitochondrial dysfunction (marked by increased activation of apoptosis, the TGF-β signaling pathway, and the WNT signaling pathway) **(Figure 2, Column 3)**, inflammation (marked by increased upregulation of T17 cytokines) **(Figure 2, Column 4)**, cytotoxicity (marked by increased LDH secretion) **(Figure 2, Column 5)**, and organotypic physiology (marked by decreased barrier function) **(Figure 2, Column 6)**—with AJ:T2-Skewed being the most sensitive genotype and phenotype. We constructed plausible linkages based on limited or no quantitative *in vitro* dose-response data between "Cytotoxicity" and "Organotypic Physiology" for AJ:Normal, B6:Normal, and B6:T2-Skewed. We constructed empirical linkages based on quantitative *in vitro* dose-response data between "Oxidative Stress" and "Mitochondrial Function", "Mitochondrial Function" and "Inflammation", "Inflammation" and "Cytotoxicity for AJ:Normal, B6:Normal, AJ:T2-Skewed, and B6:T2-Skewed as well as "Cytotoxicity" and "Organotypic Physiology", but only for AJ:T2-Skewed.

Genotype and phenotype effects on key events for AgNP-induced adverse cellular responses at subacute exposures

One *in vitro* study evaluated G×E effects on AgNP toxicity in organotypic cultures at a subacute 5×4 h exposure, and we integrated these *in vitro* data into the AOP framework

(Figure 3). Nicholas et al. (submitted) compared G×E effects on association and dissolution (marked by Ag, Au, and Ag:Au mass) **(Figure 3, Row 1)** across genotypes, phenotypes, and exposures, and observed weaker G×E effects in the "T2-Skewed phenotype" at a subacute 5×4 h exposure when normalized by ICP-MS for both AgNP association by Ag mass and by Ag^+ dissolution as estimated by Ag:Au mass. The authors also compared G×E effects on dosimetric dose-response relationships across genotypes, phenotypes, and exposures, and observed weaker G×E effects in the "T2-Skewed" phenotype at a subacute 5×4 h exposure for AgNP-induced MIE (marked by increased ROS production) **(Figure 3, Row 1)**, oxidative stress (marked by increased GSH depletion and lipid peroxidation) **(Figure 3, Column 2)**, cytotoxicity (marked by increased LDH secretion) **(Figure 3, Column 5)**, and organotypic physiology (marked by decreased barrier function) **(Figure 3, Column 6)**—with AJ:T2-Skewed being the most sensitive genotype and phenotype. We constructed plausible linkages based on limited or no quantitative *in vitro* dose-response data between "Oxidative Stress" and "Mitochondrial Function", "Mitochondrial Function" and "Inflammation", "Inflammation" and "Cytotoxicity", as well as "Cytotoxicity" and "Organotypic Physiology" for AJ:Normal, B6:Normal, and B6:T2-Skewed. We constructed empirical linkages based on quantitative *in vitro* dose-response data between "Oxidative Stress" and "Cytotoxicity" for AJ:Normal, B6:Normal, AJ:T2-Skewed, and B6:T2-Skewed as well as "Oxidative Stress" and "Organotypic Physiology", but only for AJ:T2-Skewed.

Genotype effects on key events for AgNP-induced adverse organ responses at acute exposures

One *in vivo* study evaluated G×E effects on AgNP toxicity in multiple genotypes of mice at an acute 24 h exposure, and we integrated these *in vivo* data into the AOP framework **(Figure 4)**. Scoville et al. treated 25 genotypes of male mice (including BALB/cJ, A/J, and C57BL6/J), and in our review of this study, we observed evidence of genotype effects on association (marked by increased dosimetric doses of Ag mass associated in the lungs) **(Figure 4, Row 1)** and AgNP-induced T2 lung inflammation (marked by increased pro-inflammatory cell infiltrate) **(Figure 4, Column 3)** compared to genetically-matched vehicle controls, with BALB/cJ and SWR/J mice being the most differentially sensitive

genotypes.[78] The authors used RNA-seq on lungs isolated from BALB/cJ, A/J, and C57BL6/J mice and observed an inverse relationship between AgNP-induced T2 lung inflammation and expression of E3 ubiquitin-protein ligase NEDD4-like (*Nedd4l*), anoctamin 6 (*Ano6*), and E3 ubiquitin-protein ligase RNF220 (*Rnf220*), which may function as candidate polymorphisms for AgNP-induced T2 lung inflammation. *Nedd4l* is a E3 ubiquitin ligase gene involved in ubiquitin protein ligase activity; AgNP-induced *Nedd4l* downregulation may increase amiloride-sensitive epithelial Na^+ channel (ENaC) activity and T2 lung inflammation. *Ano6* is small-conductance calcium-activated non-selective cation channel gene involved in calcium-dependent exposure of phosphatidylserine on the cell surface; AgNP-induced *Ano6* downregulation may impair ion transport, increase airway surface fluid volume and viscosity, as well as apoptosis, phagocytosis, and T2 lung inflammation and/or mast cell degranulation via the phosphatidylserine signaling pathway. *Rnf220* is another E3 ubiquitin ligase gene involved in ubiquitin protein ligase activity; AgNP-induced *Rnf220* downregulation may inhibit β-catenin stabilization and activate the WNT signaling pathway to exacerbate T2 lung inflammation.[78] We constructed plausible linkages with little or no quantitative *in vivo* exposure-response data between “Oxidative Stress”, “Lung Inflammation” and “Organ Physiology” for male BALB/cJ, A/J, and C57BL6/J mice.

Sex, genotype, and antigen effects on key events for AgNP-induced adverse organ responses at subacute exposures

Several *in vivo* studies evaluated G×E effects on AgNP toxicity in antigen-sensitized mice at subacute exposures from 4 to 21 d, and we integrated these *in vivo* data into the AOP framework **(Figure 5)**. Typically, *in vivo* studies evaluating genotype and antigen effects on AgNP toxicity in the lungs have used OVA-sensitized female BALB/cJ mice, which develop increased AHR and T2 lung inflammation than male mice or other mice genotypes. These *in vivo* studies treated OVA-sensitized, female BALB/cJ or C57BL6/J mice with AgNP of various sizes and coatings, and in our review, we observed limited evidence of genotype or antigen effects on association (marked by increased dosimetric doses of Ag mass associated in the lungs) **(Figure 5, Row 1)**. However, we observed evidence of genotype and antigen effects on exacerbation of the allergic airway

phenotype via increased AgNP-induced oxidative stress (marked by increased ROS production, NF-κB activation, leukotriene E4 [LTE_4] and 8-hydroxy-2'-deoxyguanosine [8-OHdG] production) **(Figure 5, Column 2)**, and T2 lung inflammation (marked by increased T1/T2 cytokine secretion, pro-inflammatory cell infiltrate, immunoglobulin E [IgE], AHR, and histopathological changes) **(Figure 5, Column 3)** in allergic mice compared to healthy mice and filtered air controls.[82-85] We constructed empirical linkages based on quantitative *in vivo* exposure-response data between "Oxidative Stress", "Lung Inflammation", and "Organ Physiology" for female BALB/cJ and C57BL6/J mice.

Several *in vivo* studies evaluated G×E effects on AgNP toxicity in rats at subacute exposures from 7 to 14 d, and we integrated these *in vivo* data into the AOP framework **(Figure 5)**. Typically, *in vivo* studies evaluating sex and genotype effects on AgNP toxicity in the lungs have used either Brown-Norway, Fischer 344, or Sprague-Dawley rats. These *in vivo* studies treated male and female Fischer 344 or Sprague-Dawley rats with AgNP of various sizes and coatings, and in our review, we observed evidence of sex and genotype effects on association (marked by increased dosimetric doses of Ag mass associated in the lungs) **(Figure 5, Row 1)**, AgNP-induced oxidative stress (marked by increased GSH depletion) **(Figure 5, Column 2)**, and T2 lung inflammation (marked by increased T1/T2 cytokine secretion, pro-inflammatory cell infiltrate, and histopathological changes) **(Figure 5, Column 3)** in male Fischer 344 rats compared to female Fischer 344 rats and filtered air controls, but no sex effects on AgNP-induced lung dysfunction (marked by decreased minute and tidal volume) **(Figure 5, Column 3)** in male Sprague-Dawley rats compared to female Sprague-Dawley rats and filtered air controls.[71,138,139] We constructed plausible linkages with little or no quantitative *in vivo* exposure-response data between "Lung Inflammation" and "Organ Physiology" for male and female Fischer 344 rats, and between "Oxidative Stress" and "Lung Inflammation" for male and female Sprague-Dawley rats. We constructed empirical linkages based on quantitative *in vivo* exposure-response data between "Oxidative Stress" and "Lung Inflammation" for male and female Fischer 344 rats, and between "Lung Inflammation" and "Organ Physiology" for male and female Sprague-Dawley rats.

Sex and genotype effects on key events for AgNP-induced adverse organ

responses at subchronic exposures

No *in vivo* studies have evaluated G×E effects on AgNP toxicity in mice at subchronic exposures. However, several *in vivo* studies have evaluated G×E effects on AgNP toxicity in rats at subchronic exposures from 21 to 90 d **(Figure 6).** Typically, *in vivo* studies evaluating sex and genotype effects on AgNP toxicity in the lungs have used either Brown-Norway, Fischer 344, or Sprague-Dawley rats. These *in vivo* studies treated male and female Brown-Norway (male only) or Sprague-Dawley rats with AgNP of various sizes and coatings, and in our review, we observed evidence of sex and genotype effects on association (marked by increased dosimetric doses of Ag mass associated in the lungs) **(Figure 6, Row 1)**, AgNP-induced oxidative stress (marked by increased bronchoalveolar lavage fluid [BALF] malondialdehyde [Brown-Norway]) **(Figure 6, Column 2)**, T2/T17 lung inflammation (marked by increased T1/T2/T17 cytokine secretion, pro-inflammatory cell infiltrate, and changes in histopathology [Brown-Norway]) **(Figure 6, Column 3)**, and lung dysfunction (marked by decreased airway resistance, tissue elastance [Brown Norway], as well as minute and tidal volume [Sprague-Dawley]) **(Figure 6, Column 4)** compared to genetically-matched vehicle controls, with males being the more sensitive sex and Brown-Norway rats being the more sensitive genotype.[72,73,79,80] We constructed plausible linkages with little or no quantitative *in vivo* exposure-response data between “Oxidative Stress” and “Lung Inflammation” for male Brown-Norway rats, and between “Oxidative Stress” and “Lung Inflammation” for male and female Sprague-Dawley rats. We constructed empirical linkages based on quantitative *in vivo* exposure-response data between “Lung Inflammation” and “Organ Physiology” for male Brown-Norway rats, and between “Lung Inflammation” and “Organ Physiology” for male and female Sprague-Dawley rats.

5.5 DISCUSSION

Using the AOP framework above, we showed that host genetic and acquired factors may play a role in defining sensitive populations to AgNP exposures in occupational settings. These G×E effects on AgNP toxicity are of relevance of public health as they may be broadly applicable to other types of ENM, which are used in manufacturing of many

consumer products. In the present study, we utilized mechanistic information from previous *in vitro* and *in vivo* studies to highlight how KE can be modified by host genetic and host acquired factors at acute, subacute, and subchronic exposures and identify knowledge gaps in order to more directly prioritize future research needs.

Knowledge gaps for key events of AgNP toxicity

- *In vitro* data for "Mitochondrial Function" and "Inflammation" in organotypic cultures at subacute exposures
- *In vivo* data for "Oxidative Stress" and "Organ Physiology" in mice at acute and subacute exposures

Knowledge gaps for G×E effects on AgNP toxicity

- *In vitro* data for sex, genotype, and phenotype effects on AgNP particokinetics and toxicity in organotypic cultures at acute and subacute exposures
- *In vivo* data for sex, genotype, and antigen effects on AgNP particokinetics and toxicity in mice at acute, subacute, and subchronic exposures
- *In vivo* data for sex and genotype effects on AgNP particokinetics and toxicity in rats at acute, subacute, and subchronic exposures

Benchmark dose (BMD) approaches have been used in previous *in vitro* and *in vivo* studies and could be used to anchor the KE for AgNP toxicity within the AOP framework in order to inform regulatory policy aimed at protecting all populations. Nicholas et al. (submitted) and Weldon et al. used nominal and dosimetric dose-response relationships to define exposure levels corresponding to specific changes in response;[242] or a 10% difference in response to represent a shift in one standard deviation from the mean of normally distributed data to reflect adverse cellular and organ responses in the respective studies.[243] Nicholas et al. (submitted) derived nominal and dosimetric BMD (BMDL) based upon the dosimetric dose of Ag mass associated on organotypic cultures, and observed the most sensitive adverse cellular response was ROS production in organotypic cultures

at acute and subacute exposures **(Supplementary Data)**. Weldon et al. used HEC based upon the dosimetric dose of Ag mass associated in the lungs as reported in the *in vivo* study by Sung et al. to derive a health-based OEL of 0.19 μg AgNP/m^3, and observed the most sensitive adverse organ response was lung inflammation in male Sprague-Dawley rats at subchronic exposures, which fell below the suggested NOAEL of 133 mg/m^3 **(Supplementary Data)**.[73,119] Ultimately, these BMD approaches allowed for allowed for the detection of AgNP toxicity that can be translated to physiologically-relevant units measurable in occupational settings and could be used to anchor the KE for AgNP toxicity within the AOP framework in order to inform regulatory policy aimed at protecting all populations.

Many of the *in vitro* dosimetric BMD (BMDL) for adverse cellular responses (e.g., GSH depletion, ROS production, lipid peroxidation, and cytotoxicity) fell within or below the range of *in vivo* dosimetric BMD (BMDL) and BMC (BMCL) for adverse organ responses (e.g., tidal volume, albumin, lactate dehydrogenase [LDH], and protein in BALF, as well as lung infiltrate, and lung inflammation), suggesting the possibility that adverse cellular responses may predict adverse organ responses. However, *in vitro* studies using mice and *in vivo* studies using rats are not directly comparable without accounting for uncertainty factors related to species differences as well as *in vitro* to *in vivo* extrapolation (IVIVE). Future studies should evaluate G×E effects on AgNP toxicity in mice at subchronic exposures in order to address this knowledge gap, which would also serve to reduce the uncertainty factors associated with IVIVE. Even in light of reduced uncertainty, predicting the IVIVE of ENM toxicity is difficult due to the dynamic interactions between their particokinetics and similarly complex G×E effects within biological systems. Therefore, effective and complete characterization of ENM prior to and upon entry into different biological systems is important for establishing plausible linkages between their MoA and adverse organism responses. These complex G×E effects within biological systems have been described in previous *in vitro* and *in vivo* studies.

Several *in vitro* studies by Nicholas et al. (submitted) described the importance of phenotype and exposure effects on AgNP particokinetics, as higher dosimetric doses of Ag and Au mass were detected in organotypic cultures at acute exposures, and lower

dosimetric doses of Ag and Au mass were detected in organotypic cultures at subacute exposures. The highest dosimetric doses of Ag and Au mass were detected under the “T2-Skewed” phenotype at acute exposures, suggesting the importance of phenotype effects on dosimetric doses of Ag and Au mass. The lowest dosimetric doses of Ag:Au mass were also detected under the “T2-Skewed” phenotype at subacute exposures, also suggesting the importance of phenotype effects on dosimetric doses of Ag:Au mass. The authors used the dosimetric dose of Ag:Au mass as an indirect measurement of the colocation of Ag and Au metals, and a low Ag:Au mass suggests that the two metals have separated through dissolution, potentially leading to increased AgNP bioavailability and bioactivity. Together, these data suggest that phenotype and exposure effects on AgNP particokinetics are greater for the “T2-Skewed” phenotype and for an acute exposure as opposed to a subacute exposure. While deposition and dissolution can occur throughout the conducting and respiratory airways, deposition in the conducting airway of healthy individuals will be reduced by mucociliary clearance, with a fraction of deposited Ag mass undergoing dissolution upon inhalation. However, this host defense mechanism may be impaired in individuals with pre-existing chronic respiratory diseases, and raises the potential for increased deposition, dissolution, and thus AgNP toxicity.

Several *in vivo* studies described the importance of sex effects on AgNP particokinetics. In the case of rats, Braakhuis et al. exposed male Fischer 344 rats with 15 nm and 410 nm AgNP and observed size effects on AgNP-induced T2 lung inflammation, with 15 nm AgNP exerting the strongest effects. The authors quantified dosimetric doses of Ag mass associated in the lungs and observed the original burdens after 7 d for 15 nm AgNP was 350% higher than 410 nm AgNP, and that the remaining burdens decreased to 38% and 69% of the original burdens after 7 d for 15 nm and 410 nm AgNP, respectively. Takenaka et al. exposed female Fischer 344 rats with 15 nm uncoated AgNP and observed similar levels of deposited Ag mass associated in the lungs to those reported by Braakhuis et al.; however, the remaining burdens decreased to 4% of the original burdens after 7 d, suggesting rapid dissolution and/or mucociliary clearance to other systemic pathways. Male mice and rats have been shown to be the more sensitive sex to AgNP toxicity, and therefore, we suggest a potential for airway physiology, or airway branching and mucociliary clearance, to be a contributing factor in sex effects on AgNP toxicity.

Several *in vivo* studies also described the importance of genotype effects on ENM particokinetics. In the case of mice, Scoville et al. treated 25 genotypes of male mice with AgNP and observed genotype effects on AgNP-induced T2 lung inflammation (marked by increased pro-inflammatory cell infiltrate) compared to genetically-matched vehicle controls, with BALB/cJ and SWR/J mice being the most differentially sensitive genotypes. The authors quantified dosimetric doses of Ag mass in the lungs of these differentially sensitive genotypes and detected higher burdens in A/J mice compared to C57BL/6J mice, suggesting that airway physiology (marked by alveolar size and airway branching) may be a contributing factor in genotype effects on AgNP toxicity.[75,76,78] In the case of rats, Seiffert et al. treated male Brown-Norway and Sprague-Dawley rats with AgNP and observed genotype effects on AgNP-induced lung dysfunction and T2/T17 lung inflammation, with Brown-Norway rats being the more sensitive genotype. The authors also quantified dosimetric doses of Ag mass associated in the lungs of these differentially sensitive genotypes and detected higher burdens in Brown-Norway rats compared to Sprague-Dawley rats,[80] suggesting that airway physiology (marked by mucociliary clearance) may be a contributing factor in genotype effects on AgNP toxicity.

While some of these differences in ENM particokinetics can be accounted for by using dosimetric dose-response relationships, IVIVE of AgNP toxicity from organotypic cultures to the lungs may still exhibit significant variability. This was highlighted by Bachler et al., who developed a physiologically-based pharmacokinetic/toxicokinetic (PBPK) model for AgNP toxicity in various organ systems. The authors calibrated their human respiratory tract model to estimate the deposition fraction of inhaled particles from 1 to 1000 nm among the extrathoracic, endothoracic, bronchial, bronchiolar, and alveolar-interstitial compartments, and accounted for mucociliary clearance as well as time-dependent uptake of particles to the systemic blood circulation, which emphasized the complexity of IVIVE of AgNP toxicity from organotypic cultures to the lungs.[168] Together, this highlights the importance of considering PBPK parameters within sensitive populations when using IVIVE to contribute relevant data for integration into the AOP framework in order to provide efficient characterization toward risk assessment for occupational exposures.

One limitation of the *in vitro* data integrated into the AOP framework was each study's

focus on a single mouse sex and two genotypes, which did not account for the effects of other potential interactions between host genetic and acquired factors. For example, the use of a single mouse sex ignored the potential interactions between sex and genotype with phenotype effects on AgNP toxicity in organotypic cultures. Therefore, these *in vitro* data did not fully capture the *in vitro* effects of underlying genetics or diseases which may directly modify response to AgNP exposures. This highlights the importance of also evaluating sex, genotype, and phenotype effects on AgNP toxicity in future studies that account for interactions between these host genetic and acquired factors.

One limitation of the *in vivo* data integrated into the AOP framework was each study's focus on a single mouse sex and genotype, which did not individually account for the effects of interactions between host genetic and acquired factors. For example, the use of a single mouse sex and genotype has ignored the potential interactions between sex and genotype with antigen effects on AgNP toxicity in the lungs. Therefore, these *in vivo* data did not fully capture the *in vivo* effects of underlying genetics or diseases which may directly modify response to AgNP exposures. This highlights the importance of also evaluating sex, genotype, and antigen effects on AgNP toxicity in future studies that account for interactions between these host genetic and acquired factors. A second limitation of the *in vivo* data integrated into the AOP framework was each study's focus on either a single rat sex or genotype, which did not individually account for the effects of interactions between host genetic factors. For example, the use of a single rat genotype has ignored the potential interactions between sex and genotype on AgNP toxicity in the lungs. Therefore, these *in vivo* data also did not fully capture the *in vivo* impact of underlying genetics on AgNP toxicity in the lungs. This highlights the importance of also evaluating sex and genotype effects on AgNP toxicity in future studies that account for interactions between these host genetic factors as well as acquired factors.

Despite these knowledge gaps, this study establishes organotypic cultures derived from MTEC as capable of being used within the AOP framework to organize and integrate data from *in vivo* models to evaluate G×E effects on AgNP toxicity in the respiratory system at acute to subchronic exposures. Using this framework helped us to identify plausible linkages between MoA and adverse organism responses when KE were not measured

using the same assay or the same exposure in order to derive future predictive models, guide research, and support development of tools for making risk-based, regulatory decisions on ENM. In the future, the AOP framework should be used alongside an associated knowledgebase that includes targeted functional *in vitro* and *in vivo* data to allow for better *de novo* predictions of AgNP toxicity in the respiratory system.

AUTHOR CONTRIBUTIONS

The manuscript was written through contributions of all authors. All authors have given approval to the final version of the manuscript.

FUNDING SOURCES

This work was supported by the US EPA under Grant R835738 (E.M.F., T.J.K., W.A.A); NIH under Grants P30 ES007033 (T.J.K.) and T32 ES007032-38 (T.P.N.); the Washington State Department of Labor and Industries under the Medical Aid/Accident Fund; (T.P.N.) and the University of Washington under the GO-MAP Dissertation Fellowship (T.P.N.).

NOTES

The authors declare no competing financial interest.

5.6 DATA

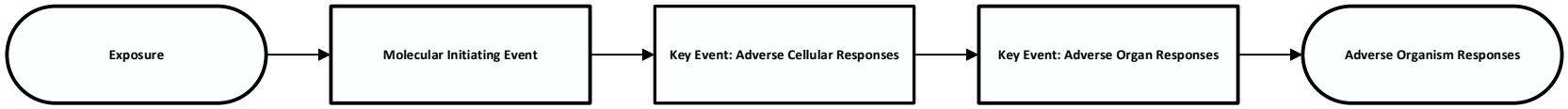

Figure 5.1. AOP framework. AOP identify modes of action (MoA) by outlining a molecular initiating event (MIE) followed by key events (KE) for adverse cellular and organ responses along a biological pathway, ending with the adverse organism response.

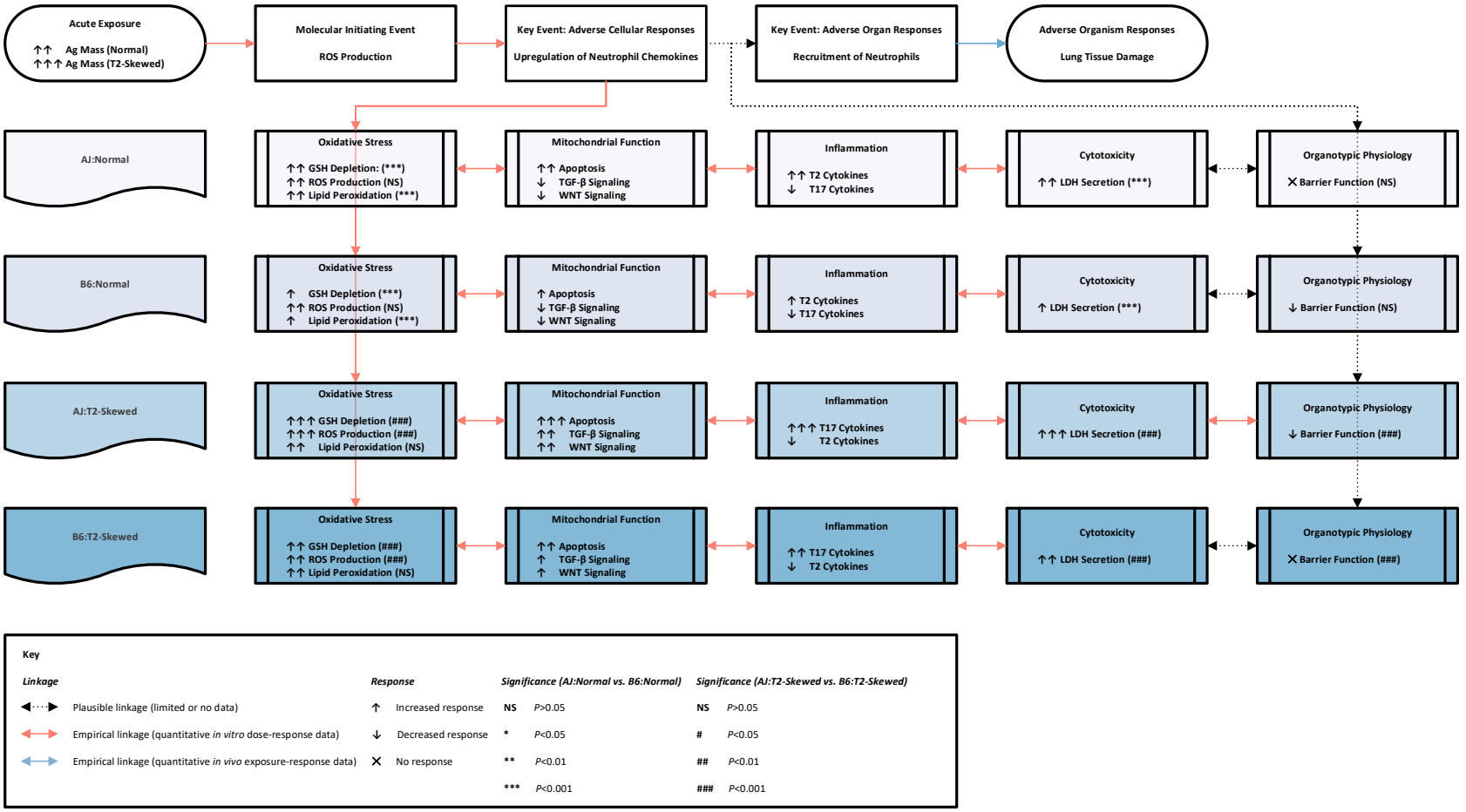

Figure 5.2. Adverse cellular responses at acute exposures. Acute Exposure (24 h): Ag mass (μg Ag/mg protein). Molecular Initiating Event: ROS (reactive oxygen species). Oxidative Stress: GSH (glutathione); ROS (reactive oxygen species). Mitochondrial Function: TGF-β (transforming growth factor beta); WNT (wingless-related integration site). Inflammation: T2 (type 2); T17 (type 17). Cytotoxicity: LDH (lactate dehydrogenase).

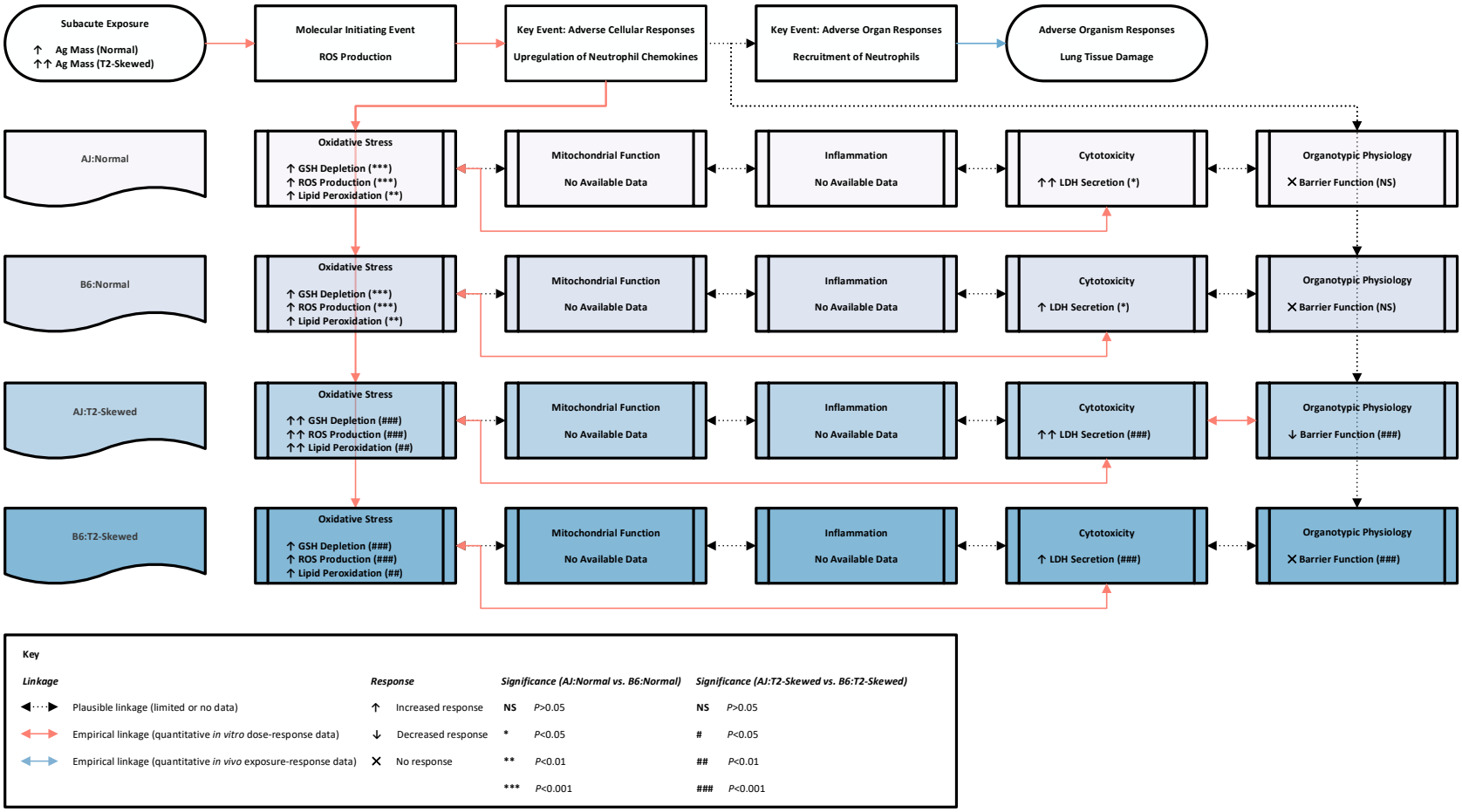

Figure 5.3. Adverse cellular responses at subacute exposures. Subacute Exposure (5×4 h): Ag mass (μg Ag/mg protein). Molecular Initiating Event: ROS (reactive oxygen species). Oxidative Stress: GSH (glutathione); ROS (reactive oxygen species). Cytotoxicity: LDH (lactate dehydrogenase).

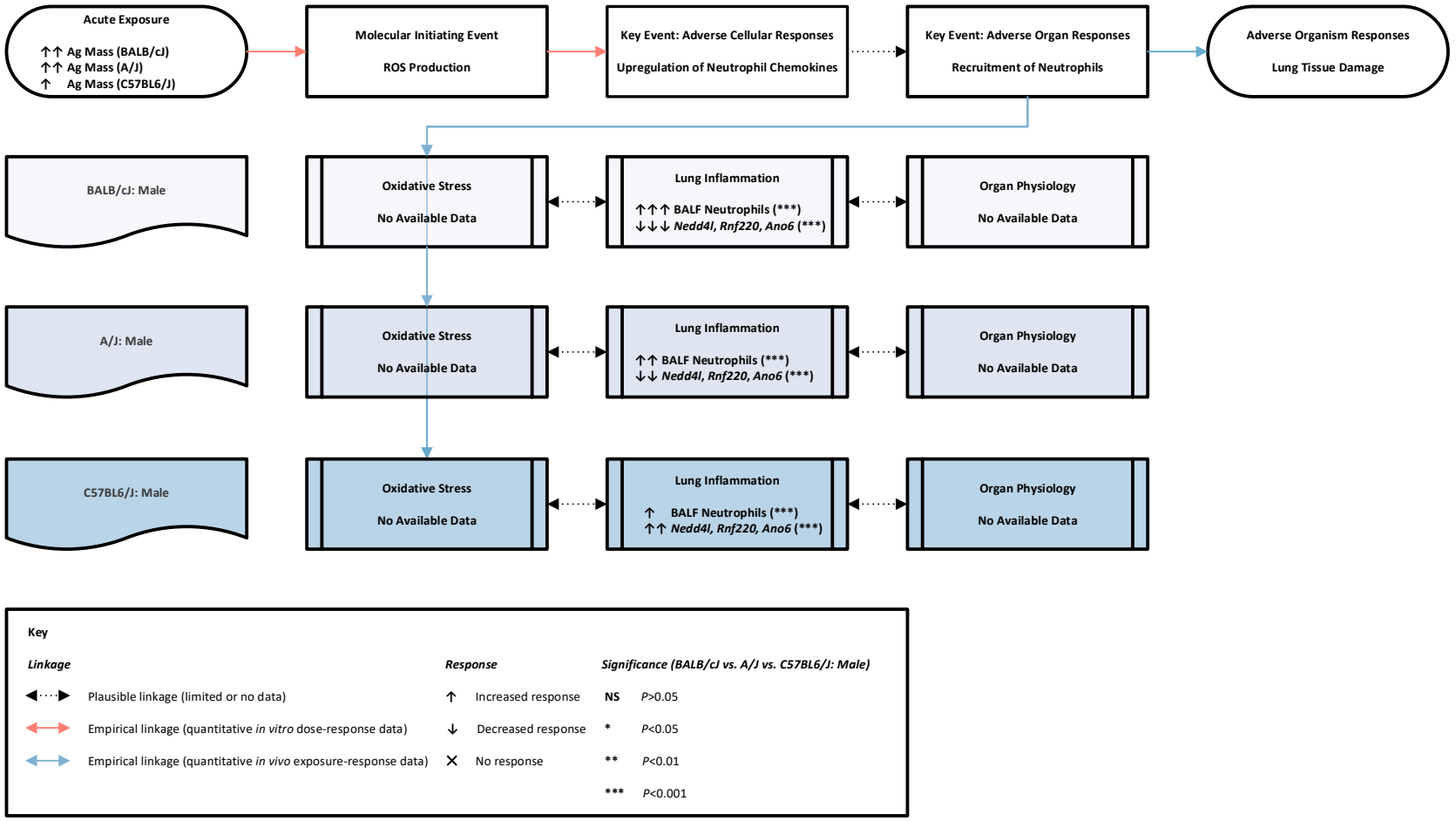

Figure 5.4. Adverse organ responses at acute exposures. Acute Exposure (24 h): Ag mass (µg Ag/mg tissue). Molecular Initiating Event: ROS (reactive oxygen species). Lung Inflammation: BALF (bronchoalveolar lavage fluid); *Ano6* (anoctamin 6); *Nedd4l* (E3 ubiquitin-protein ligase NEDD4-like); *Rnf220* (E3 ubiquitin-protein ligase RNF220).

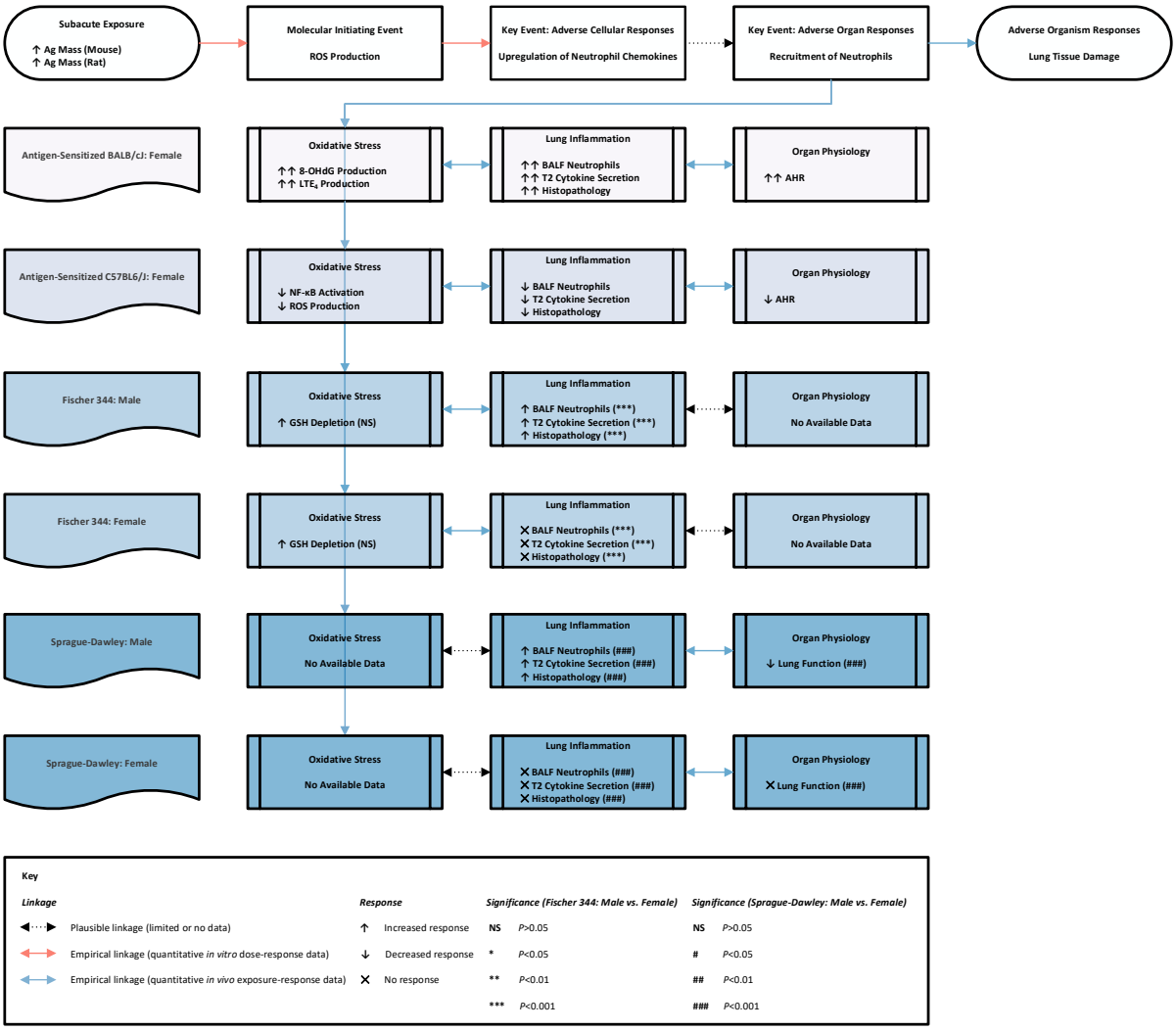

Figure 5.5. Adverse organ responses at subacute exposures. Subacute Exposure (4 to 21 d): Ag mass (μg Ag/mg tissue). Molecular Initiating Event: ROS (reactive oxygen species). Oxidative Stress: 8-OHdG (8-hydroxy-2'-deoxyguanosine); NF-κB (nuclear factor kappa-light-chain-enhancer of activated B cells); ROS (reactive oxygen species); GSH (glutathione). Lung Inflammation: BALF (bronchoalveolar lavage fluid); T2 (type 2).

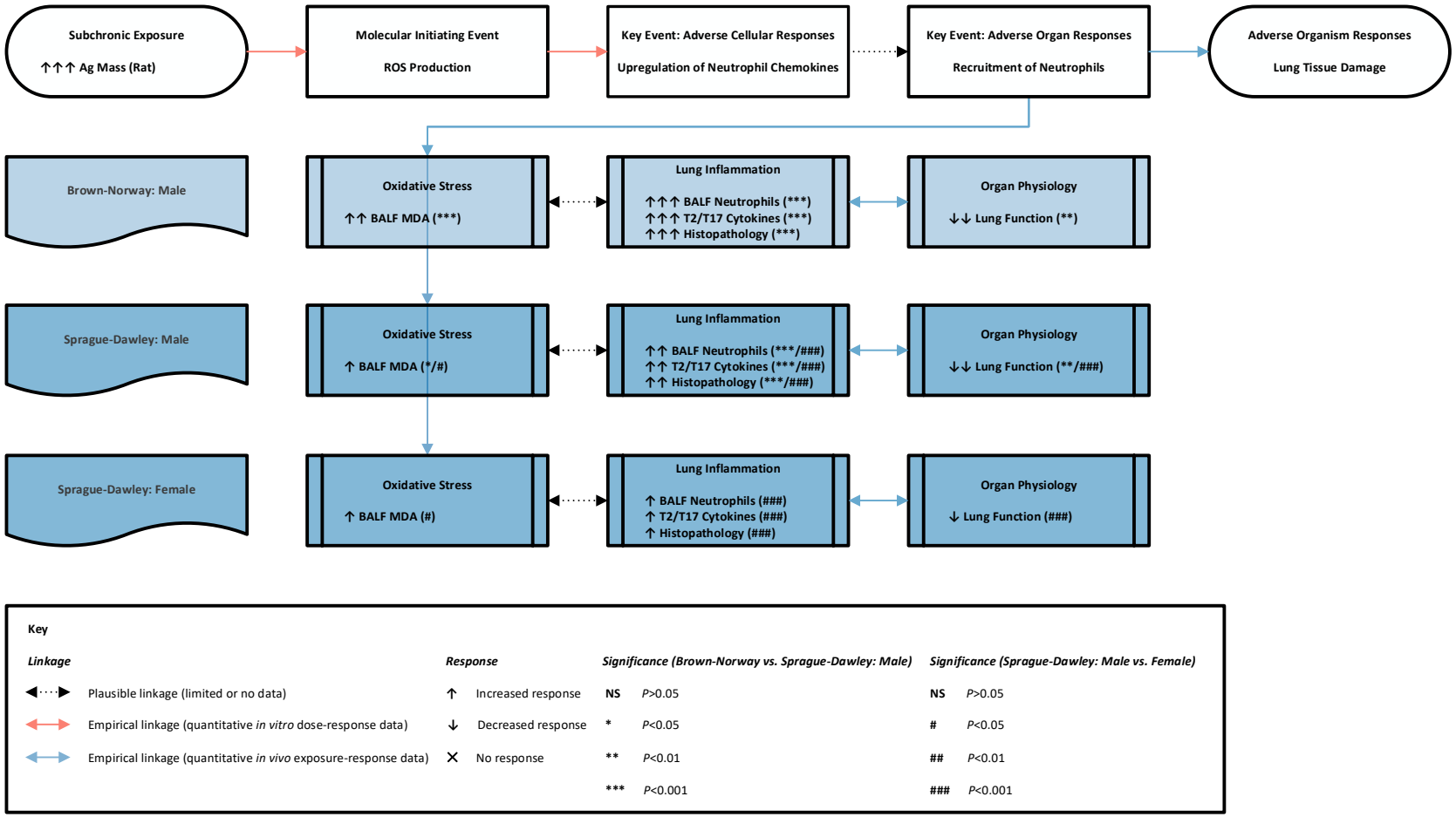

Figure 5.6. Adverse organ responses at subchronic exposures. Subchronic Exposure (21 to 90 d): Ag mass (µg Ag/mg tissue). Molecular Initiating Event: ROS (reactive oxygen species). Oxidative Stress: BALF (bronchoalveolar lavage fluid); MDA (malondialdehyde). Lung Inflammation: BALF (bronchoalveolar lavage fluid); T2 (type 2); T17 (type 17).

5.7 SUPPLEMENTARY DATA

Adverse Cellular Response	Exposure	Genotype:Phenotype	Nominal BMD (BMDL)	Significance (*P*)	Dosimetric BMD (BMDL)	Significance (*P*)
GSH depletion	24 h	AJ:Normal	27.40 (21.30)	***	17.40 (12.80)	***
		B6:Normal	51.70 (33.50)	***	17.50 (11.00)	***
		AJ:T2-Skewed	22.00 (17.90)	***	18.00 (14.10)	***
		B6:T2-Skewed	35.50 (25.90)	***	20.00 (15.20)	***
	5×4 h	AJ:Normal	39.40 (27.90)	***	2.10 (1.60)	***
		B6:Normal	55.60 (35.10)	***	4.50 (2.70)	***
		AJ:T2-Skewed	35.50 (25.90)	***	12.80 (7.70)	***
		B6:T2-Skewed	75.60 (42.20)	*	>8.70	NS
ROS production	24 h	AJ:Normal	5.30 (5.00)	***	3.90 (3.60)	***
		B6:Normal	6.70 (6.30)	***	3.20 (2.90)	***
		AJ:T2-Skewed	2.60 (2.50)	***	3.50 (3.30)	***
		B6:T2-Skewed	8.00 (7.40)	***	5.30 (4.90)	***
	5×4 h	AJ:Normal	9.90 (9.00)	***	1.10 (1.00)	***
		B6:Normal	7.90 (7.30)	***	0.60 (0.50)	***
		AJ:T2-Skewed	2.60 (2.50)	***	1.80 (1.60)	***
		B6:T2-Skewed	3.30 (3.20)	***	1.80 (1.70)	***
Lipid peroxidation	24 h	AJ:Normal	9.40 (8.50)	***	5.80 (5.20)	***
		B6:Normal	21.00 (17.20)	***	6.50 (5.30)	***
		AJ:T2-Skewed	5.20 (4.90)	***	5.60 (5.20)	***
		B6:T2-Skewed	7.00 (6.50)	***	4.50 (4.20)	***
	5×4 h	AJ:Normal	9.90 (9.00)	***	1.40 (1.20)	***
		B6:Normal	13.20 (11.60)	***	1.00 (0.90)	***
		AJ:T2-Skewed	7.30 (6.80)	***	3.50 (3.00)	***
		B6:T2-Skewed	11.90 (10.60)	***	8.30 (3.70)	***
Cytotoxicity	24 h	AJ:Normal	>50.00	NS	>24.50	NS
		B6:Normal	16.50 (14.10)	***	5.60 (4.70)	***
		AJ:T2-Skewed	7.10 (6.60)	***	>33.50	NS
		B6:T2-Skewed	10.80 (9.70)	***	7.00 (6.30)	***
	5×4 h	AJ:Normal	55.40 (35.10)	***	8.30 (3.70)	***
		B6:Normal	20.50 (16.90)	***	1.70 (1.40)	***
		AJ:T2-Skewed	7.20 (6.70)	***	2.90 (2.50)	***
		B6:T2-Skewed	7.80 (7.20)	***	2.60 (2.30)	***

Nominal vs. dosimetric BMD (BMDL) for adverse cellular responses at acute and subacute exposures. Exposure: h (hours). Genotype:Phenotype: AJ:Normal (A/J, “Normal” phenotype); B6:Normal (C57BL6/J, “Normal” phenotype); AJ:T2-Skewed (A/J, “T2-Skewed” phenotype); B6:T2-Skewed (C57BL6/J, “T2-Skewed” phenotype). Nominal BMD (BMDL): µg AgNP/mL media; Dosimetric BMD (BMDL): µg Ag/mg protein. n = 3 biological replicates with technical replicates. Data represent BMD (BMDL); NS (P>0.05); * (P<0.05); ** (P<0.01); *** (P<0.001).

Adverse Organ Response	Size (nm)	Coating	Dose	Exposure	Genotype/Sex	Nominal BMD (BMDL)	Dosimetric BMC (BMCL)
Tidal volume	18	Uncoated	49-515 μg/m^3	6 h/d, 5 d/w, 13 w	Sprague-Dawley/Male	1.45 (8.65)	296 (177)
BALF: albumin	18	Uncoated	49-515 μg/m^3	6 h/d, 5 d/w, 13 w	Sprague-Dawley/Male	13.32 (8.17)	273 (168)
					Sprague-Dawley/Female	14.45 (8.44)	318 (186)
BALF: LDH	18	Uncoated	49-515 μg/m^3	6 h/d, 5 d/w, 13 w	Sprague-Dawley/Female	7.56 (5.21)	166 (115)
BALF: protein	18	Uncoated	49-515 μg/m^3	6 h/d, 5 d/w, 13 w	Sprague-Dawley/Female	11.08 (7.02)	244 (156)
Lung infiltrate	18	Uncoated	49-515 μg/m^3	6 h/d, 5 d/w, 13 w	Sprague-Dawley/Female	6.86 (2.52)	151 (56)
Lung inflammation	18	Uncoated	49-515 μg/m^3	6 h/d, 5 d/w, 13 w	Sprague-Dawley/Male	6.06 (1.39)	124 (28)
					Sprague-Dawley/Female	6.90 (3.11)	152 (69)

Nominal BMD (BMDL) vs. dosimetric BMC (BMCL) for adverse organ responses at subchronic exposures. Exposure: h (hours); d (days); w (weeks). Nominal BMD (BMDL): μg AgNP/organ. Dosimetric BMC (BMCL): μg Ag/m^3. Data represent BMD (BMDL) and BMC (BMCL); NS (P>0.05); * (P<0.05); ** (P<0.01); *** (P<0.001).

Chapter 6. Outline of Research Findings and Implications for Risk Assessment

6.1 SIGNIFICANCE OF RESEARCH FINDINGS

The Effects of Gene × Environment Interactions on Silver Nanoparticle Toxicity in the Respiratory System

- **Research need:** There is presently a need to understand the effects of interactions between host genetic and acquired factors, or G×E, on AgNP toxicity in the respiratory system to assist in defining exposure limits to protect all populations in occupational settings.

- **Research aim:** Review host genetic and acquired factors identified across *in vitro* and *in vivo* studies and prioritize those necessary for defining exposure limits to protect all populations in occupational settings.

- **Research findings:** Host genetic and acquired factors may play a role in defining sensitive populations to AgNP exposures in occupational settings. These G×E effects on AgNP toxicity are of relevance of public health as they may be broadly applicable to other types of engineered nanomaterials (ENM), which are used in manufacturing of many consumer products. Our review focused on host acquired factors, such as asthma, but other pre-existing chronic respiratory diseases, such as acute bronchitis or chronic obstructive pulmonary disease (COPD), may also confer increased sensitivity to occupational exposures.[25-27] When defining exposure limits, it is important to determine whether sex effects on AgNP toxicity are present given the effects of sexual dimorphism on adverse health responses to oxidative stress and allergic inflammation. An additional consideration is whether there are known polymorphisms identified in the putative pathways by which different occupational exposures cause adverse health responses. It is also important to evaluate whether individuals with pre-existing chronic respiratory diseases, such as asthma, may be more sensitive to occupational exposures. Future studies should evaluate G×E effects in order to identify genes or gene

products that may contribute to risk for AgNP toxicity.

The Effects of Genotype × Phenotype Interactions on Silver Nanoparticle Toxicity in Organotypic Cultures of Murine Tracheal Epithelial Cells

- **Research need:** There is presently a need for *in vitro* models to provide a regulatory basis for sensitivity to occupational exposures.
- **Research aim:** Use organotypic cultures to characterize nominal and dosimetric dose-response relationships across genotypes, phenotypes, and exposures to understand G×P effects on AgNP toxicity.
- **Research hypothesis:** Genotype and phenotype (physiological environment) will define G×E, or genotype × phenotype interaction (G×P), effects on AgNP toxicity.
- **Research findings:** This study established organotypic cultures derived from murine tracheal epithelial cells (MTEC) as a medium-throughput, high-content *in vitro* model for the conducing airway to characterize chemical perturbation as a means to screen and prioritize potential respiratory toxicants. We characterized nominal and dosimetric dose-response relationships for AgNP-induced barrier dysfunction, GSH depletion, ROS production, lipid peroxidation, and cytotoxicity across genotypes, phenotypes, and exposures to understand G×P effects on AgNP toxicity. The “Type 2 (T2)-Skewed” phenotype was characterized as an *in vitro* model of chronic respiratory diseases and was marked by increased sensitivity to AgNP-induced barrier dysfunction, GSH depletion, ROS production, lipid peroxidation, and cytotoxicity, suggesting that asthmatics could be a sensitive population to AgNP exposures in occupational settings. This also suggests that exposure limits, which should be based upon the most sensitive population, should be derived using *in vitro* and *in vivo* models of chronic respiratory diseases. This study highlights the importance of considering dosimetry as well as G×P effects when screening and prioritizing potential respiratory toxicants. Such *in vitro* studies can be used to inform regulatory policy aimed at protecting all populations.

The Effects of Genotype × Phenotype Interactions on Transcriptional Response to

Silver Nanoparticle Toxicity in Organotypic Cultures of Murine Tracheal Epithelial Cells

- **Research need:** There is presently a need for *in vitro* models to provide a mechanistic basis for sensitivity to occupational exposures.

- **Research aim:** Use organotypic cultures to characterize global and differential gene expression, canonical pathway enrichment, and upstream transcriptional regulators to understand G×P effects on transcriptional response to AgNP toxicity.

- **Research hypothesis:** Genotype and phenotype will define G×P effects on transcriptional response to AgNP toxicity.

- **Research findings:** This study further established organotypic cultures derived from MTEC as a medium-throughput, high-content *in vitro* model for the conducing airway to characterize chemical perturbation as a means to screen and prioritize potential respiratory toxicants. We characterized global, differential, and targeted gene expression, canonical pathway enrichment, and upstream transcriptional regulation to understand G×P effects on transcriptional response to AgNP toxicity. We pursued a targeted analysis to characterize dose, genotype, and phenotype effects on expression patterns of genes involved in the secreted factors canonical pathway that were also associated with T1, pro-T2, T2, and T17 responses to AgNP toxicity. We observed the “T2-Skewed” phenotype was marked by increased pro-inflammatory T17 responses to AgNP toxicity, which are significant predictors of neutrophilic/difficult-to-control asthma and suggests that asthmatics could be a sensitive population to AgNP exposures in occupational settings. This study highlights the importance of considering G×P effects when identifying these sensitive populations, whose underlying genetics or diseases could directly modify their response to AgNP exposures.

The Effects of Gene × Environment Interactions on Silver Nanoparticle Toxicity in The Respiratory System: Toward an Adverse Outcome Pathway

- **Research need:** There is presently a need to support regulatory decision-making

for ENM through highlighting knowledge gaps where they exist in order to more directly prioritize future research needs.

- **Research aim:** Use the Adverse Outcome Pathway (AOP) framework to organize and integrate data from *in vitro* and *in vivo* models to evaluate G×E effects on AgNP toxicity in the respiratory system.

- **Research hypothesis:** Molecular initiating events (MIE) and key events (KE) for AgNP toxicity can be modified by different host genetic and host acquired factors at acute, subacute, and subchronic exposures.

- **Research findings:** Using the AOP framework, this study established that host genetic and acquired factors may play a role in defining sensitive populations to AgNP exposures in occupational settings. These G×E effects on AgNP toxicity are of relevance of public health as they may be broadly applicable to other types of ENM, which are used in manufacturing of many consumer products. We utilized mechanistic information from *in vitro* and *in vivo* studies to highlight how KE can be modified by host genetic and host acquired factors at acute, subacute, and subchronic exposures, and identified two categories of knowledge gaps in order to more directly prioritize future research needs.

  Knowledge gaps for key events of AgNP toxicity

  - *In vitro* data for “Mitochondrial Function” and “Inflammation” in organotypic cultures at subacute exposures

  - *In vivo* data for “Oxidative Stress” and “Organ Physiology” in mice at acute and subacute exposures

  Knowledge gaps for G×E effects on AgNP toxicity

  - *In vitro* data for sex, genotype, and phenotype effects on AgNP particokinetics and toxicity in organotypic cultures at acute and subacute exposures

- *In vivo* data for sex, genotype, and antigen effects on AgNP particokinetics and toxicity in mice at acute, subacute, and subchronic exposures
- *In vivo* data for sex and genotype effects on AgNP particokinetics and toxicity in rats at acute, subacute, and subchronic exposures

6.2 FUTURE DIRECTIONS

This is the first study to use organotypic cultures as a high-content *in vitro* model for the conducting airway to characterize G×P effects on AgNP toxicity, and therefore, refining this *in vitro* model in future studies is warranted. One limitation of these studies was our use of only one sex and two genotypes; the use of both sexes and additional genotypes (e.g., BALB/cJ and SWR/J mice) or knockouts (e.g., *Nedd4l*$^{-/-}$, *Nfkb1*$^{-/-}$, *Il23*$^{-/-}$, *Stat3*$^{-/-}$, or *Bcl6*$^{-/-}$ mice mice) would increase genetic diversity and assist in defining a mechanistic basis for G×P effects on AgNP toxicity in future studies.

A second limitation of these studies was our use of IL-13 to skew differentiation toward an *in vitro* model of chronic respiratory diseases; the use of co-cultures with relevant cell populations, including alveolar macrophages, mast cells, or type 2 innate lymphoid cells (ILC2), would increase cellular diversity and improve the physiological relevance of this *in vitro* model in future studies. Or alternatively, the use of additional cytokines, such as IL-17, to skew differentiation toward an *in vitro* model of more severe chronic respiratory diseases would improve the physiological relevance of this *in vitro* model by reflecting the diversity of T2-high and T17-high endotypes.

A third limitation of these studies was our administration of the nominal dose using suspensions of AgNP in differentiation media. This approach may have contributed to their dissolution; the use of a Nano Aerosol Chamber for *in vitro* Toxicity studies (NACIVT) would allow for direct deposition of ENM onto the apical surface of organotypic cultures;[50,61,182] or alternatively, the use of microfluidic systems would improve our understanding of the kinetics and dynamics of the conducing airway in future studies.[183] Both approaches would allow this *in vitro* model to better

recapitulate the physiological conditions of AgNP exposures in occupational settings.

A fourth limitation of these studies was the fact the we did not address whether these differences in gene expression translate into differences in protein expression for secreted factors in bronchoalveolar lavage fluid (BALF). Characterizing these differences in gene expression in humans depends upon invasive procedures and therefore precludes routine use, which emphasises the need to identify less invasive mechanistic-based biomarkers of AgNP toxicity still capable of producing biologically robust predictions of adverse organism responses resulting from these occupational exposures. The use of multiplex platforms would permit future studies to 1) assay *in vitro* or *in vivo* protein expression for secreted factors at multiple doses in order to identify predictive, mechanistic-based biomarkers of AgNP toxicity and, 2) use a BMD approach to define exposure levels corresponding to specific changes in response.

A fifth limitation of these studies was that we did not assay the kinetics and dynamics of ROS production, which was observed to be the most sensitive adverse cellular response at the subacute 5×4 h exposure.[157,158] The use of thiol-redox and oxidative stress responsive green fluorescent protein (GFP) probes (Grx1-roGFP and roGFP2-Orp1) in lentivirus-based vectors would permit future studies to assay the kinetics and dynamics of these important redox indicators in organotypic cultures. Though investigated preliminarily in our study, future studies could pair lentiviral transduction with the use of a defined differentiation media supplemented with antioxidants, such as glutathione-ethyl ester (GSH-EE), in order to more fully understand the kinetics and dynamics of their protective role during oxidative stress. Since GSH depletion is a clinical feature of chronic respiratory diseases that impairs host defense mechanisms against oxidative stress, these studies would aid in determining the efficacy of GSH supplementation as an intervention for sensitive populations, whose underlying genetics or diseases could directly modify their response to AgNP exposures.

Going forward, future studies should also consider how to improve upon the specificity of our RNA-seq analysis. This could be addressed, in part, by using

Translating Ribosome Affinity Purification (TRAP) on organotypic cultures for cell population-specific transcriptomics.[244,245] This approach would assist in characterizing sensitive cell populations and thus improving the specificity of transcriptional response to AgNP toxicity. However, these changes in gene expression may not correlate to functional linked endpoints, and thus organotypic cultures can be paired with proteomics or metabolomics to better correlate these changes in gene expression to functional linked endpoints.

Despite these limitations, these studies establish organotypic cultures derived from MTEC as a medium-throughput, high-content *in vitro* model for the conducing airway to characterize chemical perturbation as a means to screen and prioritize potential respiratory toxicants. Our results highlight the importance of considering dosimetry as well as G×P effects when screening and prioritizing potential respiratory toxicants. This suggests the importance of considering other host factors, such as age, gender, and epigenetic effects when screening and prioritizing potential respiratory toxicants. This is challenging and important for engineered nanomaterials, since their MoA have been shown to differ considerably but are still used in hundreds of consumer products. Prior to anticipating potential adverse organism responses arising from engineered nanomaterial toxicity, ensuring safe development of the consumer products in which they are used will be the most critical and necessary step toward safeguarding public health.

References

1 Wilson, A. G. E. in *New Horizons in Predictive Toxicology Drug Discovery* 1-8 (2011).

2 Burden, N. *et al.* Aligning the 3Rs with new paradigms in the safety assessment of chemicals. *Toxicology* **330**, 62-66, doi:10.1016/j.tox.2015.01.014 (2015).

3 Krewski, D., Andersen, M. E., Mantus, E. & Zeise, L. Toxicity testing in the 21st century: implications for human health risk assessment. *Risk Anal* **29**, 474-479, doi:10.1111/j.1539-6924.2008.01150.x (2009).

4 Judson, R. S. *et al.* Estimating toxicity-related biological pathway altering doses for high-throughput chemical risk assessment. *Chem Res Toxicol* **24**, 451-462, doi:10.1021/tx100428e (2011).

5 Berube, K., Prytherch, Z., Job, C. & Hughes, T. Human primary bronchial lung cell constructs: the new respiratory models. *Toxicology* **278**, 311-318, doi:10.1016/j.tox.2010.04.004 (2010).

6 Kavlock, R. & Dix, D. Computational toxicology as implemented by the U.S. EPA: providing high throughput decision support tools for screening and assessing chemical exposure, hazard and risk. *J Toxicol Environ Health B Crit Rev* **13**, 197-217, doi:10.1080/10937404.2010.483935 (2010).

7 Lee, J. J., Miller, J. A., Basu, S., Kee, T. V. & Loo, L. H. Building predictive in vitro pulmonary toxicity assays using high-throughput imaging and artificial intelligence. *Arch Toxicol* **92**, 2055-2075, doi:10.1007/s00204-018-2213-0 (2018).

8 Lock, E. F. *et al.* Quantitative high-throughput screening for chemical toxicity in a population-based in vitro model. *Toxicol Sci* **126**, 578-588, doi:10.1093/toxsci/kfs023 (2012).

9 NAS. in *Application of Modern Toxicology Approaches for Predicting Acute Toxicity for Chemical Defense* (2015).

10 Nichols, J. E., Niles, J. A., Vega, S. P. & Cortiella, J. Novel in vitro respiratory models to study lung development, physiology, pathology and toxicology. *Stem Cell Res Ther* **4 Suppl 1**, S7, doi:10.1186/scrt368 (2013).

11 Kim, J. *et al.* Antimicrobial effects of silver nanoparticles. *Nanomedicine: Nanotechnology, Biology and Medicine* **3**, 95-101, doi:10.1016/j.nano.2006.12.001 (2007).

12 Danilczuk, M., Lund, A., Sadlo, J., Yamada, H. & Michalik, J. Conduction electron spin resonance of small silver particles. *Spectrochimica Acta Part A: Molecular and Biomolecular Spectroscopy* **63**, 189-191, doi:10.1016/j.saa.2005.05.002 (2006).

13 Ma, R. *et al.* Size-Controlled Dissolution of Organic-Coated Silver Nanoparticles. *Environmental Science & Technology* **46**, 752-759, doi:10.1021/es201686j (2012).

14 Utembe, W., Potgieter, K., Stefaniak, A. & Gulumian, M. Dissolution and biodurability: Important parameters needed for risk assessment of nanomaterials. *Particle and Fibre Toxicology* **12**, 1-12, doi:10.1186/s12989-015-0088-2 (2015).

15 Hallstrand, T. S. *et al.* Airway epithelial regulation of pulmonary immune homeostasis and inflammation. *Clinical Immunology* **151**, 1-15, doi:10.1016/j.clim.2013.12.003 (2014).

16 Weaver, M., Batts, L. & Hogan, B. Tissue interactions pattern the mesenchyme of the embryonic mouse lung. *Developmental Biology* **258**, 169-184, doi:10.1016/s0012-1606(03)00117-9 (2003).
17 Rock, J. R. *et al.* Multiple stromal populations contribute to pulmonary fibrosis without evidence for epithelial to mesenchymal transition. *Proceedings of the National Academy of Sciences* **108**, doi:10.1073/pnas.1117988108 (2011).
18 Borok, Z. *et al.* Cell Plasticity in Lung Injury and Repair. *Proceedings of the American Thoracic Society* **8**, 215-222, doi:10.1513/pats.201012-067cb (2011).
19 Ostedgaard, L. S. *et al.* Gel-forming mucins form distinct morphologic structures in airways. *Proc Natl Acad Sci U S A* **114**, 6842-6847, doi:10.1073/pnas.1703228114 (2017).
20 Steelant, B. *et al.* Histamine and T helper cytokine-driven epithelial barrier dysfunction in allergic rhinitis. *J Allergy Clin Immunol* **141**, 951-963 e958, doi:10.1016/j.jaci.2017.08.039 (2018).
21 Flynn, A. N., Itani, O. A., Moninger, T. O. & Welsh, M. J. Acute regulation of tight junction ion selectivity in human airway epithelia. *Proc Natl Acad Sci U S A* **106**, 3591-3596, doi:10.1073/pnas.0813393106 (2009).
22 MacRedmond, R. E. *et al.* Fluticasone Induces Epithelial Injury and Alters Barrier Function in Normal Subjects. *J Steroids Horm Sci* **5**, doi:10.4172/2157-7536.1000134 (2014).
23 Matsui, H., Randell, S. H., Peretti, S. W., Davis, C. W. & Boucher, R. C. Coordinated clearance of periciliary liquid and mucus from airway surfaces. *Journal of Clinical Investigation* **102**, 1125-1131, doi:10.1172/jci2687 (1998).
24 MacPherson, J. C. *et al.* Eosinophils Are a Major Source of Nitric Oxide-Derived Oxidants in Severe Asthma: Characterization of Pathways Available to Eosinophils for Generating Reactive Nitrogen Species. *The Journal of Immunology* **166**, 5763-5772, doi:10.4049/jimmunol.166.9.5763 (2001).
25 Donaldson, K., Stone, V., Clouter, A., Renwick, L. & MacNee, W. Ultrafine particles. *Occup Environ Med* **58**, 211-216, 199 (2001).
26 Goss, C. H., Newsom, S. A., Schildcrout, J. S., Sheppard, L. & Kaufman, J. D. Effect of ambient air pollution on pulmonary exacerbations and lung function in cystic fibrosis. *Am J Respir Crit Care Med* **169**, 816-821, doi:10.1164/rccm.200306-779OC (2004).
27 Pope, C. A., 3rd. Epidemiology of fine particulate air pollution and human health: biologic mechanisms and who's at risk? *Environ Health Perspect* **108 Suppl 4**, 713-723 (2000).
28 von Mutius, E. Gene-environment interactions in asthma. *J Allergy Clin Immunol* **123**, 3-11; quiz 12-13, doi:10.1016/j.jaci.2008.10.046 (2009).
29 Molfino, N. A. & Coyle, A. J. Gene-environment interactions in chronic obstructive pulmonary disease. *Int J Chron Obstruct Pulmon Dis* **3**, 491-497 (2008).
30 Xiu, Z.-M., Ma, J. & Alvarez, P. J. J. Differential effect of common ligands and molecular oxygen on antimicrobial activity of silver nanoparticles versus silver ions. *Environmental science & technology* **45**, 9003-9008, doi:10.1021/es201918f (2011).

31 Quadros, M. E. & Marr, L. C. Environmental and Human Health Risks of Aerosolized Silver Nanoparticles. *Journal of the Air & Waste Management Association* **60**, 770-781, doi:10.3155/1047-3289.60.7.770 (2010).
32 Quadros, M. E. & Marr, L. C. Silver Nanoparticles and Total Aerosols Emitted by Nanotechnology-Related Consumer Spray Products. *Environmental Science & Technology* **45**, 10713-10719, doi:10.1021/es202770m (2011).
33 Kruis, F. E., Fissan, H. & Peled, A. Synthesis of nanoparticles in the gas phase for electronic, optical and magnetic applications—a review. *Journal of Aerosol Science* **29**, 511-535, doi:10.1016/s0021-8502(97)10032-5 (1998).
34 Nymark, P. *et al.* Genotoxicity of polyvinylpyrrolidone-coated silver nanoparticles in BEAS 2B cells. *Toxicology* **313**, 38-48, doi:10.1016/j.tox.2012.09.014 (2013).
35 Prabhu, S. & Poulose, E. K. Silver nanoparticles: mechanism of antimicrobial action, synthesis, medical applications, and toxicity effects. *International Nano Letters* **2**, 32, doi:10.1186/2228-5326-2-32 (2012).
36 O'Connell, R. *et al.* World Silver Survey 2017. *The Silver Institute and Thomson Reuters* (2017).
37 Vance, M. E. *et al.* Nanotechnology in the real world: Redeveloping the nanomaterial consumer products inventory. *Beilstein journal of nanotechnology* **6**, 1769-1780, doi:10.3762/bjnano.6.181 (2015).
38 Park, J. *et al.* Characterization of exposure to silver nanoparticles in a manufacturing facility. *Journal of Nanoparticle Research* **11**, 1705-1712, doi:10.1007/s11051-009-9725-8 (2009).
39 Lee, J. *et al.* Exposure assessment of workplaces manufacturing nanosized TiO2 and silver. *Inhalation Toxicology* **23**, 226-236, doi:10.3109/08958378.2011.562567 (2011).
40 Lee, J., Mun, J., Park, J. & Yu, I. A health surveillance case study on workers who manufacture silver nanomaterials. *Nanotoxicology* **6**, 667-669, doi:10.3109/17435390.2011.600840 (2012).
41 Kim, E. *et al.* Case Study on Risk Evaluation of Silver Nanoparticle Exposure from Antibacterial Sprays Containing Silver Nanoparticles. *Journal of Nanomaterials* **2015**, 1-8, doi:10.1155/2015/346586 (2015).
42 Hoet, P. H. M., Brüske-Hohlfeld, I. & Salata, O. V. Nanoparticles – known and unknown health risks. *Journal of Nanobiotechnology* **2**, 1-15, doi:10.1186/1477-3155-2-12 (2004).
43 Bonner, J. C. *et al.* Interlaboratory Evaluation of Rodent Pulmonary Responses to Engineered Nanomaterials: The NIEHS Nano GO Consortium. *Environmental Health Perspectives* **121**, 676-682, doi:10.1289/ehp.1205693 (2013).
44 Schug, T. T. *et al.* ONE Nano: NIEHS's Strategic Initiative on the Health and Safety Effects of Engineered Nanomaterials. *Environmental Health Perspectives* **121**, 410-414, doi:10.1289/ehp.1206091 (2013).
45 Schug, T. T., Nadadur, S. S. & Johnson, A. F. Nano GO Consortium—A Team Science Approach to Assess Engineered Nanomaterials: Reliable Assays and Methods. *Environmental Health Perspectives* **121**, doi:10.1289/ehp.1306866 (2013).

46 Maurer, L. L. & Meyer, J. N. A systematic review of evidence for silver nanoparticle-induced mitochondrial toxicity. *Environmental Science: Nano* **3**, 311-322, doi:10.1039/c5en00187k (2016).
47 Sun, Y. & Xia, Y. Shape-Controlled Synthesis of Gold and Silver Nanoparticles. *Science* **298**, 2176-2179, doi:10.1126/science.1077229 (2002).
48 Alsaleh, N. B. & Brown, J. M. Immune responses to engineered nanomaterials: Current understanding and challenges. *Current Opinion in Toxicology* **10**, 8-14, doi:10.1016/j.cotox.2017.11.011 (2018).
49 Johnson, M. *et al.* Genomic and transcriptomic comparison of allergen and silver nanoparticle-induced mast cell degranulation reveals novel non-immunoglobulin E mediated mechanisms. *PLoS One* **13**, e0193499, doi:10.1371/journal.pone.0193499 (2018).
50 Jeannet, N. *et al.* Acute toxicity of silver and carbon nanoaerosols to normal and cystic fibrosis human bronchial epithelial cells. *Nanotoxicology* **10**, 1-13, doi:10.3109/17435390.2015.1049233 (2015).
51 Hamilton, R. F., Buckingham, S. & Holian, A. The effect of size on Ag nanosphere toxicity in macrophage cell models and lung epithelial cell lines is dependent on particle dissolution. *Int J Mol Sci* **15**, 6815-6830, doi:10.3390/ijms15046815 (2014).
52 Hussain, S. *et al.* Inflammasome activation in airway epithelial cells after multi-walled carbon nanotube exposure mediates a profibrotic response in lung fibroblasts. *Part Fibre Toxicol* **11**, 28, doi:10.1186/1743-8977-11-28 (2014).
53 Liang, X. *et al.* Reactive oxygen species trigger NF-kappaB-mediated NLRP3 inflammasome activation induced by zinc oxide nanoparticles in A549 cells. *Toxicol Ind Health* **33**, 737-745, doi:10.1177/0748233717712409 (2017).
54 Allen, I. C. *et al.* An Allergic Lung Microenvironment Suppresses Carbon Nanotube-Induced Inflammasome Activation via STAT6-Dependent Inhibition of Caspase-1. *Plos One* **10**, doi:10.1371/journal.pone.0128888 (2015).
55 Hirota, J. A. *et al.* The airway epithelium nucleotide-binding domain and leucine-rich repeat protein 3 inflammasome is activated by urban particulate matter. *J Allergy Clin Immunol* **129**, 1116-1125 e1116, doi:10.1016/j.jaci.2011.11.033 (2012).
56 Zielinska, E., Zauszkiewicz-Pawlak, A., Wojcik, M. & Inkielewicz-Stepniak, I. Silver nanoparticles of different sizes induce a mixed type of programmed cell death in human pancreatic ductal adenocarcinoma. *Oncotarget* **9**, 4675-4697, doi:10.18632/oncotarget.22563 (2018).
57 Simard, J. C., Vallieres, F., de Liz, R., Lavastre, V. & Girard, D. Silver nanoparticles induce degradation of the endoplasmic reticulum stress sensor activating transcription factor-6 leading to activation of the NLRP-3 inflammasome. *J Biol Chem* **290**, 5926-5939, doi:10.1074/jbc.M114.610899 (2015).
58 Kim, H., Kim, M., Lee, S., Oh, S. & Chung, K. Genotoxic effects of silver nanoparticles stimulated by oxidative stress in human normal bronchial epithelial (BEAS-2B) cells. *Mutation Research/Genetic Toxicology and Environmental Mutagenesis* **726**, 129-135, doi:10.1016/j.mrgentox.2011.08.008 (2011).

59 Cronholm, P. *et al.* Intracellular Uptake and Toxicity of Ag and CuO Nanoparticles: A Comparison Between Nanoparticles and their Corresponding Metal Ions. *Small* **9**, 970-982, doi:10.1002/smll.201201069 (2013).
60 Gliga, A. R., Skoglund, S., Wallinder, I., Fadeel, B. & Karlsson, H. L. Size-dependent cytotoxicity of silver nanoparticles in human lung cells: the role of cellular uptake, agglomeration and Ag release. *Particle and Fibre Toxicology* **11**, 1-17, doi:10.1186/1743-8977-11-11 (2014).
61 Jeannet, N., Fierz, M., Kalberer, M., Burtscher, H. & Geiser, M. Nano Aerosol Chamber for In-Vitro Toxicity (NACIVT) studies. *Nanotoxicology* **9**, 34-42, doi:10.3109/17435390.2014.886739 (2014).
62 Schlinkert, P. *et al.* The oxidative potential of differently charged silver and gold nanoparticles on three human lung epithelial cell types. *Journal of Nanobiotechnology* **13**, 1, doi:10.1186/s12951-014-0062-4 (2015).
63 Choo, W. *et al.* Long-term exposures to low doses of silver nanoparticles enhanced in vitro malignant cell transformation in non-tumorigenic BEAS-2B cells. *Toxicology in Vitro* **37**, 41-49, doi:10.1016/j.tiv.2016.09.003 (2016).
64 Foldbjerg, R., Dang, D. & Autrup, H. Cytotoxicity and genotoxicity of silver nanoparticles in the human lung cancer cell line, A549. *Archives of Toxicology* **85**, 743-750, doi:10.1007/s00204-010-0545-5 (2011).
65 Chairuangkitti, P. *et al.* Silver nanoparticles induce toxicity in A549 cells via ROS-dependent and ROS-independent pathways. *Toxicology in Vitro* **27**, 330-338, doi:10.1016/j.tiv.2012.08.021 (2013).
66 Gurunathan, S. *et al.* Multidimensional effects of biologically synthesized silver nanoparticles in Helicobacter pylori, Helicobacter felis, and human lung (L132) and lung carcinoma A549 cells. *Nanoscale Research Letters* **10**, 1-17, doi:10.1186/s11671-015-0747-0 (2015).
67 Herzog, F. *et al.* Exposure of silver-nanoparticles and silver-ions to lung cells in vitro at the air-liquid interface. *Particle and Fibre Toxicology* **10**, 1-14, doi:10.1186/1743-8977-10-11 (2013).
68 Ahlberg, S. *et al.* PVP-coated, negatively charged silver nanoparticles: A multi-center study of their physicochemical characteristics, cell culture and in vivo experiments. *Beilstein Journal of Nanotechnology* **5**, 1944-1965, doi:10.3762/bjnano.5.205 (2014).
69 Lankoff, A. *et al.* The effect of agglomeration state of silver and titanium dioxide nanoparticles on cellular response of HepG2, A549 and THP-1 cells. *Toxicology Letters* **208**, 197-213, doi:10.1016/j.toxlet.2011.11.006 (2012).
70 Merhi, M. *et al.* Study of serum interaction with a cationic nanoparticle: Implications for in vitro endocytosis, cytotoxicity and genotoxicity. *International Journal of Pharmaceutics* **423**, 37-44, doi:10.1016/j.ijpharm.2011.07.014 (2012).
71 Sung, J. *et al.* Acute inhalation toxicity of silver nanoparticles. *Toxicology and Industrial Health* **27**, 149-154, doi:10.1177/0748233710382540 (2011).
72 Sung, J. *et al.* Lung Function Changes in Sprague-Dawley Rats After Prolonged Inhalation Exposure to Silver Nanoparticles. *Inhalation Toxicology* **20**, 567-574, doi:10.1080/08958370701874671 (2008).
73 Sung, J. *et al.* Subchronic Inhalation Toxicity of Silver Nanoparticles. *Toxicological Sciences* **108**, 452-461, doi:10.1093/toxsci/kfn246 (2009).

74 Song, K. *et al.* Recovery from silver-nanoparticle-exposure-induced lung inflammation and lung function changes in Sprague Dawley rats. *Nanotoxicology* **7**, 169-180, doi:10.3109/17435390.2011.648223 (2012).
75 Soutiere, S. E., Tankersley, C. G. & Mitzner, W. Differences in alveolar size in inbred mouse strains. *Respiratory Physiology & Neurobiology* **140**, 283-291, doi:10.1016/j.resp.2004.02.003 (2004).
76 Metzger, R. J., Klein, O. D., Martin, G. R. & Krasnow, M. A. The branching programme of mouse lung development. *Nature* **453**, doi:10.1038/nature07005 (2008).
77 Scoville, D. K. *et al.* Susceptibility to quantum dot induced lung inflammation differs widely among the Collaborative Cross founder mouse strains. *Toxicology and Applied Pharmacology* **289**, 240-250, doi:10.1016/j.taap.2015.09.019 (2015).
78 Scoville, D. K. *et al.* Genetic determinants of susceptibility to silver nanoparticle-induced acute lung inflammation in mice. *The FASEB Journal* **31**, 4600-4611, doi:10.1096/fj.201700187r (2017).
79 Seiffert, J. *et al.* Pulmonary toxicity of instilled silver nanoparticles: influence of size, coating and rat strain. *PLoS One* **10**, e0119726, doi:10.1371/journal.pone.0119726 (2015).
80 Seiffert, J. *et al.* Pulmonary effects of inhalation of spark-generated silver nanoparticles in Brown-Norway and Sprague-Dawley rats. *Respir Res* **17**, 85, doi:10.1186/s12931-016-0407-7 (2016).
81 McConnachie, L. A. *et al.* The glutathione synthesis gene Gclm modulates amphiphilic polymer-coated CdSe/ZnS quantum dot-induced lung inflammation in mice. *PLoS One* **8**, e64165, doi:10.1371/journal.pone.0064165 (2013).
82 Chuang, H.-C. *et al.* Allergenicity and toxicology of inhaled silver nanoparticles in allergen-provocation mice models. *International Journal of Nanomedicine* **8**, 4495-4506, doi:10.2147/ijn.s52239 (2013).
83 Su, C. L. *et al.* Comparative proteomics of inhaled silver nanoparticles in healthy and allergen provoked mice. *Int J Nanomedicine* **8**, 2783-2799, doi:10.2147/IJN.S46997 (2013).
84 Jang, S. *et al.* Silver nanoparticles modify VEGF signaling pathway and mucus hypersecretion in allergic airway inflammation. *International Journal of Nanomedicine* **7**, 1329-1343, doi:10.2147/ijn.s27159 (2012).
85 Park, H. *et al.* Attenuation of allergic airway inflammation and hyperresponsiveness in a murine model of asthma by silver nanoparticles. *International Journal of Nanomedicine* **Volume 5**, 505-515, doi:10.2147/ijn.s11664 (2010).
86 Alessandrini, F. *et al.* Pro-Inflammatory versus Immunomodulatory Effects of Silver Nanoparticles in the Lung: The Critical Role of Dose, Size and Surface Modification. *Nanomaterials* **7**, 300, doi:10.3390/nano7100300 (2017).
87 Zhang, H. *et al.* Mammalian Cells Exhibit a Range of Sensitivities to Silver Nanoparticles that are Partially Explicable by Variations in Antioxidant Defense and Metallothionein Expression. *Small* **11**, 3797-3805, doi:10.1002/smll.201500251 (2015).
88 Yang, D., Jin, M., Bai, C., Zhou, J. & Shen, Y. Peroxiredoxin 6 suppresses Muc5ac overproduction in LPS-induced airway inflammation through H2O2-EGFR-MAPK

signaling pathway. *Respir Physiol Neurobiol* **236**, 84-90, doi:10.1016/j.resp.2016.11.012 (2017).
89 Comhair, S. A., Bhathena, P. R., Farver, C., Thunnissen, F. B. & Erzurum, S. C. Extracellular glutathione peroxidase induction in asthmatic lungs: evidence for redox regulation of expression in human airway epithelial cells. *FASEB J* **15**, 70-78, doi:10.1096/fj.00-0085com (2001).
90 Randall, M. J., Spiess, P. C., Hristova, M., Hondal, R. J. & van der Vliet, A. Acrolein-induced activation of mitogen-activated protein kinase signaling is mediated by alkylation of thioredoxin reductase and thioredoxin 1. *Redox Biol* **1**, 265-275, doi:10.1016/j.redox.2013.02.001 (2013).
91 Kelleher, Z. T. *et al.* Thioredoxin-mediated denitrosylation regulates cytokine-induced nuclear factor kappaB (NF-kappaB) activation. *J Biol Chem* **289**, 3066-3072, doi:10.1074/jbc.M113.503938 (2014).
92 Yuan, Y. G., Wang, Y. H., Xing, H. H. & Gurunathan, S. Quercetin-mediated synthesis of graphene oxide-silver nanoparticle nanocomposites: a suitable alternative nanotherapy for neuroblastoma. *Int J Nanomedicine* **12**, 5819-5839, doi:10.2147/IJN.S140605 (2017).
93 Han, J. W. *et al.* Male- and female-derived somatic and germ cell-specific toxicity of silver nanoparticles in mouse. *Nanotoxicology* **10**, 361-373, doi:10.3109/17435390.2015.1073396 (2016).
94 Zhang, X. F., Shen, W. & Gurunathan, S. Silver Nanoparticle-Mediated Cellular Responses in Various Cell Lines: An in Vitro Model. *Int J Mol Sci* **17**, doi:10.3390/ijms17101603 (2016).
95 Choi, Y. J. *et al.* Differential Cytotoxic Potential of Silver Nanoparticles in Human Ovarian Cancer Cells and Ovarian Cancer Stem Cells. *Int J Mol Sci* **17**, doi:10.3390/ijms17122077 (2016).
96 Gurunathan, S. *et al.* Reduced graphene oxide-silver nanoparticle nanocomposite: a potential anticancer nanotherapy. *Int J Nanomedicine* **10**, 6257-6276, doi:10.2147/IJN.S92449 (2015).
97 Han, J. W., Gurunathan, S., Choi, Y. J. & Kim, J. H. Dual functions of silver nanoparticles in F9 teratocarcinoma stem cells, a suitable model for evaluating cytotoxicity- and differentiation-mediated cancer therapy. *Int J Nanomedicine* **12**, 7529-7549, doi:10.2147/IJN.S145147 (2017).
98 Orlowski, P. *et al.* Assessment of in vitro cellular responses of monocytes and keratinocytes to tannic acid modified silver nanoparticles. *Toxicol In Vitro* **27**, 1798-1808, doi:10.1016/j.tiv.2013.05.010 (2013).
99 Misiewicz, M. *et al.* Identification of a novel endoplasmic reticulum stress response element regulated by XBP1. *J Biol Chem* **288**, 20378-20391, doi:10.1074/jbc.M113.457242 (2013).
100 Zhou, J. & Chng, W. J. Roles of thioredoxin binding protein (TXNIP) in oxidative stress, apoptosis and cancer. *Mitochondrion* **13**, 163-169, doi:10.1016/j.mito.2012.06.004 (2013).
101 O'Grady, S. M. Oxidative stress, autophagy and airway ion transport. *Am J Physiol Cell Physiol*, doi:10.1152/ajpcell.00341.2018 (2018).
102 Gao, S. *et al.* Ubiquitin ligase Nedd4L targets activated Smad2/3 to limit TGF-beta signaling. *Mol Cell* **36**, 457-468, doi:10.1016/j.molcel.2009.09.043 (2009).

103 Ma, P. *et al.* The ubiquitin ligase RNF220 enhances canonical Wnt signaling through USP7-mediated deubiquitination of beta-catenin. *Mol Cell Biol* **34**, 4355-4366, doi:10.1128/MCB.00731-14 (2014).
104 Caliceti, C., Nigro, P., Rizzo, P. & Ferrari, R. ROS, Notch, and Wnt signaling pathways: crosstalk between three major regulators of cardiovascular biology. *Biomed Res Int* **2014**, 318714, doi:10.1155/2014/318714 (2014).
105 Jofre-Monseny, L., Minihane, A.-M. & Rimbach, G. Impact of apoE genotype on oxidative stress, inflammation and disease risk. *Molecular Nutrition & Food Research* **52**, 131-145, doi:10.1002/mnfr.200700322 (2008).
106 Yao, X. *et al.* Apolipoprotein E negatively regulates house dust mite-induced asthma via a low-density lipoprotein receptor-mediated pathway. *Am J Respir Crit Care Med* **182**, 1228-1238, doi:10.1164/rccm.201002-0308OC (2010).
107 Howrylak, J. A. *et al.* Gene expression profiling of asthma phenotypes demonstrates molecular signatures of atopy and asthma control. *J Allergy Clin Immunol* **137**, 1390-1397 e1396, doi:10.1016/j.jaci.2015.09.058 (2016).
108 Novershtern, N., Itzhaki, Z., Manor, O., Friedman, N. & Kaminski, N. A functional and regulatory map of asthma. *Am J Respir Cell Mol Biol* **38**, 324-336, doi:10.1165/rcmb.2007-0151OC (2008).
109 Leguillette, R. *et al.* Myosin, transgelin, and myosin light chain kinase: expression and function in asthma. *Am J Respir Crit Care Med* **179**, 194-204, doi:10.1164/rccm.200609-1367OC (2009).
110 Nalbandian, A. *et al.* Activation of the NLRP3 Inflammasome Is Associated with Valosin-Containing Protein Myopathy. *Inflammation* **40**, 21-41, doi:10.1007/s10753-016-0449-5 (2017).
111 Coll, R. C. *et al.* A small-molecule inhibitor of the NLRP3 inflammasome for the treatment of inflammatory diseases. *Nat Med* **21**, 248-255, doi:10.1038/nm.3806 (2015).
112 Ober, C., Loisel, D. A. & Gilad, Y. Sex-specific genetic architecture of human disease. *Nat Rev Genet* **9**, 911-922, doi:10.1038/nrg2415 (2008).
113 Keller, A. A., McFerran, S., Lazareva, A. & Suh, S. Global life cycle releases of engineered nanomaterials. *Journal of Nanoparticle Research* **15**, doi:10.1007/s11051-013-1692-4 (2013).
114 Royce, S. G. *et al.* Modeling population exposures to silver nanoparticles present in consumer products. *Journal of Nanoparticle Research* **16**, doi:10.1007/s11051-014-2724-4 (2014).
115 Pourzahedi, L. & Eckelman, M. J. Comparative life cycle assessment of silver nanoparticle synthesis routes. *Environmental Science: Nano* **2**, 361-369, doi:10.1039/c5en00075k (2015).
116 Hischier, R. & Walser, T. Life cycle assessment of engineered nanomaterials: State of the art and strategies to overcome existing gaps. *Science of The Total Environment* **425**, 271-282, doi:10.1016/j.scitotenv.2012.03.001 (2012).
117 Slotte, M. & Zevenhoven, R. Energy requirements and life cycle assessment of production and product integration of silver, copper and zinc nanoparticles. *Journal of Cleaner Production* **148**, 948-957, doi:10.1016/j.jclepro.2017.01.083 (2017).
118 Reidy, B., Haase, A., Luch, A., Dawson, K. A. & Lynch, I. Mechanisms of Silver Nanoparticle Release, Transformation and Toxicity: A Critical Review of Current

Knowledge and Recommendations for Future Studies and Applications. *Materials* **6**, 2295-2350, doi:10.3390/ma6062295 (2013).
119 Weldon, B. A. *et al.* Occupational exposure limit for silver nanoparticles: considerations on the derivation of a general health-based value. *Nanotoxicology* **10**, 1-13, doi:10.3109/17435390.2016.1148793 (2016).
120 NIOSH. *Current Intelligence Bulletin on the Health Effects of Occupational Exposure to Silver Nanomaterials*, <https://www.federalregister.gov/documents/2018/09/18/2018-20169/revised-draft-niosh-current-intelligence-bulletin-health-effects-of-occupational-exposure-to-silver> (2018).
121 Kim, H. *et al.* Silver nanoparticles induce p53-mediated apoptosis in human bronchial epithelial (BEAS-2B) cells. *The Journal of Toxicological Sciences* **39**, 401-412, doi:10.2131/jts.39.401 (2014).
122 VanWinkle, B. A. *et al.* Nanoparticle (NP) uptake by type I alveolar epithelial cells and their oxidant stress response. *Nanotoxicology* **3**, 307-318, doi:10.3109/17435390903121949 (2009).
123 Stępkowski, T. M., Brzóska, K. & Kruszewski, M. Silver nanoparticles induced changes in the expression of NF-κB related genes are cell type specific and related to the basal activity of NF-κB. *Toxicology in Vitro* **28**, 473-478, doi:10.1016/j.tiv.2014.01.008 (2014).
124 Aldossari, A. A., Shannahan, J. H., Podila, R. & Brown, J. M. Influence of physicochemical properties of silver nanoparticles on mast cell activation and degranulation. *Toxicology in Vitro* **29**, 195-203, doi:10.1016/j.tiv.2014.10.008 (2015).
125 Alsaleh, N. B., Persaud, I. & Brown, J. M. Silver Nanoparticle-Directed Mast Cell Degranulation Is Mediated through Calcium and PI3K Signaling Independent of the High Affinity IgE Receptor. *PLOS ONE* **11**, doi:10.1371/journal.pone.0167366 (2016).
126 Yang, W., Lee, S., Lee, J., Bae, Y. & Kim, D. Silver nanoparticle-induced degranulation observed with quantitative phase microscopy. *Journal of Biomedical Optics* **15**, 45005, doi:10.1117/1.3470104 (2010).
127 Shin, S.-H., Ye, M.-K., Kim, H.-S. & Kang, H.-S. The effects of nano-silver on the proliferation and cytokine expression by peripheral blood mononuclear cells. *International Immunopharmacology* **7**, 1813-1818, doi:10.1016/j.intimp.2007.08.025 (2007).
128 Vallières, F. *et al.* Activation of human AML14.3D10 eosinophils by nanoparticles: Modulatory activity on apoptosis and cytokine production. *Journal of Immunotoxicology*, 1-10, doi:10.1080/1547691x.2016.1203379 (2016).
129 Poirier, M., Simard, J. C., Antoine, F. & Girard, D. Interaction between silver nanoparticles of 20 nm (AgNP20) and human neutrophils: induction of apoptosis and inhibition of de novo protein synthesis by AgNP20 aggregates. *Journal of Applied Toxicology* **34**, 404-412, doi:10.1002/jat.2956 (2014).
130 Poirier, M., Simard, J.-C. & Girard, D. Silver nanoparticles of 70 nm and 20 nm affect differently the biology of human neutrophils. *Journal of Immunotoxicology* **13**, 375-385, doi:10.3109/1547691x.2015.1106622 (2015).

131 Bezemer, G. F. G. *et al.* Activation of Pulmonary Dendritic Cells and Th2-Type Inflammatory Responses on Instillation of Engineered, Environmental Diesel Emission Source or Ambient Air Pollutant Particles in vivo. *Journal of Innate Immunity* **3**, 150-166, doi:10.1159/000321725 (2010).
132 Kang, K., Jung, H. & Lim, J.-S. Cell Death by Polyvinylpyrrolidine-Coated Silver Nanoparticles is Mediated by ROS-Dependent Signaling. *Biomolecules & Therapeutics* **20**, 399-405, doi:10.4062/biomolther.2012.20.4.399 (2012).
133 Carlson, C. *et al.* Unique Cellular Interaction of Silver Nanoparticles: Size-Dependent Generation of Reactive Oxygen Species. *The Journal of Physical Chemistry B* **112**, 13608-13619, doi:10.1021/jp712087m (2008).
134 Müller, L. *et al.* Exposure to silver nanoparticles affects viability and function of natural killer cells, mostly via the release of ions. *Cell Biology and Toxicology*, 1-10, doi:10.1007/s10565-017-9403-z (2017).
135 Joksić, G., Stašić, J., Filipović, J., Šobot, A. & Trtica, M. Size of silver nanoparticles determines proliferation ability of human circulating lymphocytes in vitro. *Toxicology Letters* **247**, 29-34, doi:10.1016/j.toxlet.2016.02.007 (2016).
136 Devanabanda, M., Latheef, S. & Madduri, R. Immunotoxic effects of gold and silver nanoparticles: Inhibition of mitogen-induced proliferative responses and viability of human and murine lymphocytes in vitro. *Journal of Immunotoxicology*, 1-6, doi:10.1080/1547691x.2016.1234522 (2016).
137 Greulich, C. *et al.* Cell type-specific responses of peripheral blood mononuclear cells to silver nanoparticles. *Acta Biomaterialia* **7**, 3505-3514, doi:10.1016/j.actbio.2011.05.030 (2011).
138 Takenaka, S. *et al.* Pulmonary and Systemic Distribution of Inhaled Ultrafine Silver Particles in Rats. *Environmental Health Perspectives* **109**, 547, doi:10.2307/3454667 (2001).
139 Braakhuis, H. M. *et al.* Particle size dependent deposition and pulmonary inflammation after short-term inhalation of silver nanoparticles. *Particle and Fibre Toxicology* **11**, 1-16, doi:10.1186/s12989-014-0049-1 (2014).
140 Ji, J. *et al.* Twenty-Eight-Day Inhalation Toxicity Study of Silver Nanoparticles in Sprague-Dawley Rats. *Inhalation Toxicology* **19**, 857-871, doi:10.1080/08958370701432108 (2008).
141 USEPA. *Reviewing New Chemicals under the Toxic Substances Control Act (TSCA)*, <https://www.epa.gov/reviewing-new-chemicals-under-toxic-substances-control-act-tsca/control-nanoscale-materials-under> (2017).
142 Judson, R. S. *et al.* In vitro screening of environmental chemicals for targeted testing prioritization: the ToxCast project. *Environ Health Perspect* **118**, 485-492, doi:10.1289/ehp.0901392 (2010).
143 USEPA. *Use of High-Throughput Assays and Computational Tools in the Endocrine Disruptor Screening Program*, <https://www.epa.gov/endocrine-disruption/use-high-throughput-assays-and-computational-tools-endocrine-disruptor> (2013).
144 Yamanaka, K. *et al.* IL-13 regulates IL-17C expression by suppressing NF-kappaB-mediated transcriptional activation in airway epithelial cells. *Biochem Biophys Res Commun* **495**, 1534-1540, doi:10.1016/j.bbrc.2017.11.207 (2018).

145 Lerner, C. A., Sundar, I. K. & Rahman, I. Mitochondrial redox system, dynamics, and dysfunction in lung inflammaging and COPD. *Int J Biochem Cell Biol* **81**, 294-306, doi:10.1016/j.biocel.2016.07.026 (2016).
146 Ackerman, K. G. *et al.* Interacting genetic loci cause airway hyperresponsiveness. *Physiol Genomics* **21**, 105-111, doi:10.1152/physiolgenomics.00267.2004 (2005).
147 Levitt, R. C., Mitzner, W. & Kleeberger, S. R. A genetic approach to the study of lung physiology: understanding biological variability in airway responsiveness. *Am J Physiol* **258**, L157-164, doi:10.1152/ajplung.1990.258.4.L157 (1990).
148 Karp, C. L. *et al.* Identification of complement factor 5 as a susceptibility locus for experimental allergic asthma. *Nat Immunol* **1**, 221-226, doi:10.1038/79759 (2000).
149 Brewer, J. P., Kisselgof, A. B. & Martin, T. R. Genetic variability in pulmonary physiological, cellular, and antibody responses to antigen in mice. *Am J Respir Crit Care Med* **160**, 1150-1156, doi:10.1164/ajrccm.160.4.9806034 (1999).
150 Shinagawa, K. & Kojima, M. Mouse model of airway remodeling: strain differences. *Am J Respir Crit Care Med* **168**, 959-967, doi:10.1164/rccm.200210-1188OC (2003).
151 You, Y., Richer, E. J., Huang, T. & Brody, S. L. Growth and differentiation of mouse tracheal epithelial cells: selection of a proliferative population. *Am J Physiol Lung Cell Mol Physiol* **283**, L1315-1321, doi:10.1152/ajplung.00169.2002 (2002).
152 Petecchia, L. *et al.* Cytokines induce tight junction disassembly in airway cells via an EGFR-dependent MAPK/ERK1/2-pathway. *Lab Invest* **92**, 1140-1148, doi:10.1038/labinvest.2012.67 (2012).
153 Melgert, B. N. *et al.* Female mice are more susceptible to the development of allergic airway inflammation than male mice. *Clinical & Experimental Allergy* **35**, 1496-1503, doi:10.1111/j.1365-2222.2005.02362.x (2005).
154 Elenkov, I. J. Glucocorticoids and the Th1/Th2 balance. *Ann N Y Acad Sci* **1024**, 138-146, doi:10.1196/annals.1321.010 (2004).
155 Krause, S. *et al.* Blockade of interleukin-13-mediated cell activation by a novel inhibitory antibody to human IL-13 receptor alpha1. *Mol Immunol* **43**, 1799-1807, doi:10.1016/j.molimm.2005.11.001 (2006).
156 Dickinson, J. D. *et al.* IL13 activates autophagy to regulate secretion in airway epithelial cells. *Autophagy* **12**, 397-409, doi:10.1080/15548627.2015.1056967 (2016).
157 You, Y. & Brody, S. L. Culture and differentiation of mouse tracheal epithelial cells. *Methods Mol Biol* **945**, 123-143, doi:10.1007/978-1-62703-125-7_9 (2013).
158 Horani, A., Dickinson, J. D. & Brody, S. L. Applications of mouse airway epithelial cell culture for asthma research. *Methods Mol Biol* **1032**, 91-107, doi:10.1007/978-1-62703-496-8_7 (2013).
159 Lee, V. *et al.* Amphiphilic polymer-coated CdSe/ZnS quantum dots induce pro-inflammatory cytokine expression in mouse lung epithelial cells and macrophages. *Nanotoxicology* **9**, 336-343, doi:10.3109/17435390.2014.930532 (2015).
160 Park, J. J. *et al.* Characterization of 3D embryonic C57BL/6 and A/J mouse midbrain micromass in vitro culture systems for developmental neurotoxicity testing. *Toxicol In Vitro* **48**, 33-44, doi:10.1016/j.tiv.2017.12.009 (2018).

161 Parker, J. C. *et al.* Chronic IL9 and IL-13 exposure leads to an altered differentiation of ciliated cells in a well-differentiated paediatric bronchial epithelial cell model. *PLoS One* **8**, e61023, doi:10.1371/journal.pone.0061023 (2013).
162 Weldy, C. S. *et al.* Heterozygosity in the glutathione synthesis gene Gclm increases sensitivity to diesel exhaust particulate induced lung inflammation in mice. *Inhal Toxicol* **23**, 724-735, doi:10.3109/08958378.2011.608095 (2011).
163 Juarez-Moreno, K. *et al.* Comparison of cytotoxicity and genotoxicity effects of silver nanoparticles on human cervix and breast cancer cell lines. *Hum Exp Toxicol* **36**, 931-948, doi:10.1177/0960327116675206 (2017).
164 Long, Y. M. *et al.* Surface ligand controls silver ion release of nanosilver and its antibacterial activity against Escherichia coli. *Int J Nanomedicine* **12**, 3193-3206, doi:10.2147/IJN.S132327 (2017).
165 Weldon, B. A. *et al.* Using primary organotypic mouse midbrain cultures to examine developmental neurotoxicity of silver nanoparticles across two genetic strains. *Toxicol Appl Pharmacol*, doi:10.1016/j.taap.2018.04.017 (2018).
166 Team, R. C. *R: A language and environment for statistical computing*, <https://www.r-project.org> (2018).
167 Gereda, J. E. *et al.* Relation between house-dust endotoxin exposure, type 1 T-cell development, and allergen sensitisation in infants at high risk of asthma. *The Lancet* **355**, 1680-1683, doi:10.1016/s0140-6736(00)02239-x (2000).
168 Bachler, G., von Goetz, N. & Hungerbuhler, K. A physiologically based pharmacokinetic model for ionic silver and silver nanoparticles. *Int J Nanomedicine* **8**, 3365-3382, doi:10.2147/IJN.S46624 (2013).
169 Yasuo, M. *et al.* Relationship between calcium-activated chloride channel 1 and MUC5AC in goblet cell hyperplasia induced by interleukin-13 in human bronchial epithelial cells. *Respiration* **73**, 347-359, doi:10.1159/000091391 (2006).
170 Kimura, T. *et al.* Deletion of the ubiquitin ligase Nedd4L in lung epithelia causes cystic fibrosis-like disease. *Proc Natl Acad Sci U S A* **108**, 3216-3221, doi:10.1073/pnas.1010334108 (2011).
171 Campbell, C. D. *et al.* Whole-genome sequencing of individuals from a founder population identifies candidate genes for asthma. *PLoS One* **9**, e104396, doi:10.1371/journal.pone.0104396 (2014).
172 Nam, J. H. *et al.* Interleukin-13/-4-induced oxidative stress contributes to death of hippocampal neurons in abeta1-42-treated hippocampus in vivo. *Antioxid Redox Signal* **16**, 1369-1383, doi:10.1089/ars.2011.4175 (2012).
173 Kato, T. *et al.* Endocrine disruptors that deplete glutathione levels in APC promote Th2 polarization in mice leading to the exacerbation of airway inflammation. *Eur J Immunol* **36**, 1199-1209, doi:10.1002/eji.200535140 (2006).
174 Utsugi, M. *et al.* Glutathione redox regulates lipopolysaccharide-induced IL-12 production through p38 mitogen-activated protein kinase activation in human monocytes: role of glutathione redox in IFN-gamma priming of IL-12 production. *J Leukoc Biol* **71**, 339-347 (2002).
175 Haddad, J. J. & Fahlman, C. S. Redox- and oxidant-mediated regulation of interleukin-10: an anti-inflammatory, antioxidant cytokine? *Biochem Biophys Res Commun* **297**, 163-176 (2002).

176 Meng, Q. *et al.* Nuclear Factor-kappaB modulates cellular glutathione and prevents oxidative stress in cancer cells. *Cancer Lett* **299**, 45-53, doi:10.1016/j.canlet.2010.08.002 (2010).
177 Hadzic, T. *et al.* The Role of Low Molecular Weight Thiols in T Lymphocyte Proliferation and IL-2 Secretion. *The Journal of Immunology* **175**, 7965-7972, doi:10.4049/jimmunol.175.12.7965 (2005).
178 Short, S., Merkel, B. J., Caffrey, R. & McCoy, K. L. Defective antigen processing correlates with a low level of intracellular glutathione. *Eur J Immunol* **26**, 3015-3020, doi:10.1002/eji.1830261229 (1996).
179 Kuppner, M. C. *et al.* Ifosfamide impairs the allostimulatory capacity of human dendritic cells by intracellular glutathione depletion. *Blood* **102**, 3668-3674, doi:10.1182/blood-2003-05-1408 (2003).
180 Murata, Y., Ohteki, T., Koyasu, S. & Hamuro, J. IFN-gamma and pro-inflammatory cytokine production by antigen-presenting cells is dictated by intracellular thiol redox status regulated by oxygen tension. *Eur J Immunol* **32**, 2866-2873, doi:10.1002/1521-4141(2002010)32:10<2866::AID-IMMU2866>3.0.CO;2-V (2002).
181 Peterson, J. D., Herzenberg, L. A., Vasquez, K. & Waltenbaugh, C. Glutathione levels in antigen-presenting cells modulate Th1 versus Th2 response patterns. *Proc Natl Acad Sci U S A* **95**, 3071-3076 (1998).
182 Svensson, C. R. *et al.* Validation of an air-liquid interface toxicological set-up using Cu, Pd, and Ag well-characterized nanostructured aggregates and spheres. *J Nanopart Res* **18**, 86, doi:10.1007/s11051-016-3389-y (2016).
183 Huh, D. *et al.* Reconstituting organ-level lung functions on a chip. *Science* **328**, 1662-1668, doi:10.1126/science.1188302 (2010).
184 Marshall, C. B. *et al.* p73 Is Required for Multiciliogenesis and Regulates the Foxj1-Associated Gene Network. *Cell Reports* **14**, 2289-2300, doi:10.1016/j.celrep.2016.02.035 (2016).
185 Smith, M. K., Koch, P. J. & Reynolds, S. D. Direct and indirect roles for beta-catenin in facultative basal progenitor cell differentiation. *Am J Physiol Lung Cell Mol Physiol* **302**, L580-594, doi:10.1152/ajplung.00095.2011 (2012).
186 Martin, F. J. & Prince, A. S. TLR2 Regulates Gap Junction Intercellular Communication in Airway Cells. *The Journal of Immunology* **180**, 4986-4993, doi:10.4049/jimmunol.180.7.4986 (2008).
187 Rock, J. R. *et al.* Basal cells as stem cells of the mouse trachea and human airway epithelium. *Proc Natl Acad Sci U S A* **106**, 12771-12775, doi:10.1073/pnas.0906850106 (2009).
188 You, Y. *et al.* Role of f-box factor foxj1 in differentiation of ciliated airway epithelial cells. *Am J Physiol Lung Cell Mol Physiol* **286**, L650-657, doi:10.1152/ajplung.00170.2003 (2004).
189 Wang, X. Y. *et al.* Novel method for isolation of murine clara cell secretory protein-expressing cells with traces of stemness. *PLoS One* **7**, e43008, doi:10.1371/journal.pone.0043008 (2012).
190 Fahy, J. V. Goblet cell and mucin gene abnormalities in asthma. *Chest* **122**, 320S-326S (2002).

191 Buchweitz, J. P., Harkema, J. R. & Kaminski, N. E. Time-dependent airway epithelial and inflammatory cell responses induced by influenza virus A/PR/8/34 in C57BL/6 mice. *Toxicol Pathol* **35**, 424-435, doi:10.1080/01926230701302558 (2007).
192 Cai, Y., Kumar, R. K., Zhou, J., Foster, P. S. & Webb, D. C. Ym1/2 promotes Th2 cytokine expression by inhibiting 12/15(S)-lipoxygenase: identification of a novel pathway for regulating allergic inflammation. *J Immunol* **182**, 5393-5399, doi:10.4049/jimmunol.0803874 (2009).
193 Ong, C. B. *et al.* Ozone-Induced Type 2 Immunity in Nasal Airways. Development and Lymphoid Cell Dependence in Mice. *Am J Respir Cell Mol Biol* **54**, 331-340, doi:10.1165/rcmb.2015-0165OC (2016).
194 Chu, H. W. *et al.* Expression and activation of 15-lipoxygenase pathway in severe asthma: relationship to eosinophilic phenotype and collagen deposition. *Clin Exp Allergy* **32**, 1558-1565 (2002).
195 Hallstrand, T. S. *et al.* Relationship between levels of secreted phospholipase A(2) groups IIA and X in the airways and asthma severity. *Clin Exp Allergy* **41**, 801-810, doi:10.1111/j.1365-2222.2010.03676.x (2011).
196 Hallstrand, T. S. *et al.* Regulation and function of epithelial secreted phospholipase A2 group X in asthma. *Am J Respir Crit Care Med* **188**, 42-50, doi:10.1164/rccm.201301-0084OC (2013).
197 Aoki, Y., Qiu, D., Uyei, A. & Kao, P. N. Human airway epithelial cells express interleukin-2 in vitro. *Am J Physiol* **272**, L276-286, doi:10.1152/ajplung.1997.272.2.L276 (1997).
198 Ahdieh, M., Vandenbos, T. & Youakim, A. Lung epithelial barrier function and wound healing are decreased by IL-4 and IL-13 and enhanced by IFN-gamma. *Am J Physiol Cell Physiol* **281**, C2029-2038, doi:10.1152/ajpcell.2001.281.6.C2029 (2001).
199 Saatian, B. *et al.* Interleukin-4 and interleukin-13 cause barrier dysfunction in human airway epithelial cells. *Tissue Barriers* **1**, e24333, doi:10.4161/tisb.24333 (2013).
200 Neurath, M. F., Finotto, S. & Glimcher, L. H. The role of Th1/Th2 polarization in mucosal immunity. *Nat Med* **8**, 567-573, doi:10.1038/nm0602-567 (2002).
201 Gordon, E. D., Locksley, R. M. & Fahy, J. V. Cross-Talk between Epithelial Cells and Type 2 Immune Signaling. The Role of IL-25. *Am J Respir Crit Care Med* **193**, 935-936, doi:10.1164/rccm.201512-2534ED (2016).
202 Uchida, M. *et al.* Oxidative stress serves as a key checkpoint for IL-33 release by airway epithelium. *Allergy* **72**, 1521-1531, doi:10.1111/all.13158 (2017).
203 Miyata, M. *et al.* Thymic stromal lymphopoietin is a critical mediator of IL-13-driven allergic inflammation. *Eur J Immunol* **39**, 3078-3083, doi:10.1002/eji.200939302 (2009).
204 Salvi, S. *et al.* Interleukin-5 production by human airway epithelial cells. *Am J Respir Cell Mol Biol* **20**, 984-991, doi:10.1165/ajrcmb.20.5.3463 (1999).
205 Xie, X. H. *et al.* Lipopolysaccharide induces IL-6 production in respiratory syncytial virus-infected airway epithelial cells through the toll-like receptor 4 signaling pathway. *Pediatr Res* **65**, 156-162, doi:10.1203/PDR.0b013e318191f5c6 (2009).

206 Lim, S. *et al.* Differential expression of IL-10 receptor by epithelial cells and alveolar macrophages. *Allergy* **59**, 505-514, doi:10.1111/j.1398-9995.2004.00455.x (2004).
207 Tyner, J. W. *et al.* Blocking airway mucous cell metaplasia by inhibiting EGFR antiapoptosis and IL-13 transdifferentiation signals. *J Clin Invest* **116**, 309-321, doi:10.1172/JCI25167 (2006).
208 Thavagnanam, S. *et al.* Effects of IL-13 on mucociliary differentiation of pediatric asthmatic bronchial epithelial cells. *Pediatr Res* **69**, 95-100, doi:10.1203/PDR.0b013e318204edb5 (2011).
209 Laoukili, J. *et al.* IL-13 alters mucociliary differentiation and ciliary beating of human respiratory epithelial cells. *Journal of Clinical Investigation* **108**, 1817-1824, doi:10.1172/jci200113557 (2001).
210 Kidd, P. Th1/Th2 balance: the hypothesis, its limitations, and implications for health and disease. *Altern Med Rev* **8**, 223-246 (2003).
211 Choy, D. F. *et al.* TH2 and TH17 inflammatory pathways are reciprocally regulated in asthma. *Sci Transl Med* **7**, 301ra129, doi:10.1126/scitranslmed.aab3142 (2015).
212 Woodruff, P. G. *et al.* T-helper type 2-driven inflammation defines major subphenotypes of asthma. *Am J Respir Crit Care Med* **180**, 388-395, doi:10.1164/rccm.200903-0392OC (2009).
213 Choy, D. F. *et al.* Gene expression patterns of Th2 inflammation and intercellular communication in asthmatic airways. *J Immunol* **186**, 1861-1869, doi:10.4049/jimmunol.1002568 (2011).
214 Colobran, R., Pujol-Borrell, R., Armengol, M. P. & Juan, M. The chemokine network. I. How the genomic organization of chemokines contains clues for deciphering their functional complexity. *Clin Exp Immunol* **148**, 208-217, doi:10.1111/j.1365-2249.2007.03344.x (2007).
215 Commins, S. P., Borish, L. & Steinke, J. W. Immunologic messenger molecules: cytokines, interferons, and chemokines. *J Allergy Clin Immunol* **125**, S53-72, doi:10.1016/j.jaci.2009.07.008 (2010).
216 Dobin, A. *et al.* STAR: ultrafast universal RNA-seq aligner. *Bioinformatics* **29**, 15-21, doi:10.1093/bioinformatics/bts635 (2013).
217 Brown, K. R. *et al.* Endotypes of difficult-to-control asthma in inner-city African American children. *PLoS One* **12**, e0180778, doi:10.1371/journal.pone.0180778 (2017).
218 Yang, X. O. *et al.* STAT3 regulates cytokine-mediated generation of inflammatory helper T cells. *J Biol Chem* **282**, 9358-9363, doi:10.1074/jbc.C600321200 (2007).
219 Lee, H. S. *et al.* IL-23 secreted by bronchial epithelial cells contributes to allergic sensitization in asthma model: role of IL-23 secreted by bronchial epithelial cells. *Am J Physiol Lung Cell Mol Physiol* **312**, L13-L21, doi:10.1152/ajplung.00114.2016 (2017).
220 Yen, D. *et al.* IL-23 is essential for T cell-mediated colitis and promotes inflammation via IL-17 and IL-6. *J Clin Invest* **116**, 1310-1316, doi:10.1172/JCI21404 (2006).
221 Wu, H. *et al.* An Inhibitory Role for the Transcription Factor Stat3 in Controlling IL-4 and Bcl6 Expression in Follicular Helper T Cells. *J Immunol* **195**, 2080-2089, doi:10.4049/jimmunol.1500335 (2015).

222 Mondal, A., Sawant, D. & Dent, A. L. Transcriptional repressor BCL6 controls Th17 responses by controlling gene expression in both T cells and macrophages. *J Immunol* **184**, 4123-4132, doi:10.4049/jimmunol.0901242 (2010).
223 Lee, S., Hwang, H. J. & Kim, Y. Modeling the role of TGF-beta in regulation of the Th17 phenotype in the LPS-driven immune system. *Bull Math Biol* **76**, 1045-1080, doi:10.1007/s11538-014-9946-6 (2014).
224 Suryawanshi, A. *et al.* Canonical wnt signaling in dendritic cells regulates Th1/Th17 responses and suppresses autoimmune neuroinflammation. *J Immunol* **194**, 3295-3304, doi:10.4049/jimmunol.1402691 (2015).
225 Browne, P., Noyes, P. D., Casey, W. M. & Dix, D. J. Application of Adverse Outcome Pathways to U.S. EPA's Endocrine Disruptor Screening Program. *Environ Health Perspect* **125**, 096001, doi:10.1289/EHP1304 (2017).
226 Combes, R. & Balls, M. Intelligent testing strategies for chemicals testing -- a case of more haste, less speed? *Altern Lab Anim* **33**, 289-297 (2005).
227 Hartung, T., Luechtefeld, T., Maertens, A. & Kleensang, A. Integrated testing strategies for safety assessments. *ALTEX* **30**, 3-18 (2013).
228 OECD. *New Guidance Document on an Integrated Apporach on Testing and Assessment (IATA) for Skin Corrosion and Irritation*, <http://www.oecd.org/chemicalsafety/risk-assessment/iata-integrated-approaches-to-testing-and-assessment.htm> (2014).
229 Meek, M. E. *et al.* A framework for human relevance analysis of information on carcinogenic modes of action. *Crit Rev Toxicol* **33**, 591-653, doi:10.1080/713608373 (2003).
230 OECD. *Proposal for a Template, and Guidance on Developing and Assessing the Completeness of Adverse Outcome Pathways*, <http://www.oecd.org/chemicalsafety/risk-assessment/iata-integrated-approaches-to-testing-and-assessment.htm> (2012).
231 Groh, K. J. & Tollefsen, K. E. The Challenge: Adverse outcome pathways in research and regulation-Current status and future perspectives. *Environmental Toxicology and Chemistry* **34**, 1935-1937, doi:10.1002/etc.3042 (2015).
232 Sturla, S. J. *et al.* Systems Toxicology: From Basic Research to Risk Assessment. *Chemical Research in Toxicology* **27**, 314-329, doi:10.1021/tx400410s (2014).
233 Harris, S., Hermsen, S. A. B., Yu, X., Hong, S. W. & Faustman, E. M. Comparison of toxicogenomic responses to phthalate ester exposure in an organotypic testis co-culture model and responses observed in vivo. *Reproductive Toxicology* **58**, 149-159, doi:10.1016/j.reprotox.2015.10.002 (2015).
234 Harris, S. *et al.* The presence of macrophages and inflammatory responses in an in vitro testicular co-culture model of male reproductive development enhance relevance to in vivo conditions. *Toxicol In Vitro* **36**, 210-215, doi:10.1016/j.tiv.2016.08.003 (2016).
235 Harris, S., Wegner, S., Hong, S. W. & Faustman, E. M. Phthalate metabolism and kinetics in an in vitro model of testis development. *Toxicology in Vitro* **32**, 123-131, doi:10.1016/j.tiv.2015.12.002 (2016).
236 Ankley, G. T. *et al.* Adverse outcome pathways: a conceptual framework to support ecotoxicology research and risk assessment. *Environ Toxicol Chem* **29**, 730-741, doi:10.1002/etc.34 (2010).

237 Warheit, D. B. How Meaningful are the Results of Nanotoxicity Studies in the Absence of Adequate Material Characterization? *Toxicological Sciences* **101**, 183-185, doi:10.1093/toxsci/kfm279 (2008).
238 Sayes, C. M. & Warheit, D. B. Characterization of nanomaterials for toxicity assessment. *Wiley Interdiscip Rev Nanomed Nanobiotechnol* **1**, 660-670, doi:10.1002/wnan.58 (2009).
239 Boyes, W. K. *et al.* A comprehensive framework for evaluating the environmental health and safety implications of engineered nanomaterials. *Crit Rev Toxicol* **47**, 767-810, doi:10.1080/10408444.2017.1328400 (2017).
240 Vietti, G., Lison, D. & van den Brule, S. Mechanisms of lung fibrosis induced by carbon nanotubes: towards an Adverse Outcome Pathway (AOP). *Part Fibre Toxicol* **13**, 11, doi:10.1186/s12989-016-0123-y (2016).
241 Gerloff, K. *et al.* The Adverse Outcome Pathway approach in nanotoxicology. *Computational Toxicology* **1**, 3-11, doi:10.1016/j.comtox.2016.07.001 (2017).
242 Edler, L. in *Regulatory Toxicology* Ch. Chapter 93, 359-375 (2014).
243 Kavlock, R. J., Allen, B. C., Faustman, E. M. & Kimmel, C. A. Dose-response assessments for developmental toxicity. IV. Benchmark doses for fetal weight changes. *Fundam Appl Toxicol* **26**, 211-222 (1995).
244 Sanz, E. *et al.* Cell-type-specific isolation of ribosome-associated mRNA from complex tissues. *Proc Natl Acad Sci U S A* **106**, 13939-13944, doi:10.1073/pnas.0907143106 (2009).
245 Heiman, M., Kulicke, R., Fenster, R. J., Greengard, P. & Heintz, N. Cell type-specific mRNA purification by translating ribosome affinity purification (TRAP). *Nat Protoc* **9**, 1282-1291, doi:10.1038/nprot.2014.085 (2014).